

PRESSURE DROP AND FILTRATION THROUGH FIBROUS POROUS MEDIA ON
THE SUMP STRAINER OF LIGHT WATER REACTORS

A Dissertation

by

SAYA LEE

Submitted to the Office of Graduate and Professional Studies of
Texas A&M University
in partial fulfillment of the requirements for the degree of

DOCTOR OF PHILOSOPHY

Chair of Committee,	Yassin A. Hassan
Committee Members,	William H. Marlow
	Kalyan Annamalai
	Hamm-Ching Chen
Head of Department,	Yassin A. Hassan

December 2014

Major Subject: Nuclear Engineering

Copyright 2014 Saya Lee

ABSTRACT

Fibrous porous media has been found in a variety of industrial applications including filters and insulation materials. In nuclear power plants, fibrous media are found as insulation materials to prevent heat loss and protect the containment structures and other components from thermal effects. However, in spite of efficient thermal insulation, fibrous media have been focused on as a hazard in the Emergency Core Cooling Systems (ECCSs). Fibrous debris generated from fiberglass insulation materials during a Loss of Coolant Accident (LOCA) might accumulate on the containment sump strainer causing loss of Net Positive Suction Head (NPSH), called the upstream effect, or it might penetrate through the strainer becoming a source of clogging for flow channels in the core (downstream effect). In the present work, head loss through fibrous porous media made of the same fiberglass insulation material used in pressurized water reactors (PWRs) were experimentally investigated to study upstream effects. Porosity of fibrous porous media was also considered by measuring build-up of debris beds. In order to study downstream effects, quantity of debris bypass was examined by changing the type of water, concentration of debris, fluid approach velocity, and temperature. As results, a head loss model, a compression model, and a debris bypass model were proposed for the given conditions in this study. Additionally, a microscope system was developed to characterize size distribution of irregular-shaped fibrous debris. The methodology was applied to three samples and the maximum fraction of debris bypass was found in the size range of 10 to 250 μm .

ACKNOWLEDGEMENTS

I would like to express my deepest gratitude to my advisor, Dr. Yassin A. Hassan, for his excellent guidance, caring, and providing the best research atmosphere throughout the course of this study. I would also like to thank my committee members, Dr. William H. Marlow, Dr. Kalyan Annamlai, and Dr. Hamm-Ching Chen, for their exceptional advice for doing research.

I would like to thank Dr. Rodolfo Vaghetto for his technical guidance and personal mentoring. Thanks also go to my friends, Suhaeb Abdulsattar, Mathew J. Kappes, and Huhu Wang, for their help and sharing the difficulties in the research. I would like to thank two undergraduate students, Jean Lim and Landon Brockmeyer, for their excellent and diligent performance. Also, I would like to thank Junsoo Yoo, Carlos Estrada, Dr. Shinkyu Kang, and Dr. Elvis Dominguez for their comments and practical help.

I would like to thank Debbie Greer, one of the department staff, for her very efficient support in all required procurement for the research.

Finally, thanks to my parents and parents-in-law, for their encouragement and to my wife, Myung, for her cheering me up and love.

NOMENCLATURE

a – empirical constant

a_p – particle radius

b – empirical constant

c – packing ratio of a porous medium

k – Kozeny constant

h – distance of separation between materials (m)

m – empirical constant for the compression model in this study

m_{chem} – mass of chemicals remaining in a filter (kg)

t – time for a test or the t-value for a statistical analysis

t_{crit} – critical t value

t_{dry} – drying time required to completely remove the water from the filter (hour)

t_{end} – time at the end of a test (hour)

t_{eq} – equilibrium time necessary for the dried filter to reach the equilibrium (hour)

w_{bypass} – quantity of debris bypass per unit surface area of a strainer (g/cm^2)

w_{max} – maximum quantity of debris bypass per unit surface area (g/cm^2)

$w_{injected}$ – quantity of debris injected per unit surface area (g/cm^2)

w_{∞} – maximum quantity of debris bypass per unit surface area with the maximum debris injection in this study (g/cm^2)

A – surface area of the strainer (m^2)

A_i – projected surface area of the i^{th} fraction to the strainer (m^2)

A_{total} – total surface area of the strainer (m^2)

C_f – filtration efficiency

D – particle diameter (m)

D_f – diameter of fiberglass (m)

I – ionic strength

K – Darcy permeability (m^{-2})

L – thickness of debris bed (m)

L_{avg} – averaged bed thickness (m)

L_i – bed thickness (m) at predefined location P_i

N_ε – empirical constant for the compression model in this study

N_{group2} – number of samples of group 2

N_T – number of turnovers of the water in the tank

L_0 – theoretical thickness of a fiber bed (m)

L_m – actual thickness of a fiber bed (m)

M – empirical constant for compression models

M_0 – initial quantity of NUKON in the tank (kg)

M_C – empirical constant for Grahn et al.'s model

M_{debris} – mass of debris collected in a filter bag (kg)

$M_{initial}$ – mass of a filter bag before test (kg)

M_{final} – mass of a filter bag after test (kg)

M_{solid} – mass of the solid material (kg)

$M_{s,t}$ – quantity of NUKON on the strainer at time t (kg)

N – empirical constant for compression models

N_C – empirical constant for Grahn et al.'s model

N_{group1} – number of samples of group 1

P – pressure (Pa)

P_i – i^{th} point to measure the debris thickness

p_k – total pressure on the bed (Pa)

Re_m – modified Reynolds number

U – approach velocity (m/s)

S_{group1}^2 – variance of group 1

S_{group2}^2 – variance of group 2

S_{DI}^2 - variance of the weight of the debris bypass of DI water tests

S_{HT}^2 - variance of the weight of the debris bypass of high temperature water tests

S_{TT}^2 - variance of the weight of the debris bypass of TAMU tap water tests

S_{1xBB}^2 - variance of the Weight of the debris bypass of 1xBB-DI water tests

S_{2xBB}^2 - variance of the Weight of the debris bypass of 2xBB-DI water tests

S_v – specific surface area (m^2/m^3)

T_{surfae} – surface temperature of the drying plate ($^{\circ}\text{C}$)

V_t – volume of water in the tank (m^3)

V_{DLR} – double layer repulsion energy (J)

\bar{W}_{group1} – mean value of group 1

\bar{W}_{group2} – mean value of group 2

$W_{group1,i}$ – value of the i^{th} sample of group 1

$W_{group2,i}$ – value of the i^{th} sample of group 2

$W_{DI,i}$ - weight of the debris bypass of the i^{th} DI water test

\bar{W}_{DI} - average weight of the debris bypass of the DI water tests

$W_{TT,i}$ - weight of the debris bypass of the i^{th} TAMU tap water test

\bar{W}_{TT} - average weight of the debris bypass of the TAMU tap water tests

$W_{HT,i}$ - weight of the debris bypass of the i^{th} high temperature tap water test

\bar{W}_{HT} - average weight of the debris bypass of the high temperature tap water tests

$W_{1xBB,i}$ - weight of the debris bypass of the i^{th} 1x BB-DI water test

\bar{W}_{1xBB} - average weight of the debris bypass of the 1x BB-DI water tests

$W_{2xBB,i}$ - weight of the debris bypass of the i^{th} 2x BB-DI water test

\bar{W}_{2xBB} - average weight of the debris bypass of the 2x BB-DI water tests

α – material dependent constant

β_v – compressibility of the void volume

ε – porosity of a porous medium or the dielectric constant

ε_0 – porosity at zero pressure

ε_∞ – porosity an infinite pressure

ε_m – mixed bedd porosity

ψ_{01} – electric potential on material 1

ψ_{02} – electric potential on material 2

κ – Deby-Hücke parameter

μ – viscosity of the fluid (Pa·s)

ρ – liquid density (kg/m³)

ρ_m – fiber mat density (kg/m³)

ρ_f – fiber density (kg/m³)

ρ_w – water density (kg/m³)

ρ_{solid} – density of the solid material (kg/m³)

$\sigma_{Ms,t}$ – uncertainty of quantity of debris transported to the strainer at time t (kg)

σ_U – uncertainty of approach velocity (m/s)

σ_{V_t} – uncertainty of volume of water in tank (m³)

σ_{C_f} – uncertainty of filtration efficiency

τ – experimentally determined time constant for N_T

τ_w – experimentally determined constant for the bypass model

BA – boric acid

BB – buffered borated

CDF – cumulative distribution function

DI – deionized

Co – cotton

Dw – down

EC – electrical conductivity ($S = \Omega^{-1}$)

Gf – glass fiber

Go – goat wool

Gw – glass wool

HT – high temperature test

HT-F – high temperature test with fluctuation

ID – inner diameter

K – kapok

M – merino cotton

MPP – mesh added perforated plate

N/A – not applicable

N/Q – not quoted

OD – outer diameter

Pe – Polyester

R – Rayon

RO – reversed osmosis

SBT – simulated Boston tap water

Si – Silk

SPP – simply perforated plate

Stdev – standard deviation

STT – simulated TAMU tap water

TSP – tri-sodium phosphate

TT – TAMU tap water

1xBB – 1x concentration (typical concentration) buffered borated

2xBB – 2x concentration buffered borated

3xBB – 3x concentration buffered borated

ARL – Alden Research Laboratory

BWR – Boiling Water Reactor

DBA - Design Basis Accident

ECCS – Emergency Core Cooling System

FIR – Finite Impulse Response

GE – General Electric

GL – Generic Letter

GSI-191 – Generic Safety Issue 191

IPSM – Imaging Particle Size Measurement system

LDV – Laser Doppler Velocimetry

LOCA – Loss-of-Coolant Accident

LWR – Light Water Reactor

NEI – Nuclear Energy Institute

NIST – National Institute of Standards and Technology

NPSH – Net Positive Suction Head

NRC – Nuclear Regulatory Commission

PCI – Performance Contracting INC.

PWR – Pressurized Water Reactor

RMSE – Root Mean Square Error

RWST – Refuel Water Storage Tank

SNC – Southern Nuclear Company

SRM – Standard Reference Material

SSE – Sum of Squares due to Error

STP – South Texas Project

TABLE OF CONTENTS

	Page
ABSTRACT	ii
ACKNOWLEDGEMENTS	iii
NOMENCLATURE	iv
TABLE OF CONTENTS	xii
LIST OF FIGURES	xv
LIST OF TABLES	xxii
CHAPTER I INTRODUCTION AND LITERATURE REVIEW	1
CHAPTER II EXPERIMENTAL FACILITIES	15
II.1. Low temperature horizontal head loss and debris bypass test facility	16
II.2. High temperature horizontal head loss and debris bypass test facility	22
II.3. Vertical head loss and debris bypass test facility	29
II.4. Debris size characterization system	35
II.5. Instrumentations	42
CHAPTER III EXPERIMENTS	46
III.1. Debris preparation	47
III.1.1. Shredder method	47
III.1.2. NEI method	49
III.2. Head loss experiment	55
III.3. Debris bypass experiment	59
III.3.1. General procedure of debris bypass test	59
III.3.2. Buffered borated water and aqueous chemical solutions preparation	65
III.3.3. Heating procedure	69
III.3.4. Debris quantity measurement	69
III.3.4.1. Drying time estimation	70
III.3.4.2. Equilibrium time estimation	71
III.3.4.3. Washout	72
III.4. Debris size characterization	73

CHAPTER IV RESULTS AND ANALYSES.....	76
IV.1. Head loss and compression of fibrous beds.....	77
IV.1.1. Thickness of fibrous beds.....	79
IV.1.2. Porosity of fibrous beds.....	92
IV.1.3. Head loss through fibrous beds	95
IV.1.4. Compression of fibrous bed.....	106
IV.1.5. Vertical head loss test results	114
IV.1.6. Uncertainty analysis	125
IV.1.6.1. Systematic errors	125
IV.1.6.2. Random errors	133
IV.2. Debris bypass.....	135
IV.2.1. Water type sensitivity test results.....	136
IV.2.1.1. Experimental results	137
IV.2.1.2. Summary of water type test results.....	139
IV.2.1.3. Statistical analysis.....	142
IV.2.2. Water chemistry effect analysis.....	146
IV.2.3. Temperature effect test results.....	151
IV.2.4. Effect of debris concentration	156
IV.2.5. Effect of fluid approach velocity	162
IV.2.6. Effect of flow fluctuation	164
IV.3. Debris size characterization.....	166
CHAPTER V CONCLUSIONS.....	177
REFERENCES	181
APPENDIX A. PRELIMINARY INVESTIGATION ON THE MIXING PROPELLER EFFECTS.....	189
APPENDIX B. DRYING TIME AND EQUILIBRIUM TIME ESTIMATION.....	191
APPENDIX C. PRELIMINARY MEASUREMENTS FOR THE FILTER WASHOUT PROCEDURE	193
APPENDIX D. HEAD LOSS AND COMPRESSION - MATLAB CODE.....	194
APPENDIX E. TEXAS A&M TAP WATER VS. BORATED WATER STATISTICAL ANALYSIS PROCEDURE BY JEREMY TEJADA.....	208
APPENDIX F. WATER QUALITY REPORTS	210
APPENDIX G. VISCOSITY MEASUREMENT	221

APPENDIX H. DEBRIS BED SNAPSHOTS – END OF TEST	224
APPENDIX I. DEBRIS SIZE CHARACTERIZATION MATLAB CODE	230
APPENDIX J. FIBROUS DEBRIS SEM IMAGES.....	236

LIST OF FIGURES

	Page
Figure I. 1. The sources of coolant and chemical solutions (a) break, (b) sprays	2
Figure I. 2. Containment sump strainers	3
Figure I. 3. Mechanisms of filtration.....	12
Figure II.1. 1. 3-D design of the low temperature horizontal head loss and debris bypass test facility	16
Figure II.1. 2. Low temperature horizontal experimental facility & instruments	17
Figure II.1. 3. Water tank of the low temperature horizontal facility	18
Figure II.1. 4. Strainer Plate (left) and its installation between two flanges (right).....	19
Figure II.1. 5. Centrifugal pump and flow control	20
Figure II.2. 1. Experimental Facility Overview	22
Figure II.2. 2. Polycarbonate water tank	23
Figure II.2. 3. T-Shape mixing propeller	24
Figure II.2. 4. Strainer plate (right) and its location in the test section (left).....	25
Figure II.2. 5. High temperature chemical resistant pump.....	26
Figure II.2. 6. Magnetic flow meter	26
Figure II.2. 7. Heating loop (7kW).....	27
Figure II.2. 8. Control panel interface	28
Figure II.3. 1. The design concept (a) and overview (b) of the vertical head loss and debris bypass test facility	29
Figure II.3. 2. Stainless steel water tank of the high temperature vertical facility.....	30
Figure II.3. 3. Pressure measurement and sampling point: (a) test section and (b) dynamic sampling port	31

Figure II.3. 4. Vertical test section in parts	32
Figure II.3. 5. Filter bag in the vertical test facility	32
Figure II.3. 6. Electro-magnetic flow meter and pressure transducer	33
Figure II.3. 7. Heating loop (7kw)	34
Figure II.4. 1. Overview of imaging particle size measurement system developed at Texas A&M University (IPSM-TAMU).....	35
Figure II.4. 2. Microscopy image calibration - (a) 20x with KR-851 (KLARMANN RULINGS, INC.) and (b) 2x with grids.....	37
Figure II.4. 3. Validation of particle size distribution using NIST 8631a standard particles	39
Figure II.4. 4. Mono-sized particle size measurement	40
Figure II.4. 5. Mono-sized particles – original images (left) and processed images (right).....	41
Figure III.1. 1. Debris preparation using shredder method (a) NUKON prepared using a leaf shredder and (b) and (c) boiled for 10 minutes in 2-liter stainless steel jar	48
Figure III.1. 2. Debris classes prepared by shredder method	48
Figure III.1. 3. One-side baked NUKON® mat	49
Figure III.1. 4. Debris final quantity – 6.6g (left), 40g (right)	50
Figure III.1. 5. Layers separation	51
Figure III.1. 6. Debris size reduction	52
Figure III.1. 7. Debris size reduction in a bucket – 6.6g (left), 40g (right).....	52
Figure III.1. 8. Pressure washer mixing – (a) outside and (b) inside of the bucket	53
Figure III.1. 9. Final state of debris sample – (a) in the bucket and (b) in the tray.....	54
Figure III.2. 1. Two different types of strainers - (a) simply perforated plate (SPP) and (b) mesh added perforated plate (MPP)	56

Figure III.2. 2. Comparison of viscosity of different water types	57
Figure III.3. 1. Filter bag (before test).....	60
Figure III.3. 2. Test section filter bag insertion.....	60
Figure III.3. 3. Filter bag in the low temperature horizontal test facility	61
Figure III.3. 4. Filter Bag in the high temperature horizontal test facility	61
Figure III.3. 5. Venting valve	62
Figure III.3. 6. Water tank isolation cap.....	64
Figure III.3. 7. Boric acid (left) and TSP (right) final quantities	65
Figure III.3. 8. Chemicals in the tank before mixing	66
Figure III.3. 9. Water jet and chemical dissolution	67
Figure III.3. 10. Chemicals dissolved in the water tank before test start	68
Figure III.4. 1. General procedures	74
Figure III.4. 2. 200 micro-liter of wet debris sample on the slide glass.....	75
Figure IV.1. 1. Fibrous bed thickness measurement for shredder method tests	80
Figure IV.1. 2. Fibrous bed on the strainer at steady state for different approaching velocities - (a) 0.52 cm/s, (b) 1.17 cm/s, and (c) 3.11 cm/s.....	81
Figure IV.1. 3. Fibrous bed growth on the strainer at different approach velocities - (a) 0.52 cm/s, (b) 1.17 cm/s, and (c) 3.11 cm/s	82
Figure IV.1. 4. Growth of fibrous bed at different approach velocities with 40g of NUKON prepared using shredder method.....	83
Figure IV.1. 5. Build-up of fibrous debris bed on the strainer, at $U = 0.52$ cm/s	84
Figure IV.1. 6. Build-up of fibrous debris bed on the strainer, at $U = 1.17$ cm/s	85
Figure IV.1. 7. Build-up of fibrous debris bed on the strainer, at $U = 3.11$ cm/s	86
Figure IV.1. 8. Build-up of fibrous debris bed on the MPP strainer, at $U = 0.31$ cm/s ...	87

Figure IV.1. 9. Build-up of fibrous debris bed on the MPP strainer, at $U = 1.17$ cm/s ...	88
Figure IV.1. 10. Build-up of fibrous debris bed on the MPP strainer, at $U = 3.11$ cm/s .	89
Figure IV.1. 11. Measurement of fibrous debris bed growth for each approaching velocity on the SPP strainer	90
Figure IV.1. 12. Measurement of fibrous debris bed growth for each approaching velocity on the MPP strainer	91
Figure IV.1. 13. Average bed thickness of the fibrous beds with NEI preparation	92
Figure IV.1. 14. Porosity change over the period of fibrous debris accumulation on the SPP strainer with shredder method.....	93
Figure IV.1. 15. Porosity vs. quantity of debris with NEI method	95
Figure IV.1. 16. Pressure drop vs. time with shredder method.....	96
Figure IV.1. 17. Pressure drop vs. averaged fibrous bed thickness at different approach velocities with shredder method	96
Figure IV.1. 18. Kozeny constant, k vs. Porosity, ε for NUKON samples prepared using shredder method in the horizontal test facility	98
Figure IV.1. 19. Head loss prediction and comparison with experimental data	102
Figure IV.1. 20. Pressure drop results at 1.17cm/s and 3.11 cm/s	103
Figure IV.1. 21. Pressure drop results at 0.31 cm/s and 0.52 cm/s	103
Figure IV.1. 22. Kozeny constant for NEI samples in the horizontal test facility	104
Figure IV.1. 23. Porosity vs. pressure drop of fibrous bed prepared using NEI method.....	108
Figure IV.1. 24. Pressure and porosity distribution in a fibrous bed	109
Figure IV.1. 25. Head loss vs. quantity of debris on the strainer with NEI preparation at different approach velocities	110
Figure IV.1. 26. Average bed thickness vs. quantity of debris using NEI preparation, (lines: model, dots: experiment).....	111

Figure IV.1. 27. Head loss vs. quantity of debris on the strainer with shredder preparation.....	112
Figure IV.1. 28. Average bed thickness vs. quantity of debris using shredder method .	113
Figure IV.1. 29. Build-up of debris bed on SPP strainer at approach velocity of 0.31 cm/s	115
Figure IV.1. 30. Build-up of debris bed on SPP strainer at approach velocity of 3.11 cm/s	116
Figure IV.1. 31. Build-up of debris bed on MPP strainer at approach velocity of 0.31 cm/s	117
Figure IV.1. 32. Graphical growth of debris bed on SPP strainer at approach velocity of 0.31 cm/s (PD-13)	118
Figure IV.1. 33. Graphical growth of debris bed on SPP strainer at approach velocity of 3.11 cm/s (PD-14)	119
Figure IV.1. 34. Graphical growth of debris bed on MPP strainer at approach velocity of 0.31 cm/s (PD-15)	120
Figure IV.1. 35. Average thickness of debris bed in the vertical test facility	121
Figure IV.1. 36. Head loss vs. time through fibrous beds in the vertical test loop	122
Figure IV.1. 37. Head loss vs. quantity of debris transported to the strainer in the vertical test loop	123
Figure IV.1. 38. Average thickness of debris bed vs. quantity of debris transported to the strainer in the vertical test loop	124
Figure IV.1. 39. Uncertainty in measurement of debris quantity on the strainer at different time	127
Figure IV.1. 40. Measurement of uncertainty in porosity of the fibrous beds at different time	128
Figure IV.1. 41. Measurement of the thickness of the fibrous bed	129
Figure IV.1. 42. Area weighted thickness measurement in the vertical test facility	130
Figure IV.1. 43. Comparison of 10 point method and image processing	131

Figure IV.1. 44. Head loss with random error (standard deviation)	134
Figure IV.2. 1. Bypass of the buffered borated water tests and the di water test.....	141
Figure IV.2. 2. pH effect on the weight of debris penetration	147
Figure IV.2. 3. pH vs. zeta potential of glass (a, b) and silica (c, d) materials	149
Figure IV.2. 4. EC effect on the weight of debris penetration	150
Figure IV.2. 5. Temperature history of high temperature test.....	153
Figure IV.2. 6. Effect of average temperature on weight of debris bypass for high temperature tests.....	154
Figure IV.2. 7. Quantity of debris bypass as a function of debris injection concentration in the horizontal test facility	158
Figure IV.2. 8. Quantity of debris bypass vs. time at different concentrations in the horizontal test facility.....	159
Figure IV.2. 9. Quantity of debris bypass as a function of debris injection concentration in the vertical test facility	160
Figure IV.2. 10. Quantity of debris bypass vs. time at different concentrations in the vertical test facility	161
Figure IV.2. 11. Quantity of debris bypass vs. approach velocity for different injection concentrations.....	163
Figure IV.2. 12. Flow fluctuations at (a) room temperature, (b) high temperature without external heaters, and (c) high temperature with external heaters.....	165
Figure IV.3. 1. Debris samples in containers - four sets of samples for STP (top) and three samples for Vogtle (bottom).....	167
Figure IV.3. 2. Samples in glass vials	168
Figure IV.3. 3. Maximum ferret length (caliper diameter)	169
Figure IV.3. 4. Picture of samples with 2x magnification	170
Figure IV.3. 5. Picture of samples with 20x magnification	171

Figure IV.3. 6. Volume % vs. debris size (feret length), x-axis linear scale.....	172
Figure IV.3. 7. Volume % vs. debris size (feret length), x-axis log scale.....	173
Figure IV.3. 8. Volume % CDF vs. debris size (feret length), x-axis linear scale.....	173
Figure IV.3. 9. Volume % CDF vs. debris size (feret length), x-axis log scale.....	174
Figure IV.3.10. Count vs. debris size (feret length), x-axis linear scale.....	174
Figure IV.3.11. Count vs. Debris size (feret length), x-axis log scale.....	175
Figure IV.3.12. Count CDF vs. debris size (feret length), x-axis linear scale.....	175
Figure IV.3.13. Count CDF vs. debris size (feret length), x-axis log scale.....	176

LIST OF TABLES

	Page
Table I. 1. Fibrous debris classification by shape [11].....	13
Table II.2. 1. Buffered/borated water tests results	22
Table II.2. 2. Main components of the control panel	28
Table II.4. 1. High speed camera specification	36
Table II.4. 2. Microscopic objectives specifications	36
Table II.4. 3. Mechanical system	37
Table II.4. 4. Particle size distribution results (NIST 8631a).....	39
Table II.4. 5. Size information of mono-sized particles.....	40
Table III.2. 1. Parameters in a 4 loop Westinghouse PWR.....	55
Table III.2. 2. Experimental conditions.....	55
Table IV.1. 1. List of head loss tests with different conditions.....	78
Table IV.1. 2. Kozeny constant and permeability of fibrous porous media	100
Table IV.1. 3. Comparison of head loss data	106
Table IV.1. 4. Uncertainty of measurement of vertically deposited debris bed thickness	131
Table IV.1. 5. Comparison of thickness measurement methods: 10 points method and image processing	132
Table IV.1. 6. List of random error test cases	134
Table IV.1. 7. Head loss and random error at steady state.....	135
Table IV.2. 1. DI water test results	137
Table IV.2. 2. TAMU tap water test results	137

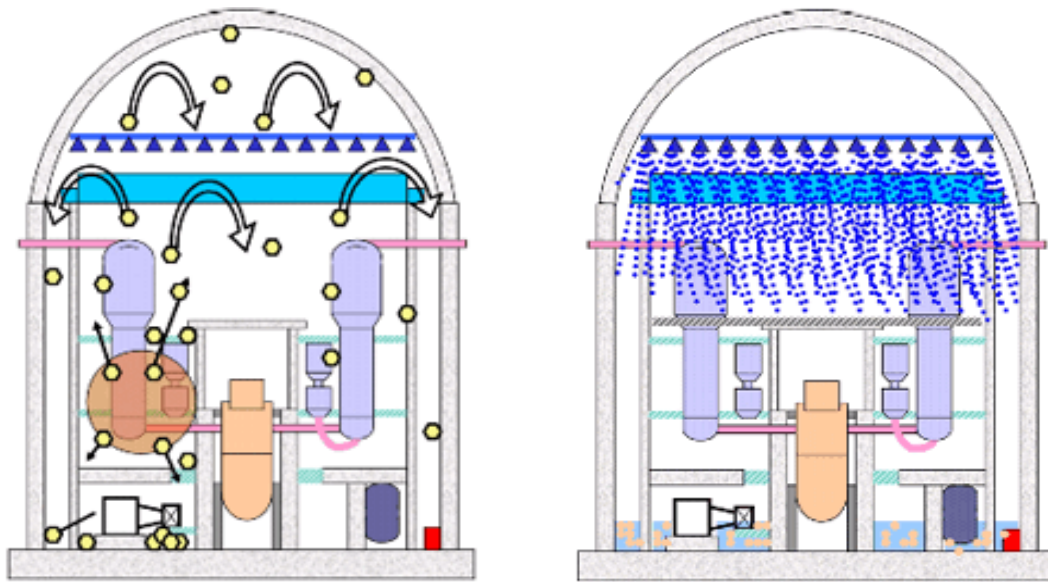
Table IV.2. 3. 1x buffered borated water test results	138
Table IV.2. 4. 2x buffered borated water test results	138
Table IV.2. 5. Additional water type test results.....	139
Table IV.2. 6. Summary of debris bypass quantity in different water types.....	140
Table IV.2. 7. Summary of debris bypass quantity in different water types.....	145
Table IV.2. 8. Summary of statistical analyses	145
Table IV.2. 9. Water chemistry conditions	146
Table IV.2. 10. High temperature TAMU tap water test results.....	152
Table IV.2. 11. Debris bypass in the horizontal loop* experiments.....	157
Table IV.2. 12. Debris bypass in the vertical loop* experiments	157
Table IV.2. 13. Summary of fluid approach velocity effect tests	162
Table IV.2. 14. Quantity of debris bypass at different flow fluctuations.....	164

CHAPTER I

INTRODUCTION AND LITERATURE REVIEW

Fibrous porous media has been found in a variety of industrial applications including thermal insulation [1, 2], filtration [3-5], textile manufacturing [6, 7], and paper production [8, 9]. However, because of complexity of the media and diversity of systems, a generalized model of liquid or gas flow through fibrous porous media has not been developed. Many researchers developed their own permeability model or modified others' for different fibrous materials with different fluids either theoretically or empirically [10]. In nuclear power plants, fibrous media have been used to insulate the reactor vessel and the pipe lines in order to prevent heat loss from the system and protect the containment structures and other components from thermal effects. Though a fibrous medium provides efficient thermal insulation, it has been focused on as a source of the Generic Safety Issue 191 (GSI-191) "Assessment of Debris Accumulation on PWR Sump Performance" in NUREG-0933 [11]. Every nuclear power plant is required by regulation (10 CFR 50.46) to have an Emergency Core Cooling System (ECCS) to mitigate a design basis accident (DBA) that a nuclear facility must be designed and built to withstand without loss to the systems, structures, and components necessary to ensure public health and safety. The ECCS can be affected by fibrous debris generated during a Loss-of-Coolant Accident (LOCA) which is the DBA of Light Water Reactors (LWRs) by the high energy jet impingement from the break on surrounding surfaces and materials. The fibrous debris, then, may be transported through the reactor containment

and reach the sump strainers, which are components of the ECCS. The containment sump collects reactor coolant leaked from breaks and chemically reactive solutions from sprays following a LOCA (see Figure I.1); it then serves as the water source to support long-term recirculation.



(a) Coolant leaked from a break

(b) Chemical solutions from sprays

Figure I. 1. The sources of coolant and chemical solutions (a) break, (b) sprays
(<http://www.nrc.gov/reactors/operating/ops-experience/pwr-sump-performance/safety-concern.html>)

Since the debris collected in the containment sump can block or damage the ECCS pumps and pipe lines, the containment sump is surrounded by strainers to prevent debris from entering the pump suction lines as shown in Figure I.2.



Figure I. 2. Containment sump strainers

(<http://www.nrc.gov/reactors/operating/ops-experience/pwr-sump-performance/function-containment-sump.html>)

There were many efforts to resolve this safety issue including Ziegler et al. [12] for Boiling Water Reactors (BWRs) and by Rao et al. [13] for Pressurized Water Reactors (PWRs). In 2004 Generic Letter (GL) 2004-02 [14] requested to perform a mechanistic evaluation of the recirculation functions and, as appropriate, take additional actions to ensure system functionality. GL 2004-02 categorized the safety issue into the upstream effect and the downstream effect (also known as the in-vessel effect). The upstream effect is caused by accumulation of debris on the surface of strainers, which may result in a loss of Net Positive Suction Head (NPSH). For the downstream effect, the quantity of debris bypass through the strainer, which may negatively affect the capability of core cooling by clogging inside the reactor core or the components in the flow path, still remains as an unclosed issue.

The safety issue related to fibrous porous media in a nuclear reactor is a complex topic. The characteristics of debris may be different according to the location where the debris is found. On the surface of the sump strainer, the debris may be found as a filter

bed which is composed of fibrous porous media. Upstream and downstream of the strainer, the debris will be found as dilute suspensions of fibers.

The behavior of debris or the phenomena in different locations may be different. Until the debris reaches the strainer, it may behave like solid-liquid two-phase flow. Once it reaches the strainer, it may generate a fibrous porous medium resulting in pressure drop. To develop a head loss model of fibrous porous media generated on the sump strainer, pressure drop through the media will be measured varying liquid velocity. Additionally, in order to obtain the permeability as a function of porosity, buildup of fibrous porous media and the porosity at each thickness will be measured. Then, the measured values will be correlated to the pressure drop. When the focus is moved downstream of the strainer, bypass of debris will be encountered. Then, concentration of debris, water type and temperature, and liquid approach velocity may affect head loss and filtration by altering viscosity and water chemistry. To investigate these complex phenomena, the present research defined three research objectives:

- Head loss through fibrous porous media,
- Debris bypass through fibrous porous media, and
- Size characterization of irregular shaped fibrous debris

For each topic, an experimental facility was constructed and several conditions were examined to understand the phenomena as a function of different parameters. The results may also establish a basis to continue studying on the fibrous porous media not only for nuclear engineering but also for general engineering applications.

The fibrous debris bed is a fibrous porous medium. The models of fluid flow resistance through porous media have been developed based on Darcy's law, as shown in Equation (I.1).

$$\frac{\Delta P}{\Delta L} = -\frac{\mu U}{K} \quad (\text{I.1})$$

where P is the pressure (Pa) through a porous medium, L is the thickness (m) of the porous medium, μ is viscosity of the fluid (Pa·s), U is the approach velocity (m/s) of the fluid, and K is Darcy permeability (m²). This relationship only holds for very low liquid flow rates at which the viscous force dominates. Musket [15] proposed a model of head loss composed of a viscous term (first order of velocity) and an inertial term (second order of velocity), as shown in Equation (I.2) with coefficients a and b as functions of porosity of a porous medium, ε .

$$\frac{\Delta P}{\Delta L} = a(\varepsilon)\mu U + b(\varepsilon)\rho U^2 \quad (\text{I.2})$$

Blake [16] suggested the modified Reynolds number, Re_m , defined in Equation (I.3) using particle diameter (m), D , porosity, liquid density (kg/m³), ρ , to treat the pressure drop in a packed system by an approach analogous to pressure drop in a circular pipe.

$$Re_m = \frac{\rho UD}{\mu(1-\varepsilon)} \quad (I.3)$$

Kaviany [17] categorized the permeability models into capillary models, drag models, and hydraulic radius models. The hydraulic radius models were mainly focused on the present experimental study. Fluid flow in porous media can be categorized with Re_m as Ergun [18] showed. When $Re_m < 10$, a viscous flow regime, Kozeny-Carman equation, Equation (I.4), showed good agreement with experimental data of packed beds where porosity is smaller than 0.5.

$$\frac{\Delta P}{\Delta L} = -k S_v^2 \frac{(1-\varepsilon)^2}{\varepsilon^3} \mu U \quad (I.4)$$

where k is Kozeny constant and S_v is specific surface area (m^2/m^3). Equation (I.4) can be rearranged as shown in Equation (I.5) to calculate the Kozeny constant from experimental data. Carman [19] suggested k for uniform spheres to be 4.8 and the most probable range of variation to be 4.5~5.1.

$$k = \frac{\varepsilon^3}{U \mu S_v^2 (1-\varepsilon)^2} \frac{\Delta P}{\Delta L} \quad (I.5)$$

Despite good predictions of Equation (I.5) for packed beds, Davies [20] found that the Kozeny constant for packed bed was not applicable for fibrous beds at high porosity. He proposed k as a function of porosity shown in Equation (I.6) based on a number of experimental data of filter pads used for air filtration (for $Re_m < 1$).

$$k = a \frac{\varepsilon^3}{(1-\varepsilon)^{0.5}} \left[1 + b(1-\varepsilon)^3 \right] \quad (I.6)$$

Davies suggested the coefficients $a = 4.0$ and $b = 56$. Later, Ingmanson et al. [21] conducted head loss experiments using air through a fiberglass bed and modified Davies' model to have coefficients $a = 3.5$ and $b = 57$. Zigler et al. [12] developed the NUREG/CR-6224 model, Equation (I.7), based on Ingmanson et al.'s model.

$$\frac{\Delta P}{\Delta L_0} = \left[3.5 S_v^2 (1-\varepsilon_m)^{1.5} [1 + 57(1-\varepsilon_m)^3] \mu U + 0.66 S_v \frac{(1-\varepsilon_m)}{\varepsilon_m^3} \rho_w U^2 \right] \left(\frac{\Delta L_m}{\Delta L_0} \right) \quad (I.7)$$

where P is pressure, L_m and L_0 are the actual bed thickness (m) and the fiber bed theoretical thickness (m), respectively, U is approach velocity (m/s), S_v is specific surface area (m^2/m^3), ε_m is mixed bed porosity, ρ_w is water density (kg/m^3), and μ is viscosity (Pa·s) of water. Since the viscous term of this model was developed for air flow through fibrous beds with porosity smaller than 0.98 and with relatively large diameter fibers compared to NUKON™ diameter, it is required to validate whether the

model is applicable for the conditions after the replacement of the sump strainer in PWRs. Lord [7] proposed a head loss model, Equation (I.8), for air flow through plugs of textile fibers such as Viscose rayon, Cuprammonium rayon, wool, and silk, the diameters of which are similar to NUKON™, in a different way from Davies.

$$k = \frac{1}{0.903} \frac{(1-\varepsilon)^{\alpha-2}}{\varepsilon^2} \quad (\text{I.8})$$

where α is a material dependent constant.

Drag models proposed by Happel[22], Equation (I.9), and Kuwabara [23], Equation (I.10), also have been applied to fibrous bed. They solved Navier-Stokes equation for flow normal to an array of cylinders using the circular unit cell with an assumption: zero shear stress and zero vorticity, respectively, at the perimeter of the cylinder.

$$k = \frac{\varepsilon^3}{(1-\varepsilon) \left[-\frac{1}{2} \ln(1-\varepsilon) - \frac{1}{2} \frac{1-(1-\varepsilon)^2}{1+(1-\varepsilon)^2} \right]} \quad (\text{I.9})$$

$$k = \frac{\varepsilon^3}{(1-\varepsilon) \left[-\frac{1}{2} \ln(1-\varepsilon) - 0.75 + 2(1-\varepsilon) + \frac{(1-\varepsilon)^2}{4} \right]} \quad (\text{I.10})$$

Happel [22] also calculated the Kozeny constant for flow parallel to an array of cylinders as shown in Equation (I.11).

$$k = \frac{2\varepsilon^3}{(1-\varepsilon)\left[-2\ln(1-\varepsilon)-3+4(1-\varepsilon)-(1-\varepsilon)^2\right]} \quad (\text{I.11})$$

Jackson and James [10] proposed a revised prediction of the Kozeny constant based on Drummond and Tahir's [24] equation as shown in Equation (I.12) to include three dimensional effect of fiber deposition.

$$k = \frac{5\varepsilon^3}{3(1-\varepsilon)\left[-\ln(1-\varepsilon)-0.931+\ln(1-\varepsilon)^{-1}\right]} \quad (\text{I.12})$$

Later, the authors of NUREG/CR-1862 [25] recommended a head loss model using Happel's theoretical model for the viscous term and Wu et al.'s [26] model for the inertial term. In their work, the model was expressed in terms of void ratio, and it was rearranged with porosity here as shown in Eq. (I.13).

$$\frac{\Delta P}{\Delta L} = \frac{2\varepsilon^3}{(1-\varepsilon)\left[-\ln(1-\varepsilon)-\frac{1-(1-\varepsilon)^2}{1+(1-\varepsilon)^2}\right]} S_v^2 \mu U + 1.95 \left(\frac{(1-\varepsilon)\mu S_v}{6\rho_w U} \right)^{0.071} \frac{S_v}{6} \frac{(1-\varepsilon)}{\varepsilon^3} \rho_w U^2 \quad (\text{I.13})$$

A fibrous porous medium is usually highly compressible, thus, compression models were suggested in several works including Ingmanson et al. (Equation (I.14)) [21], Jonsson and Jonsson (Equation (I.15)) [27], Meyer (Equation (I.16)) [28], and Grahn et al. (Equation (I.17)) [29].

$$c = Mp_k^N \quad (\text{I.14})$$

where c is the packing ratio, M and N are empirical constants, and p_k is the total pressure (Pa) on the bed.

$$\beta_v = Np_k^{-b} \quad (\text{I.15})$$

where β_v is the compressibility of the void volume, N and b are constants, and p_k .

$$\varepsilon = 1 - Mp_k^N \quad (\text{I.16})$$

$$\varepsilon = \varepsilon_\infty + (\varepsilon_0 - \varepsilon_\infty)e^{-M_c p_k^{N_c}} \quad (\text{I.17})$$

where $\varepsilon_0 = 0.9833$, $\varepsilon_\infty = 0.9147$, $M_c = 0.00712467 \text{ Pa}^{-0.5197}$, and $N_c = 0.5197$. Grahn et al.'s model was developed using mechanical compression which applied uniform

pressure through a bed. Nevertheless, in the present study the compression models will be reviewed based on pressure drop generated by liquid flow which applies cumulative pressure through a bed.

Debris transport through a fibrous bed may be understood as particle filtration through a nonwoven filter. Hutten [30] summarized four filtration mechanisms described by Purchas and Sutherland [31] such as surface straining, depth straining, depth filtration, and cake filtration. In surface straining, the particle is larger than the pores and simply cannot pass through. The sump strainer behaves in this mechanism at the beginning of the debris bed build-up. In depth straining, the filter thickness is relatively greater than pore diameters. The particles penetrate the filter medium through the channel made of pores with variable diameters until reaching a necking point where particles are trapped. Depth filtration removes a particle from a fluid even though the particle is smaller than the size of the pore in the filter medium. This mechanism will be discussed in detail since the effect of water chemistry on the transport of small debris in the present experiment is expected to be mainly influenced by this. Cake filtration is another important liquid filtration mechanism in which the capture of solid particles on the surface of a filter medium results in the build-up of particulate matter into a layer of filter cake. In the containment sump, once the strainer is covered by fibrous debris via surface straining, a large fraction of fibrous debris becomes the filter medium as a cake filter. Initially, debris with a size of millimeters can bypass the perforated plate which is the strainer. Once the debris starts generating a fibrous cake on the strainer, the cake filtration removes large fraction of debris from the water. Although the cake filtration

removes the largest fraction of debris, since most of the debris penetrating the filter medium is the debris smaller than millimeters, the depth filtration would be the main mechanism in the transport of debris through the fibrous bed and the strainer.

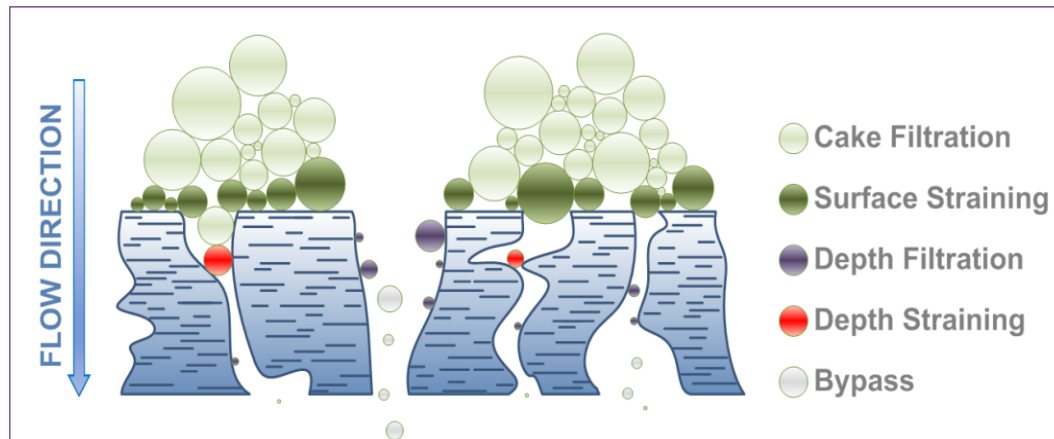









Figure I. 3. Mechanisms of filtration

As mentioned, the depth filtration may be strongly affected by water chemistry. Therefore, sensitivity studies of different chemical solutions and water chemistry including pH and electrical capacitance on debris bypass are required. Additional thermal-hydraulic effects such as liquid approach velocity and temperature should be investigated.

The fibrous debris generated from fiberglass insulation materials shall have irregular shapes and the size distribution shall have a large span as reported by Zigler et al. [12] in Table I.1.

Table I. 1. Fibrous debris classification by shape [11]

Class	Description
1 	Very small pieces of “microscopic” fines which appear to be cylinders
2 	Single strand of fiberglass, essentially acts as a suspended strand
3 	Multiple attached or interwoven strands that exhibit considerable flexibility
4 	Fiber clusters with more rigidity reacting to drag forces more as a semi-rigid body
5 	Clumps of fibrous debris which were noted to sink.
6 	Larger clumps of fibers. Forms an intermediate between Classes 5 and 7
7 	Precut pieces to simulate small debris using manual/mechanical methods

Krepper et al. [32, 33] reported a size range of a metal wool, named MD. However, the size smaller than 5mm was not investigated, which are most important size range in debris penetration through the strainer. There are several particle size measurement techniques as summarized by Markus [34] and Allen [35]. Markus categorized the size of particulate material as following.

Nano: $\leq 100 \text{ nm}$ / Ultrafine: $100 \text{ nm} \sim 1 \text{ }\mu\text{m}$ / Fine: $1 \text{ }\mu\text{m} \sim 10 \text{ }\mu\text{m}$
 Medium: $10 \text{ }\mu\text{m} \sim 1 \text{ mm}$ / Coarse: $1 \text{ mm} \sim 10 \text{ mm}$

There will be all categories of debris upstream of the strainer. The strainer will filter most of coarse debris with the surface straining in the initial phase of debris transport and the cake filtration after building up enough thickness of the debris bed. These mechanisms shift the size distribution of debris downstream of the strainer to the smaller sizes from the original distribution. If the change of size distribution is compared against size bins and time, the filtration efficiency for each size category can be studied in detail. There are several techniques to measure regular shape particles. However, the main concern in this study is irregular shaped debris ranging between the categories of fine and medium. Optical methods of size characterization are heavily relied upon for particles of irregular shape. Optical microscopy is often used for particle sizes ranging from 3 μm to 150 μm . Any particles that are larger than this can be sized using a magnifying glass. Therefore, this study developed an optical size measurement system utilizing multistage magnifications and an image processing code to analyze statistically meaningful number of debris.

CHAPTER II

EXPERIMENTAL FACILITIES*

In order to investigate head loss and debris bypass through NUKON fibrous beds and debris size distribution, three experimental facilities including two horizontal head loss and debris bypass test facilities and a debris size characterization system were constructed. Both the horizontal and vertical head loss and debris bypass test facilities were designed to develop a reliable head loss model of fibrous porous media generated on the sump strainer and a debris bypass model as a function of quantity of debris injected and time. The facilities required capabilities of varying liquid velocity, measuring buildup of fibrous beds, integral and dynamic debris sampling, and logging pressure drop during each experiment. For the debris size characterization system, it was required to develop a methodology for measuring irregularly shaped fibrous debris and perform experiments to obtain debris samples upstream and downstream of a fibrous porous medium as a filter. A measurement technique was developed for a use of visual inspection to obtain the statistically meaningful numbers of size measurements for the shape characterization and the size distribution. Also, a nano-particle sizer using Brownian motion, a scanning electron microscope (SEM) for 10 nm to 100 μ m, and an electrical sensing zone method with a Coulter-counter for 1 to 1000 μ m can be utilized.

*Parts of this chapter are reprinted with permission from “Experimental study of head loss through an LOCA-generated fibrous debris bed deposited on a sump strainer for Generic Safety Issue 191” by Saya Lee et al., 2014, Progress in Nuclear Energy, 74, 166-175, Copyright [2014] by ELSEVIER.

II.1. Low temperature horizontal head Loss and debris bypass test facility

The design of the experimental facility and its overview with all instrumentations are presented in Figure II.1.1 and Figure II.1.2, respectively. The experimental facility consists of a transparent water tank (60.96 cm × 60.96 cm × 76.20 cm, width × length × height, respectively), a vertically installed strainer (a perforated stainless-steel plate with 10.16 cm (4 inch) inner diameter) in the transparent test section, centrifugal pumps, and a mixing propeller.

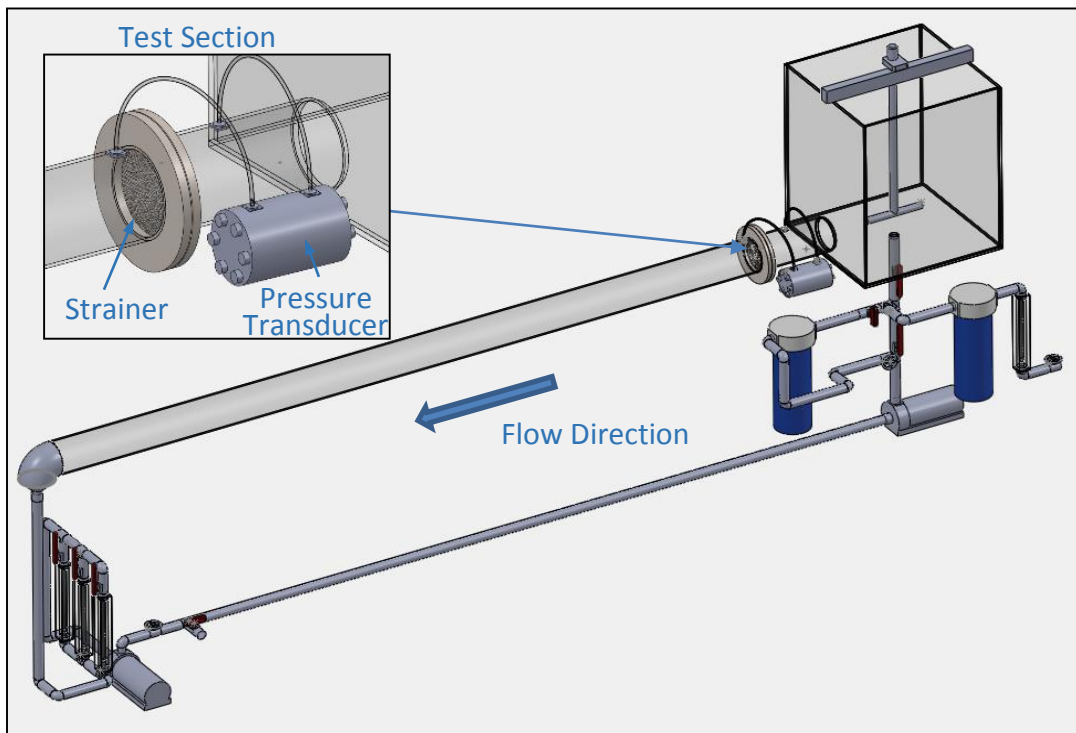


Figure II.1. 1. 3-D design of the low temperature horizontal head loss and debris bypass test facility

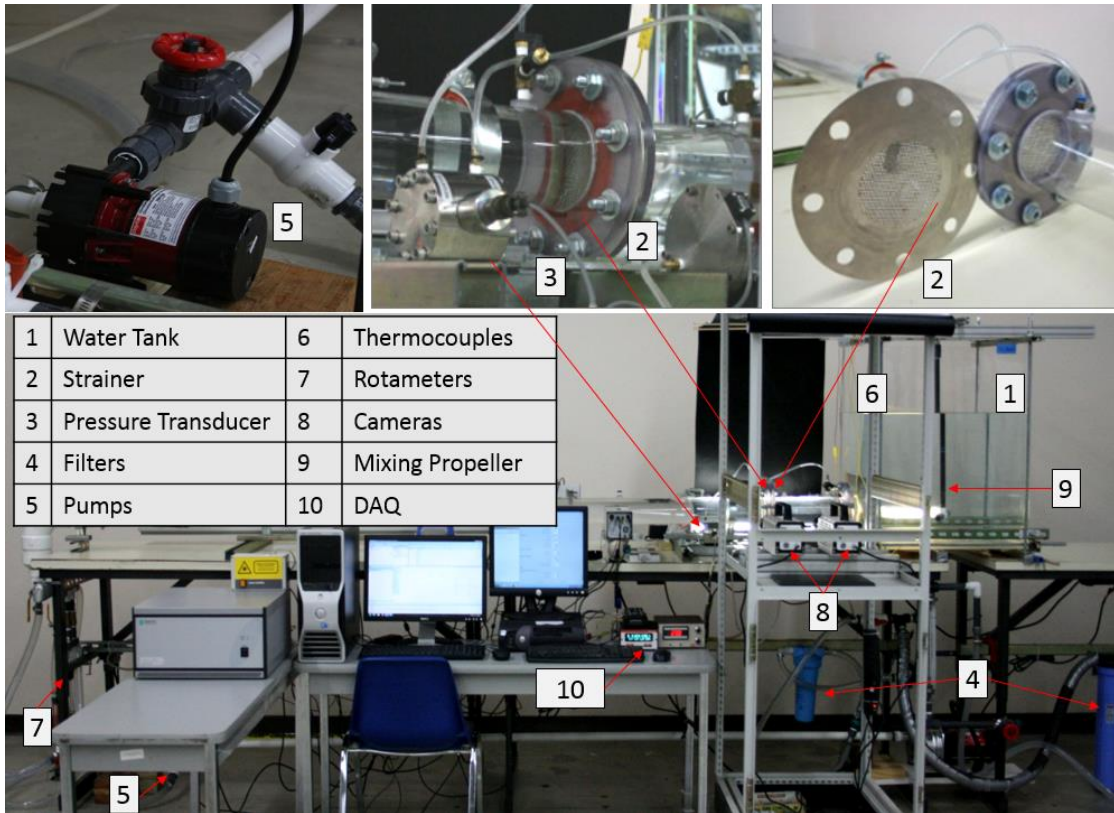


Figure II.1. 2. Low temperature horizontal experimental facility & instruments

To measure head loss through fibrous beds, a differential pressure transducer (Honeywell[®] differential pressure transducer, range: 1psid, accuracy: 0.1% full-scale) was installed. A camera recorded the growth of the debris bed for each test. Temperature was measured using a K-type thermocouple ($\pm 1^{\circ}\text{C}$) in the water tank. Three rotameters (227 liter/h (60 GPH) with 3% full-scale accuracy, 19 liter/h (5 GPM), and 38 liter/h (10 GPM) with 5% full-scale accuracy) were used to control the flow rate with a multi-rotatable valve.

The water tank is made of acrylic panels of 1.27 cm (0.5 inch) thickness to allow visualization of the debris as shown in Figure II.1.3. To keep a uniform concentration of the debris in the tank, a rotating propeller mixes the debris. The water exits the tank through the holes (10.16 cm (4 inch) inner diameter) located on the side of the tank where the horizontal test section is attached.

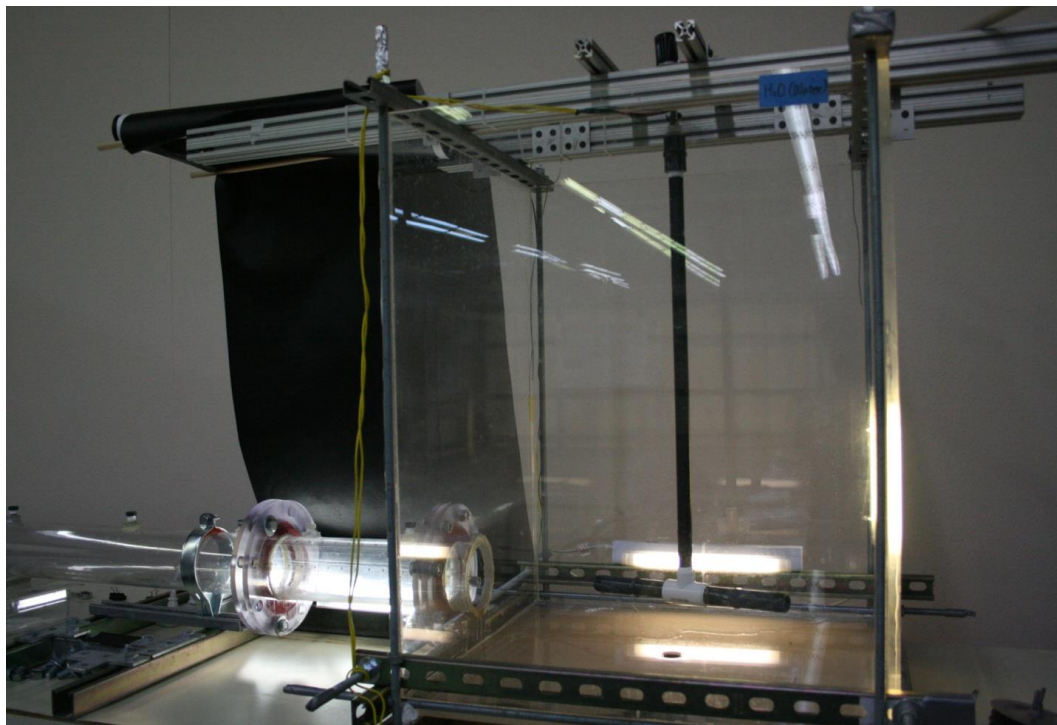


Figure II.1. 3. Water tank of the low temperature horizontal facility

A 10.16 cm (4 inch) ID and 11.43 cm (4.25 inch) OD polycarbonate pipe makes the test section. This section is subdivided in different parts connected with flanges. A perforated stainless steel plate was manufactured to simulate sump strainers following the given specifications of:

- Hole Diameter
- Hole x and y pitch
- Plate Thickness and Material

The plate has a perforated section of 10.16 cm (4 inch) in diameter which fits the flow section of the polycarbonate pipe. Eight holes were machined at the edge of the plate to allow its connection between the flanges. A detailed view of the perforated plate and its installation are presented in Figure II.1.4.

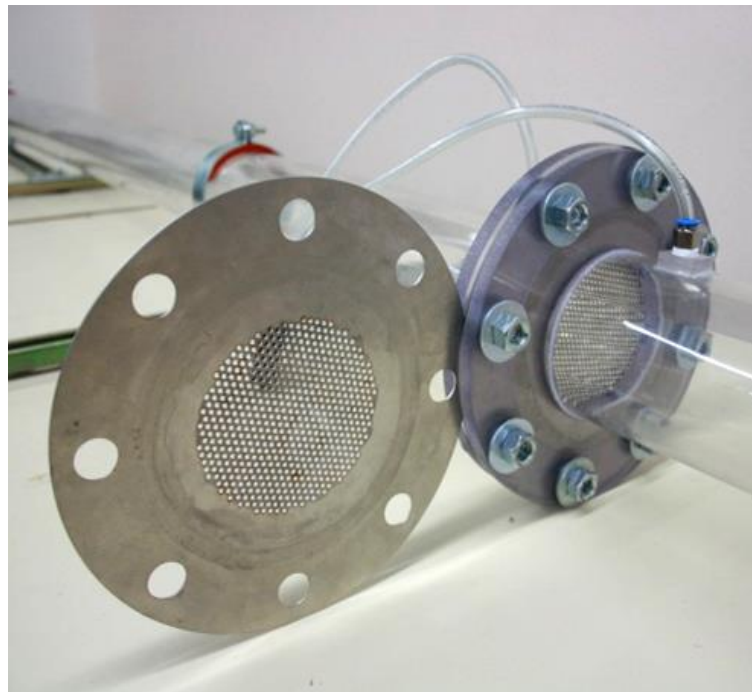


Figure II.1. 4. Strainer Plate (left) and its installation between two flanges (right)

A centrifugal pump (5, in Figure II.1.1) provides the required volumetric flow rate in the test section to reach the desired approaching velocity. A rotameter is installed upstream of the mentioned pump to read the volumetric flow rate. The flow rate is set up by changing the opening position of a PVC gate valve. Figure II.1.5 shows the centrifugal pump and the mentioned devices used to setup the desired approaching velocity.

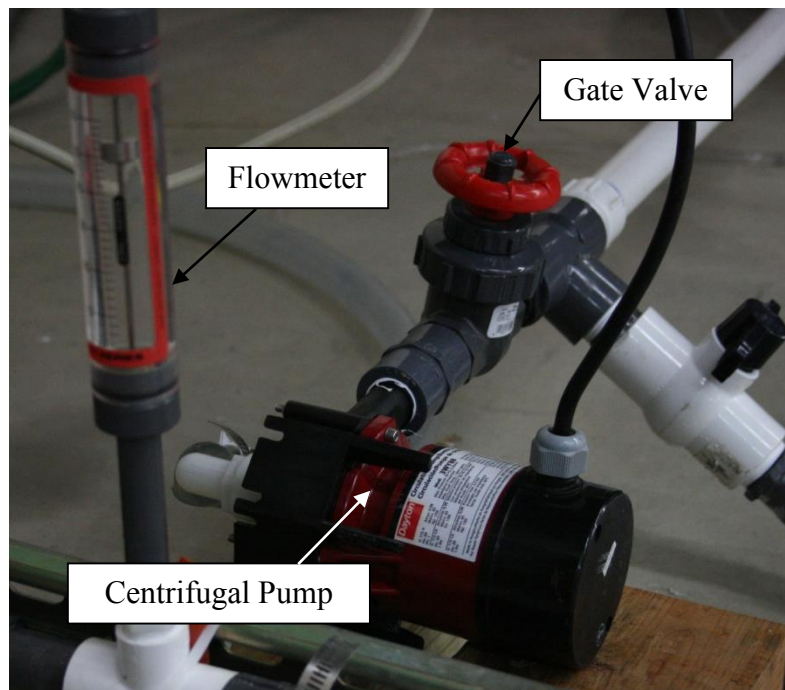


Figure II.1. 5. Centrifugal pump and flow control

An additional pump was installed and is in use only during the cleaning operations between tests; it allows recirculation of the water within a battery of filters with high volumetric flow rates. There are other PVC valves that facilitate the drainage and filling operations. All of the components installed in the facility, including the pumps and valves, are made with plastic materials or stainless steel to avoid any reaction with the buffered and borated water used during the tests. The total volume of the facility, including tank, pipelines and other components is 315 liter (83.3 gallons). The volume of the water used for each test (corresponding to a final liquid level in the tank of 50.8 cm (20 inch)) was 221 liter (58.4 gallons). The amount of water in the water tank and in the test section was 189 liter (49.9 gallons). The buffered and borated water used in the tests, which will be described in details in the next chapter, was produced with a Reversed Osmosis / De-Ionized (RO/DI) water purifying system (Vertex ® Deluxe PuraTek) which provided treated water at 379 liter/day (100 gallons/day).

II.2. High temperature horizontal head loss and debris bypass test facility

Figure II.2.1 shows an overview of the high temperature horizontal (up to 99°C) experimental facility. The components in Figure II.2.1 are defined in Table II.2.1.

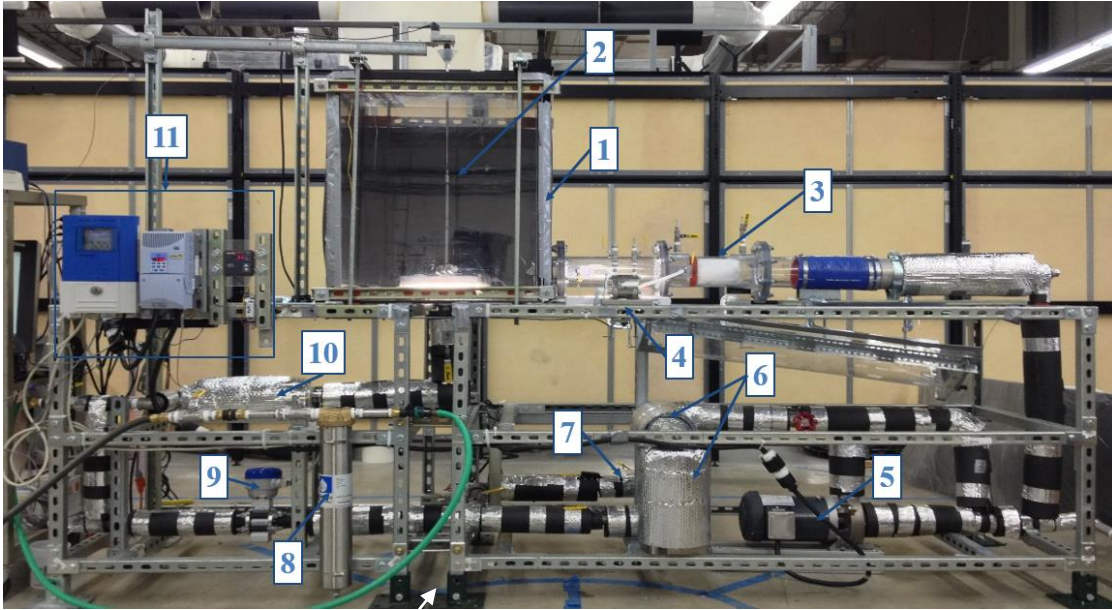


Figure II.2. 1. Experimental Facility Overview

Table II.2. 1. Buffered/borated water tests results

#	Component	#	Component
1	Polycarbonate Water Tank	6	External Flexible Heaters (1kw)
2	Mixing Propeller	7	Submerged Main Heaters (7kw)
3	Test Section	8	1µm Tap Water Filter
4	Pressure Transducer	9	Magnetic Flow Meter
5	High Temperature Chemical Resistant Pump	10	Temperature Controlling External Heater
		11	Control Panel

The Water Tank is made of polycarbonate panels (60.96 cm × 60.96 cm × 76.20 cm, width × length × height, respectively) which can be heated up to 120°C. The tank is equipped with an insulated removable lid on the top used during the experiments to minimize the heat losses.

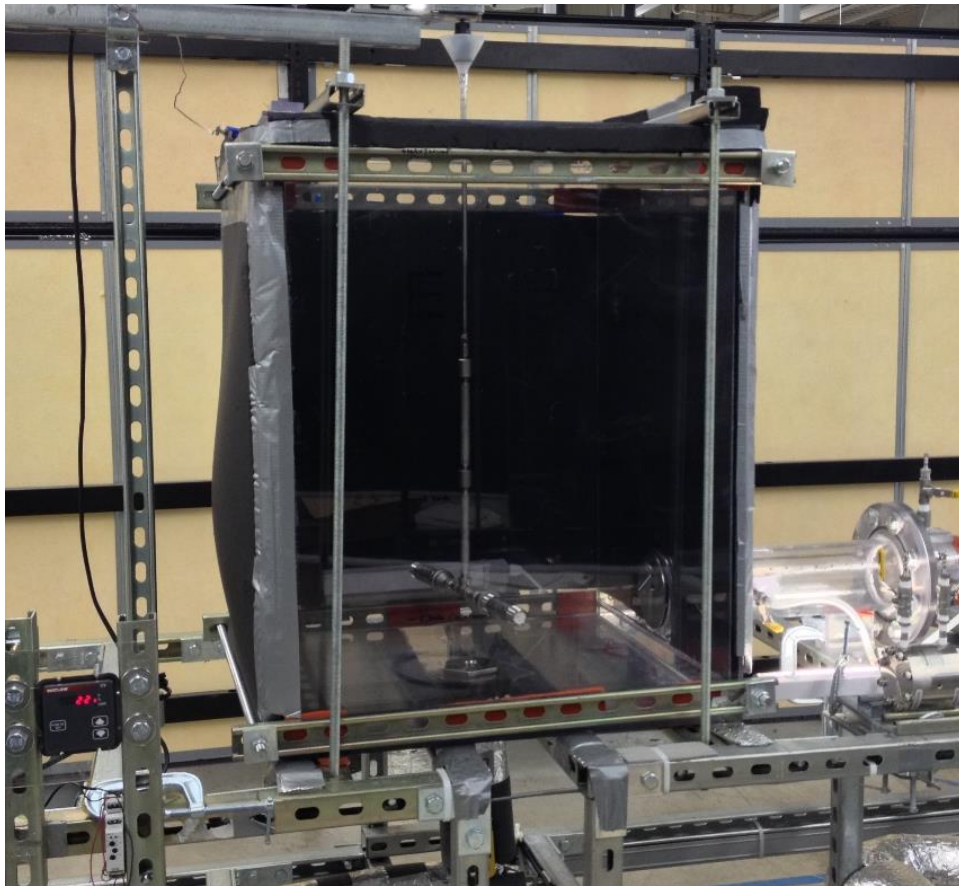


Figure II.2. 2. Polycarbonate water tank

The mixing propeller is made of stainless steel (SS-304) pipes with of $\frac{1}{2}$ inch NPT for the body and $\frac{3}{4}$ inch NPT for the arms, forming a T-shape mixer as shown in Figure II.2.3. The mixing propeller was controlled by time-adjustable relays (shown in section II.2.9) that switched the direction of rotation every 1 minute.

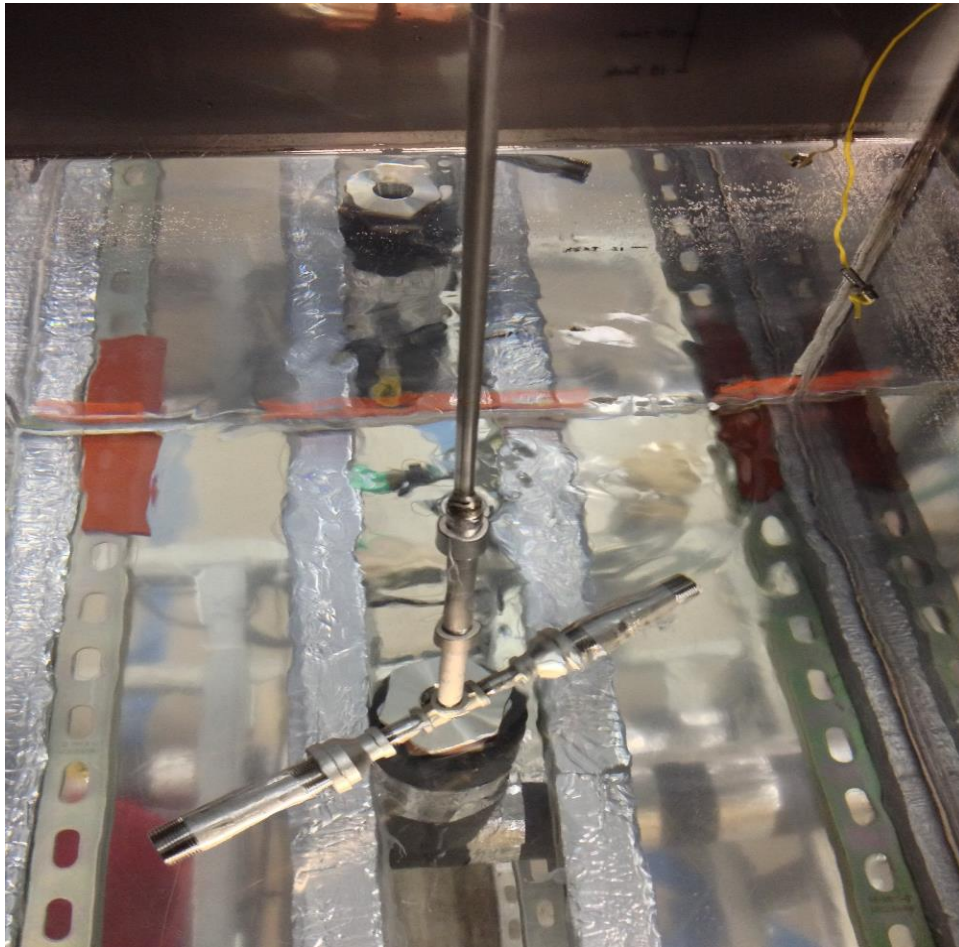


Figure II.2. 3. T-Shape mixing propeller

The test section is made of polycarbonate tube (10.16 cm ID, 11.43 cm OD). This section is subdivided into two parts connected with flanges as shown in Figure II.2.4. The test section has two flanges to install the strainer which follows the same design of the low temperature horizontal facility in the previous section.

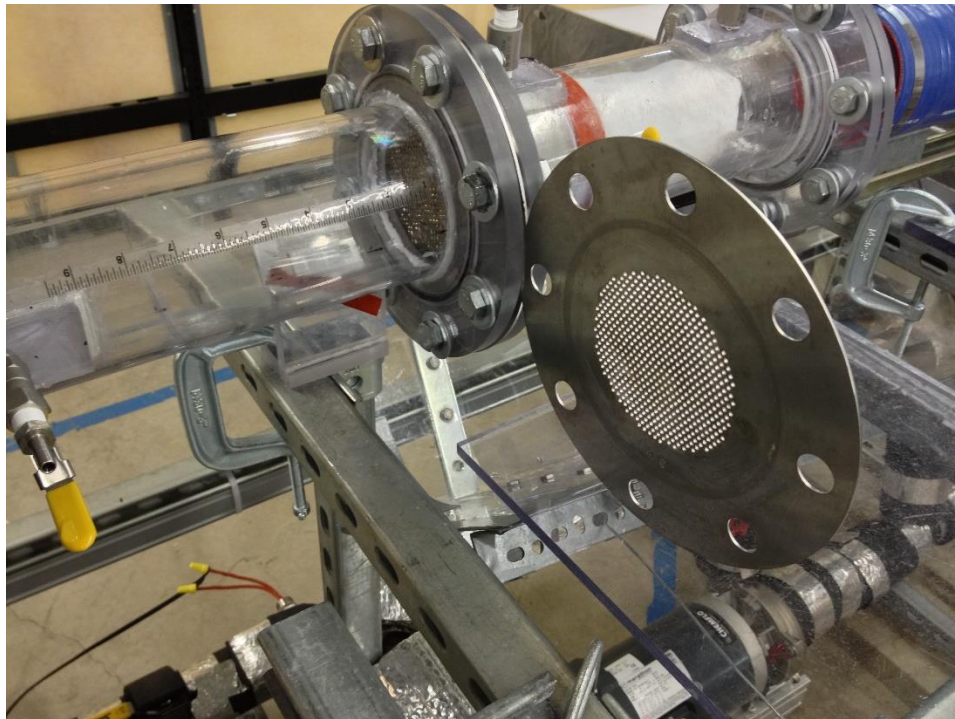


Figure II.2. 4. Strainer plate (right) and its location in the test section (left)

A stainless-steel centrifugal pump (Figure II.2.5) provides the required volumetric flow rate in the test section to reach the desired approaching velocity at high temperature.



Figure II.2. 5. High temperature chemical resistant pump

An Optiflux-1300 magnetic flow meter (Krohne®) was installed downstream of the pump to read the volumetric flow rate (Figure II.2.6). The accuracy at the target flow velocity (0.3 cm/s) is 1.7% of the reading.



Figure II.2. 6. Magnetic flow meter

Immersed heaters (total power = 7kW) are installed downstream of the pump, inside a circulating loop (Figure II.2.7). Before starting the experiment, the water was forced to circulate through the heating loop until the desired temperature was achieved. During the experiment, the heating loop was isolated by valves.

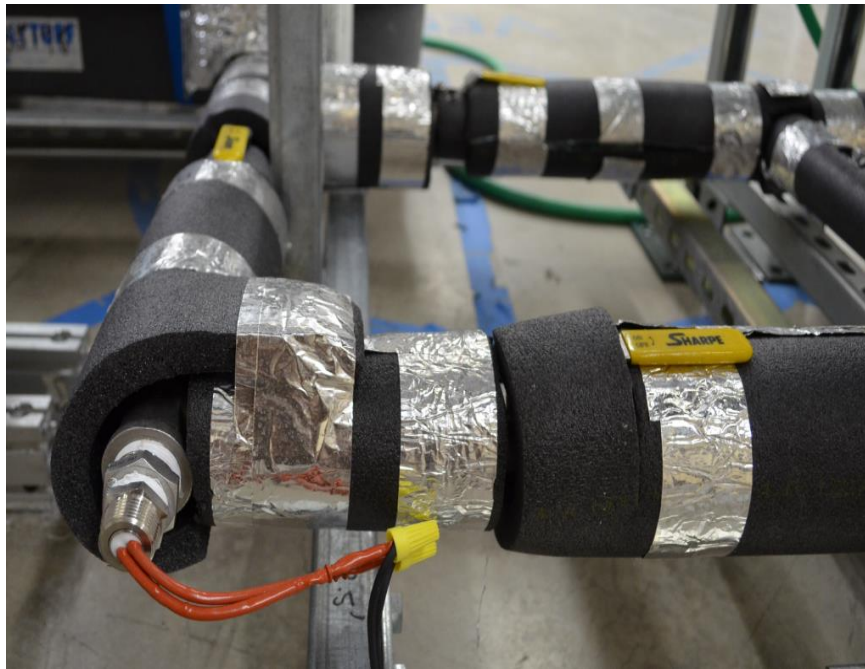


Figure II.2. 7. Heating loop (7kW)

The control panel is the operator interface. Figure II.2.8 shows the main components included in the control panel, and the components are listed in Table II.2.2.

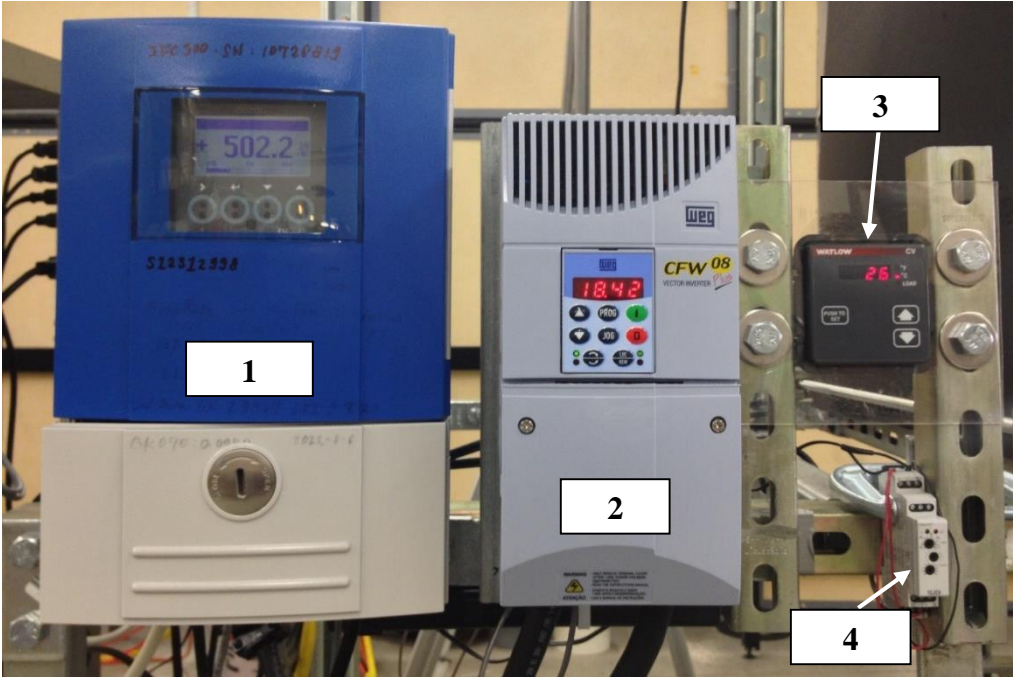


Figure II.2. 8. Control panel interface

Table II.2. 2. Main components of the control panel

#	Component	#	Component
1	Signal converter for the flowmeter	3	Temperature controller
2	Frequency inverter	4	Time delay relay

II.3. Vertical head loss and debris bypass test facility

The design concept of the vertical head loss and debris bypass test facility and its overview are shown in Figure II.3.1.

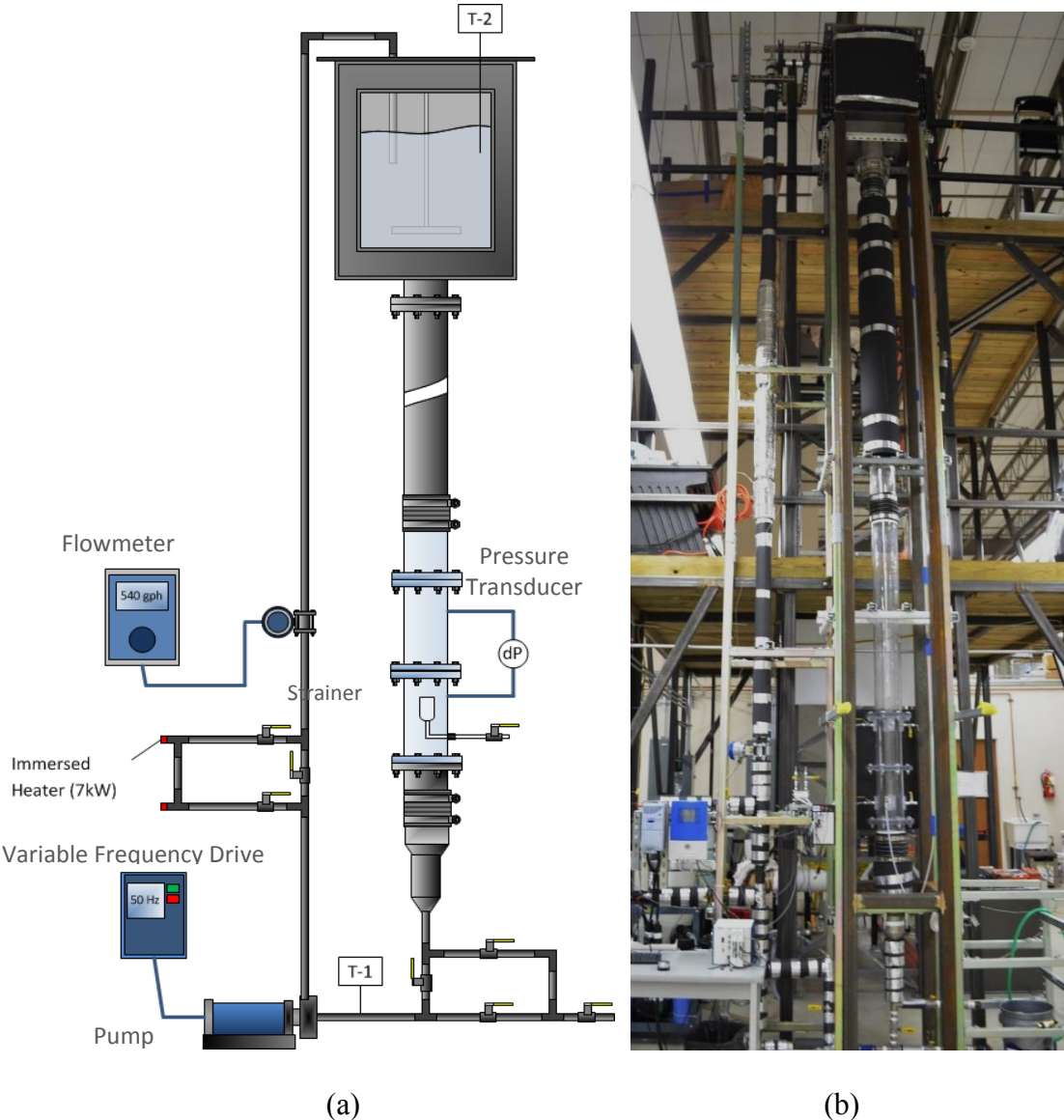
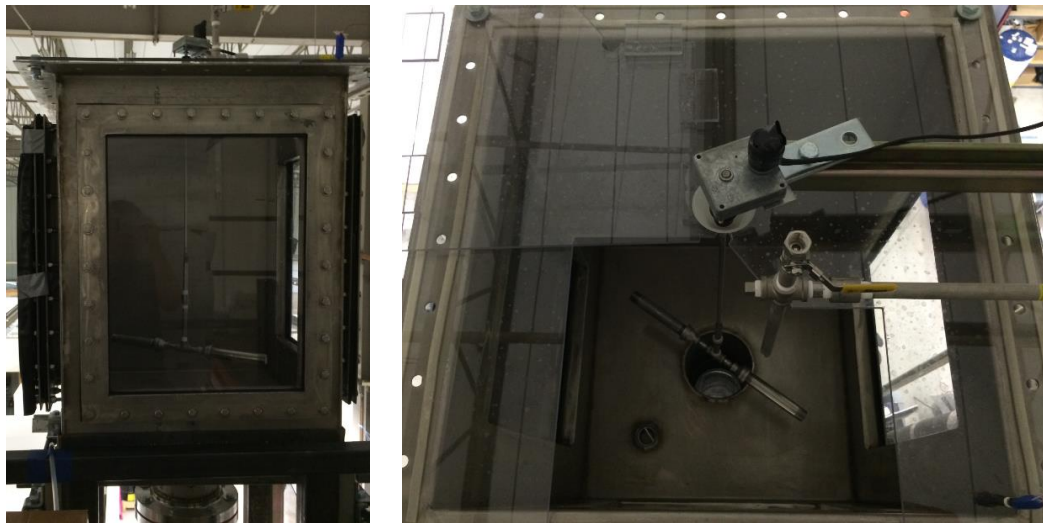


Figure II.3. 1. The design concept (a) and overview (b) of the vertical head loss and debris bypass test facility

The experimental facility consists of a transparent water tank, a horizontally installed strainer in the transparent test section, a centrifugal, and a mixing propeller. Since the water tank of the high temperature vertical facility was installed at 6 m elevated from the floor and filled with high temperature water, the main frame was made of stainless steel (60.96 cm × 60.96 cm × 76.20 cm, width × length × height, respectively). The tank is equipped with a lid on the top used during the experiments to minimize the heat losses. For the visualization 3 polycarbonate windows were attached. Figure II.3.2 shows the water tank from different points of view.



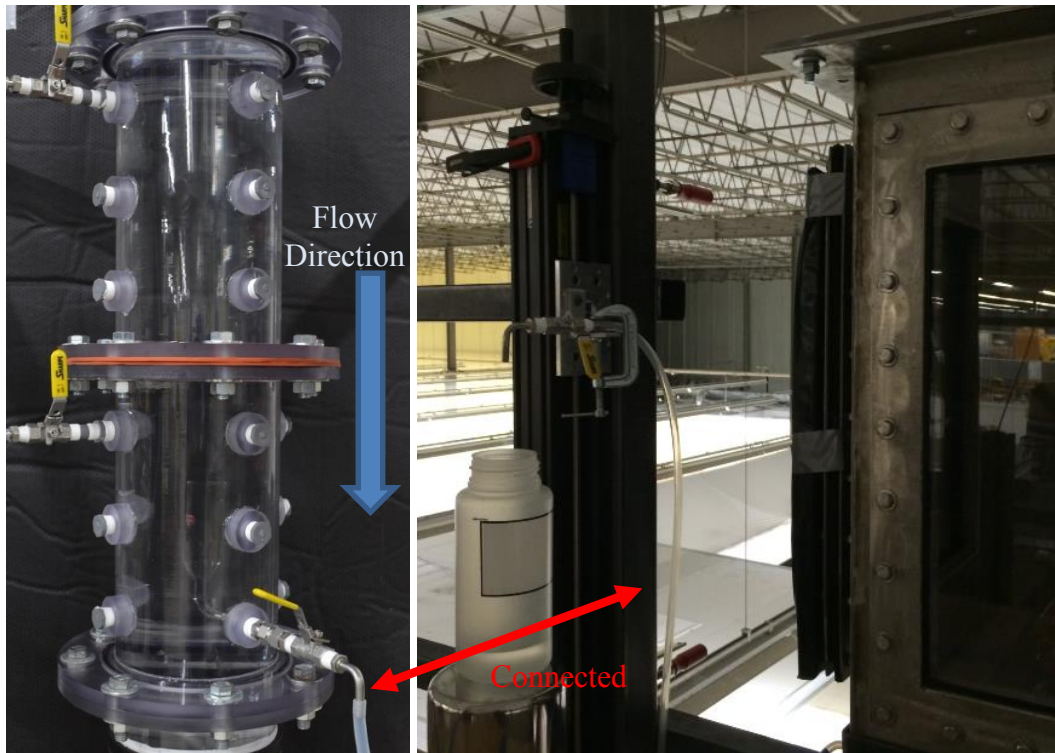
(a) Tank side view

(b) Tank top view

Figure II.3. 2. Stainless steel water tank of the high temperature vertical facility

The mixing propeller was made of stainless steel (SS-304) pipes with of ½ inch NPT for the body and ¾ inch NPT for the arms, forming a T-shape mixer and controlled by a time-adjustable relay that switched the direction of rotation every 1 minute. Figure

II.3.3 shows the test section and dynamic sampling port connected to the top of the facility to use gravity without disturbing the sampling by sampling pumps.



(a) (b)
Figure II.3. 3. Pressure measurement and sampling point: (a) test section and (b) dynamic sampling port

The test section consists of two polycarbonate tubes (15.24 cm ID, 16.51 cm OD), a strainer, and a sampling port. The test section has two flanges to install the strainer which follows the same design of the low temperature horizontal facility as shown in Figure II.3.4.

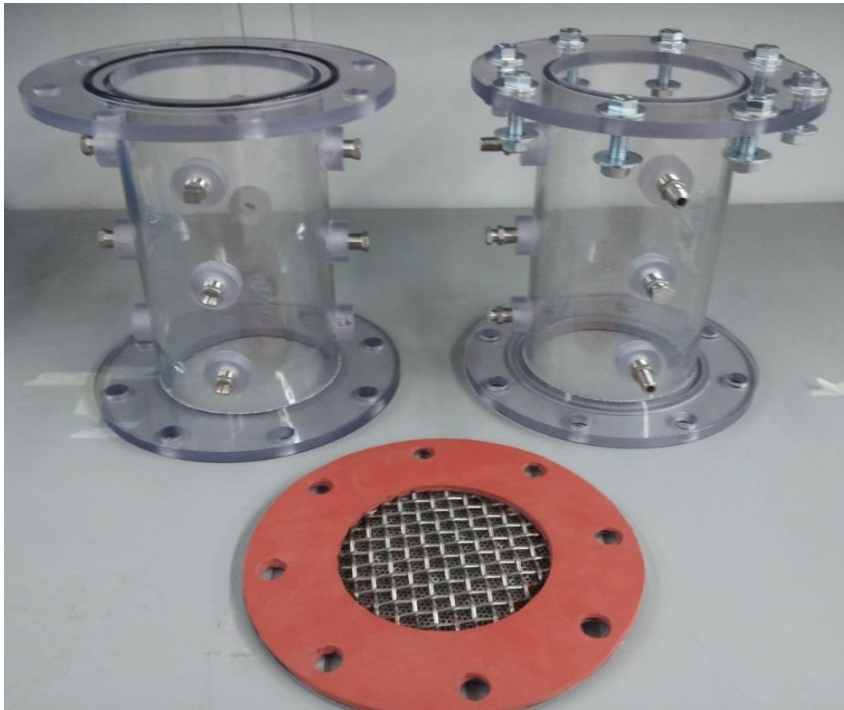


Figure II.3. 4. Vertical test section in parts



Figure II.3. 5. Filter bag in the vertical test facility

A stainless-steel centrifugal pump provides the required volumetric flow rate in the test section to reach the desired approach velocity at high temperature. An Optiflux-1300 magnetic flow meter (Krohne®) was installed downstream of the pump to read the volumetric flow rate (Figure II.3.6). The accuracy at the target flow velocity (0.3 cm/s) is 2 % of the reading. To measure head loss through fibrous beds, a differential pressure transducer (Honeywell® differential pressure transducer, range: 1psid, accuracy: 0.1% full-scale) was installed.

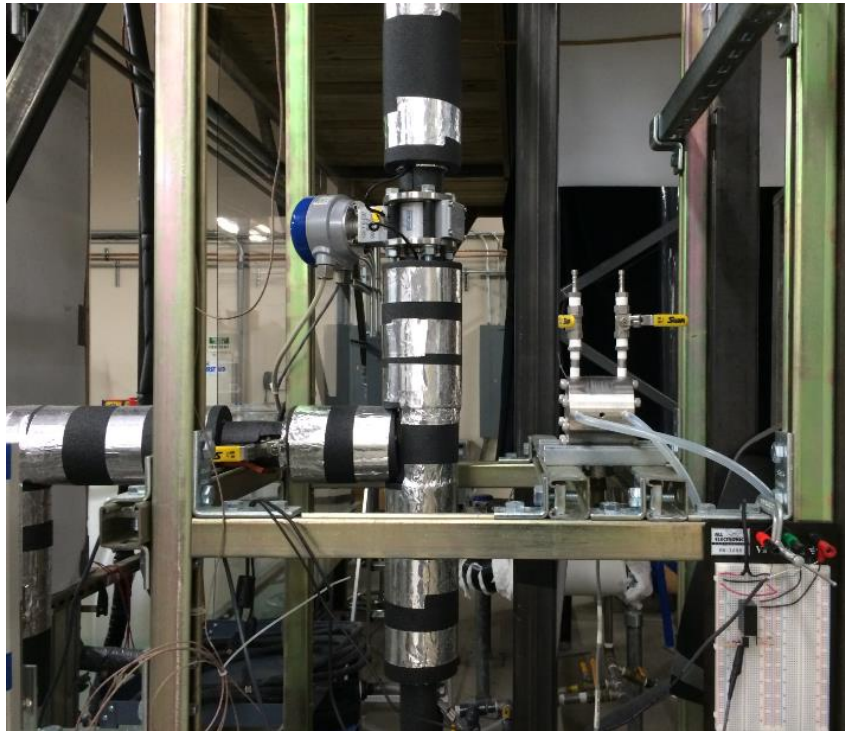


Figure II.3. 6. Electro-magnetic flow meter and pressure transducer

Submerged heaters (total power = 7kW) are installed downstream of the pump as shown in Figure II.3.7. Before starting the experiment, the water was forced to circulate through the heating loop until the desired temperature was achieved. During the experiment, the heating loop was isolated by valves. The vertical head loss and debris bypass test facility has a control panel same to that shown in Figure II.2.8 and Table II.2.2.



Figure II.3. 7. Heating loop (7kw)

II.4. Debris size characterization system

An Imaging Particle Size Measurement system was developed at Texas A&M University (IPSM-TAMU) for debris size characterization. Figure II.4.1 shows the overview of IPSM-TAMU with a sample image of NUKON debris prepared with NEI protocol [18]. For this version of IPSM-TAMU, NAC GX-3 high speed camera was used to take pictures of magnified debris sample images. The specification of the camera is shown in Table II.4.1.

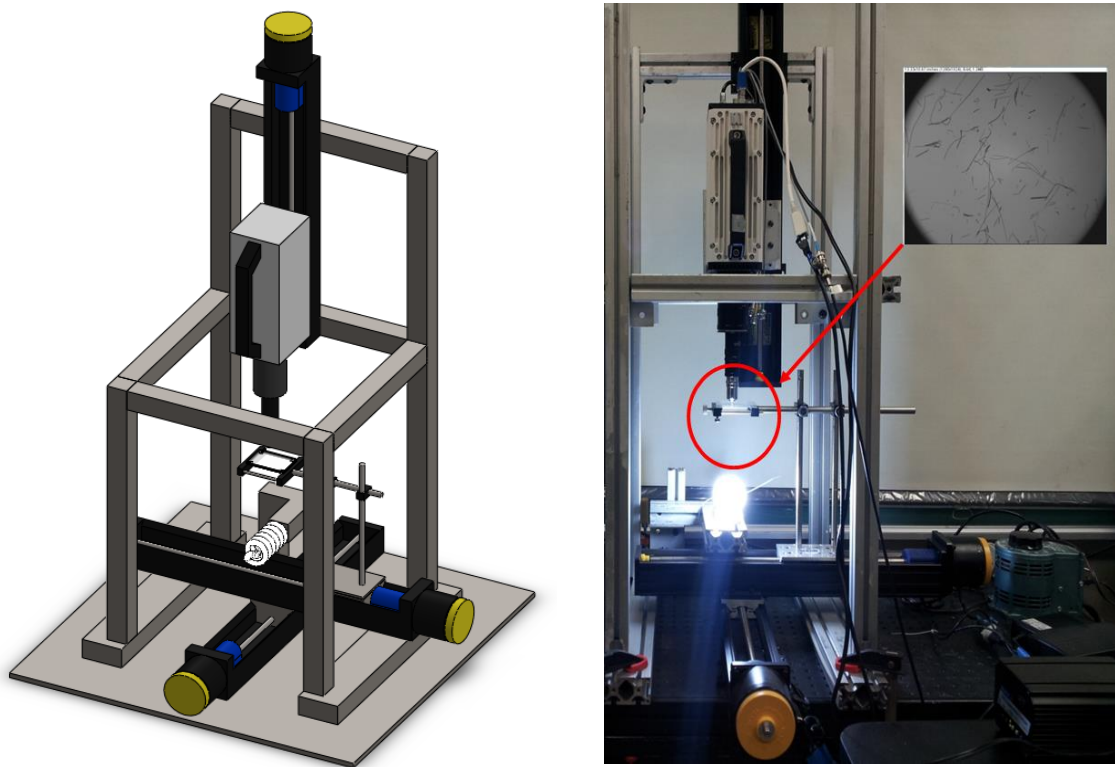


Figure II.4. 1. Overview of imaging particle size measurement system developed at Texas A&M University (IPSM-TAMU)

Table II.4. 1. High speed camera specification

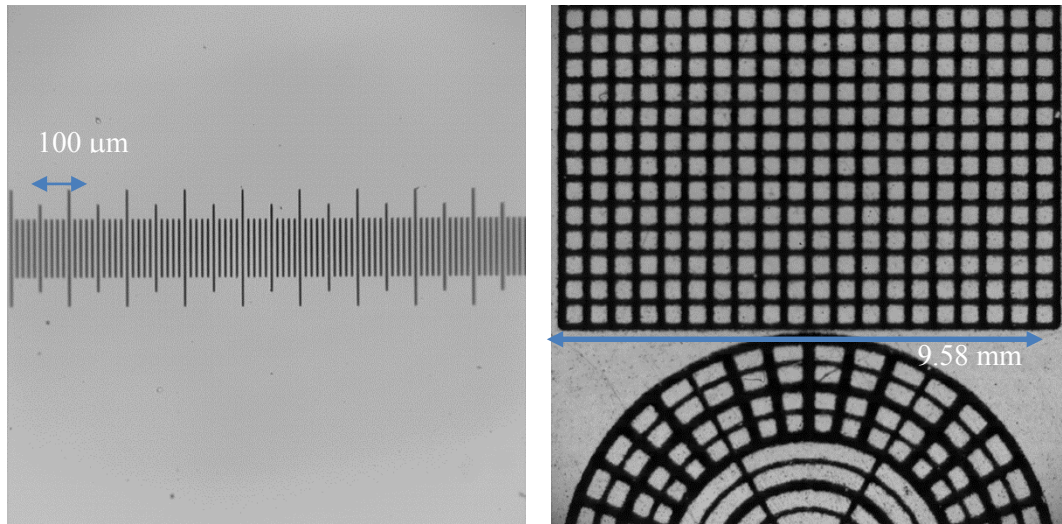
Model	Resolution	Frame rate at max Resolution
MEMRECAM GX-3	1280 × 1024 pixels	1679 frame per second

A 20x microscope objective was used to cover the range from 5 μm to 225 μm , and a 2x lens was used to cover the range from 50 μm to 2449 μm . The specifications are shown in Table II.4.2.

Table II.4. 2. Microscopic objectives specifications

Magnification	20x	2x
Actual length of 1 pixel	0.88 μm	9.57 μm

Several light sources such as 1) halogen lamps, 2) a 2500K fluorescent bulb, 3) a 6500K fluorescent bulb, 4) a white LED panel with 60 LEDs, and 5) a white light screen were tested, and the 6500K fluorescent bulb showed the best imaging. More complicated illumination such as Köhler illumination was not applied since the fluorescent illumination allowed the enough quality. Two Different calibrations were applied to the different magnifications. Figure II.4.2 shows the calibrations of (a) 20x lens and (b) 2x lens. Each division in Figure II.4.2.a is 10 μm , thus each pixel measured 0.88 μm . The distance between the two ends of the outer square in Figure II.4.2.b measured 9.58mm, which corresponded to 9.57 μm per pixel.



(a) (b)
 Figure II.4. 2. Microscopy image calibration - (a) 20x with KR-851 (KLARMANN RULINGS, INC.) and (b) 2x with grids

A two-dimensional slider system driven with stepping motors was installed. The stepping motor shifted the sample by $450\ \mu\text{m}$ to overlap the half of $900\ \mu\text{m}$ size images and take images to cover the whole target area. For 2x magnification, the same area was scanned to provide images of 1cm by 1cm size with 5mm overlapping. The specification of the system with a controller is shown in Table III.4.3. The controller also sent a triggering signal to the camera to synchronize two systems.

Table II.4. 3. Mechanical system

Resolution	Repeatability	Speed Range
6.35 μm	5 μm	$\sim 76.2\ \text{mm/s}$ at 11b load

A set of images for each sample was taken by scanning a target sample. A 900 μm by 900 μm square region was selected as a target area for 20x magnification with a resolution of 0.88 μm per pixel. 1681 images covered 18.9 mm by 18.9 mm area for each sample. 16 images with the size of 9.80 mm \times 9.80 mm covered the area of 29.4 mm \times 29.4 mm for the 2x magnification. A 2-D Finite Impulse Response (FIR) filter was applied to separate the debris from background. Once a binary image was obtained using the filter, the image was processed again to fill the empty space in the debris and smooth out the rough boundaries. Then, the perimeter, the area, the feret lengths, and the location of the debris were measured in pixels. The final goal of image processing is to obtain a binary image to separate debris from the background and measure the size and shape. Several threshold algorithms, such as Huang, Max-Entropy, Otsu, and so on, were applied and compared to the filtering method, then the filtering method showed the best result. Once a binary image was obtained, the image was processed again to fill the empty space in the debris and smooth out the rough boundaries. Then, the perimeter, the area, the feret lengths, and the location of the debris were measured in pixels. The present technique was validated using two different types of particles (National Institute of Standard and Technology (NIST) traceable).

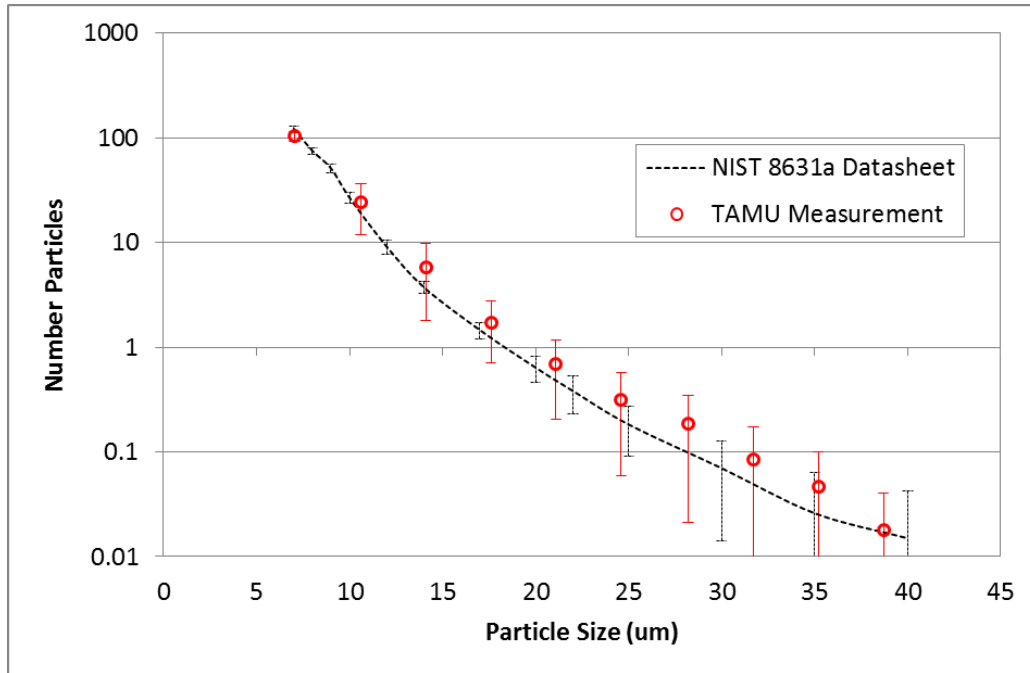


Figure II.4. 3. Validation of particle size distribution using NIST 8631a standard particles

Table II.4. 4. Particle size distribution results (NIST 8631a)

BIN (μm)	TAMU Measurement					NIST SRM 8631a Datasheet		
	S1	S2	S3	Mean	STDEV	BIN (μm)	Mean	Expanded Uncertainty
7.04	93.2	104	113	103.4	9.9136	7	122	7.61
10.6	13.4	21.8	37.8	24.333	12.3957	8	75.1	5.52
14.1	2.98	4.02	10.3	5.7667	3.9603	9	50.9	4.82
17.6	1.02	1.26	2.88	1.72	1.0117	10	26.7	3.24
21.1	0.412	0.404	1.24	0.6853	0.4804	12	9.09	1.3
24.6	0.182	0.151	0.606	0.313	0.2542	17	1.46	0.273
28.2	0.127	0.0588	0.37	0.1853	0.1636	20	0.639	0.174
31.7	0.0496	0.0202	0.185	0.0849	0.0879	25	0.183	0.091
35.2	0.020	0.01	0.109	0.0465	0.0544	30	0.07	0.056
38.7	0.0033	0.0067	0.0436	0.0179	0.0224	40	0.015	0.027

Five different mono-sized particles were used to validate the accuracy of size measurement. Figure II.4.4 presents the results of 5 μm , 10 μm , 20 μm , 65 μm , and 90 μm particles. The maximum uncertainty of the measurement, 1.9 μm , was found in 5 μm particles. The detailed particle size information is presented in Table II.4.5 and Figures II.4.5 is the example images of mono-sized particles and processed images.

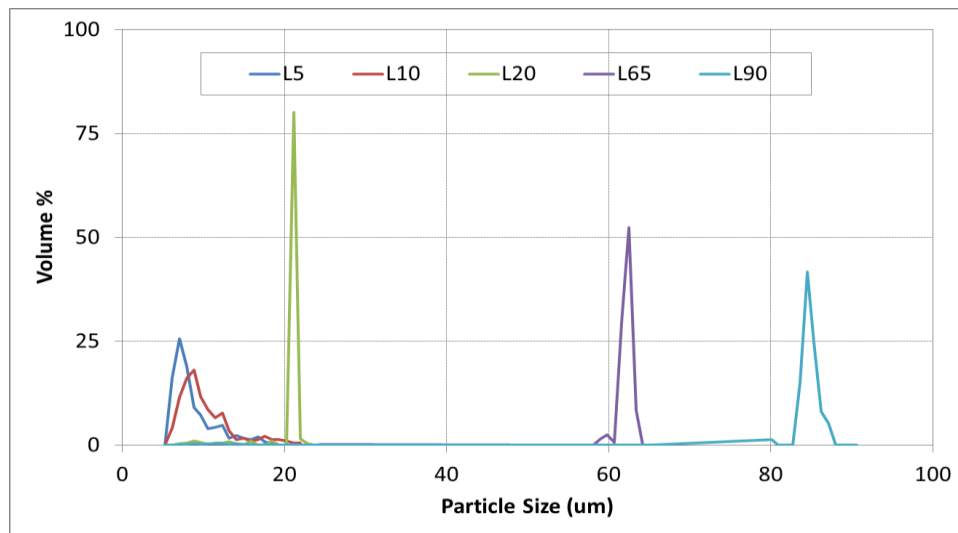
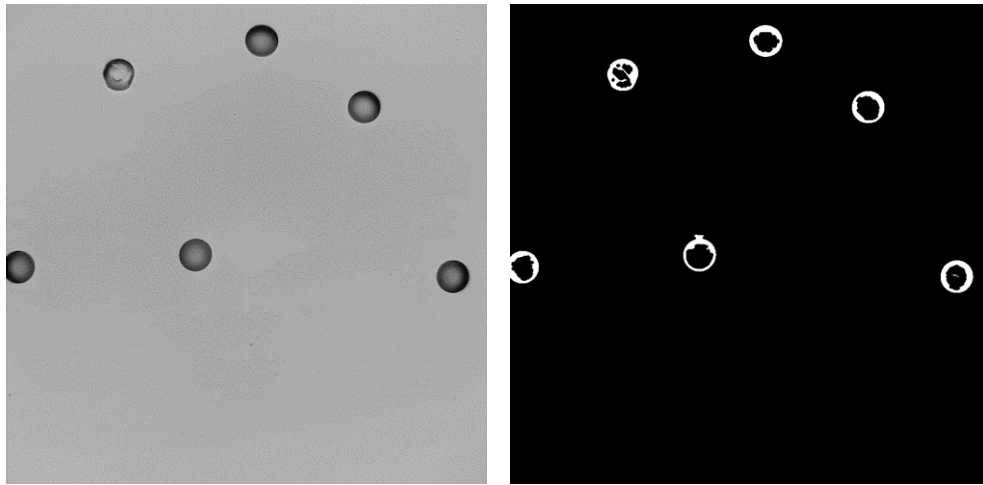


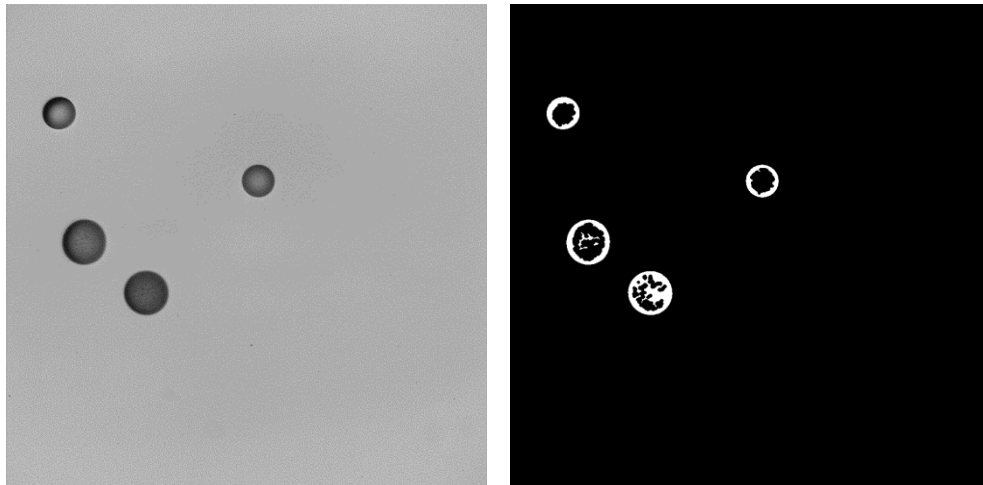
Figure II.4. 4. Mono-sized particle size measurement

Table II.4. 5. Size information of mono-sized particles

Particles*	Nominal Size (μm)	Assay Value (μm)	Measured Value (μm)	Difference (μm)
L5	5	5.052	7.04	1.99
L10	10	10.35	8.8	1.55
L20	20	20.5	21.12	0.62
L65	65	63.13	62.48	0.65
L90	90	85.42	84.48	0.94
Maximum Difference :				1.99 μm
* COULTER CC Size Standard LXX, (NIST Traceable Latex Beads)				



(a) 65 μm particles (L65)



(b) Mixture of 65 μm and 90 μm particles (L65 and L90)

Figure II.4. 5. Mono-sized particles – original images (left) and processed images (right)

II.5. Instrumentations

This section provides a description of the instrumentation installed in the facility and used during the experiments. This includes instruments for the analysis of the debris bypass quantity such as scale, hygrometer and thermometer. The following devices were installed and used during the experiments:

- Electro-magnetic Flowmeter

As previously mentioned (Figure II.2.6), an electro-magnetic flow meter (Optiflux-1300, Krohne®) was installed to measure the flow rate of the water through the test facility. The accuracy of the flow-meter is 1.7% at the working flow rate of 24 gallon/h which corresponds 0.3 cm/s or 0.01 ft/s.

- Rotameters

Three King Instrument rotameters were installed to measure the flow rate of the water through the test facility.

- Low flow rate: 227 liter/h (60 GPH) with 3% full-scale accuracy
- Intermediate flow rate: 19 liter/min (5 GPM) with 5% full-scale accuracy
- High flow rate: 38 liter/min (10 GPM) with 5% full-scale accuracy

- Thermocouple

- T-type thermocouple probe (Omega® EN60584-2, Class 1) was used with an NI-SCXI-1000 data logger to read the temperature of the water in the high temperature horizontal and vertical water tanks. The accuracy of the system is ± 0.5 °C.
- K-Type Thermocouple and Thermocouple Reader. A Fluke® 52II thermocouple reader was used with a K-type thermocouple probe (Omega® EN60584-2, Class 1) to read the temperature of the water in the water tank at the beginning of each test in the low temperature horizontal test facility. The accuracy of the system is ± 0.3 °C. All the test were performed at room temperature.

- pH Meter

A SevenCompact™ S220 (METTLER TOLEDO®) pH/Ion meter was used to measure the pH of the water. The accuracy of the meter is ± 0.002 . It was calibrated using reference solutions of pH – 4.01, 7.01, 9.21, and 10.01.

- Electrical Conductivity Meter

A PCSTestr™35 (Eutech Instruments OAKTON®) was used to measure the electrical conductivity (EC) of the water. The range is 0.0 to 199.9 $\mu\text{S}/\text{cm}$, 200 to 1999 $\mu\text{S}/\text{cm}$ or 2.00 to 20.00 mS/cm and the accuracy is $\pm 1\%$ full

scale. The sensor was calibrated using 84 $\mu\text{S}/\text{cm}$ and 1413 $\mu\text{S}/\text{cm}$ standard conductivity solutions.

- Viscometer

The viscosity of the tap water at room and high temperature was measured using MCR 300 Modular Rheometer (Anton Paar, Ashland, VA). The accuracy of the system is 0.5% for viscosity and $\pm 0.1^\circ\text{C}$ for temperature. The calibration of the viscometer was validated using DI water which will be presented in Figure III.2.2.

- Scale

- A Acculab® VI-2400 was used to weigh the TSP and boric acid to be added to the DI-water during the buffered/borated water experiments. Due to the limited measuring range (0 – 2400g) of the scale in use, the boric acid quantity used on each test (3535g) was prepared in two batches. The readability of this scale is 0.1g. The calibration of the scale used during the experiment was verified using NIST certified weights.

The following certified weights were used:

- 1 g \pm 0.0009 g
- 5 g \pm 0.0015 g
- 10 g \pm 0.002 g
- 50 g \pm 0.01 g
- All the possible combinations of these weights were verified.

- A Acculab® VI-350 was used to weight the debris to be added to each experiment. The range of this scale is 0 – 350g with a readability of 0.01g. The same scale was used to measure the weight of the filter bags during the phases of the analysis. The calibration of this scale was verified using the same NIST certified weights.

- Digital Hygrometer/Thermometer

This device (Dwyer® 485-2) supported the measurements of the relative humidity and temperature of the air in the laboratory where the experiments were conducted. The accuracy and resolution for the relative humidity are $\pm 2\%$ and 0.1% respectively. Temperature measurements have a $\pm 1^\circ\text{F}$ accuracy and 0.1 $^\circ\text{F}$ resolution.

- Thermo-Hygrometer

This device (Lufft® C200) supported the measurements of the relative humidity and temperature of the air in the laboratory where the experiments were conducted. The accuracy and resolution for the relative humidity are $\pm 2\%$ and 0.1% respectively. Temperature measurements were conducted with $\pm 0.3^\circ\text{C}$ accuracy and 0.1 $^\circ\text{C}$ resolution.

CHAPTER III

EXPERIMENTS

This study includes three topics: head loss through fibrous porous media generated from dilute fiberglass suspensions, debris penetration through the fibrous porous media, and the size characterization of the debris. In order to investigate head loss through the fibrous porous media, the low temperature horizontal test facility was firstly used with the debris samples prepared by shredder method [12]. This result was utilized to modify the previous researchers' head loss model. Then, the same facility was used with the debris prepared by NEI method [36]. At the end, two tests were performed in the vertical loop with the debris samples prepared by NEI method. To understand debris bypass through NUKON[®] fibrous beds, two conditions with TAMU tap water and the typical boric acid and buffer solution were tested in the low temperature horizontal test facility. After constructing the high temperature horizontal test facility, additional TAMU tap water tests were conducted to prove that the two horizontal facilities produce the same results. Then eight different conditions of water chemistry and two different temperatures were examined. Also, the effect of different approach velocity of the fluid was investigated. The quantity of debris bypass was also measured at different time with different concentration to develop a bypass model as a function of time and concentration of debris injected. Debris size characterization was applied to potential particles and fiberglass debris generated using NEI method. Debris preparation is a general procedure for all three experiments and is described further in section III.1.

Details of each experiment are described in the following section. Section III.1 will present the procedure and measurement techniques used in head loss measurement and debris bed build-up. Section III.4 describes the procedure of the bypass test including the preparation of the debris and chemical solutions, measurement of water chemistry, and the post processing for the filter weight measurement. Section III.4 describes the validation of the debris size characterization system developed by the author and the process of the size characterization.

III.1. Debris preparation

Debris samples were prepared using shredder method or NEI method. Shredder method was originally used in NUREG/CR-6224 [12]. Recently, to produce more representative debris samples NEI method [36] was developed by the Nuclear Energy Institute (NEI).

III.1.1. Shredder method

For the sample preparation using shredder method, unbaked NUKON was shredded with a commercial leaf shredder (provided by the manufacturer (PCI, LOT ID: Lo-18-10: NUKON-1168*LN-1107-7) and then boiled for 10 minutes as shown in Figure III.1.1.



(a)

(b)

(c)

Figure III.1. 1. Debris preparation using shredder method (a) NUKON prepared using a leaf shredder and (b) and (c) boiled for 10 minutes in 2-liter stainless steel jar

Figure III.1.2 presents the size classification of NUKON (following the criteria in Table I.1) prepared using shredder method.

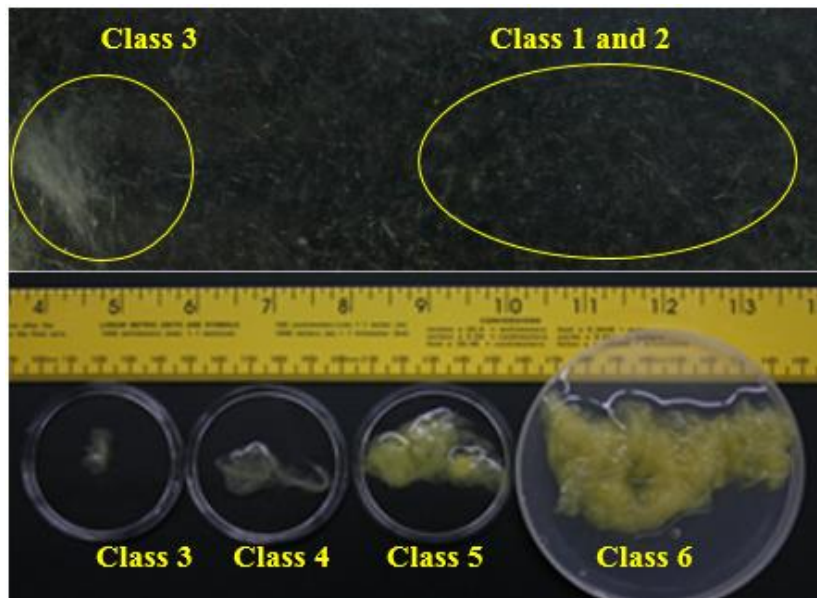


Figure III.1.2. Debris classes prepared by shredder method

III.1.2. NEI method

This protocol was developed by the NEI in 2012, and the procedure adopted aimed to produce fine debris defined in the NEI protocol. A brief description of the steps followed to produce the debris used for each test is as following.

STEP 1: NUKON debris sampling and weighing

The desired quantity of NUKON (6.6g or 40.0g) was sampled from a NUKON heat treated mat (PCI 2.5'' x 24'' x 48'', Lot #10958HT). The NUKON mat where the samples were taken is shown in Figure III.1.3.



Figure III.1. 3. One-side baked NUKON® mat

The sample cut from the mat was repeatedly trimmed on the edges in order to achieve the target weight. All the cuts on the samples were performed in a way that the full thickness of the sample was preserved in order to conserve the original characteristics of the heat-treated mat. Once an accurate mass was obtained on a digital balance as shown in Figure III.1.4, the sample was moved to the next step. The technical information of the scale used during the experiment preparation was described in section II.5.



Figure III. 1. 4. Debris final quantity – 6.6g (left), 40g (right)

STEP 2: Sample size reduction

The sample was initially separated into four layers of approximately the same thickness: two dark layers, corresponding to the side of the mat in contact with the hot surface used during the heat treatment, and two light layers, the opposite side of the mat (Figure III.1.5).



Figure III.1.5. Layers separation

These layers were then cut in small pieces of approximately $2.54 \text{ cm} \times 2.54 \text{ cm}$. The pieces originating from the light layers were additionally torn and all pieces were put in a plastic bucket (total capacity ≈ 20 liter) (Figure III.1.6).



Figure III.1.6. Debris size reduction

Approximately 2 liters of water were poured into the bucket to slightly cover the debris pieces (Figure III.1.7).

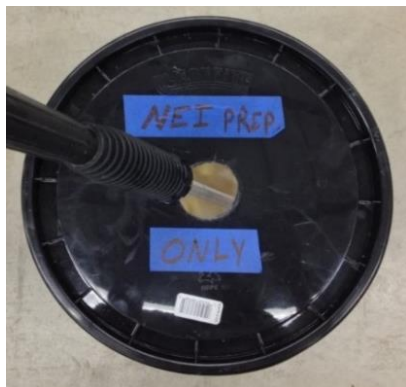


Figure III.1. 7. Debris size reduction in a bucket – 6.6g (left), 40g (right)

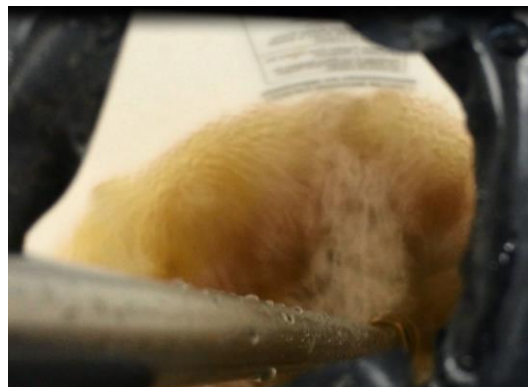
In practice, the procedures from Figure III.1.5 to Figure III.1.7 were conducted inside the plastic bucket to avoid any possible debris loss during the preparation. Those figures seen here are solely to demonstrate the final shape and size of the debris during the sample size reduction phase.

STEP 3: High pressure washer jet mixing

A high pressure (12.4MPa / 1800 psi) washer was used to further break down and mix the debris previously stored in the plastic bucket (Figure III.1.8). The jet was kept submerged into the water in the bucket while it was turned on. The jet gun was moved randomly inside the bucket to allow uniform breaking and mixing. A 40° angle nozzle was used during this phase. Spraying ceased when the final amount of water in the bucket was approximately 4 gallons. This allowed uniform debris tearing and mixing. During the pressure washer phase, a lid with a small hole was applied in order to avoid spill of water from the bucket.



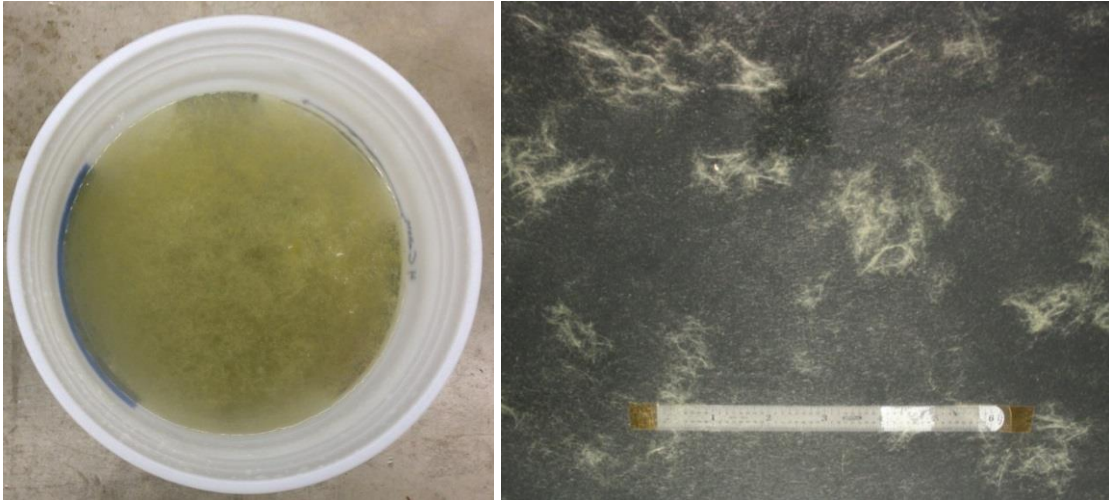
(a)



(b)

Figure III.1. 8. Pressure washer mixing – (a) outside and (b) inside of the bucket

Figure III.1.9 shows the final status of the NEI prepared NUKON debris sample in a 5 gallon bucket and the sample presented in an observation tray.



(a) (b)
Figure III.1. 9. Final state of debris sample – (a) in the bucket and (b) in the tray

When Figure III.1.9 was compared to Figure III.1.2, it was clear that NEI method produced greater fraction of smaller size debris with loose density (increased porosity) than shredder method.

III.2. Head loss experiment

Head loss tests were mainly conducted in the low temperature horizontal test facility. Additional tests to support the horizontal test results were also conducted in the high temperature vertical test facility. Table III.2.1 lists the reference parameters from a 4 Loop Westinghouse PWR [37], and Table III.2.2 presents the conditions used in the head loss experiment.

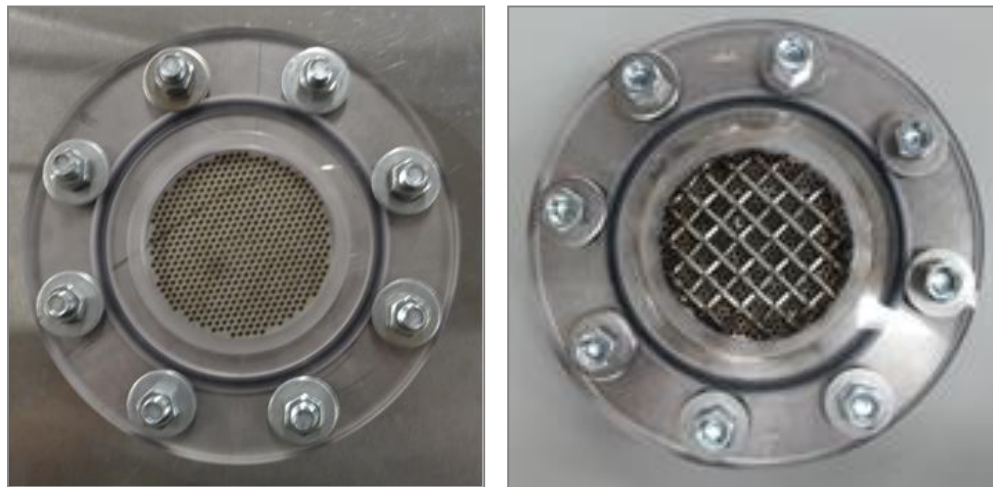
Table III.2. 1. Parameters in a 4 loop Westinghouse PWR

Maximum flow rate per train	7020 gallon/minutes
Strainer surface area per train	1818.5 ft ²
Typical approaching velocity	0.3 cm/s
Fibrous insulation material	NUKON [®] (PCI)
Strainer nominal hole size	2.4 mm
Strainer hole pitch (center to center)	
Mesh screen opening size	
Mesh screen wire diameter	
Fiber diameter	7 μm
Fiber mat density, ρ_m	0.0384 g/cm ³ (2.4 lb/ft ³)
Fiber density, ρ_f	2.5469 g/cm ³ (159 lb/ft ³)

Table III.2. 2. Experimental conditions

Experiment temperature	26 ± 3 °C
Test liquid	Tap water
Test strainer surface area	81.073 cm ²

Based on the calculated approach velocity, test velocity was selected to be up to 3.11 cm/s which resulted in the modified Reynolds Number to be 22 when the porosity was assumed to be 0.99. A simply perforated plate (SPP) type strainer designed by PCI was the primary focus during the testing phase. Additional tests with a mesh added perforated plate (MPP) type strainer manufactured by General Electric (GE) were performed to investigate the effect of strainer design on head loss. Figure III.2.1 shows the two different types of strainers. The sizes of holes and the pitches are almost the same. Without debris injection two strainers did not result in appreciable pressure drop under the test approaching velocity. The size of openings and the wire diameter of the mesh screen are 1.27cm and 3mm, respectively.



(a) SPP

(b) MPP

Figure III.2. 1. Two different types of strainers - (a) simply perforated plate (SPP) and (b) mesh added perforated plate (MPP)

As shown in the Darcy's law in Equation (I.1), head loss is a function of the fluid viscosity and the thickness of the medium. During a LOCA, boric acid solution is injected to the reactor from Refuel Water Storage Tank (RWST). Therefore, the coolant collected in the containment sump is not pure water. Thus, in order to use TAMU tap water, the viscosity of the boric acid solution at a typical concentration was compared with TAMU tap water viscosity and DI water viscosity before conducting the head loss experiments. The result shown in Figure III.2.2 confirmed that there is no significant difference between boric acid solution and TAMU tap water in overall head loss. The viscosity measurement is described in detail in Appendix G.

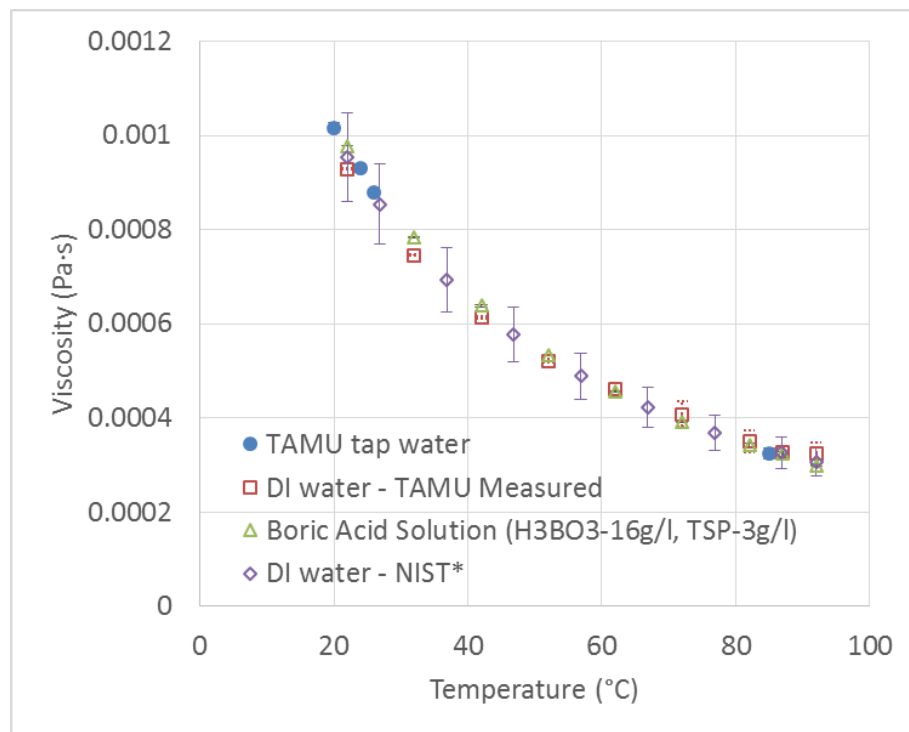


Figure III.2. 2. Comparison of viscosity of different water types (*NIST data is obtained from <http://wtt-pro.nist.gov/wtt-pro/>)

While the debris sample was being prepared using one of the methods previously discussed, the facility was filled with water up to 47 cm from the bottom of the water tank. This allowed the level of the water after injecting the prepared debris to reach 51 cm, corresponding to the volume of water in the tank of 189 liters. Venting valves were then opened to remove air trapped in the pipeline during the filling phase. After the circulation centrifugal pump was turned on, the valves were controlled until the target flow rate was achieved. The debris previously prepared (total water volume with debris was 15 liters (4 gallons) was poured into the water tank over a short (~ 5 sec) time period while the mixing propeller spun. The effect of the mixing propeller on head loss was tested, as described in Appendix A, before the experiments, and it was confirmed that the effect was negligible. Forty grams of NUKON was used to produce five times higher concentration of NUKON (0.09 volume percent (vol.%), corresponding to 0.0034 weight percent (wt.%) which covers 99% of LOCAs in the NRC report submitted by STP [37]. The camera and the data logger for the pressure transducer and thermocouples were triggered at the moment of the debris injection. The effects on the pressure drop by the pipe wall, the clean strainer, and the mixing propeller were accounted for in the pressure drop measurement. Pressure drop caused by the wall of the test section and the strainer was measured as less than 0.6895 Pa, which is below the detection range for the instrument. The effect of the mixing propeller on the pressure fluctuation was tested by comparing the change in pressure with and without mixing. This observation was also smaller the detection limit of 0.6895 Pa. Pressure drops were recorded for more than 18 hours until it reached a steady state. The experimental procedure for the vertical test

facility was exactly the same as described for the horizontal systems except for the flow rate. The flow rate in the vertical systems was 2.25 times greater than that in the horizontal system because of its strainer size ratio, 15.24 cm to 10.16 cm in diameter, which increased the surface area by 2.25 times.

III.3. Debris bypass experiment

The procedures of debris bypass experiments can be split into a general procedure and optional procedures. The general procedure is of common use for all types of water tests and optional procedures are specific methodologies applied for the different types of chemical solutions preparation. Before conducting an experiment the experimental facility was cleaned following the protocol in section III.3.1.2 and a debris sample was prepared using the method illustrated in section III.3.1.1. After each experiment, the draining and cleaning procedure was repeated for the next experiment. A filter bag collecting the debris bypass during the experiment was weighed with the methodology in section III.3.3.

III.3.1. General procedure of debris bypass test

Once the facility was cleaned from the previous experiment, the strainer bypass filter was installed downstream of the strainer. The filter selected for these experiments was a 1 μ m heat-welded polyester felt bag with a plastic ring head of 10.16 cm, which attached within the polycarbonate pipe inner surface. The filter bag plastic head was

lined with vinyl tape and inserted into the polycarbonate pipe. Figures III.3.1 ~ III.3.3 show the filter preparation steps including tape lining (Figure III.3.1), filter insertion (Figure III.3.2), and final configuration (Figure III.3.3) in the low temperature horizontal test facility.

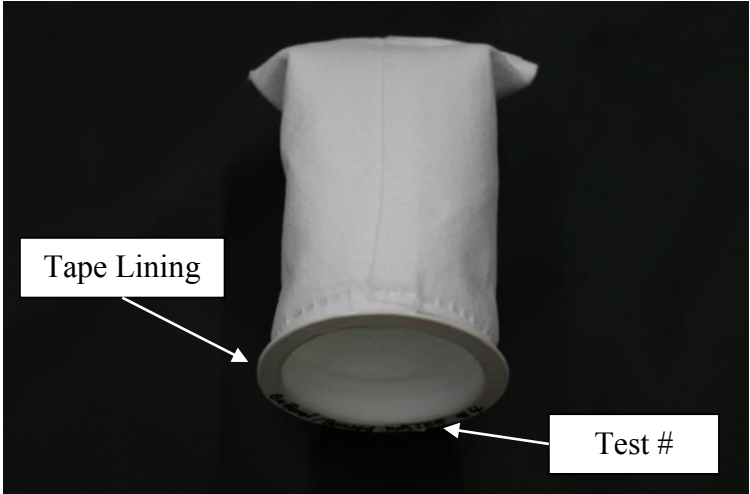


Figure III.3. 1. Filter bag (before test)

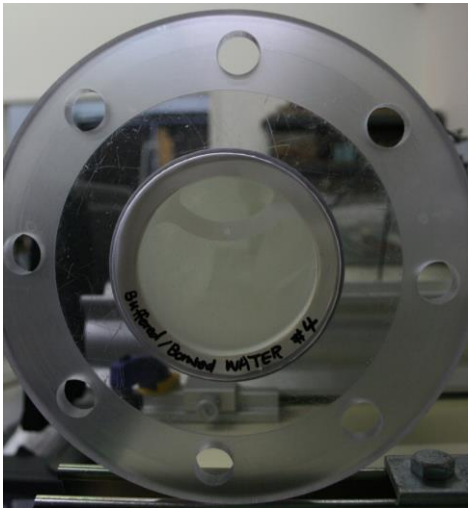


Figure III.3. 2. Test section filter bag insertion

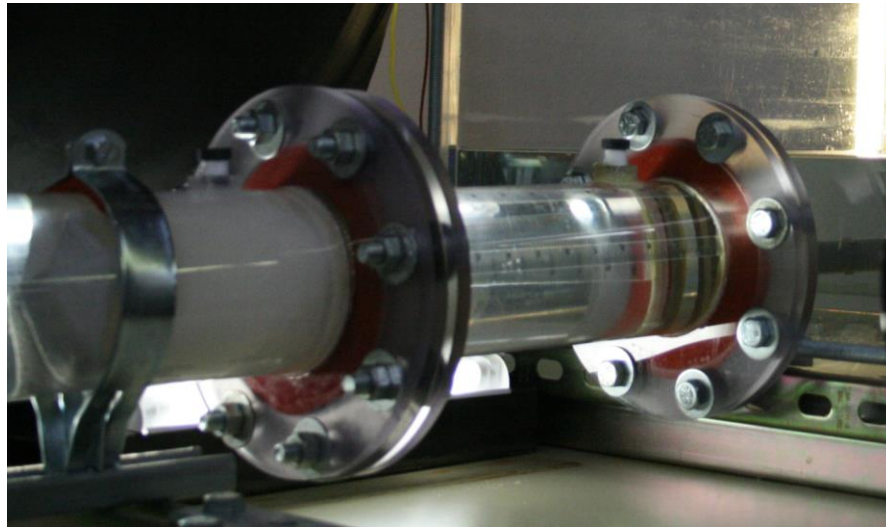


Figure III.3. 3. Filter bag in the low temperature horizontal test facility

Figure III.3.4 shows the final configuration of the filter bag installed in the high temperature horizontal test facility with lining tape and sealing silicone gasket.



Figure III.3. 4. Filter Bag in the high temperature horizontal test facility

The facility was then filled with water (tap or buffered/borated depending on the test type). The final water level in the tank was selected to be 47 cm. This allowed the final level of the water (including the water injected with the debris) to reach 51 cm, corresponding to the volume of water in the tank of 189 liters. Six venting valves were installed on the top side of the horizontal pipe section to allow air trapped in the pipeline to be vented out during the filling phase. Figure III.3.5 shows one of these venting valves used during this phase.

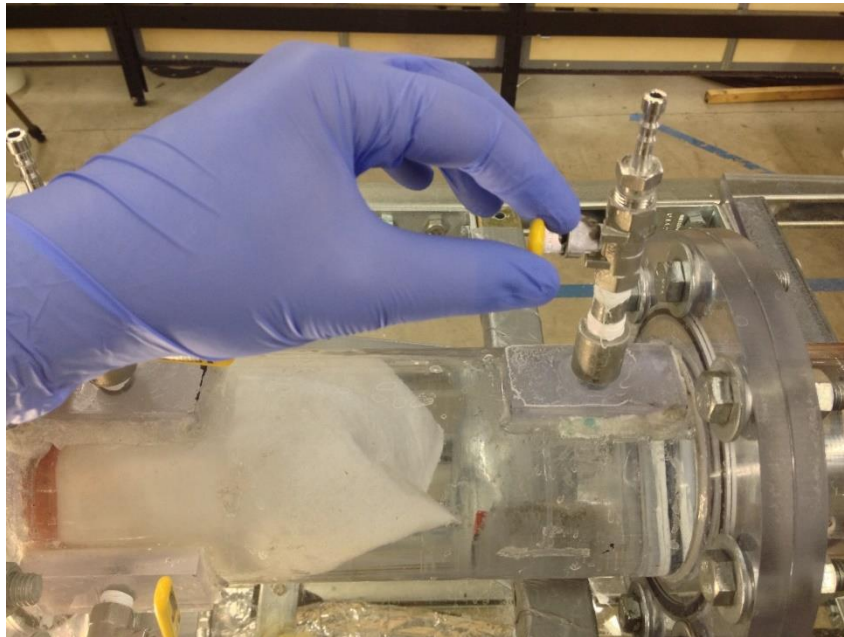


Figure III.3. 5. Venting valve

After the circulation centrifugal pump was turned on, for the low temperature horizontal test facility the PVC gate valve was controlled until the nominal volumetric flow rate of 91 liter/h (24 gallon/h) was achieved. For the high temperature horizontal test facility,

the frequency inverter was adjusted gradually to achieve the target flow rate. This flow rate was selected in order to reach the desired water approaching velocity in the test section 0.3 cm/s (0.01 ft/s). The debris previously prepared using the NEI protocol described in section III.1.1.2 (total water volume with debris was 15 liters (4 gallons) was poured into the water tank over a short (~ 5 sec) time period while the mixing propeller spun. The selected debris concentration in the water tank at the beginning of each experiment was 0.09 volume percent (vol.%), corresponding to 0.0034 weight percent (wt.%). The total weight of debris used for each experiment was 6.6 g. Each experiment was terminated when one turnover time was achieved. Nevertheless, the thickness of the debris bed was monitored at the end of each experiment to ensure a minimum bed thickness. The following formula, Equation (III.1), was used to estimate the turnover time.

$$Turnover\ Time = \frac{water\ volume}{flow\ rate} = \frac{189l}{1.51l / min} = 125\ min \quad (III.1)$$

During the experiment a camera, installed in front of the test section, recorded the flow and the debris bed generation. The movie recorded during each experiment was also used to estimate the final debris bed thickness (at $t = t_{end}$). The debris bed thickness at the end of each test was found to be larger than 2.54 cm. At the end of each experiment the system was carefully drained and cleaned in order to take the filter bag out of the test section without disruption and to remove residual debris from the previous experiment.

After the recirculation pump was turned off, the test section was isolated from the water tank using a 4-inch end cap as shown in Figure III.3.6.

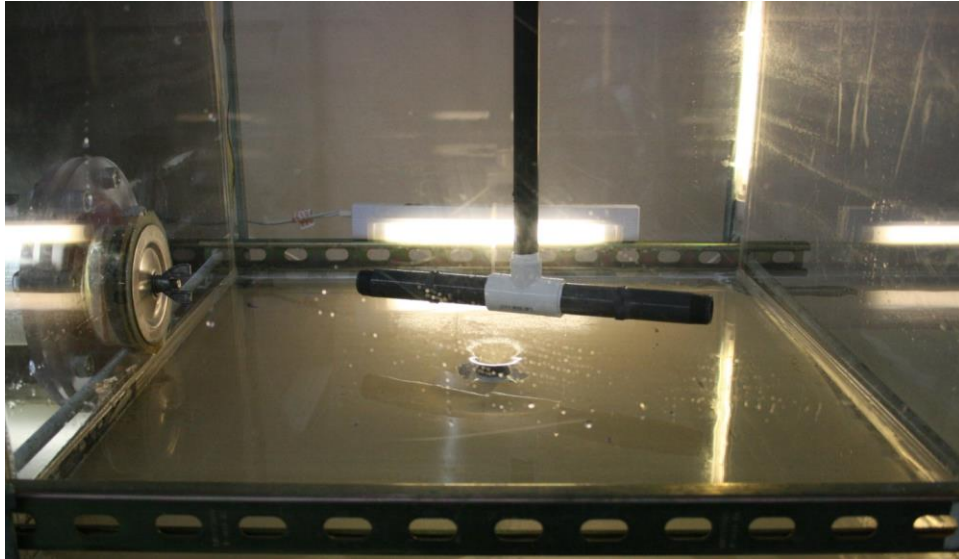


Figure III.3. 6. Water tank isolation cap

End cap placement avoided any undesired flow through the filter bag that could have potentially caused a perturbation in the debris bypass quantity captured during the experiment. After isolating the test section, the water in the test section was drained slowly over 30 minutes. Once the test section was emptied, the filter bag was carefully removed from the test section. The flanged connection was re-established with a new filter bag, and the facility was filled with tap water which was recirculated through the pipelines, pumps and other components for approximately 10 turn overs to remove the remaining debris (One turnover reduces approximately 70% of contaminants). The water was completely drained and the procedure was repeated with clean tap water with a new

filter bag. Through the whole cleaning procedure, the water was forced to flow through a 1 µm filter cartridge before being injected into the facility. For the test with buffered/borated water, an additional cleaning step was run using DI-water. The following steps describe in detail the additional precautions adopted at the end of each test to minimize the loss of debris from the filter bag.

III.3.2. Buffered borated water and aqueous chemical solutions preparation

The typical concentration (1x) buffered borated water was prepared dissolving 16 g/l of Boric acid (Optibor® Orthoboric Acid, H_3BO_3) and 3 g/l of Trisodium Phosphate (TSP) in DI water. For the given volume of the tank with the final liquid level of 20” (see section 2.1), the total amount of boric acid and TSP was (Figure III.3.7) 3535 g and 663 g, respectively.



Figure III.3. 7. Boric acid (left) and TSP (right) final quantities

For other chemical conditions, selected chemicals such as NaCl, CN_2O_3 , HCl, and H_3BO_3 were dissolved in DI water following the same protocol of buffered borated water preparation. The target quantities of chemicals were poured into the water tank where approximately 40 liters of DI-water were previously added (Figure III.3.8).

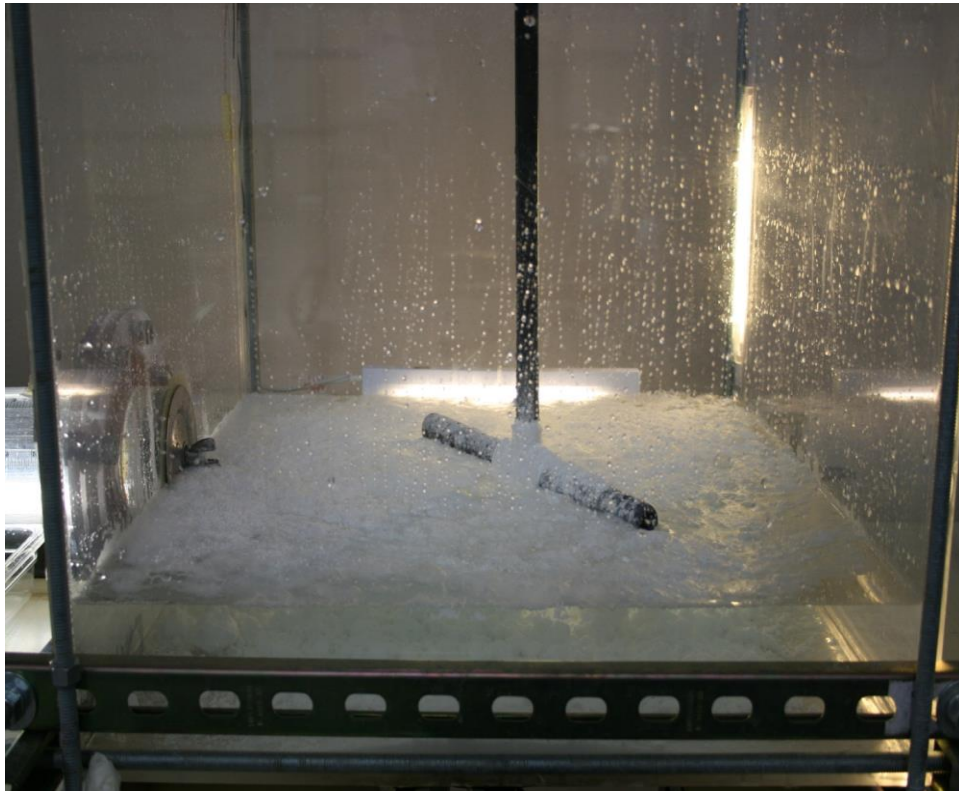


Figure III.3. 8. Chemicals in the tank before mixing

Before the chemicals were added, the tank was isolated from the test section using the end cap method mentioned previously. Additional DI-water was injected into the tank using the high-pressure washer to allow a faster dissolving of the chemicals into water (III.3.9).

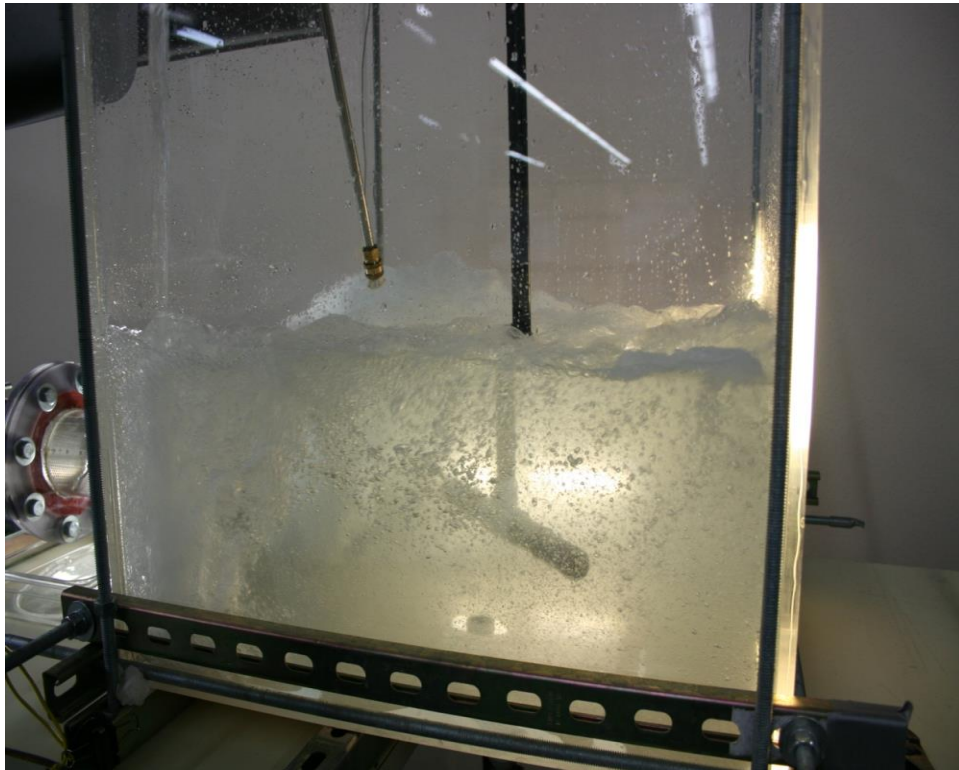


Figure III.3. 9. Water jet and chemical dissolution

The mixing was continued using propeller installed in the water tank until the water appeared clear and all the small chemical particles were totally dissolved (Figure III.3.10).

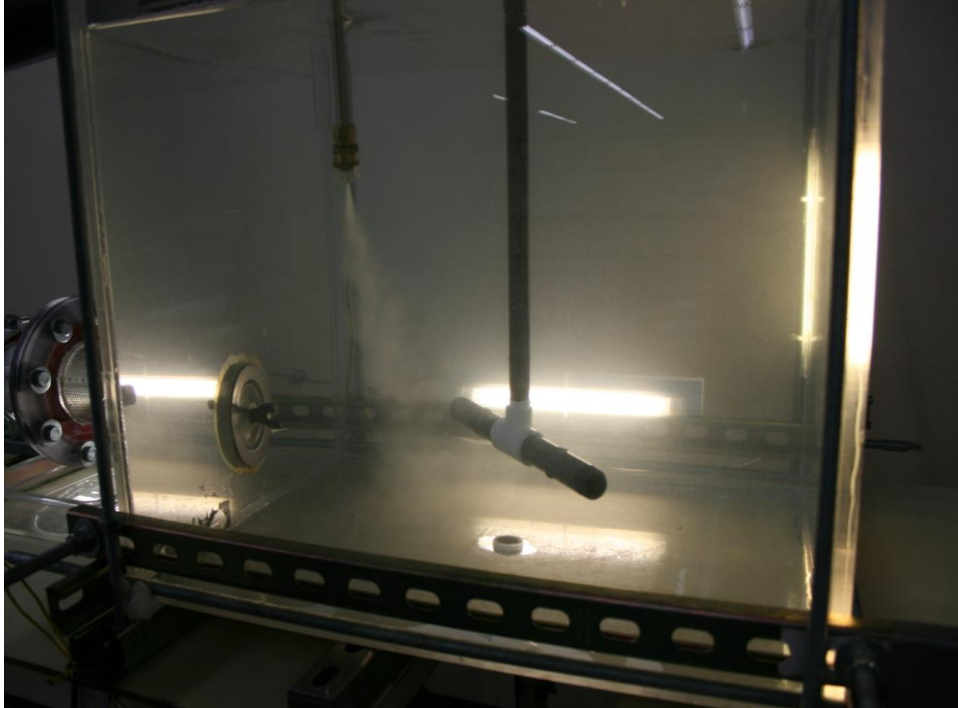


Figure III.3. 10. Chemicals dissolved in the water tank before test start

The end cap was then removed and the facility was filled with additional DI-water. The recirculation pump was turned on at high flow rate for approximately 10 minutes to allow the mixing of the water in the tank with the water in the remaining sections of the facility. The final pH of the solution prepared was measured at the beginning of each test. The flow rate was then adjusted to the nominal flow rate for the experiment and debris was injected into the water tank.

III.3.3. Heating procedure

For high temperature experiments, a heating process took place after filling up the water to the designated level. Two 3.5 kW heaters installed in the bypass loop and three external wire type heaters on the pipe line were turned on while the main loop was closed. After reaching the desired temperature (93°C), the two 3.5 kW heaters were turned off. The three wire type heaters were used in conjunction with a thermostat to maintain a constant temperature. It was noted later on that the three wire type heaters generated flow fluctuation, hence these heaters were also turned off to avoid any other effect than pure temperature effect on quantity of debris bypass. Since the heater was turned off, the temperature change was monitored and recorded during each experiment. After turning off the heaters the heating loop was closed and the main loop was opened.

III.3.4. Debris quantity measurement

Each filter bag used during the experiments was labeled with a letter and a number identifying the type of water and the test number respectively. The filter was weighed at the beginning of each experiment. During this phase, the time of measurement, the relative humidity of the laboratory where the experiments were carried out and the ambient temperature were also recorded. The filter bag removed from the test section at the end of each test were hung vertically for a few minutes, to remove any excess, and then were placed on a horizontal heated plate ($T_{surface} = 120\text{ }^{\circ}\text{F}$) for approximately 15 hours. The drying time was estimated using a preliminary test. At the

end of the drying period the filter was removed from the heated plate and left under the room conditions for approximately one hour. This allowed the filter to reach the equilibrium with the environment under which the weight of the clean filter was taken. Relative humidity and ambient temperature were also recorded at this time. The difference of the two weights recorded for each test was associated with the total debris bypass deposited in the filter during the experiment:

$$M_{debris} = M_{initial} - M_{final} \quad (III.2)$$

Preliminary verifications were required in order to assess:

- The drying time (t_{dry}) required to completely remove the water from the filter after each test.
- The equilibrium time (t_{eq}) necessary for the dry filter to reach the equilibrium (humidity and temperature) of the environment after each test.
- The washout methodology to remove the chemicals collected in the filter after each of the buffered/borated water experiment.

III.3.4.1. Drying time estimation

A clean filter was used for preliminary verification. The clean filter bag was weighed at the beginning of the verification and then immersed in tap water for a few minutes. The excess water was removed by hanging the filter bag vertically for a few minutes. The bag was then moved on the heated plate and consecutive measurements of

the sample weight were taken until the value reached a steady-state. The dry weight of the sample was found to be lower than the original weight (including the air moisture) which confirmed the total sample dry out. The drying time estimated with this procedure was:

$$t_{dry} \cong 15 \text{ hours}$$

III.3.4.2. Equilibrium time estimation

The sample was then left in the environment, and its weight was continuously monitored until the filter bag reached its previously recorded weight. The time estimated with this method was:

$$t_{eq} \cong 1 \text{ hour}$$

To account for uncertainty and changes in the filter bags' properties, the times estimated were assumed to be approximate and used as reference values. During the evaluation of the filter bags during each test the same methodology was applied in order to confirm drying period completion and equilibrium achievement. Measurements of the weight of the filter bag were taken over the time to estimate the drying time and the equilibrium time. A plot of the weight change over the time is shown in Appendix B.

III.3.4.3. Washout

Due to the amount of chemicals dissolved in the water during these experiments, a non-negligible quantity of these chemicals was expected to deposit in the filter bags with the water absorbed by the filter. A preliminary measurement on clean filter revealed that the approximate amount of water absorbed by the filters was 114 grams. This was done by weighing a clean and dry filter and comparing the value with the one obtained after immersion in tap water. Given the total concentration of chemicals in water used for the buffered/borated water experiments ($16 + 3 = 19$ g/l), the amount of chemicals stored in the filter bag was found to be approximately:

$$m_{chem} = \frac{114}{998} \times 19 = 2.17 \text{ (g)} \quad \text{(III.3)}$$

In order to remove this additional weight which may cause errors in the debris weight estimation, washing of the filter bags with DI-water was required after each experiment, before the drying period. To verify the methodology and confirm that no impact was made on the debris quantity accumulation in the filter bag, two preliminary tests were executed. The first test used a clean dry filter (weight recorded at the beginning of the test). The bag was immersed in buffered/borated water until the filter was fully wet. The filter bag was then immersed in clean DI-water several times and then dried out using the standard drying procedure previously described. The weight measured at the end of the test was found to be the same as the mass recorded at the beginning. This confirmed

that the method removed the chemicals stored in the filter bag. The second test used a filter bag where a given amount of debris was previously collected to verify that the defined methodology would not impact the debris bypass quantity collected in the filter. The bag was immersed in buffered/borated water until the filter was fully wet and then immersed in clean DI-water with extreme care to avoid collected debris from being removed from the bag. The filter was then dried out using the standard drying procedure previously described, and its weight was recorded at the end. Also in this case the final weight was found to be the same of the initial weight which confirmed that the methodology adopted did not impact the debris quantity collected by the filter. The methodology described was applied for all the filters used for the buffered/borated water tests. The measurements obtained during these preliminary tests are reported in Appendix C.

III.4. Debris size characterization

The general procedures followed during debris size analysis with microscopy-based techniques are illustrated in the flowchart in Figure III.4.1. [38]

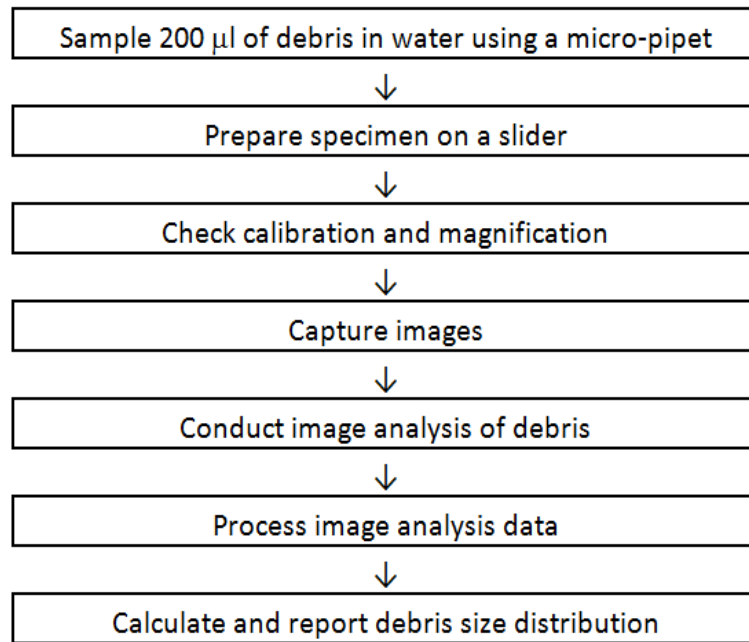


Figure III.4. 1. General procedures

Samples were prepared on a slide glass cleaned in three steps: DI water - Acetone – DI water. This cleaning procedure removed any dusts or particles on the slide glass. A cover slides then was applied with four 200um thick supporters to have that size of gap between slides as shown in Figure III.4.2.

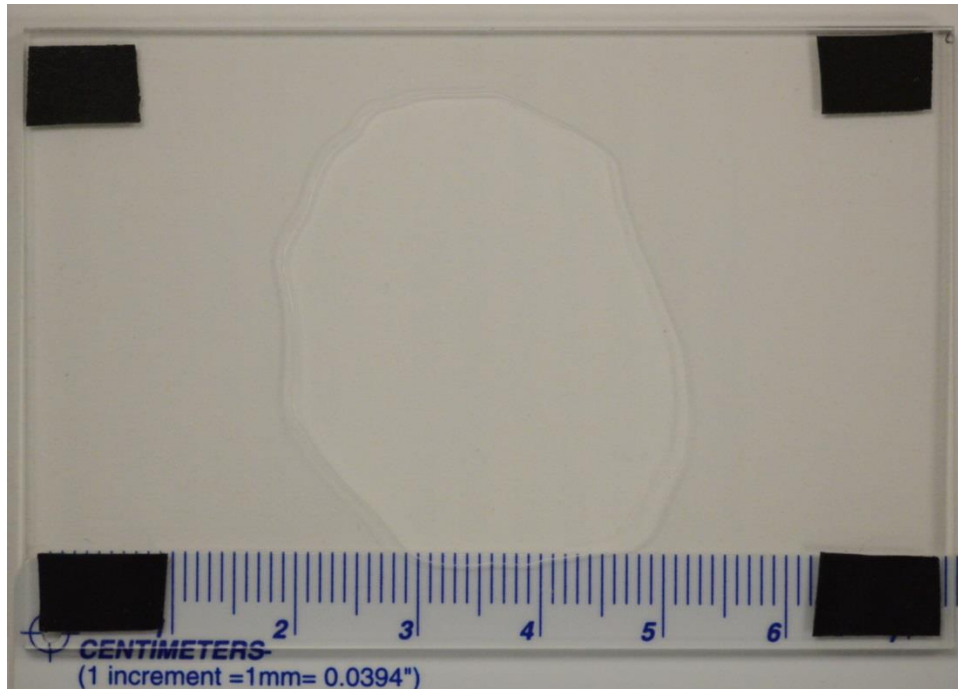


Figure III.4. 2. 200 micro-liter of wet debris sample on the slide glass

It allowed 200 micro-liter of sample to have 3.2cm by 3.2cm projection area. Each sample was taken from center of a 50 ml plastic tube after being well mixed. The sharp end of the pipet was cut to increase the opening size to be 5mm in order to suck in the fibers larger than 3mm. The capacity at 200 micro-liter setup with enlarged opening was checked with a 4 digit scale. 200 micro-liter of distilled water showed 0.2014g at room temperature.

CHAPTER IV

RESULTS AND ANALYSES*

The objectives of this research are categorized into (i) development of a modified head loss model of fibrous porous media generated from dilute suspended NUKON fiberglass debris, (ii) study on effects of debris concentration, approach velocity, temperature, water chemistry on quantity of debris bypass, (iii) development of a technique for size characterization of irregular shape debris. To develop a head loss model, the low temperature horizontal facility and the high temperature vertical facility were used. A compression model of NUKON fibrous bed was suggested to accurately predict build-up of the bed. Head loss was observed at different approach velocities and growth of debris bed was recorded. For the debris bypass, all three test facilities were used. Sensitivities of debris concentration, approach velocity, temperature, water chemistry on quantity of debris bypass were analyzed. To develop a protocol to measure the wide range of particle size with irregular shape, multiple techniques including an electric sensing zone system, a scanning electron microscope, and an automatized optical microscope were adopted. The main particle size distribution ranged in micrometers but the range of nanometers to millimeters was also obtained.

*Parts of this chapter are reprinted with permission from “Experimental study of head loss through an LOCA-generated fibrous debris bed deposited on a sump strainer for Generic Safety Issue 191” by Saya Lee et al., 2014, Progress in Nuclear Energy, 74, 166-175, Copyright [2014] by ELSEVIER.

IV.1. Head loss and compression of fibrous beds

A head loss model of fibrous beds is a function of thickness of the beds at given pressure drop. The model also contains a coefficient called Kozeny constant which is a function of porosity. By the definition in Equation (IV.1.1), porosity is calculated using the total volume of the fibrous porous media, V_{total} (m^3), and the volume of solid material, V_{solid} (m^3) in the fibrous porous media.

$$\varepsilon \equiv 1 - \frac{V_{solid}}{V_{total}} \quad (V_{solid} = \frac{M_{solid}}{\rho_{solid}}) \quad (IV.1.1)$$

where M_{solid} is the mass of the solid material (kg) and ρ_{solid} is the density of the solid material (kg/m^3). Therefore, the main parameters to measure or calculate are the thickness and the volume of the fibrous bed, pressured drop at the given thickness, and the quantity of fibrous material deposited on the bed. Approach velocity of fluid is another parameter of the head loss model, and in this study, it was used as a controlled parameter. Table IV.1.1 summarizes the tests conducted with different conditions.

Table IV.1. 1. List of head loss tests with different conditions

#	Test Facility	Strainer Type	Approach Velocity (cm/s)	NUKON Preparation	Number of Tests
PD-1	Horizontal	SPP	0.31	Shredder	1
PD-2	Horizontal	SPP	0.52	Shredder	1
PD-3	Horizontal	SPP	1.17	Shredder	1
PD-4	Horizontal	SPP	3.11	Shredder	2
PD-5	Horizontal	SPP	0.31	NEI	1
PD-6	Horizontal	SPP	0.52	NEI	3
PD-7	Horizontal	SPP	1.17	NEI	4
PD-8	Horizontal	SPP	3.11	NEI	2
PD-9	Horizontal	MPP	0.31	NEI	4
PD-10	Horizontal	MPP	0.52	NEI	2
PD-11	Horizontal	MPP	1.17	NEI	3
PD-12	Horizontal	MPP	3.11	NEI	3
PD-13	Vertical	SPP	0.31	NEI	1
PD-14	Vertical	SPP	3.11	NEI	1
PD-15	Vertical	MPP	0.31	NEI	1

IV.1.1. Thickness of fibrous beds

Thickness and porosity of fibrous beds were measured using an averaged bed thickness, L_{avg} defined in Equation (IV.1.2), to substitute the thickness, L , in Equation (I.4) as a characteristic thickness of the bed for non-uniformly deposited fibrous beds in the horizontal pipe,

$$L_{avg} = \frac{1}{N} \sum_{i=1}^N L_i \quad (IV.1.2)$$

where L_i is the measured fibrous bed thickness (m) at predefined location P_i from the strainer surface as shown in Figure IV.1.1. In this study, L_{avg} was calculated by averaging 10 measured points equally distributed which represented a linearly interpolated line (red dash line in Figure IV.1.1), thus, $N=10$.

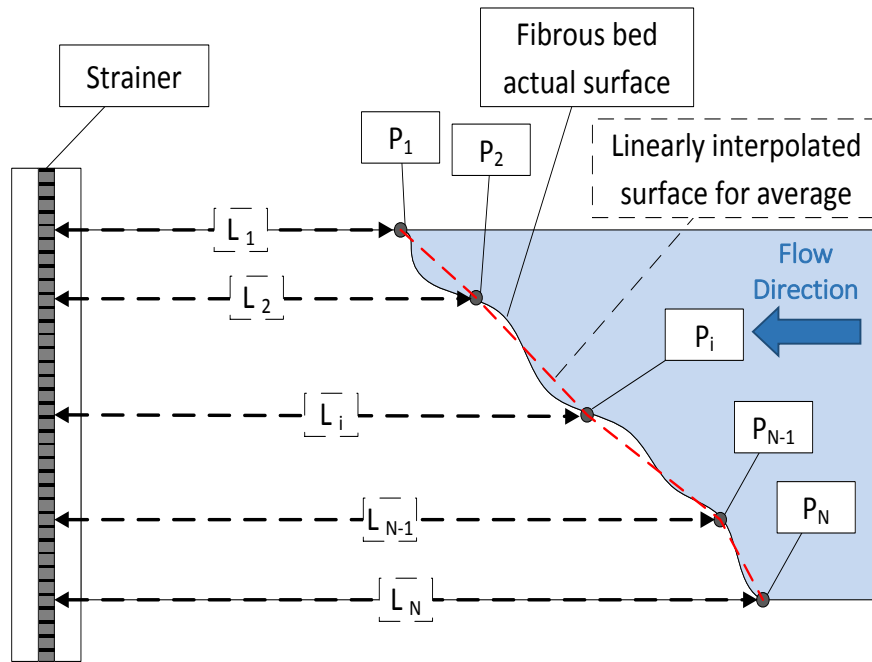
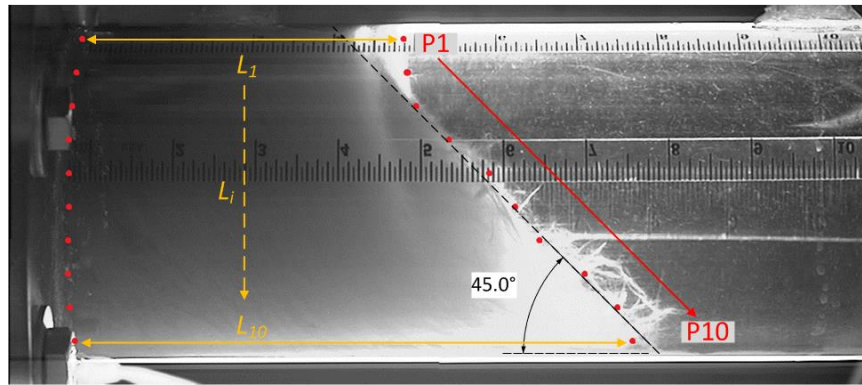
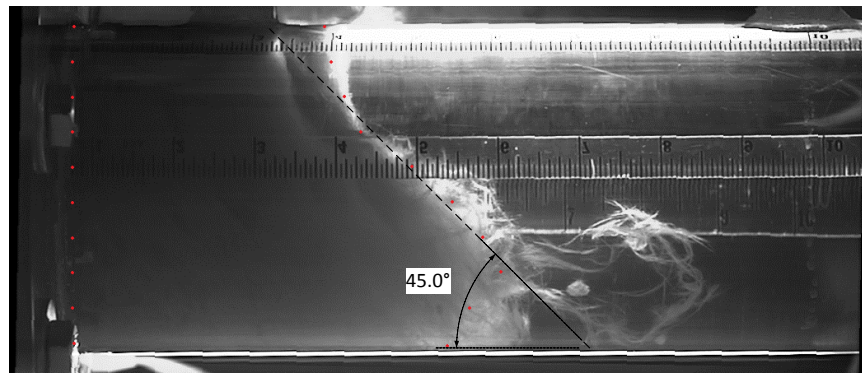


Figure IV.1. 1. Fibrous bed thickness measurement for shredder method tests

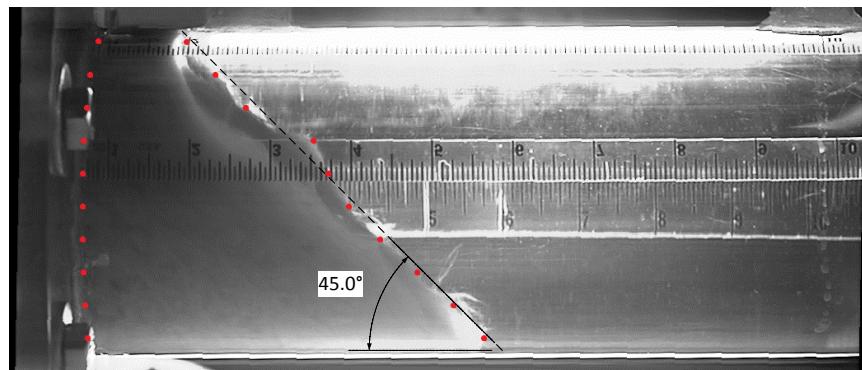
Figure IV.1.2 shows the fibrous beds generated using shredder method at steady state with bed thickness measurement points. Growth of the fibrous beds was recorded in Figure IV.1.3. Figure IV.1.4 shows the average debris bed thickness defined in Equation (IV.1.2) against time. Fibrous beds at higher approaching velocities developed quicker and reached thinner steady state thickness than lower approaching velocities. It means that higher approach velocity compresses the fibrous bed more than lower approach velocity.



(a) $U = 0.52 \text{ cm/s}$

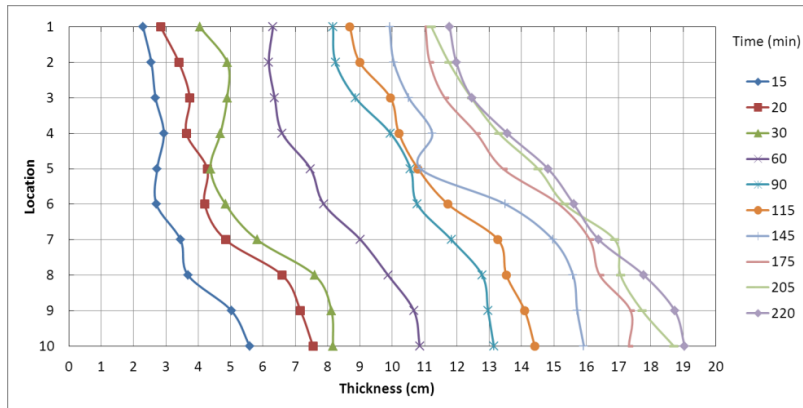


(b) $U = 1.17 \text{ cm/s}$

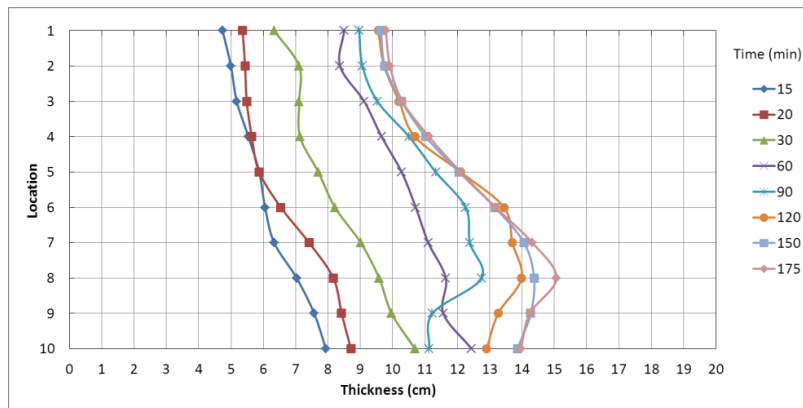


(c) $U = 3.11 \text{ cm/s}$

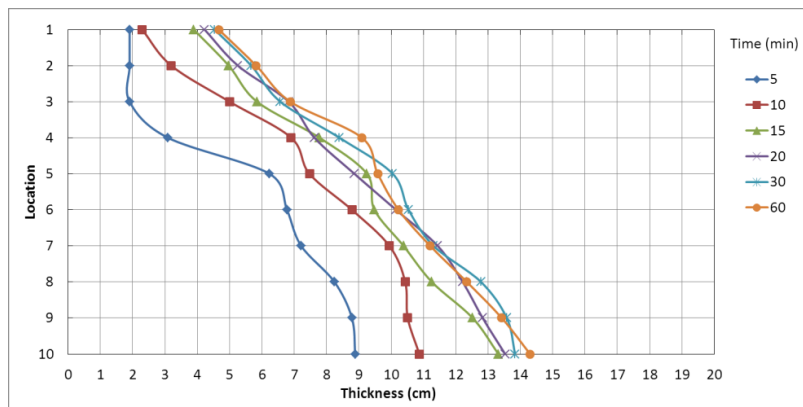
Figure IV.1. 2. Fibrous bed on the strainer at steady state for different approaching velocities - (a) 0.52 cm/s, (b) 1.17 cm/s, and (c) 3.11 cm/s



(a) $U = 0.52 \text{ cm/s}$



(b) $U = 1.17 \text{ cm/s}$



(c) $U = 3.11 \text{ cm/s}$

Figure IV.1. 3. Fibrous bed growth on the strainer at different approach velocities - (a) 0.52 cm/s , (b) 1.17 cm/s , and (c) 3.11 cm/s

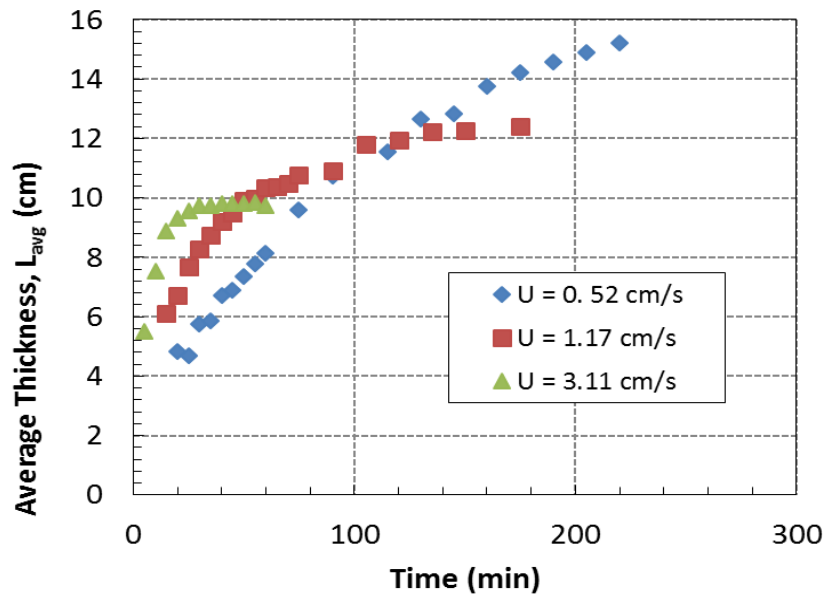
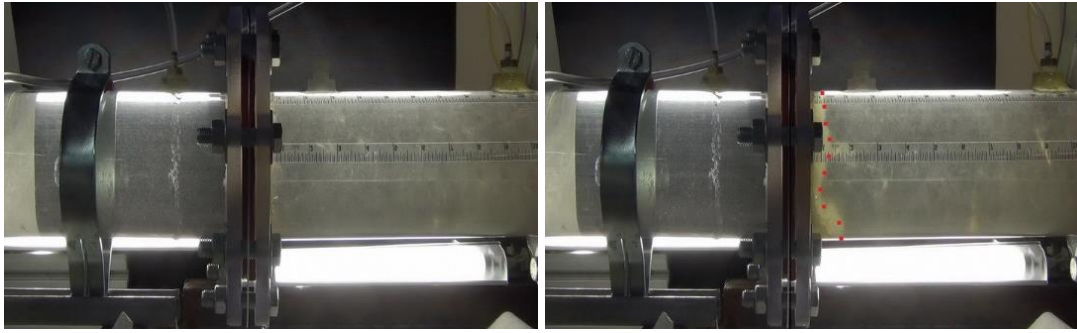


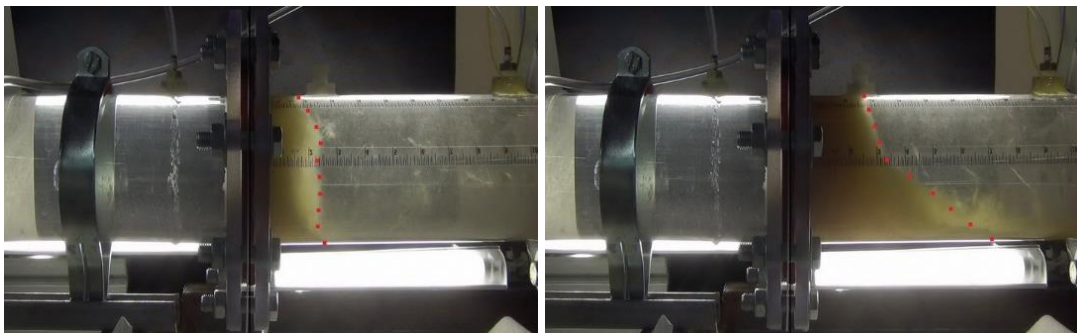
Figure IV.1. 4. Growth of fibrous bed at different approach velocities with 40g of NUKON prepared using shredder method

Figures IV.1.5 – IV.1.7 and IV.1.8 – IV.1.10 show the growth of debris beds prepared using NEI method. Figures IV.1.11 and IV.1.12 are the records of fibrous beds generated on the SPP strainer and the MPP strainer, respectively. When the approach velocities were the same, the two strainers showed similar buildup process and final thickness of the beds. At high approach velocities, the debris bed deposited with a stiffer surface angle and more compression. Figure IV.1.13 presents the change of average bed thickness. As shown for the debris bed with shredder method, higher approach velocities developed the beds more quickly and reached thinner steady state thickness than lower approach velocities. Compared to shredder method, NEI preparation resulted in a thicker fibrous bed at lower approaching velocity of 0.52 cm/s. At higher approach velocities of 1.17 cm/s and 3.11 cm/s resulted in similar bed thickness.



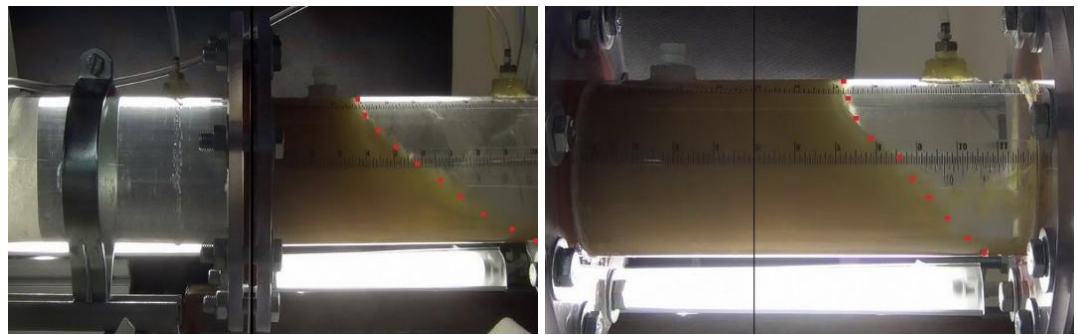
(a) 5 min

(b) 10 min



(c) 20 min

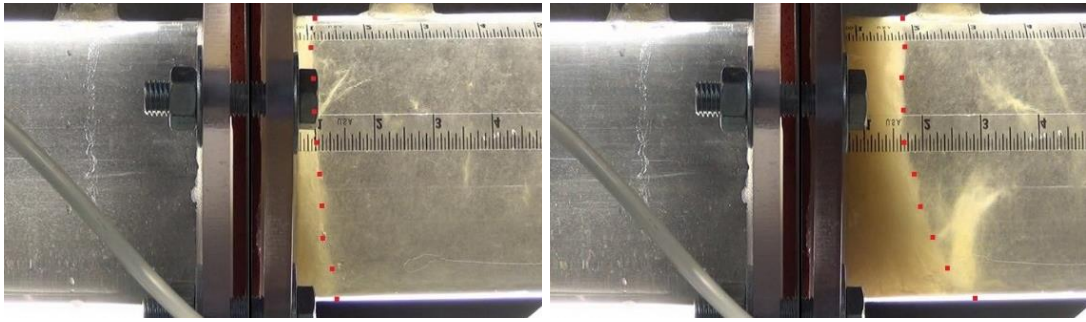
(d) 45 min



(e) 90 min

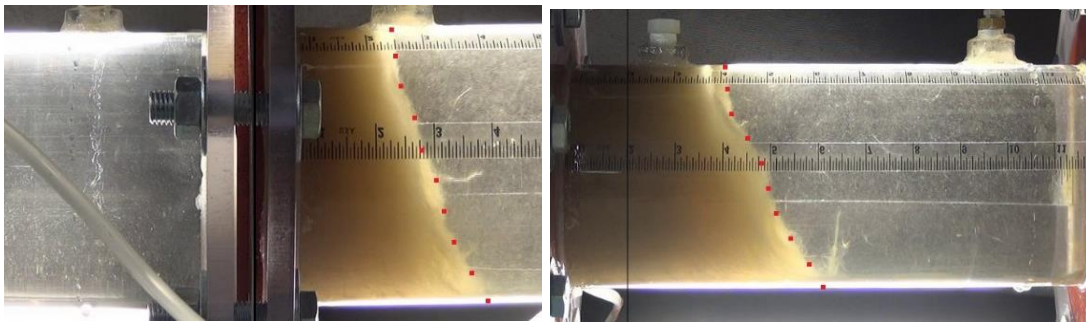
(f) 900 min

Figure IV.1. 5. Build-up of fibrous debris bed on the strainer, at $U = 0.52$ cm/s



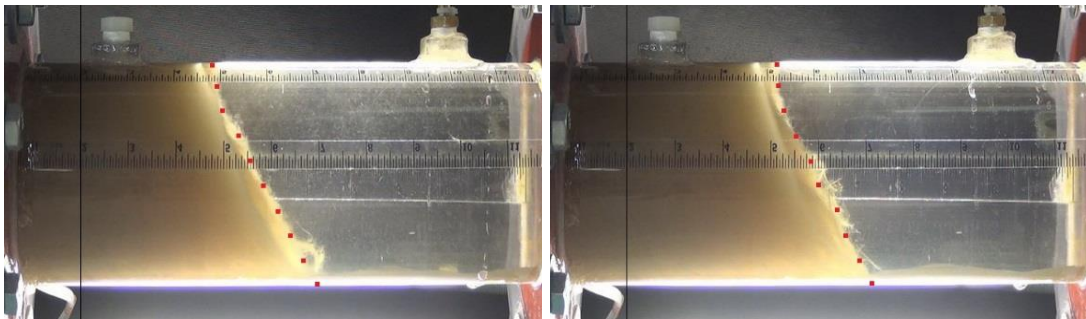
(a) 5 min

(b) 10 min



(c) 20 min

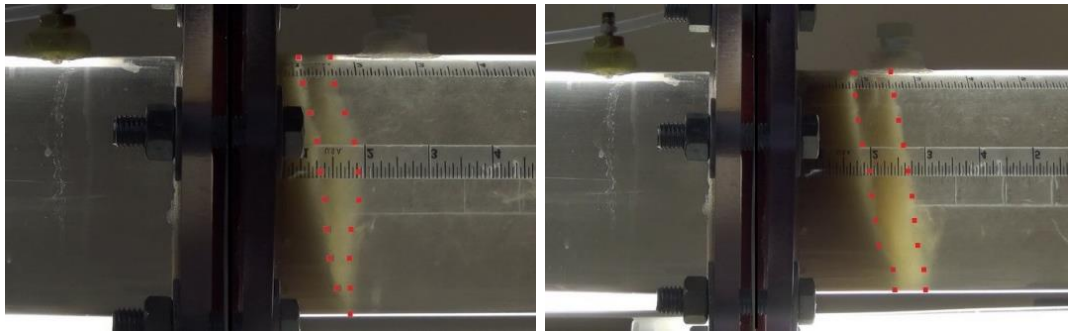
(d) 45 min



(e) 90 min

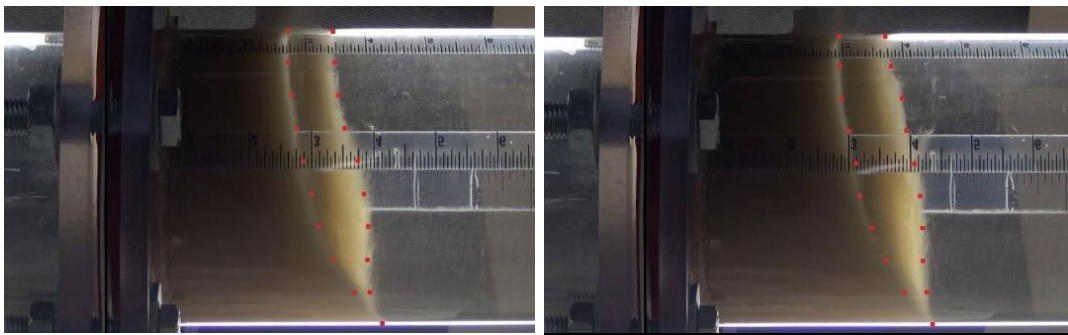
(f) 780 min

Figure IV.1. 6. Build-up of fibrous debris bed on the strainer, at $U = 1.17$ cm/s



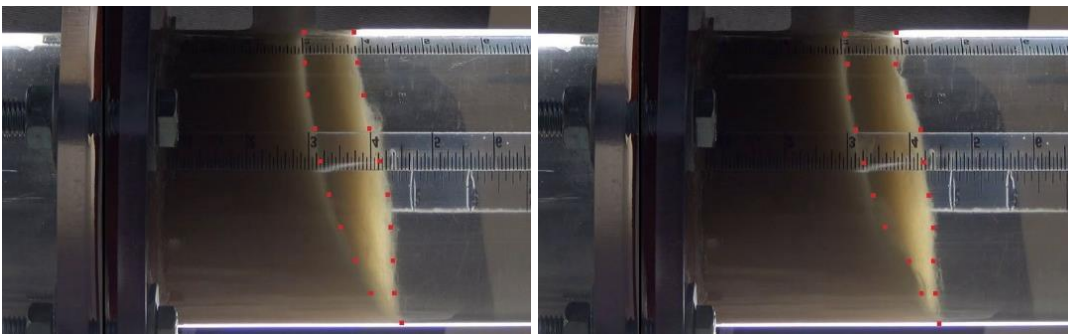
(a) 5 min

(b) 10 min



(c) 20 min

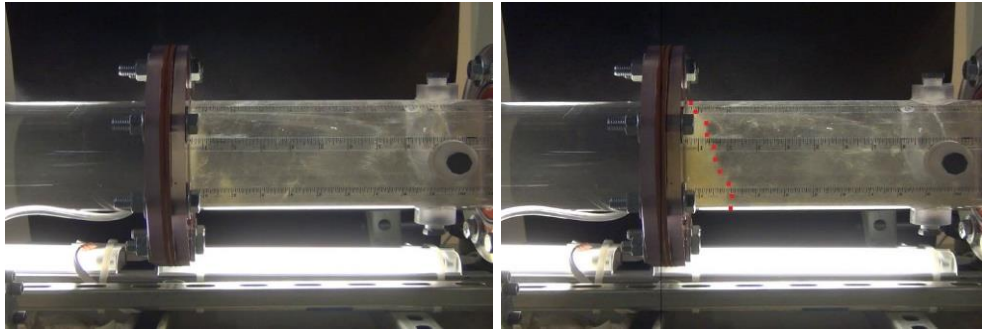
(d) 30 min



(e) 40 min

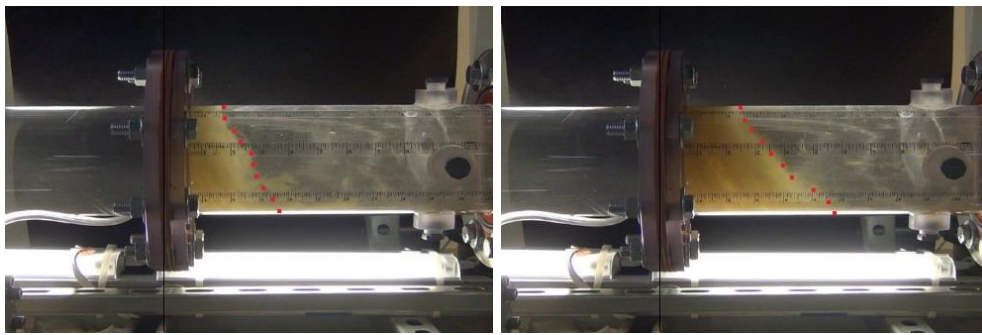
(f) 180 min

Figure IV.1. 7. Build-up of fibrous debris bed on the strainer, at $U = 3.11$ cm/s



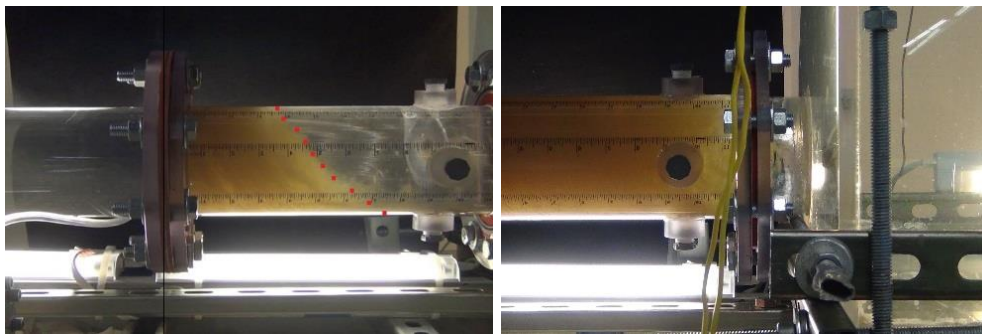
(a) 5 min

(b) 10 min



(c) 20 min

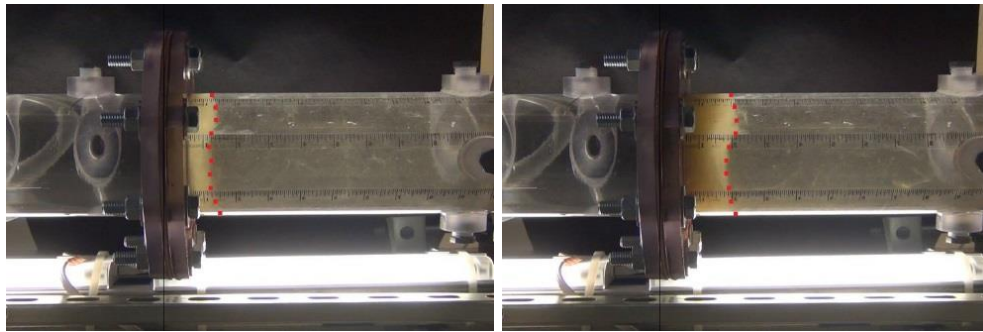
(d) 40 min



(e) 60 min

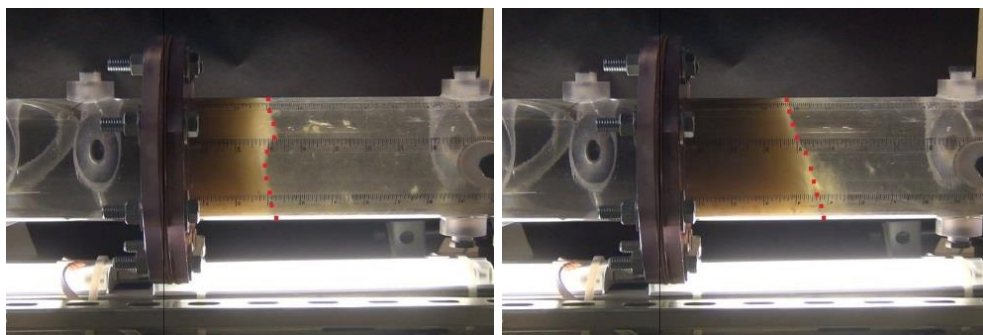
(f) 780 min

Figure IV.1. 8. Build-up of fibrous debris bed on the MPP strainer, at $U = 0.31$ cm/s



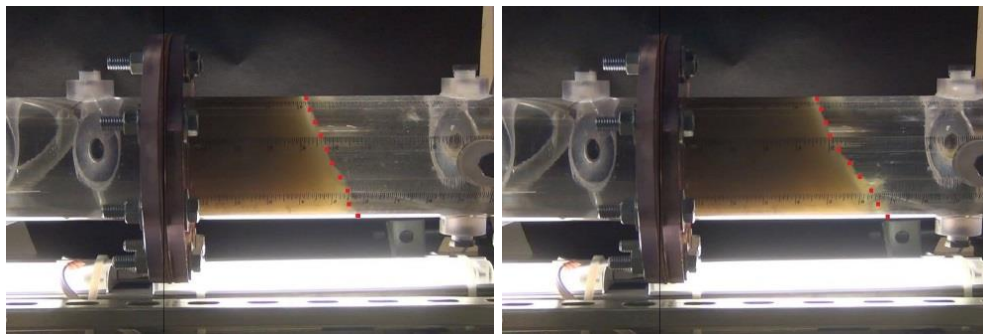
(a) 5 min

(b) 10 min



(c) 20 min

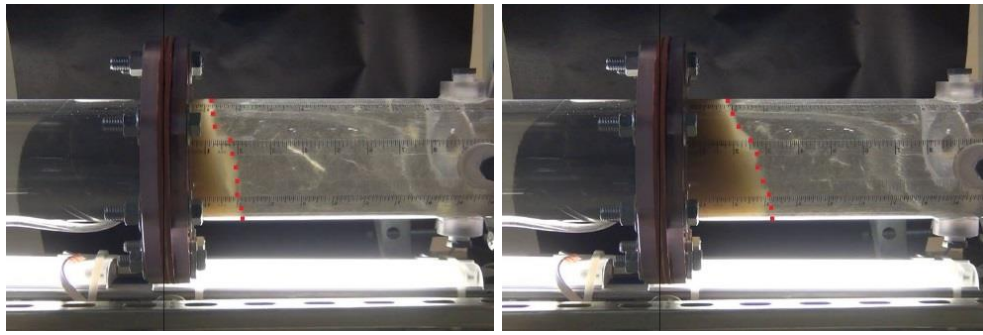
(d) 40 min



(e) 60 min

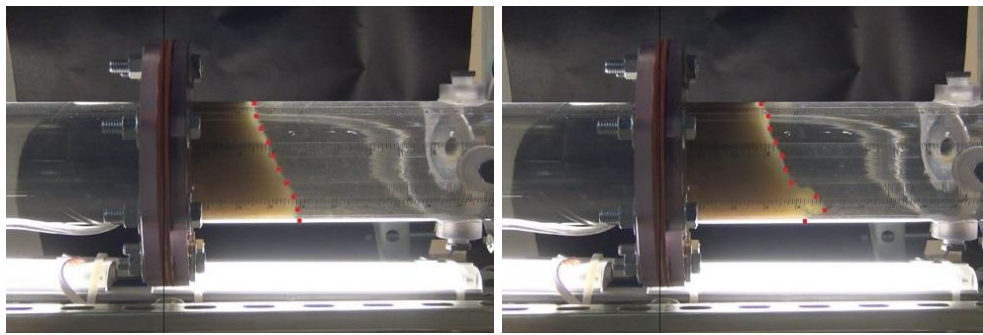
(f) 760 min

Figure IV.1. 9. Build-up of fibrous debris bed on the MPP strainer, at $U = 1.17$ cm/s



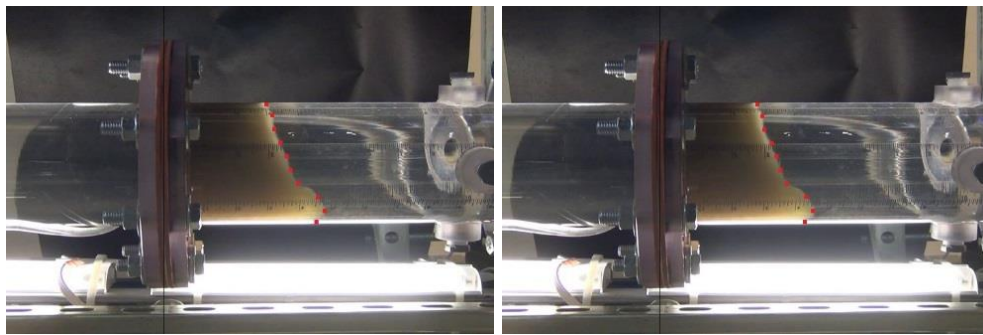
(a) 5 min

(b) 10 min



(c) 20 min

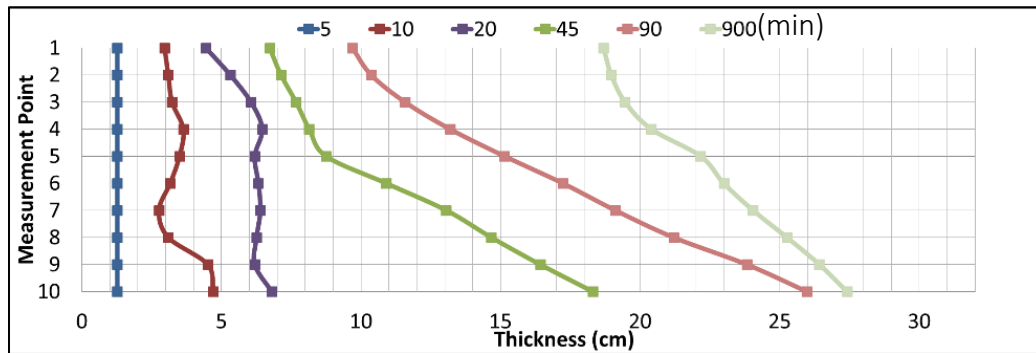
(d) 40 min



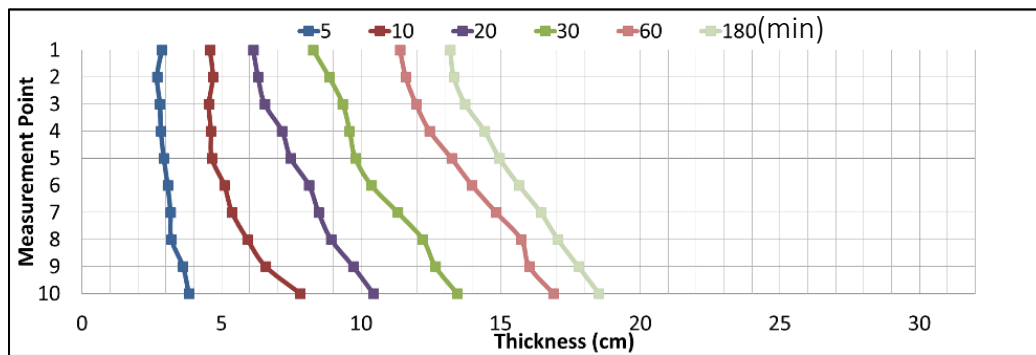
(e) 60 min

(f) 760 min

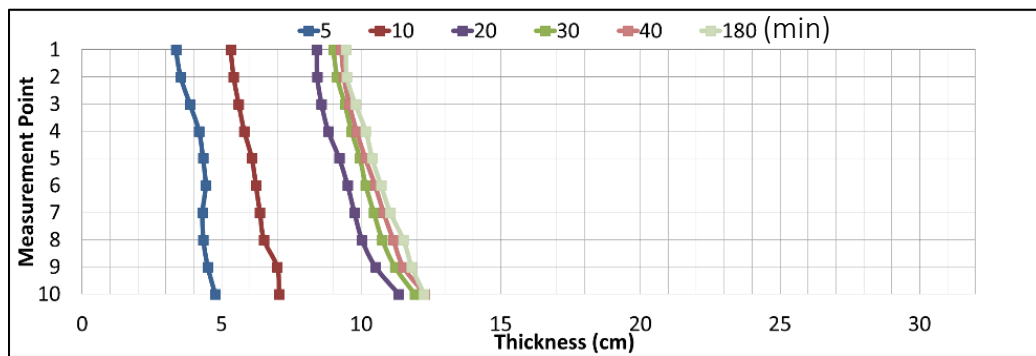
Figure IV.1. 10. Build-up of fibrous debris bed on the MPP strainer, at $U = 3.11$ cm/s



(a) $U = 0.52$ cm/s

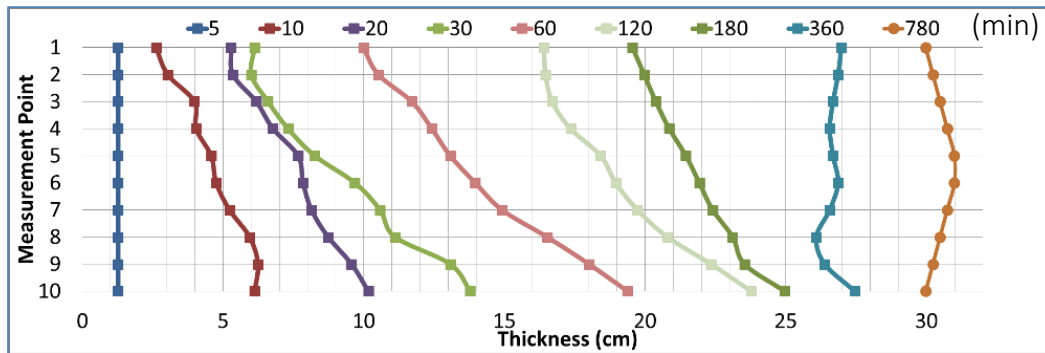


(b) $U = 1.17$ cm/s

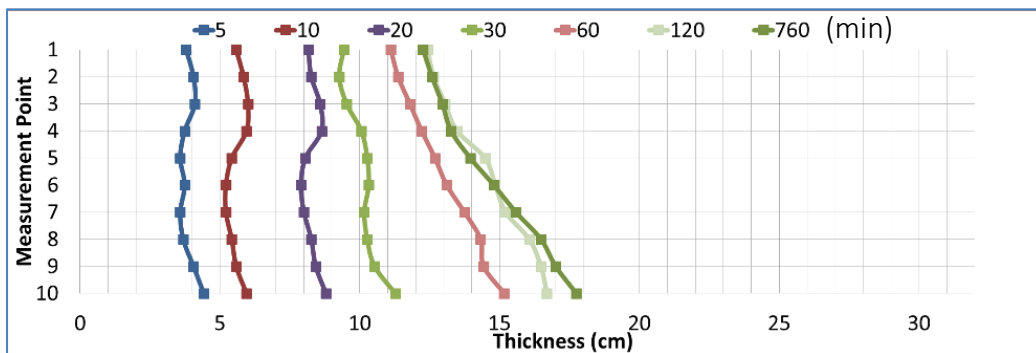


(c) $U = 3.11$ cm/s

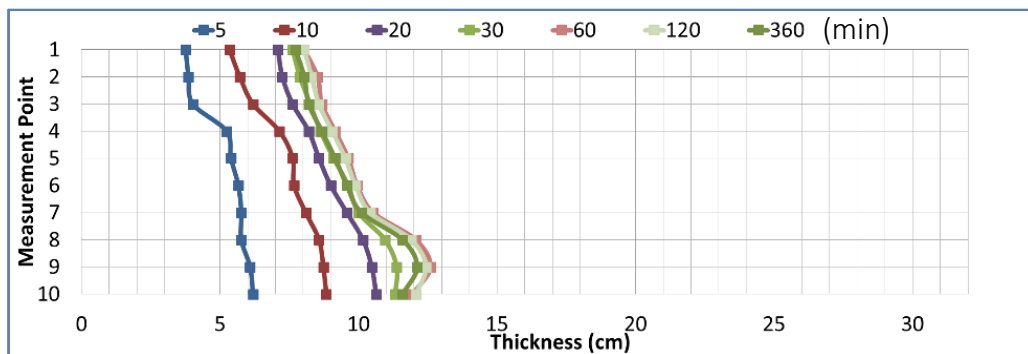
Figure IV.1. 11. Measurement of fibrous debris bed growth for each approaching velocity on the SPP strainer



(a) $U = 0.31$ cm/s



(b) $U = 1.17$ cm/s



(c) $U = 3.11$ cm/s

Figure IV.1. 12. Measurement of fibrous debris bed growth for each approaching velocity on the MPP strainer

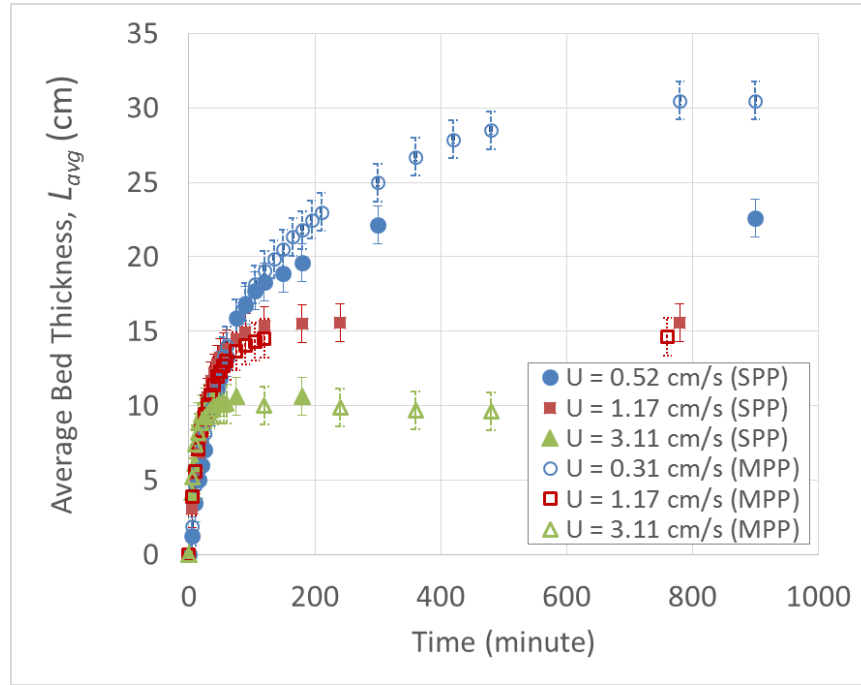


Figure IV.1. 13. Average bed thickness of the fibrous beds with NEI preparation

IV.1.2. Porosity of fibrous beds

The fibrous bed volume was measured using the average bed thickness and surface area of the strainer. The mass of the fibers on the strainer was calculated using Equation (IV.3).

$$M_{s,t} = M_0 \left[1 - e^{-\frac{AUC_f t}{V_r}} \right] \quad (IV.1.3)$$

where $M_{s,t}$ is the quantity (kg) of NUKON on the strainer at time t (s), M_0 is the initial quantity (kg) of NUKON in the tank, A is the surface area of the strainer (m^2), U is the

approaching velocity (m/s), C_f is the filtration efficiency, and V_t is the volume of water in the tank (m^3). It was assumed that the debris in the tank was uniformly mixed.

Constant flow rate was applied and the filtration efficiency was assumed to be 1.

Porosity of the fibrous bed was calculated using Equation (IV.1.4) and the quantity of fibers from Equation (IV.1.3). The result over the period of fibrous bed accumulation for each approaching velocity was plotted in Figure IV.1.14.

$$\varepsilon = \frac{AL_{avg} - M_{s,t} / \rho}{AL_{avg}} = 1 - \frac{M_{s,t}}{AL_{avg} \rho} \quad (IV.1.4)$$

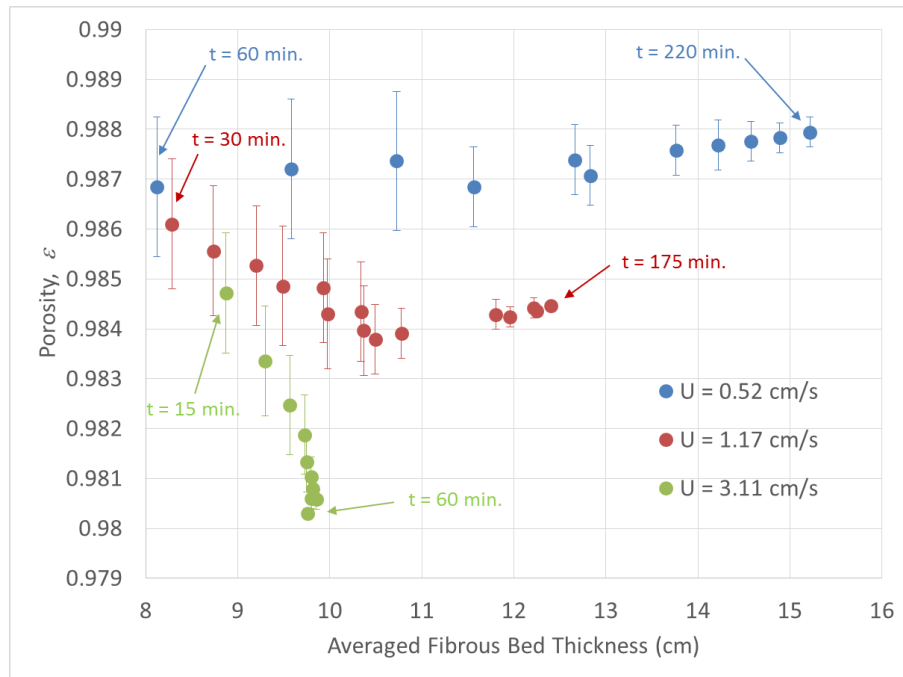


Figure IV.1. 14. Porosity change over the period of fibrous debris accumulation on the SPP strainer with shredder method

This figure shows that higher approach velocity caused greater compression resulting in lower porosity. The highest approaching velocity which is in the transient region produced continuous compression, while two tests performed in the viscous region reached more or less steady state. These results have an important implication for future work that the approaching velocity must be carefully determined during fibrous bed generation on the strainer when the fibrous bed preparation is a separate process from the main experiments such as pressure drop measurement and debris penetration tests. Several experimental studies on chemical effects [35, 36, 39, and 40] produced the fibrous beds at higher approaching velocity (3~6 cm/s) in their vertical flow loops to prevent settling by gravity in advance to the chemical effect measurements. Since the internal structure of the fibrous beds in those experiments might be different from one prepared at a prototypical approaching velocity, an experiment with a fibrous bed formed at low approaching velocity would provide an important comparison in mixture beds with particles or chemicals. Figure IV.1.15 exhibits the average porosity calculated using Equations (IV.1.3) and (IV.1.4) as a function of time. As the debris bed thickened, greater pressure drop occurred, in which the debris bed was more compressed. This trend is more clearly observed at higher approaching velocity. Because of this recursive effect between pressure and compression, the average bed thickness did not linearly increase as the debris transported to the strainer, as shown in Figure IV.1.13. The uncertainty of porosity was calculated using the uncertainties of debris quantity on the strainer and thickness measured. The details are presented in section IV.1.5.

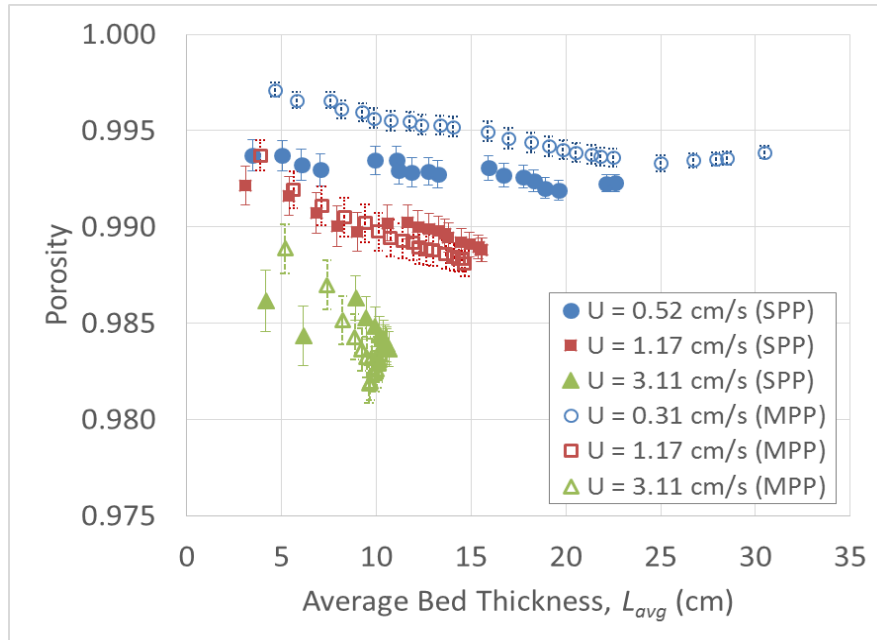


Figure IV.1. 15. Porosity vs. quantity of debris with NEI method

IV.1.3. Head loss through fibrous beds

The pressure drop through the fibrous beds prepared using shredder method is plotted for different approaching velocities in Figure IV.1.16. Pressure drop was measured for more than 18 hours until it reached at steady state. Head loss with bed thickness at the three approaching velocities was plotted in Figure IV.1.17. Two lower approaching velocities, 0.5188 cm/s and 1.1673 cm/s, showed linear pressure drop with thickness increment; however the highest one, 3.1128 cm/s, showed non-linear increment caused by compression.

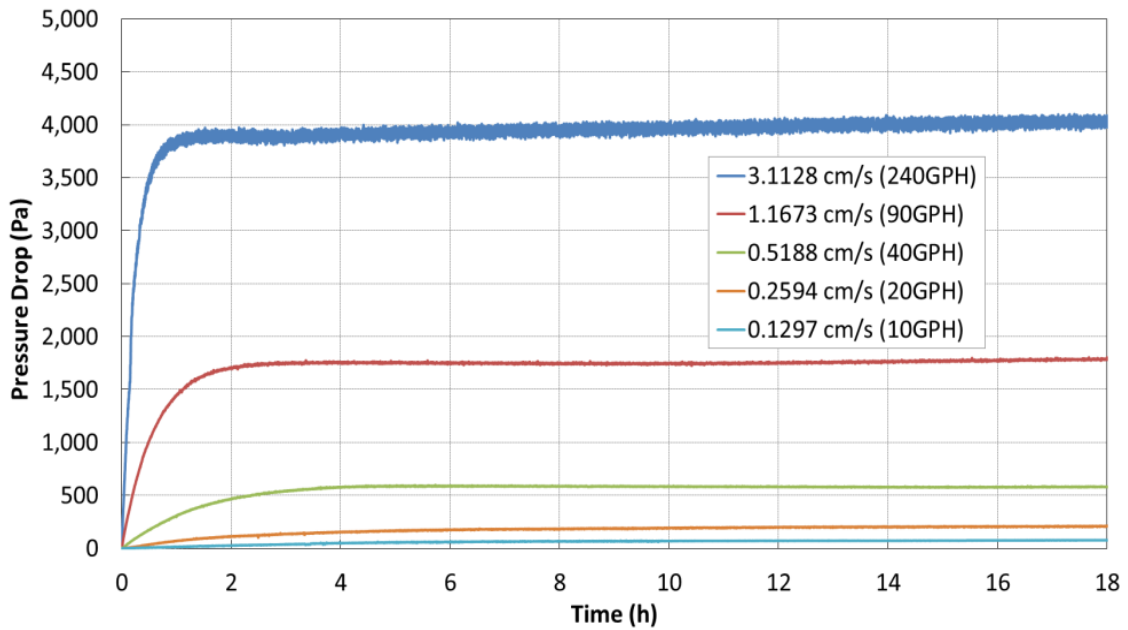


Figure IV.1. 16. Pressure drop vs. time with shredder method

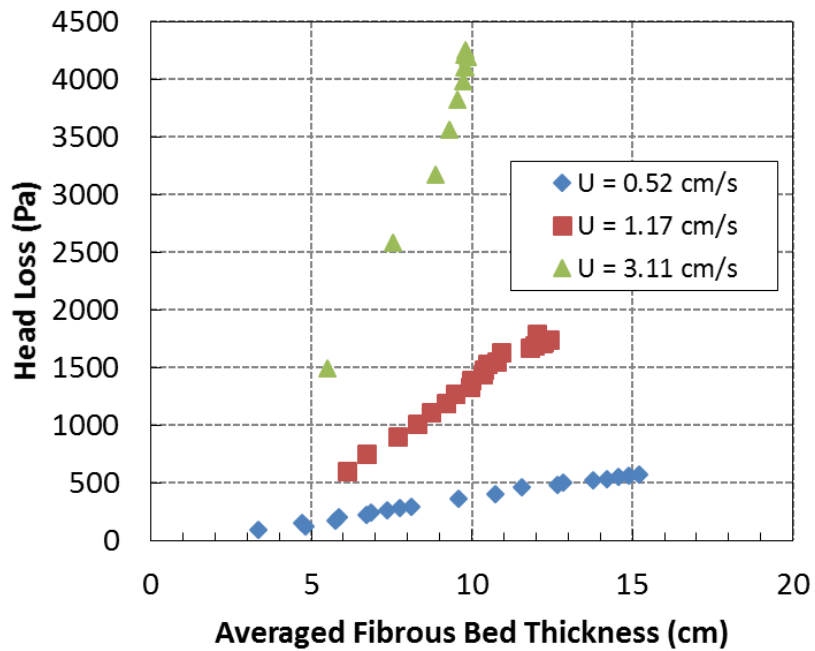


Figure IV.1. 17. Pressure drop vs. averaged fibrous bed thickness at different approach velocities with shredder method

A set of Kozeny constants shown in Figure IV.1.18 was obtained using the bed thickness measured in Figure IV.1.4 and the pressure drop in Figure IV.1.17 with Equation (IV.1.2). Based on these experimental data, new coefficients 1.9 and 125 for a and b , respectively, in Equation (IV.1.5) were suggested to modify Davies' and Ingmanson et al.'s correlations in Eq. (I.6).

$$k = 1.9 \frac{\varepsilon^3}{(1-\varepsilon)^{0.5}} \left[1 + 125(1-\varepsilon)^3 \right] \quad (\text{IV.1.5})$$

Another model was proposed by modifying Lord's model in Eq. (IV.1.6) with $\alpha = 1.41$, since the result showed better agreement with the data of Lord [7], Brown [39], and Wiggins et al. [40] rather than those of Ingmanson et al [20].

$$k = \frac{1}{0.903} \frac{(1-\varepsilon)^{\alpha-2}}{\varepsilon^3} \quad (\text{IV.1.6})$$

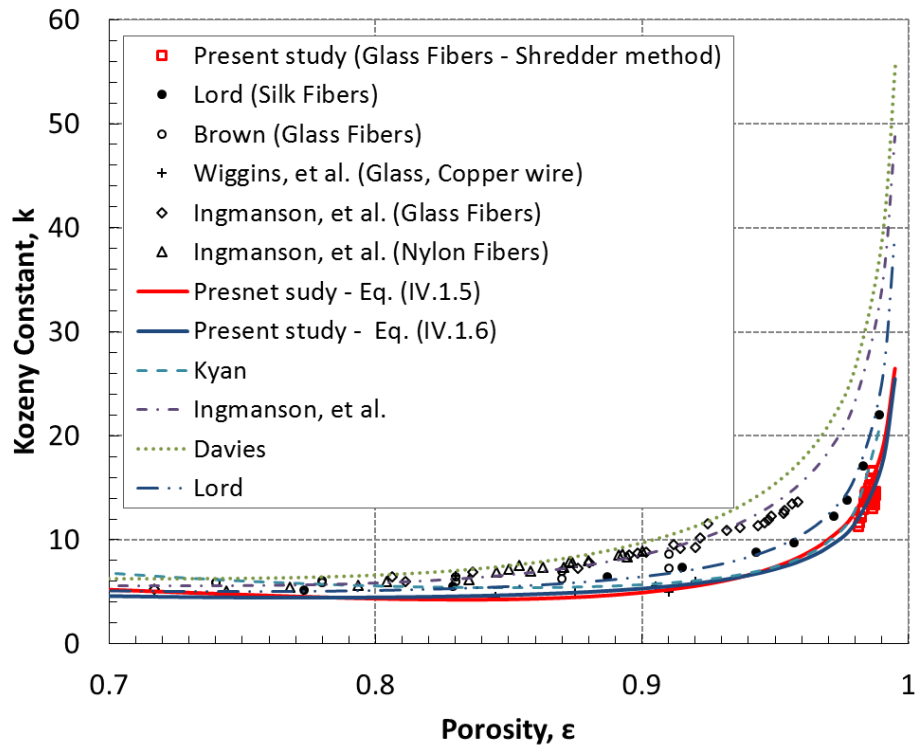


Figure IV.1. 18. Kozeny constant, k vs. Porosity, ϵ for NUKON samples prepared using shredder method in the horizontal test facility (lines - correlations / marks -experimental data)

Experimentally, the Kozeny constant is a function of specific surface area in addition to porosity, while the theoretical model suggested a function of porosity alone. When a fibrous bed material is assumed to be cylindrical, specific surface area of the fiber is to be $4/D_f$. The present study used the specific surface area, $571,428 \text{ m}^{-1}$, calculated using the diameter, $7.0 \text{ }\mu\text{m}$, reported in NEI 04-07[40]. This was in better agreement with other results than with results proposed in NUREG-1862 [25] for the specific surface area. The authors of NUREG-1862 recommended new specific surface area values which achieved reasonable head loss prediction while maintaining the other

parameters and the formulation of the Kozeny constant model. However the suggested specific surface area resulted in a significant difference from those reported by other researchers listed in Table II. One of the reasons of this difference is attributed to the limitations of Happel's theoretical model, used in the NUREG-1862 head loss model. The Happel's model was developed for a perpendicular flow across cylinders, which resulted in overestimation for randomly deposited fibrous beds. Also, Happel's model assumed uniform pore size which is the result of bulk compression, however, the fibrous bed generated from suspended debris is mainly compressed in the flow direction which maintains the larger pore size compared to the assumed uniform pore size. Although NUKON is a kind of glass fiber, the obtained Kozeny constants showed better agreement with silk and cotton fibers which have similar fiber diameters, than they showed with the large diameter glass fibers in Ingmanson et al.'s data. This result arises from the fact that fiber diameter affected Kozeny constant in addition to specific surface area and porosity.

Table IV.1. 2. Kozeny constant and permeability of fibrous porous media

Author (Year)	D_f (m)	S_v (m ⁻¹)	K (m ²)	K/D_f^2	k	ε	Re_m	Material	Fluid
Davies	N/Q	N/Q	N/Q	N/Q	38.8 27.6	0.99 0.98	<100	M, R, K Dw, Gw	Air
Ingmans on et al.	16.5 x10 ⁻⁶	242000	0.54 x10 ⁻⁹	1.99	13.5	0.955	<22	Gf	Air
	N/A	N/A	N/A	N/A	28.4 ^m 31.4 ^m	0.986 0.9884	<71* <86*		
Lord	9.73 x 10 ^{-6*}	410997	2.04 x10 ⁻⁹	21.5	22.0	0.9887	<4	Si	Air
			1.14 x10 ⁻⁹	12.0	17.1	0.9830			
	2.91 x10 ⁻¹⁰	3.1	9.77	0.9573					
	11.6 x 10 ^{-6*}	344827	3.41 x10 ⁻⁹	25.5	17.9	0.9885	<5	Co	
Kyan et al. ^[42]	8 x 10 ⁻⁶	500000	6.84 x10 ^{-11*}	1.07	6.92	0.919	6	Gf	Water
Brown ^[39]	92 x 10 ⁻⁶	43478	7.10 x10 ⁻⁹	0.839	7.3	0.912	<11	Gw	Air
Wiggins ^[38]	7 x 10 ⁻⁶	571428	0.51 x10 ⁻¹⁰	1.035	9.9	0.930	114	Gf	Water
Marmore t et al. ^[1]	13 x 10 ⁻⁶	307692	2.69 x10 ⁻¹⁰	1.592	38.7	0.9696	<164	Gw	Air
	14 x 10 ⁻⁶	285714	3.36 x10 ⁻¹⁰	1.714	15.1	0.9542	<112		
Crawford et al. ^[41]	40 x 10 ⁻⁶	100000	2.8 x10 ⁻⁸	17.5	34.7	0.99	N/Q	Pe	Air
	13 x 10 ⁻⁶	307692	6.2 x10 ⁻⁹	36.7	16.5	0.99	N/Q		
	10 x 10 ⁻⁶	400000	5.3 x10 ⁻⁹	53	11.4	0.99	N/Q		
NUREG- 1862	7.1 x 10 ^{-6**}	984252	1.42 x10 ⁻¹⁰	2.81	14.0	0.978	2.1	Gw	Water
	7.1 x 10 ^{-6**}	984252	6.98 x10 ⁻¹¹	1.38	12.3	0.967	6.9		
NUREG/ CR- 6917 ^[43]	7.1 x 10 ^{-6**}	562430	1.42 x10 ⁻¹⁰	2.81	42.8	0.978	2.1		
	7.1 x 10 ^{-6**}	562430	6.98 x10 ⁻¹¹	1.38	37.5	0.967	6.9		
NUREG- 1862	7.1 x 10 ^{-6**}	562430	3.62 x10 ⁻¹⁰	7.16	42.7*	0.986**	16.2	Gw	Water
	7.1 x 10 ^{-6**}	562430	3.62 x10 ⁻¹⁰	7.16	10.2*	0.972**	8.1		
NUREG/ CR- 6874 ^[44]	7.1 x 10 ^{-6**}	984252	3.62 x10 ⁻¹⁰	7.16	13.9*	0.986**	16.2		
	7.1 x 10 ^{-6**}	984252	3.62 x10 ⁻¹⁰	7.16	3.4*	0.972**	8.1		
NUREG/ CR-6224 NUREG/ CR- 6367 ^[45]	7.1 x 10 ⁻⁶	562430	4.02 x10 ⁻¹⁰	7.95	38.4	0.986	44.2	Gw	Water
	7.1 x 10 ⁻⁶	562430	4.92 x10 ⁻¹⁰	9.72	20.4	0.986	18.3		
	7.1 x 10 ⁻⁶	562430	4.02 x10 ⁻¹⁰	7.95	9.2	0.972*	22.1		
	7.1 x 10 ⁻⁶	562430	3.78 x10 ⁻¹⁰	7.48	9.8	0.972*	9.2		
	7.1 x 10 ⁻⁶	984252	4.02 x10 ⁻¹⁰	7.95	12.6	0.986	44.2		
	7.1 x 10 ⁻⁶	984252	4.92 x10 ⁻¹⁰	9.72	3.1	0.986	18.3		
	7.1 x 10 ⁻⁶	984252	4.02 x10 ⁻¹⁰	7.95	1.6	0.972*	22.1		
	7.1 x 10 ⁻⁶	984252	3.78 x10 ⁻¹⁰	7.48	3.2	0.972*	9.2		
Present Study	7.0 x 10 ^{-6***}	571428	1.15x10 ⁻⁹	23.40	19.0	0.9884	18.7	Gw	Water
	7.0 x 10 ^{-6***}	571428	8.03 x10 ⁻¹⁰	16.39	13.8	0.9838	5.0		
	7.1 x 10 ^{-6**}	562430	1.2 x10 ⁻⁹	22.75	19.2	0.9884	18.9		
	7.1 x 10 ^{-6**}	562430	8.3 x10 ⁻¹⁰	15.93	14.3	0.9838	5.1		
	7.1 x 10 ^{-6**}	984252	1.2 x10 ⁻⁹	22.75	6.4	0.9884	18.9		
	7.1 x 10 ^{-6**}	984252	8.3 x10 ⁻¹⁰	15.93	4.7	0.9838	5.1		

N/A: not applicable, N/Q: not quoted

Gf: Glass fiber, Gw: Glass wool, Go: Goat wool, M: Merino cotton, R: Rayon, K: kapok, Dw: Down, Pe: Polyester
Co: Cotton, Si: Silk

* Calculated from the parameters found in the article, ** Value from NUREG/CR-6224, *** Value from NEI-04-07

^m Value calculated the model in the article

Crawford et al.'s [41] data showed clearly that smaller fiber diameter leads to smaller Kozeny constant in the same material, although it was not clear for different materials found in different researchers' data. Since no significant pressure drops by inertia effects were found, the modified Ergun's model was applied for the second order term of approaching velocity, U and a modified correlation of head loss for NUKON fibrous bed prepared using shredder method is proposed in Equation (IV.1.7) with $\alpha = 1.41$.

$$\frac{\Delta P}{\Delta L} = -\frac{1}{0.903} \frac{(1-\varepsilon)^\alpha}{\varepsilon^5} S_v^2 \mu U + 0.66 S_v \frac{(1-\varepsilon)}{\varepsilon^3} \rho_w U^2 \quad (\text{IV.1.7})$$

Head loss at different approaching velocities was predicted using Equation (IV.1.7), and the comparison to the experimental data and predicted values by other researchers was provided in Figure IV.1.19. Equation (IV.1.7) predicted the head loss close to the experimental data at low Re_m (at $U < 3.1128$ cm/s), then approached to the NUREG/CR-6224 model when $U > 50$ cm/s.

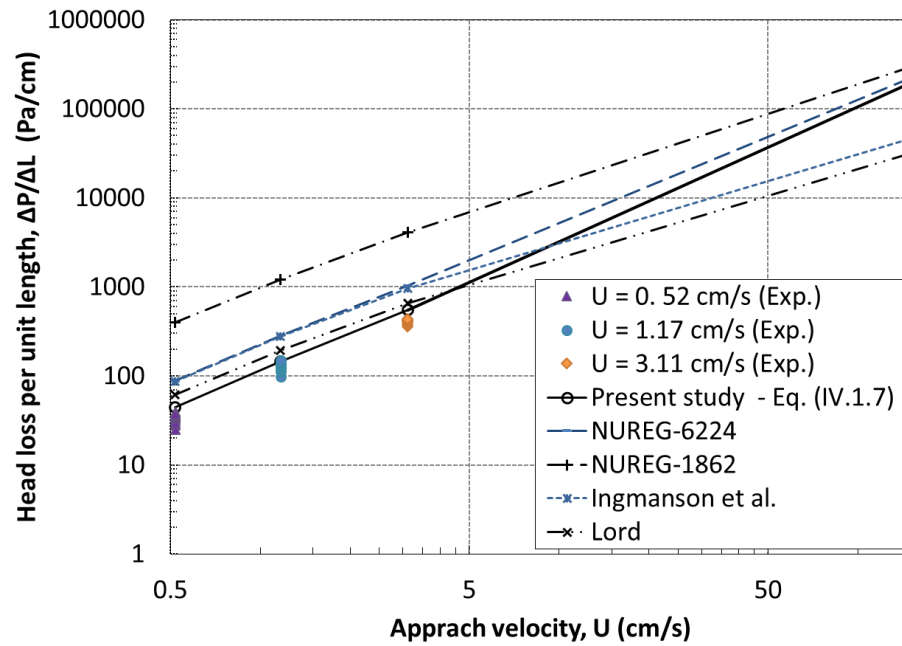


Figure IV.1. 19. Head loss prediction and comparison with experimental data

For the fibrous debris prepared using NEI method, pressure drop was measured for longer than 16 hours at four different approach velocities: 3.11 cm/s, 1.17 cm/s, 0.52 cm/s, and 0.31 cm/s. For the approaching velocities of 3.11 cm/s and 1.17 cm/s, the results from two strainers were presented in Figure IV.1.20, and the pressure drop of the SPP strainer at 0.52 cm/s and the pressure drop of the MPP strainer at 0.31 cm/s were presented in Figure IV.1.21.

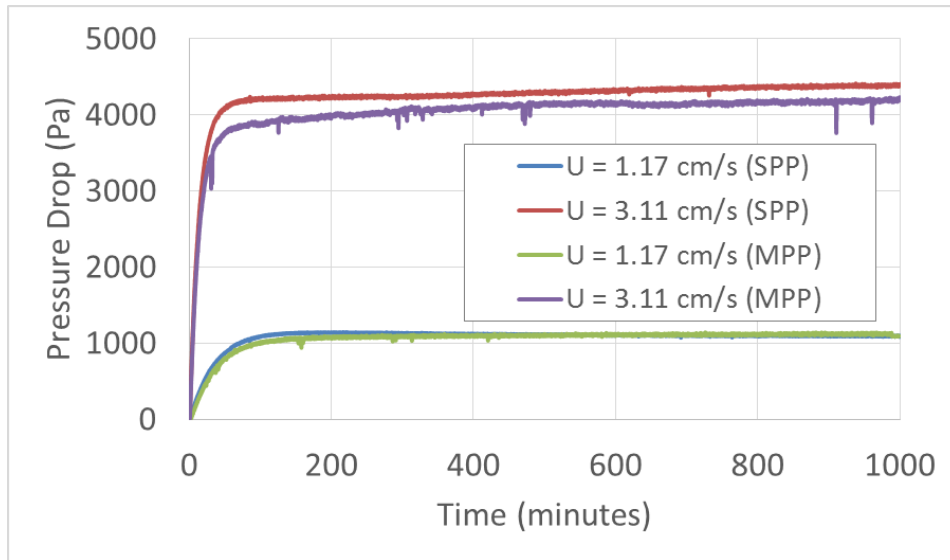


Figure IV.1. 20. Pressure drop results at 1.17cm/s and 3.11 cm/s

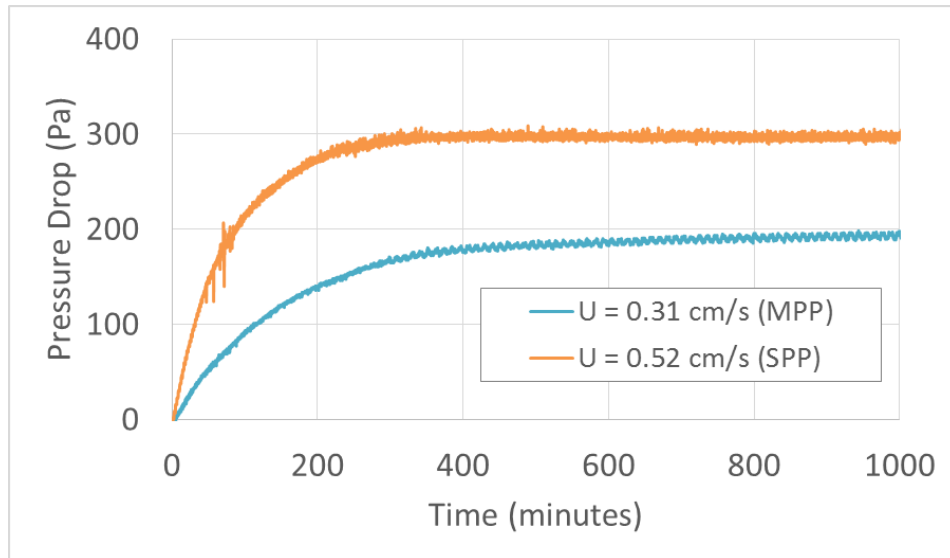


Figure IV.1. 21. Pressure drop results at 0.31 cm/s and 0.52 cm/s

The Kozeny constant was calculated in Figure IV.1.22 using the parameters previously obtained at $U=0.31$ cm/s and $U=0.52$ cm/s ($1.7 < Re_m < 2.8$). The results from both strainers followed the model proposed in Eq. (IV.1.6) which was developed for NUKON fibrous debris prepared using shredder method introduced in NUREG/CR-6224 [12].

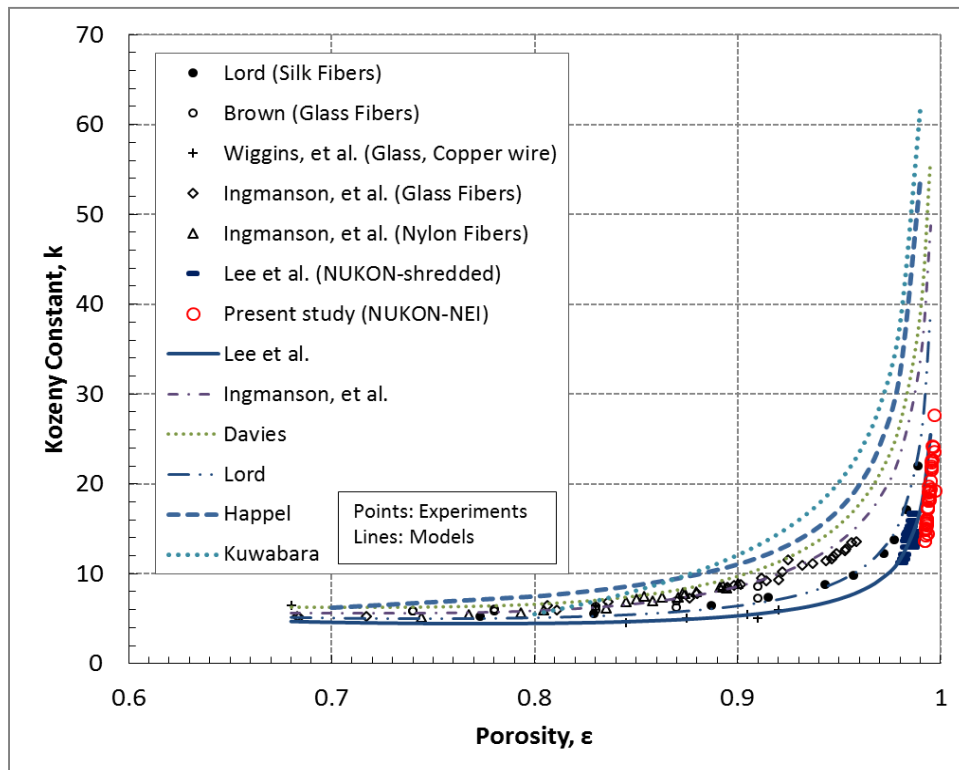


Figure IV.1. 22. Kozeny constant for NEI samples in the horizontal test facility

Davies' and Ingmanson et al.'s models overestimated the results in the present test conditions. Ingmanson et al. used fibers, approximately $20 \mu\text{m}$ in diameter, and their experimental data showed smaller Kozeny constant which means less head loss than Davies' model. The present experiment was conducted with fibers of $7\mu\text{m}$ in diameter,

which is close to the size of Lord's experiment. The models suggested by Lord and Kyan et al. [42] predicted the results within an acceptable range. The experimental results reported by Wiggins et al. [38], Lord, and Brown [39] followed the models. Theoretical models proposed by Happel [22] and Kuwabara [23] predicted the first and the second largest Kozeny constants, respectively. These overestimations were caused by their assumption that the flow is perpendicular to the cylinders, whereas the fibrous debris transported to the strainers were randomly deposited. Also, theoretical models assumed uniform pore size which is the result of bulk compression, however, the fibrous bed generated from suspended debris is mainly compressed in the flow direction which maintains the larger pore size compared to the assumed uniform pore size. This trend can be found even between experiments. Davies' experimental data which showed the largest head loss were mainly obtained from filter pads. Ingmanson et al.'s experiments were conducted with a pipe flow system which is similar to the present study, but the initial porosity was lower than the present study. Their data located between the present research and Davies' data. These observations are organized in Table IV.1.3. Although it cannot conclude that the difference in head loss was caused by the pore size, it should be worthy to investigate the effect of pore size and bed generation mechanism on head loss in the future works.

Table IV.1. 3. Comparison of head loss data

Authors	Happle Kuwabara	Davies	Ingmanson et al.	Present study
Research type	Theoretical	Experimental	Experimental	Experimental
Characteristics of fibrous porous media	Uniform pore size assumption	Compressed filter pads	Compressed fibrous bed already existing in an air flow pipe	Compressed fibrous bed generated from dilute suspensions during experiments in a water flow pipe
Head Loss	Highest	>	>	Lowest

IV.1.4. Compression of fibrous bed

In order to predict a correct head loss, therefore, a compression model was proposed based on the average porosity and additional adjustment. This study applied Meyer's model and Jonsson and Jonsson's model which were the bases of the Grahn et al.'s study and NUREG-1862, respectively. In a compression test with mechanical stress as found in Grahn et al.'s work a fibrous bed is deformed uniformly. However, stress applied by flow is cumulative, as a result, if the compression models are applied to a given pressure drop, those predict the porosity of the layer closest to the strainer in a fibrous bed. The present experiment provided the mean porosity at a given pressure drop through a fibrous bed. Therefore the unknown coefficients N and m were determined by taking average over the given pressure drop as shown in Equations (IV.1.9) and (IV.1.10).

$$\varepsilon_{mean} = \frac{\int_0^P \varepsilon dP}{\int_0^P dP} = \frac{\int_0^P \varepsilon_0 - N_\varepsilon P^m dP}{\int_0^P dP} = \frac{\varepsilon_0 P - \frac{N_\varepsilon}{m+1} P^{m+1}}{P} = \varepsilon_0 - \frac{N_\varepsilon}{m+1} P^m \quad (IV.1.9)$$

For dilute suspensions depositing on a fibrous bed, the volume fraction of suspensions would be a reasonable initial porosity. The volume fraction of debris was 0.9998 and approximately 1 at the beginning and at the end of an experiment, respectively, in this study. When the initial porosity is close to $\varepsilon_0 \approx 1$, Equation (IV.1.9) approaches Ingmanson's model and Wallis' [46] model. Using the experimental data in Figure IV.1.23, the coefficients in Equation (IV.1.9) were determined to be $N_\varepsilon = 0.0022$, and $m = 0.288$ for generation of NUKON fibrous beds on the strainer.

$$\varepsilon = \varepsilon_0 - 0.0022P^{0.288} \quad (IV.1.10)$$

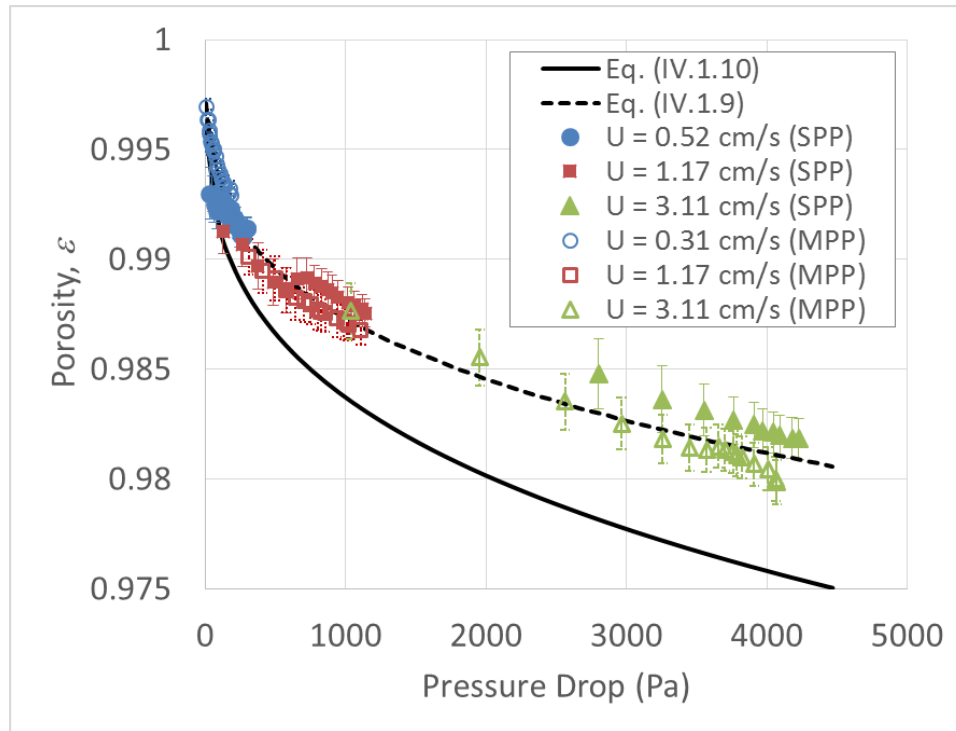


Figure IV.1. 23. Porosity vs. pressure drop of fibrous bed prepared using NEI method

A head loss model and a compression model were coupled to predict the bed thickness and the pressure drop for given quantity of fibrous debris and approach velocity. Figure IV.1.24 shows how porosity and pressure affect each other.

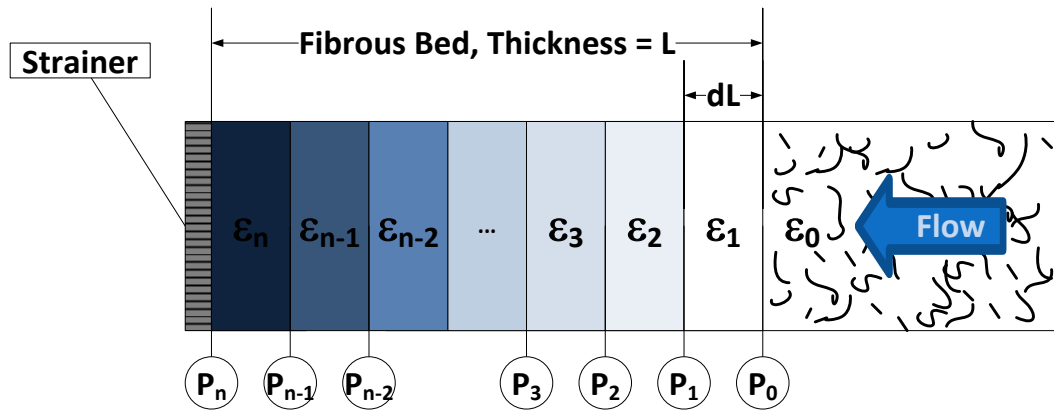


Figure IV.1. 24. Pressure and porosity distribution in a fibrous bed

Equation (IV.1.11) solves a head loss model and a compression model as shown in Figure IV.1.24.

$$\begin{aligned}
 \varepsilon_0 &= 0.9998 \text{ (Concentration of suspensions)} \\
 P_0 &\approx 0 \text{ (Pressure applied by flow)} \\
 \varepsilon_1 &= \varepsilon(P_0) \approx \varepsilon_0 \\
 P_1 &= P_0 + dP(\varepsilon_1) \\
 &\vdots \\
 \varepsilon_n &= \varepsilon(P_{n-1}) \\
 P_n &= P_{n-1} + dP(\varepsilon_n)
 \end{aligned}
 \tag{IV.1.11}$$

Equations (IV.1.7) and (IV.1.10) were numerically solved with $dL = 0.0001$ (m) for Equation (IV.1.11) using a Matlab code in Appendix D, and the results at different approach velocities are presented in Figures IV.1.25 and IV.1.26.

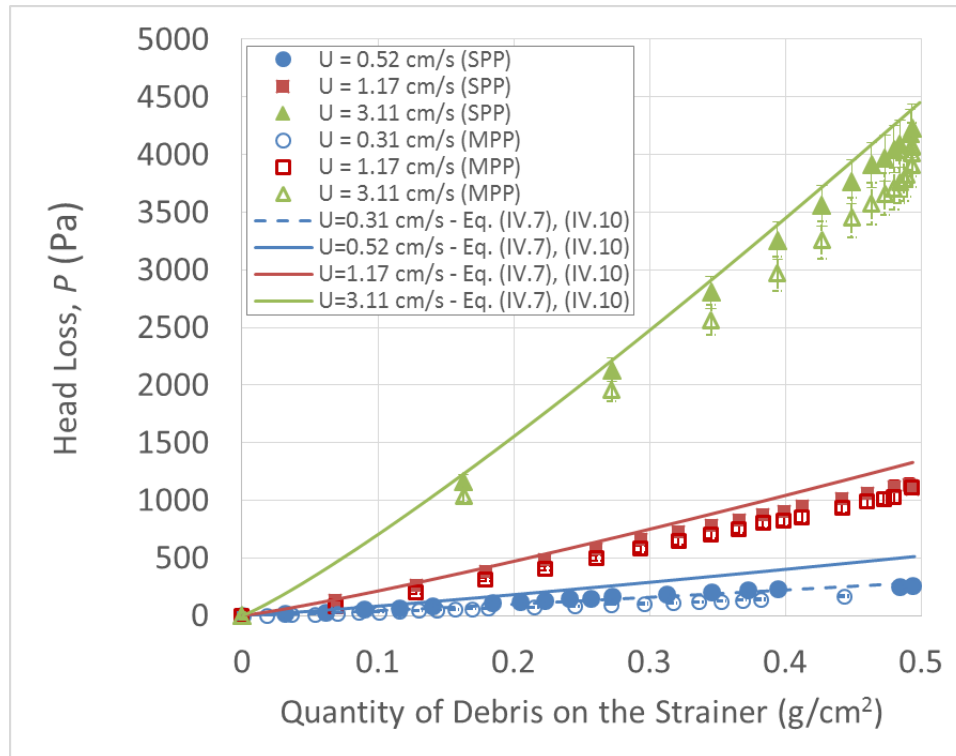


Figure IV.1. 25. Head loss vs. quantity of debris on the strainer with NEI preparation at different approach velocities, (lines: model, dots: experiment)

The models in Equations (IV.1.7) and (IV.1.10) predicted slightly higher pressure drop. This over prediction might be the limitation of the model assuming that the pore size is simply proportional to the porosity of the bed even during a compression process.

Figure IV.1.26 presents the build-up of the fibrous bed prepared using NEI method with different quantity of debris at different approach velocities.

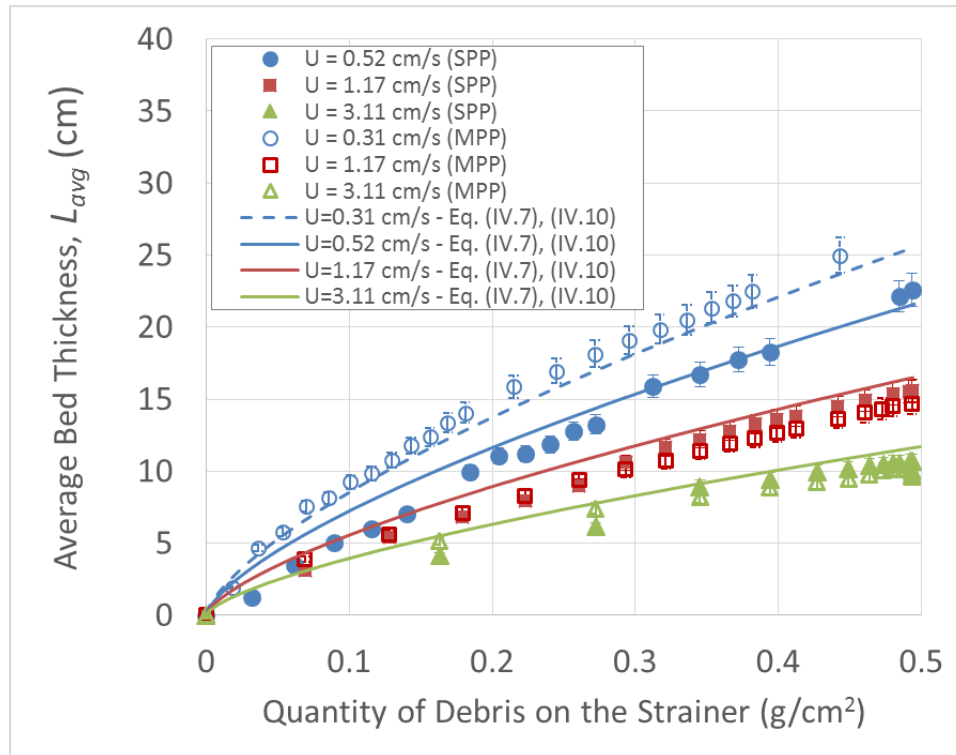


Figure IV.1. 26. Average bed thickness vs. quantity of debris using NEI preparation, (lines: model, dots: experiment)

Although, the models showed slight difference from the experimental results, the results of both strainers followed the model within acceptable ranges proposed in this study developed for NUKON fibrous debris prepared using shredder method.

The compression model developed for NEI method was applied to the results prepared using shredder method to check applicability of the model as shown in Figures IV.1.27 and IV.1.28. Since Equation (IV.1.7) was developed for debris prepared using shredder

method, head loss was predicted more accurately. However, it was found that the compression model developed using NEI method was not applicable to shredder method.

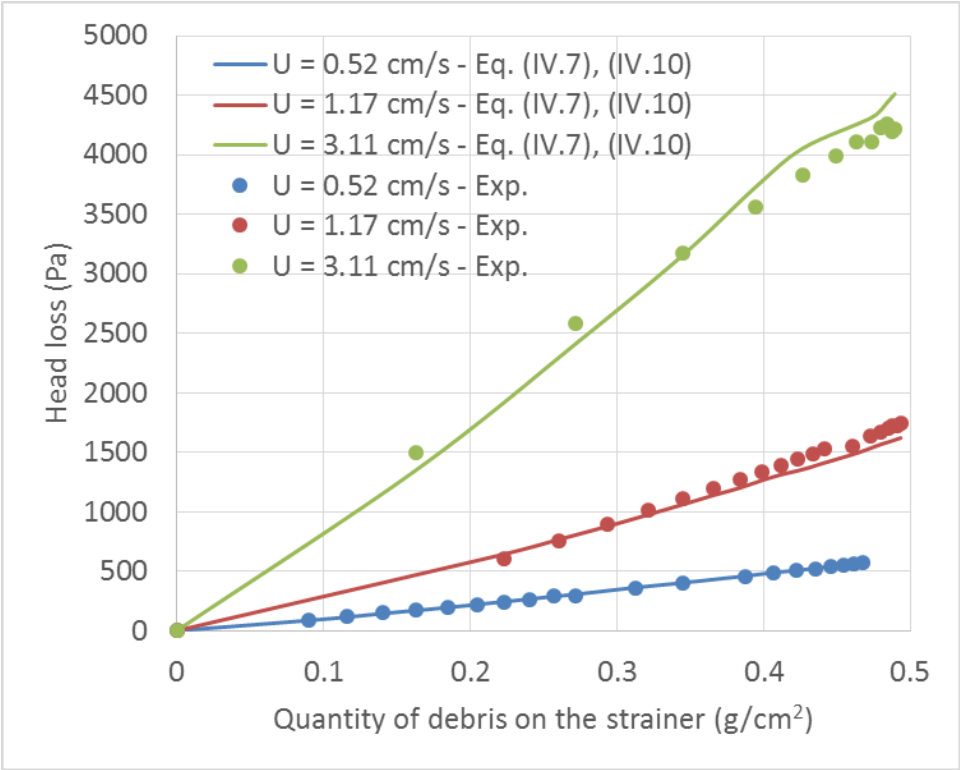


Figure IV.1. 27. Head loss vs. quantity of debris on the strainer with shredder preparation

Shredder method produced larger debris maintaining the original porosity of the NUKON mat, 0.986, which is much smaller than the initial porosity value in the NEI experiments, 0.9998. Hence, the compression model only predicted correct value for the case of the maximum approach velocity, 3.11 cm/s, where the porosity was calculated correctly. Therefore, even in the case of the same pressure drop for two different types of fibrous beds, debris generation mechanism should be considered to correctly understand the internal structure of the media.

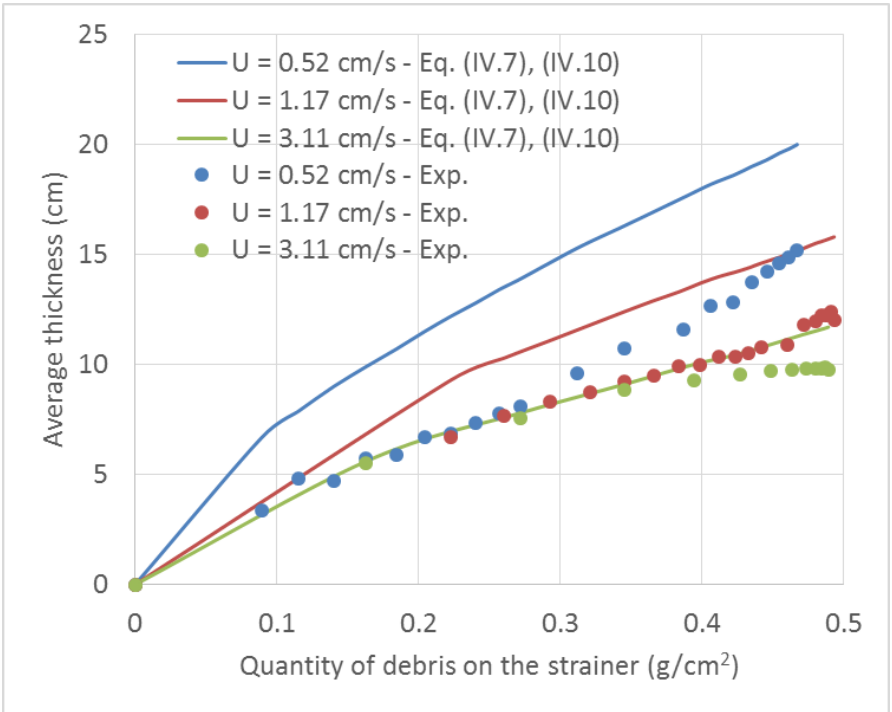
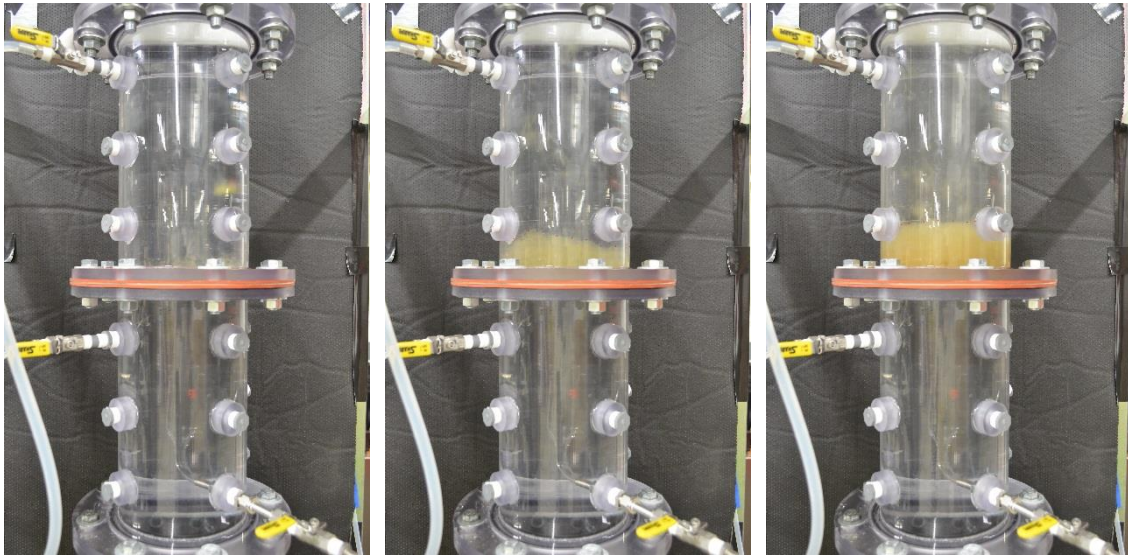


Figure IV.1. 28. Average bed thickness vs. quantity of debris using shredder method

IV.1.5. Vertical head loss test results

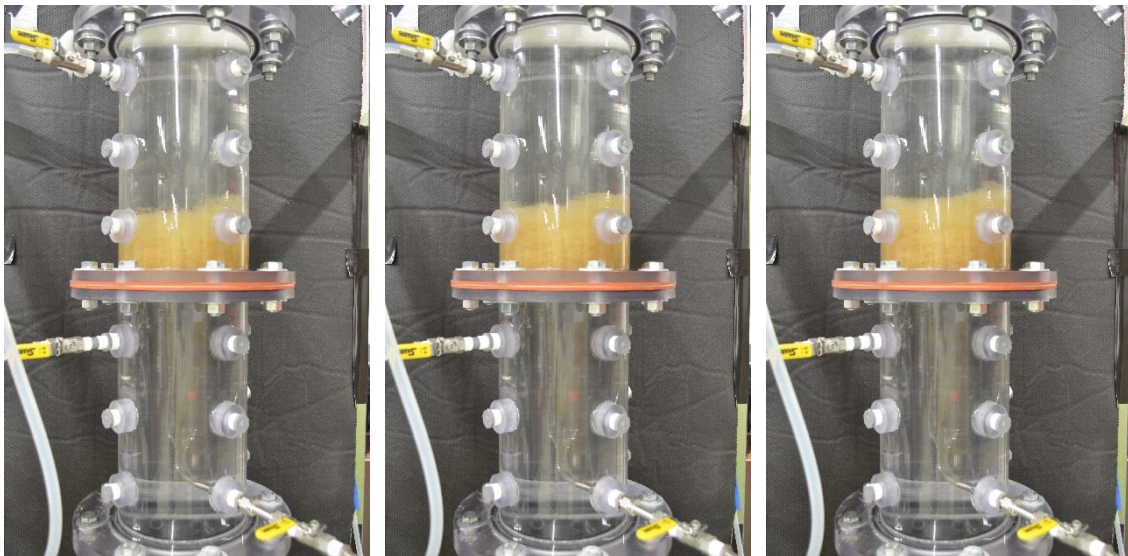
In the vertical head loss test facility, three head loss tests with NEI prepared NUKON were performed to produce validation data for the head loss model and the compression model developed previously. Figures IV.1.29 and IV.1.30 presents two tests with SPP strainer at 0.31 cm/s (PD-13) and 3.11 cm/s, (PD-14) respectively, and Figure IV.1.31 presents the test with MPP strainer at 0.31 cm/s (PD-15). PD-13 was conducted for two turnovers as a part of debris bypass test, and thus it did not reach steady state. A benefit of a horizontally installed strainer in the vertical flow loop is that gravity has less of an effect on the porosity at the same distance from the strainer than the one on the vertically installed strainers in the horizontal flow loop. Therefore, PD-14 resulted in clearly flat surface which could not be found in the horizontal system. However, PD-13 and PD-15 still showed non-uniformly deposited debris bed despite being vertically installed, hence the thickness of each fibrous bed was measured using the same method applied to the horizontal head loss tests. Figures IV.1.32, IV.1.33, and IV.1.34 are the graphical build-up of PD-13, PD-14, and PD-15, respectively.



(a) 5 min

(b) 10 min

(c) 20 min

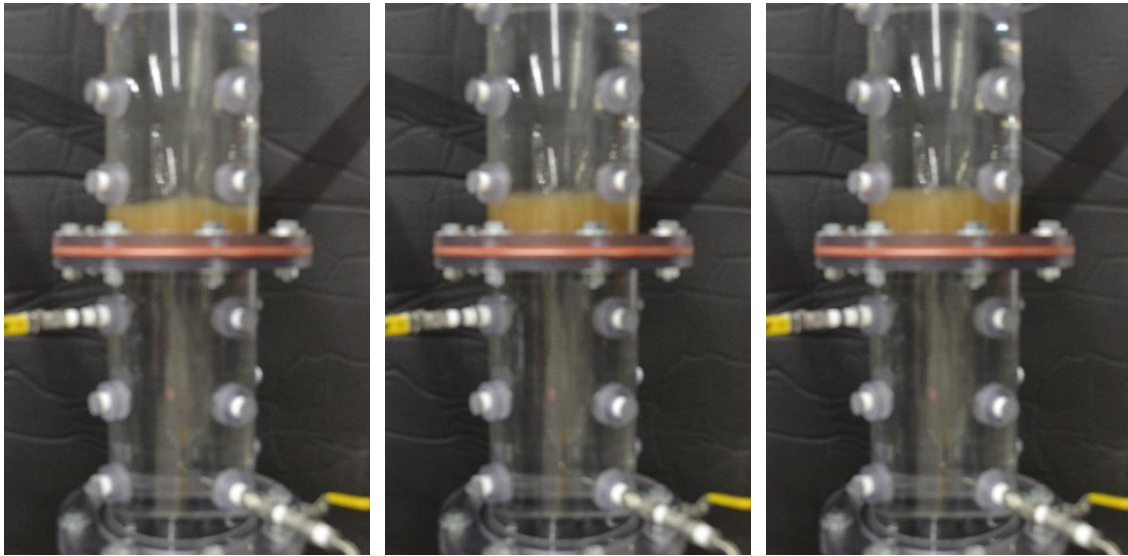


(d) 30 min

(e) 40 min

(f) 50 min

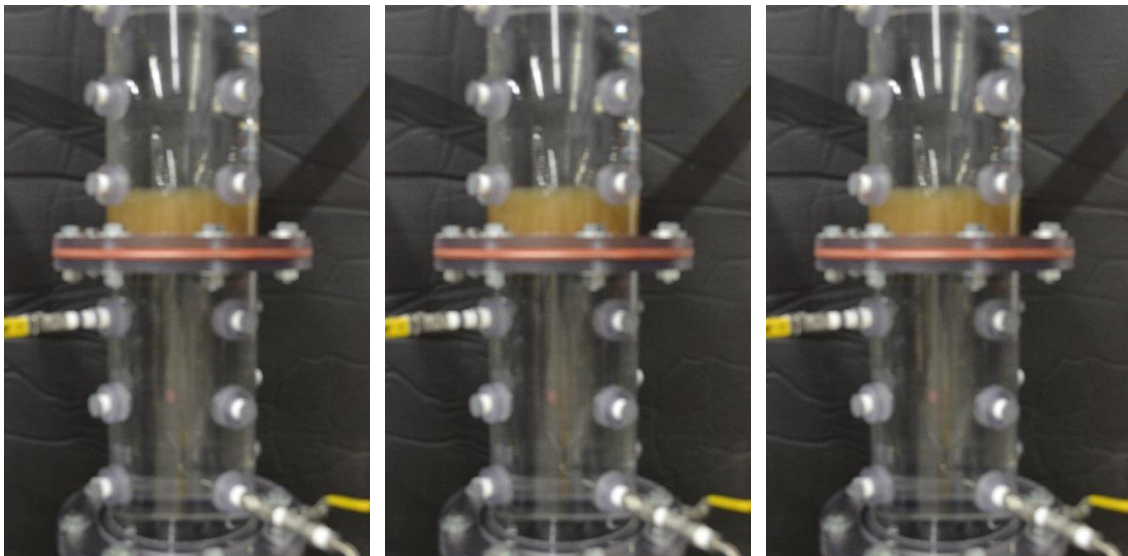
Figure IV.1. 29. Build-up of debris bed on SPP strainer at approach velocity of 0.31 cm/s



(a) 5 min

(b) 10 min

(c) 15 min

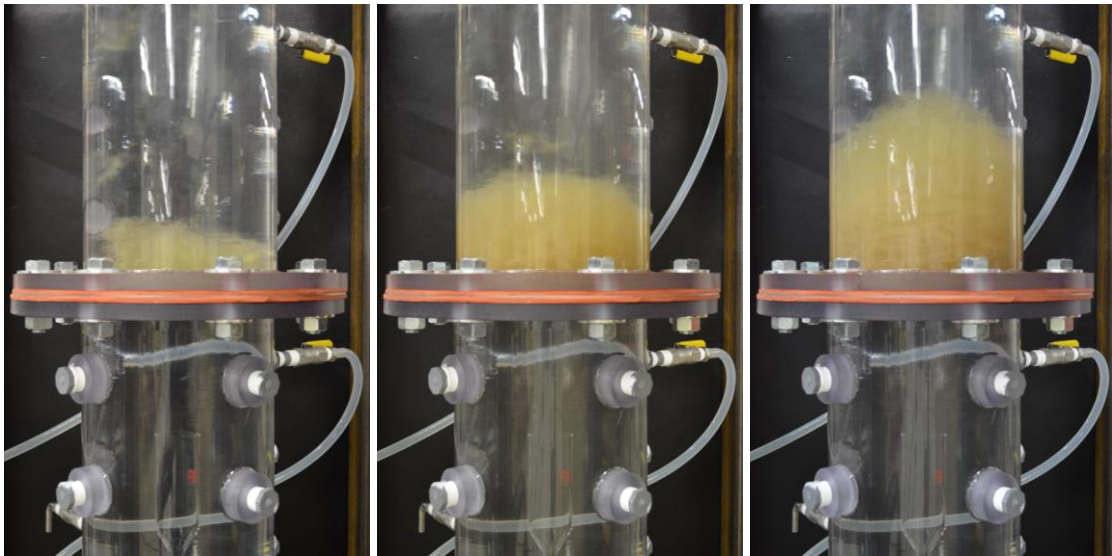


(d) 20 min

(e) 120 min

(f) 125 min

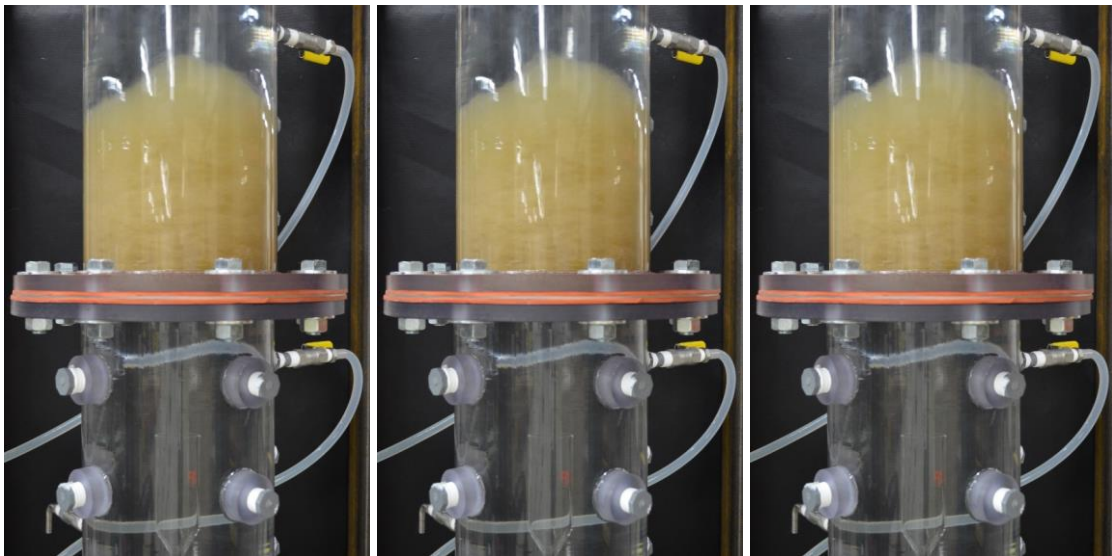
Figure IV.1. 30. Build-up of debris bed on SPP strainer at approach velocity of 3.11 cm/s



(a) 10 min

(b) 30 min

(c) 60 min



(d) 180 min

(e) 210 min

(f) 240 min

Figure IV.1. 31. Build-up of debris bed on MPP strainer at approach velocity of 0.31 cm/s

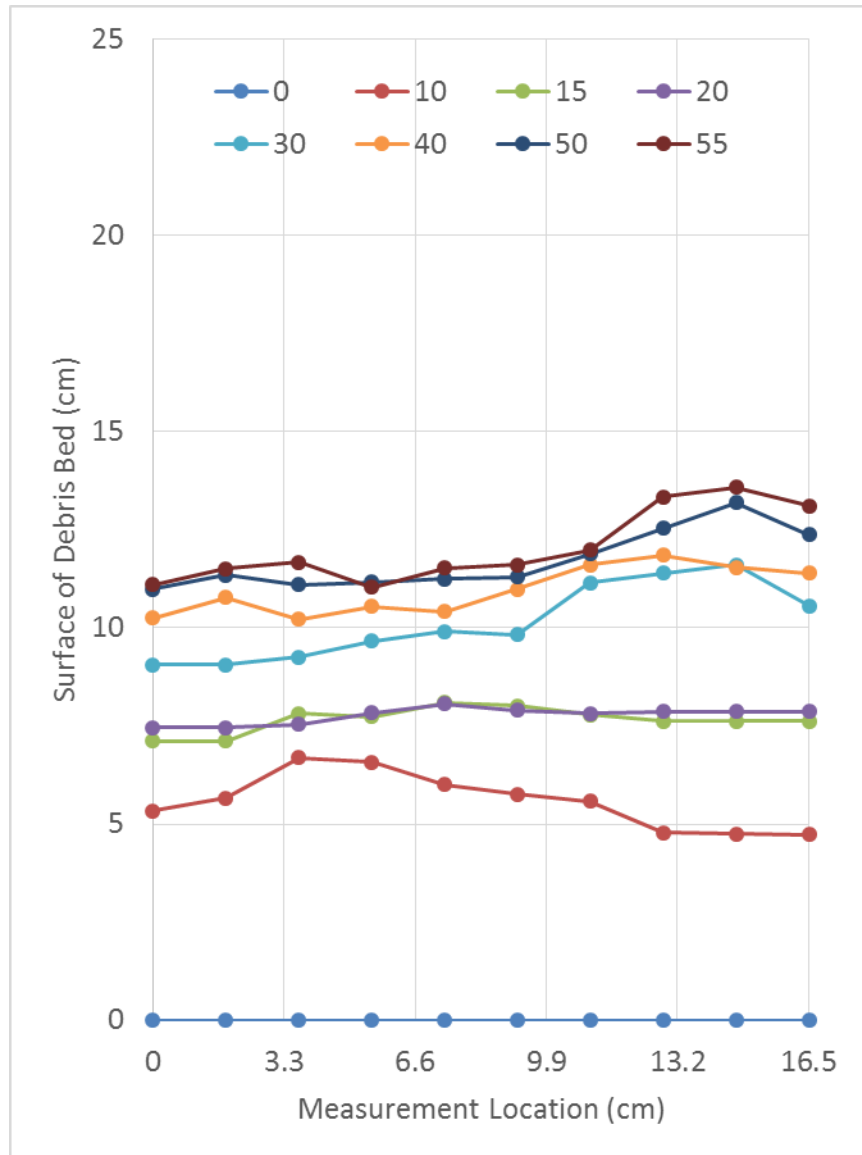


Figure IV.1. 32. Graphical growth of debris bed on SPP strainer at approach velocity of 0.31 cm/s (PD-13)

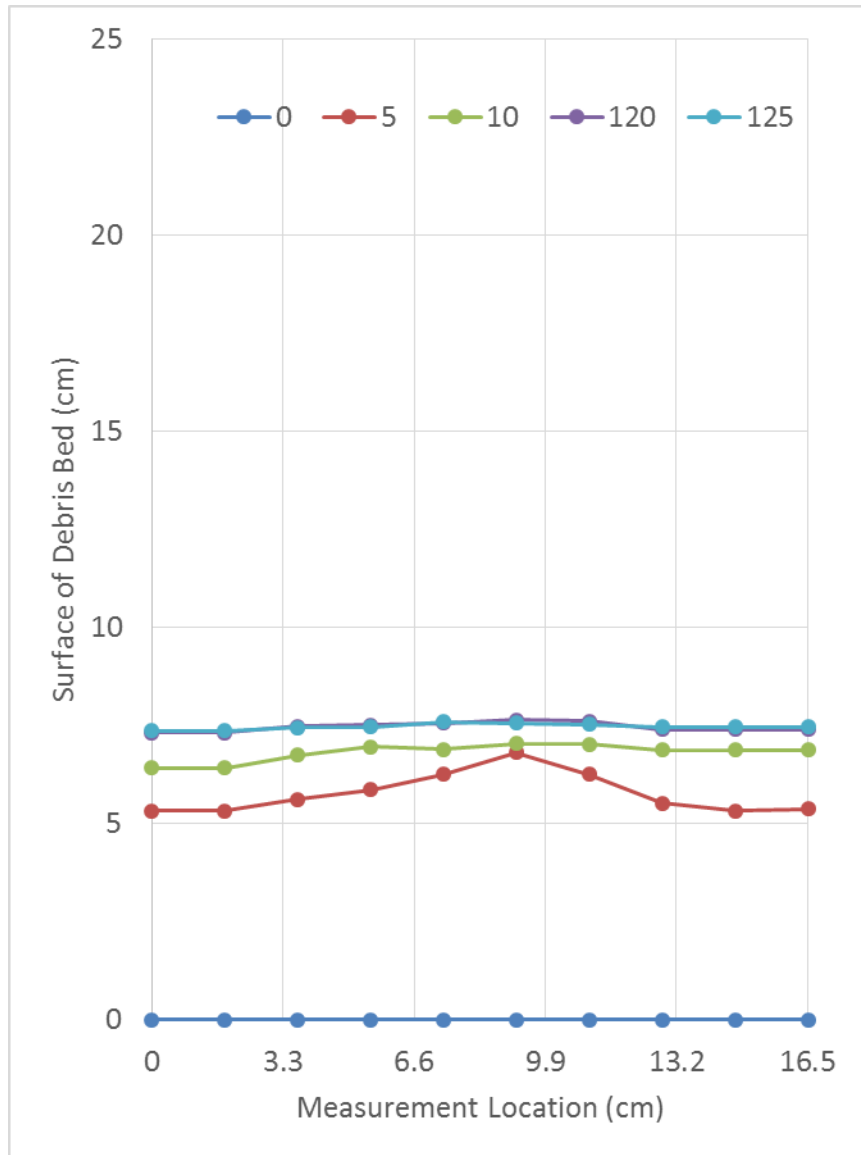


Figure IV.1. 33. Graphical growth of debris bed on SPP strainer at approach velocity of 3.11 cm/s (PD-14)

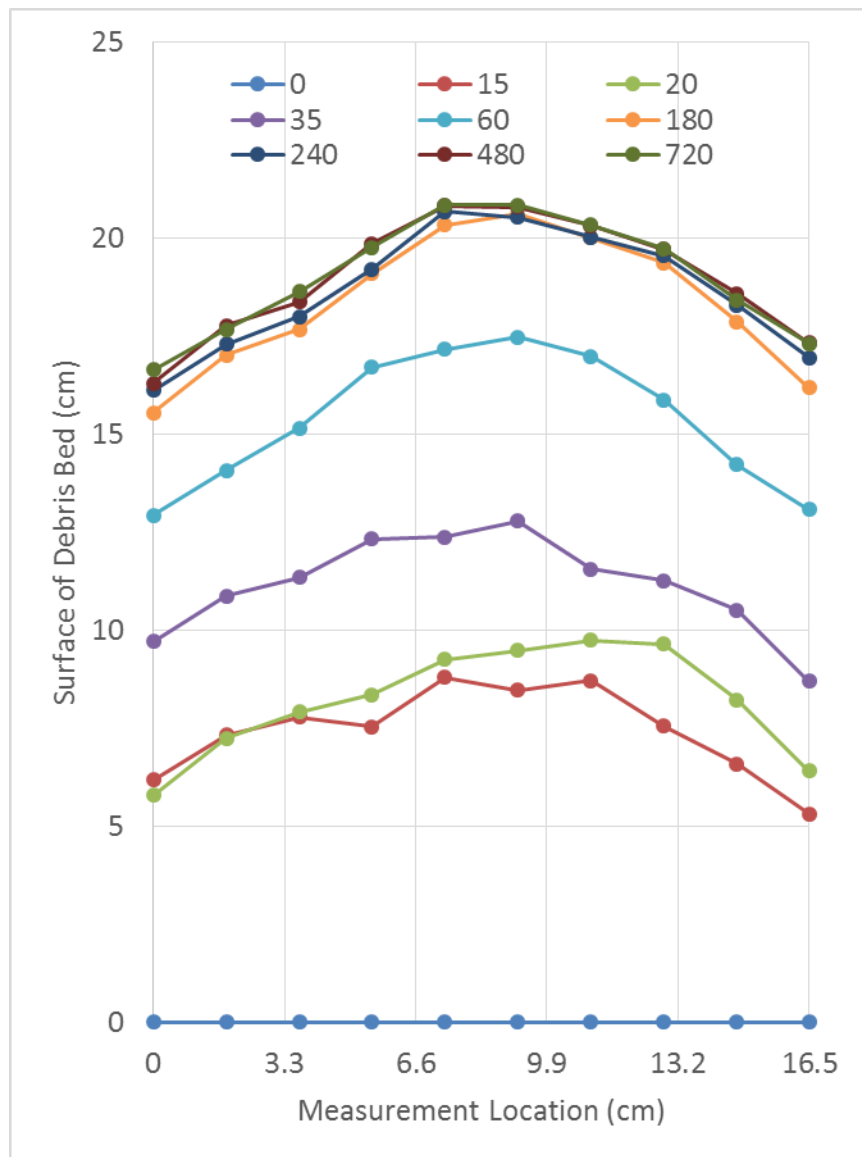


Figure IV.1. 34. Graphical growth of debris bed on MPP strainer at approach velocity of 0.31 cm/s (PD-15)

Figure IV.1.35 presents the average bed thickness measured using the previous Figures IV.1.32 to IV.1.34. Both MPP and SPP at 0.31 cm/s showed good agreement to each other. SPP strainer at 3.11 cm/s showed slightly increasing thickness even after several numbers of turnovers. This increased thickness was analyzed using the pressure drop data and other parameters in Figures IV.1.36.

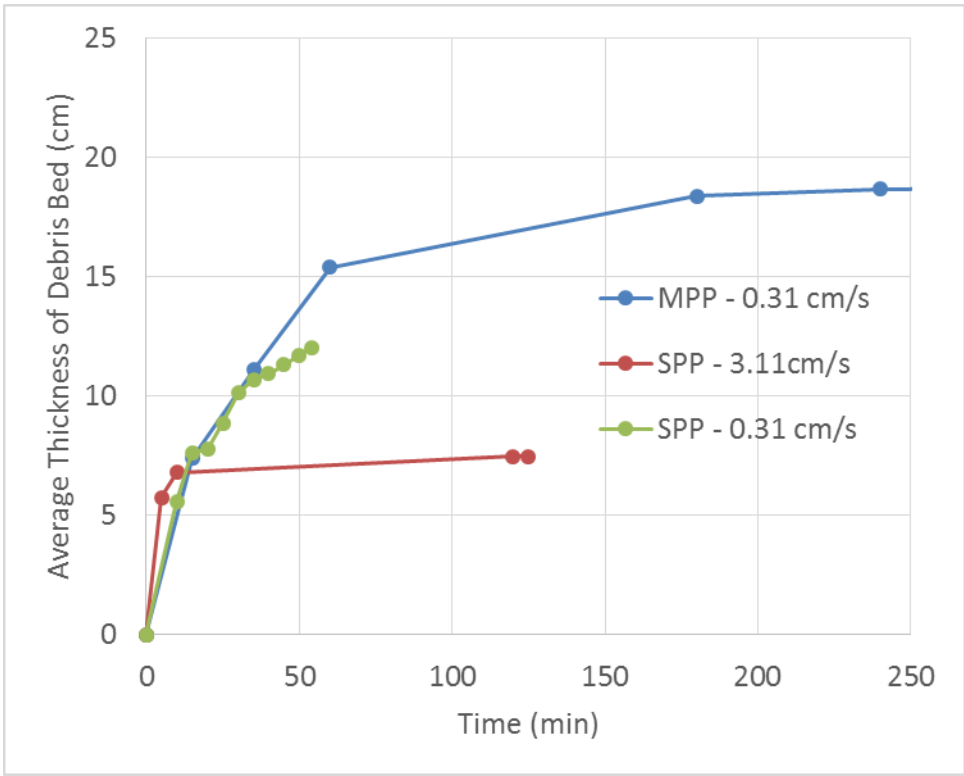


Figure IV.1. 35. Average thickness of debris bed in the vertical test facility

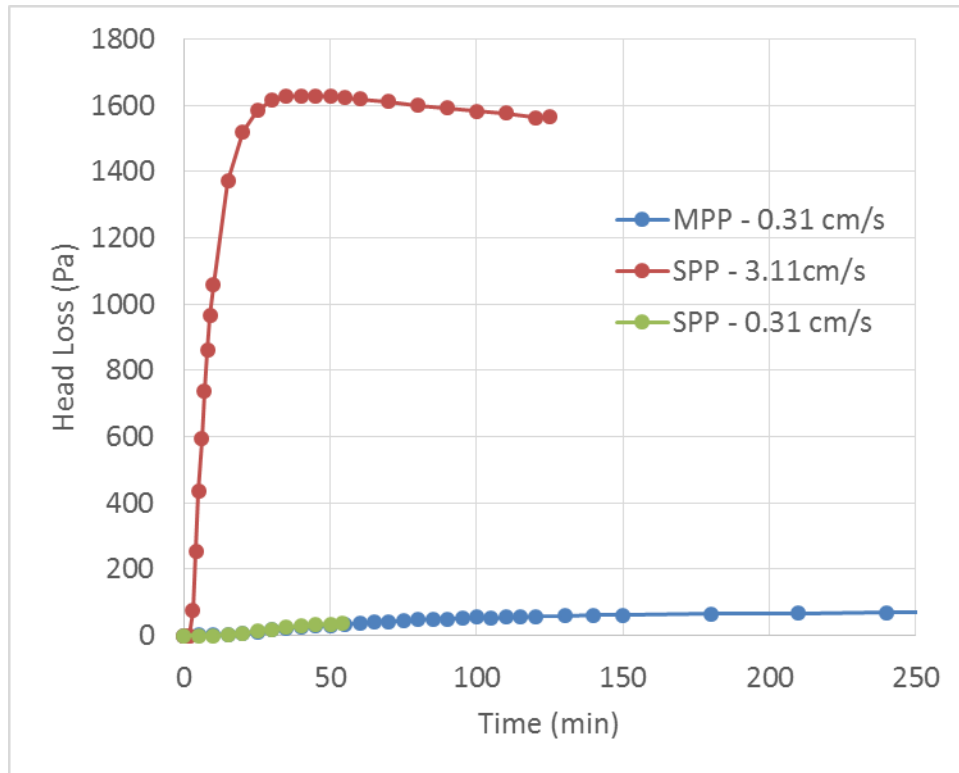


Figure IV.1. 36. Head loss vs. time through fibrous beds in the vertical test loop

Decreasing head loss at 3.11 cm/s after reaching the highest value, as shown in Figure IV.1.35, was analyzed by comparing the pressure drop record with the fluid velocity and temperature data log. The velocity data showed constant value. However, the temperature increased during the same period that the pressure drop decreased. When the viscosity change due to temperature change was applied to the head loss model, Equation (IV.1.7), the head loss model was in good agreement with the experimental results.

The head loss model, Equation (IV.1.7) and the compression model, Equation (IV.1.10) were applied to the experimental test results performed in the vertical test facility as shown in Figures IV.1.37 and IV.1.38, respectively.

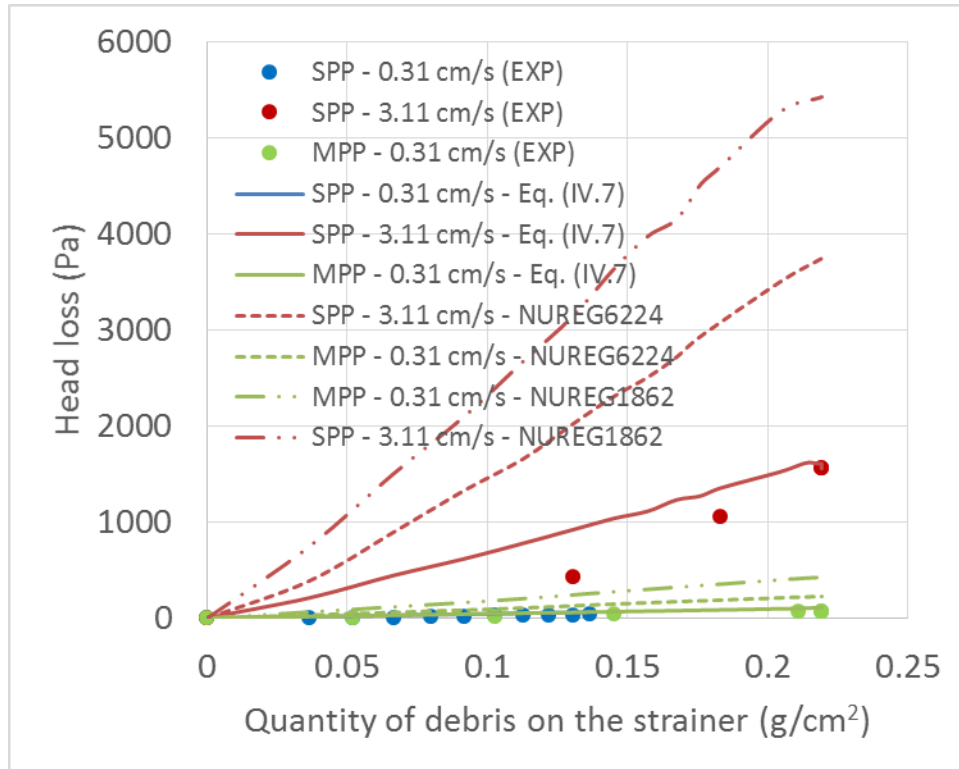


Figure IV.1. 37. Head loss vs. quantity of debris transported to the strainer in the vertical test loop

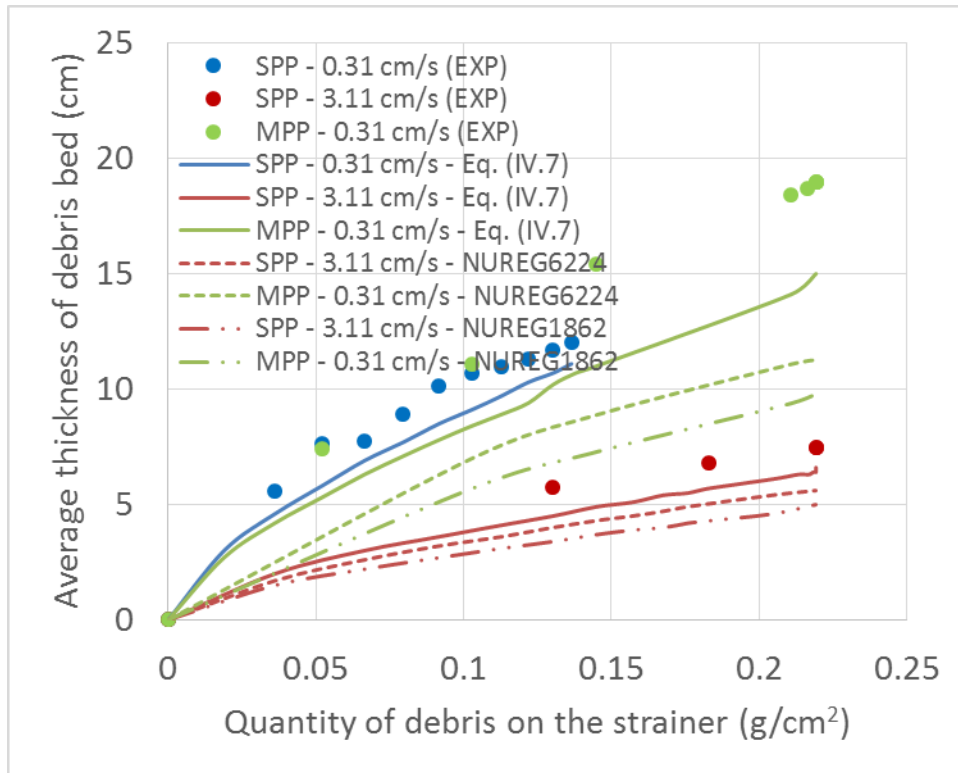


Figure IV.1. 38. Average thickness of debris bed vs. quantity of debris transported to the strainer in the vertical test loop

Although the models developed in this study for the horizontal test facility showed better prediction within acceptable ranges for the vertical test facility than NUREG/CR-6224 model and NUREG-1862 model, additional tests are required to study the discrepancy found in the early period of the bed build-up.

IV.1.6. Uncertainty analysis

Uncertainty of head loss tests were analyzed in terms of systematic errors and random errors. Systematic errors were mainly caused by inaccuracy of flow control, quantity of debris, volume of water, pressure measurement, and debris bed thickness measurement. Random errors were analyzed for the tests conducted more than two times at same condition.

IV.1.6.1. Systematic errors

Uncertainty of the quantity of debris transported to the strainer was estimated by applying measurement uncertainties in approaching velocity, volume of the water in the tank, and filtration efficiency as shown in Equation (IV.1.12)

$$\sigma_{M_{s,t}}^2 = \left(\frac{\partial M_{s,t}}{\partial U} \right)^2 \sigma_U^2 + \left(\frac{\partial M_{s,t}}{\partial C_f} \right)^2 \sigma_{C_f}^2 \quad (\text{IV.1.12})$$

where, $\sigma_{M_{s,t}}$, σ_U , σ_{V_t} , and σ_{C_f} are measurement uncertainties of $M_{s,t}$, U , V , and C_f ,

respectively. Using Equation (IV.1.3), Equation (IV.1.12) becomes Equation (IV.1.13)

$$\sigma_{M_{s,t}}^2 = \left(M_0 \frac{AC_f t}{V_t} e^{-\frac{AUC_f t}{V_t}} \right)^2 \sigma_U^2 + \left(M_0 \frac{AUt}{V_t} e^{-\frac{AUC_f t}{V_t}} \right)^2 \sigma_{C_f}^2 \quad (\text{IV.1.13})$$

To estimate filtration efficiency a preliminary test was performed with 40g of NUKON. The test resulted in that debris bypass through the fibrous bed was around 3% (~1g) for the first turnover and less than 5% (~1.4g) at the end of the test after 10 turnovers. The flow rate of this study was controlled in the range of 10% of approaching velocity. Based on these observations, σ_U and σ_{C_f} were assumed to be $0.1U$ and $0.05C_f$, respectively, to estimate the uncertainty in debris quantity on the strainer when the initial NUKON quantity was 40g in the tank. Since NUKON weight was measured with a two-digit scale, the uncertainty caused by initial NUKON quantity was less than 0.025%, which was negligible. $\sigma_{M_s,t}$ was calculated as shown in Figure IV.1.39. The uncertainty decreased below 8% in 30 minutes, 1 hour, and 2 hours for 3.11 cm/s, 1.17 cm/s, and 0.52 cm/s respectively. This calculation still assumed that the debris penetrating through the strainer went back to the tank. However, these debris might deposit in the pipeline, thus, the minimum uncertainty at steady state should be consider the measured value of 5% bypass.

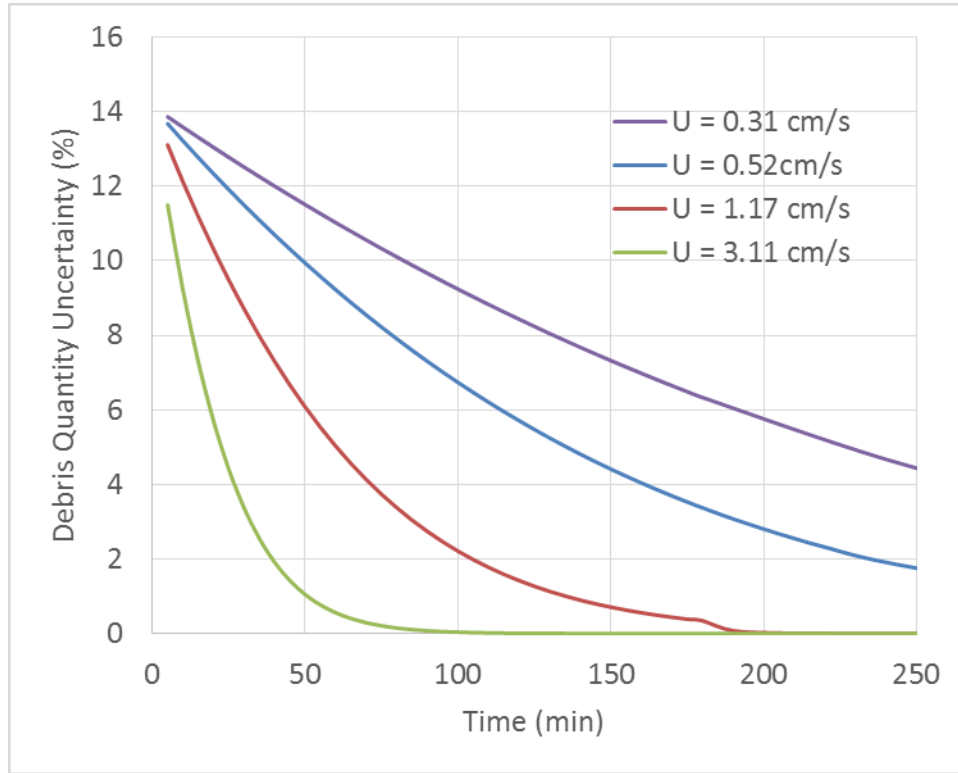


Figure IV.1. 39. Uncertainty in measurement of debris quantity on the strainer at different time

The uncertainty of fibrous bed porosity, ε defined in Equation (IV.1.4), was calculated using Equation (IV.1.14) and the uncertainty of debris quantity on the strainer obtained in Figure IV.1.28. The maximum uncertainty was found to be less than 0.0014.

$$\sigma_{\varepsilon}^2 = \left(\frac{\partial \varepsilon}{\partial M_{s,t}} \right)^2 \sigma_{M_{s,t}}^2 = \left(-\frac{1}{AL_{avg} \rho} \right)^2 \sigma_{M_{s,t}}^2 \quad (IV.1.14)$$

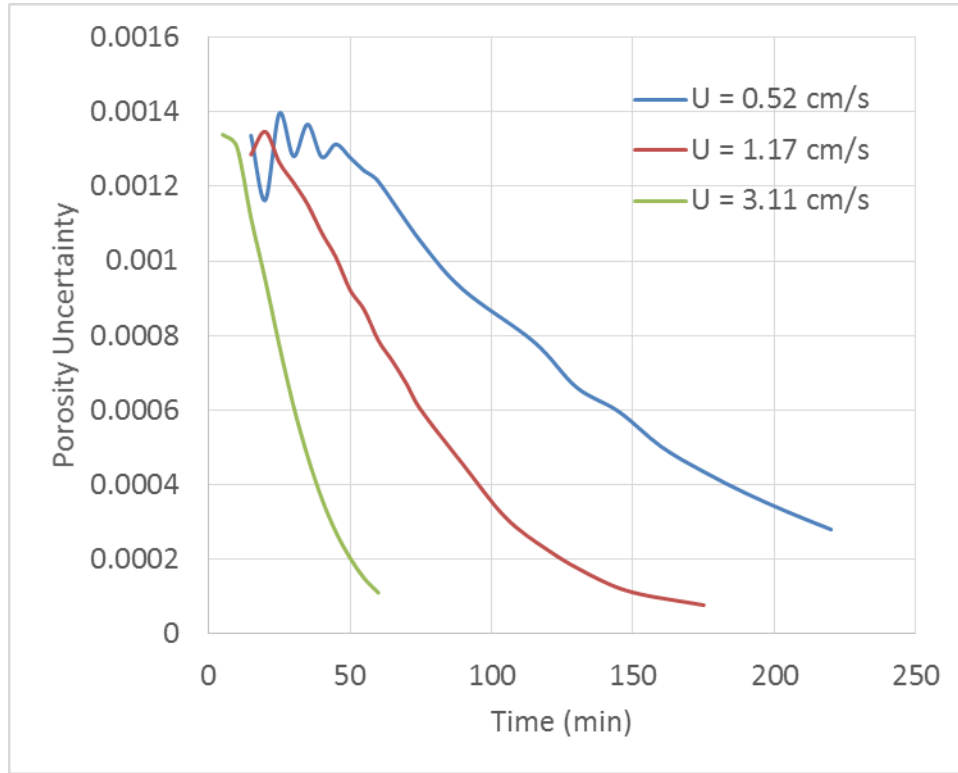


Figure IV.1. 40. Measurement of uncertainty in porosity of the fibrous beds at different time

Two additional assessments of thickness measurement were conducted to estimate accuracy of the ten-point method proposed in the beginning of this section. The first test was performed by applying a weighting method using the fraction of projected surface area as defined in Equation (IV.1.15) and Figure IV.1.40.

$$L_{avg} = \sum_{i=1}^N L_i \frac{A_i}{A_{total}} \quad (IV.1.15)$$

where L_i is the measured thickness (m) at the i^{th} point, P_i in Figure IV.1.41, N is the number of points, A_i is the projected surface area of the i^{th} fraction to the strainer, and A_{total} is the total surface area of the strainer as defined in Equation (IV.1.16).

$$A_{total} = \sum_{i=1}^N A_i \quad (IV.1.16)$$

10 equally distributed points (1cm distance between two points) were used as well as for the shredder preparation method.

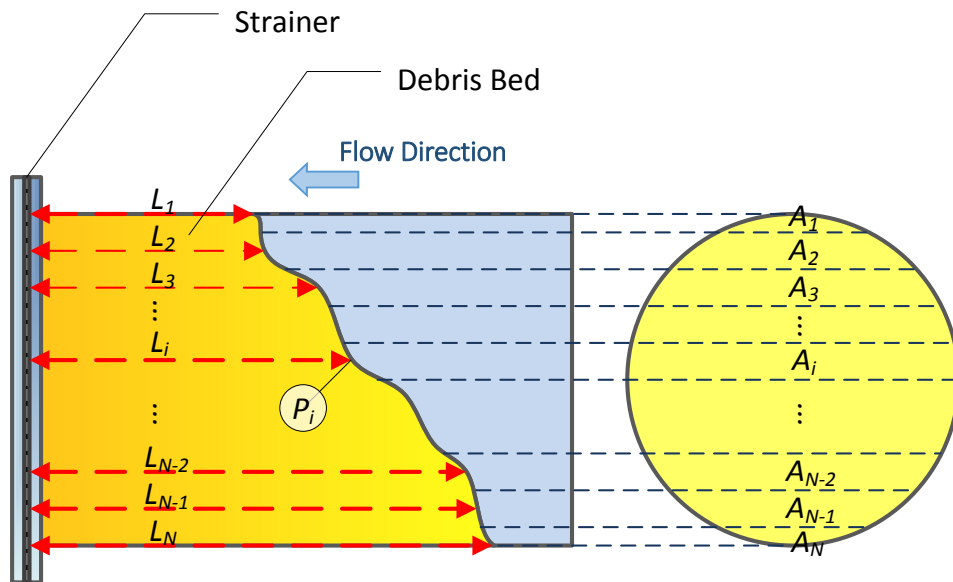


Figure IV.1. 41. Measurement of the thickness of the fibrous bed

This method did not result in appreciable difference in this study, since debris deposited along almost straight lines with certain angles.

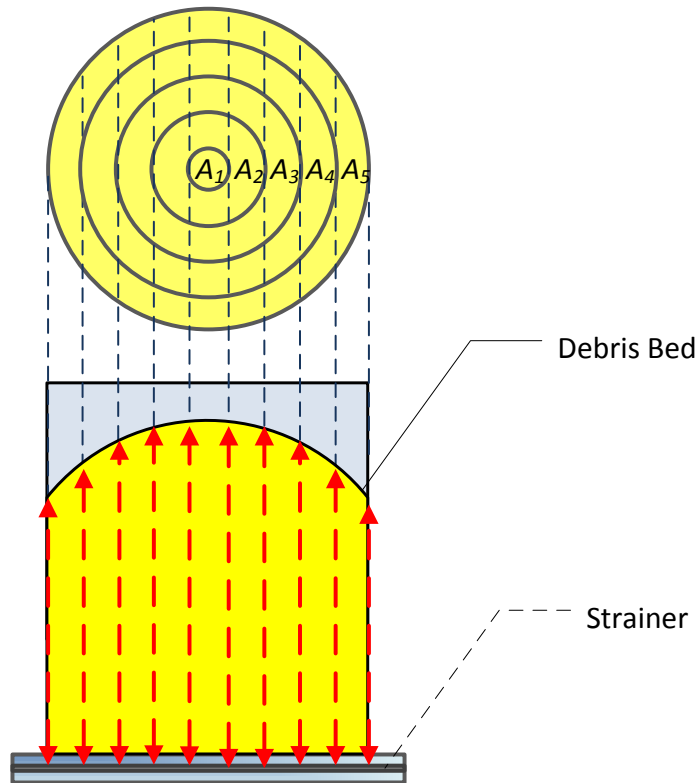


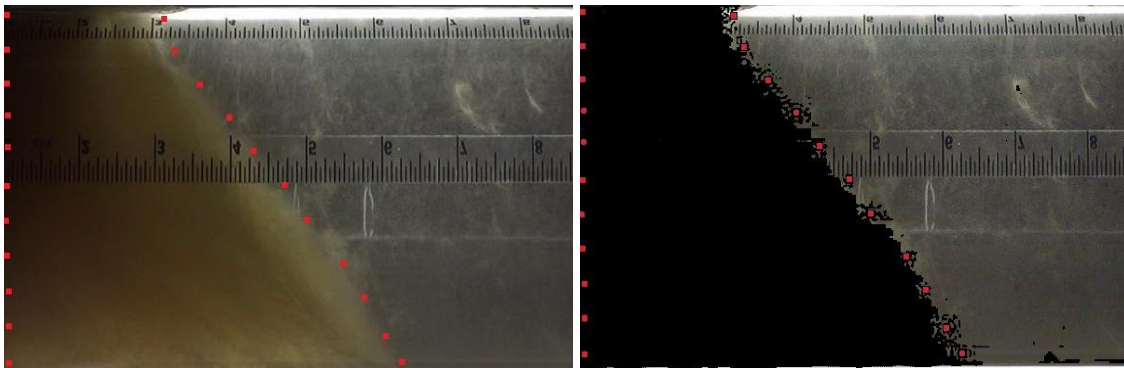
Figure IV.1. 42. Area weighted thickness measurement in the vertical test facility

Two extreme cases at 60 min and 720 min selected from PD-15 (0.31 cm/s, MPP in Figure IV.1.34) were examined using the area weighed in Figure IV.1.42 resulted in 6.6 %. This maximum value can be a reasonable boundary of the uncertainty of the method used for the thickness measurement of vertically deposited debris beds in this study.

Table IV.1. 4. Uncertainty of measurement of vertically deposited debris bed thickness

Linearly interpolated average thickness (cm)	Area weighted average thickness (cm)	Difference (%)
15.2	16.3	6.6
18.7	19.7	5.1

In the second test, 16 still shots were selected from tests performed at 0.31 cm/s and 0.52 cm/s on the SPP strainer using NEI preparation, and the thickness was precisely measured using image processing to trace the actual surface as shown in Figure IV.1.43. In image processing method, the total area measured by number of pixels was divided by the pipe cross sectional area to obtain the average thickness. The comparison showed the average difference was 2.5% with the standard deviation of 1.2%. The detailed results are presented in Table IV.1.4.



(a) 10 points interpolation

(b) Image processing

Figure IV.1. 43. Comparison of 10 point method and image processing

Table IV.1. 5. Comparison of thickness measurement methods: 10 points method and image processing

U = 0.31 cm/s, SPP, NEI			
Time (min)	Image Processing (cm)	Interpolation with 10 points (cm)	Difference (%)
20	5.889413	6.01599	2.149224
30	7.13232	7.336028	2.856125
45	9.536853	9.631426	0.991655
50	9.907129	10.06348	1.578168
90	13.87179	13.72946	1.036637
180	17.37868	17.84934	2.708272
240	18.40484	19.21434	4.398289
360	20.15631	21.2918	5.633436
U = 0.52 cm/s, SPP, NEI			
Time (min)	Image Processing (cm)	Interpolation with 10 points (cm)	Difference (%)
15	5.531556	5.67055	2.512755
30	8.867987	9.167876	3.381707
45	11.57676	11.91336	2.907606
60	13.51393	13.82395	2.294086
90	16.348	16.5989	1.534717
120	18.06674	18.38147	1.742064
150	19.41802	20.04162	3.211441
180	20.51022	20.79015	1.364862

Thickness measurement does not have clear criteria, hence the difference, 2.5%, found in this comparison might be a reasonable value to calculate the uncertainty of porosity in the horizontal experiments. For the uncertainty of thickness measurement in the vertical experimental data, 6.6% is a conservative value for the uncertainty of porosity. These uncertainty analysis were implemented in Equation (IV.1.17) by adding a term to Equation (IV.1.14).

$$\begin{aligned}\sigma_{\varepsilon}^2 &= \left(\frac{\partial \varepsilon}{\partial M_{s,t}} \right)^2 \sigma_{M_{s,t}}^2 + \left(\frac{\partial \varepsilon}{\partial L_{avg}} \right)^2 \sigma_{L_{avg}}^2 \\ &= \left(-\frac{1}{AL_{avg} \rho_{NUKON}} \right)^2 \sigma_{M_{s,t}}^2 + \left(\frac{M_{s,t}}{AL_{avg}^2 \rho_{NUKON}} \right)^2 \sigma_{L_{avg}}^2\end{aligned}\tag{IV.1.17}$$

IV.1.6.2. Random errors

Random errors might be caused by randomness in debris preparation, flow fluctuation, and other unknown perturbations. Three cases of SPP – NEI tests, one case of SPP – Shredder test, and four cases of MPP – NEI tests were selected to estimate the random errors as shown in Table IV.1.5.

Table IV.1. 6. List of random error test cases

#	Test Facility	Strainer Type	Approach Velocity (cm/s)	NUKON Preparation	Number of Tests
PD-4	Horizontal	SPP	3.11	Shredder	2
PD-6	Horizontal	SPP	0.52	NEI	3
PD-7	Horizontal	SPP	1.17	NEI	4
PD-8	Horizontal	SPP	3.11	NEI	2
PD-9	Horizontal	MPP	0.31	NEI	4
PD-10	Horizontal	MPP	0.52	NEI	2
PD-11	Horizontal	MPP	1.17	NEI	3
PD-12	Horizontal	MPP	3.11	NEI	3

Figure IV.1.44 presents the head loss data with standard deviation of the tests repeated more than twice, and the head loss at steady state with % random errors are extracted in Table IV.6. The average random error was 7.1%, and the maximum random error was 12%.

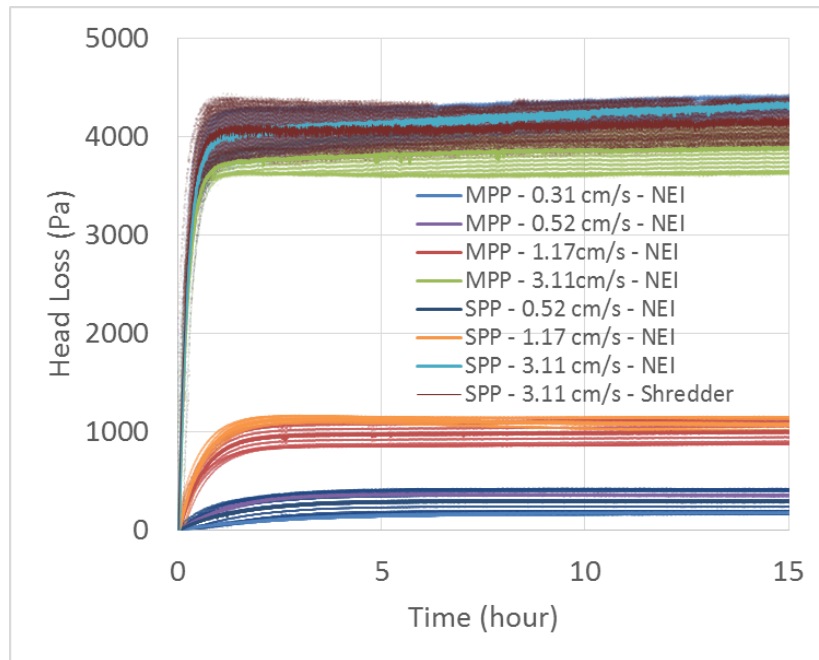


Figure IV.1. 44. Head loss with random error (standard deviation)

Table IV.1. 7. Head loss and random error at steady state

#	Pressure Drop at Steady State (Pa)	Standard Deviation (Pa)	Standard Deviation (%)	Number of Tests
PD-4	4167	231	5.5	2
PD-6	288	15	5.1	3
PD-7	1062	69	6.5	4
PD-8	4329	123	2.8	2
PD-9	177	20	11.4	4
PD-10	350	8	2.2	2
PD-11	999	119	12.0	3
PD-12	3883	243	6.3	3

IV.2. Debris bypass

The results of debris bypass were analyzed in terms of water type, fluid temperature, concentration of debris, and fluid velocity. For the detailed analysis of water type effect, a statistical comparison of the test results was carried out. Also, additional test results were obtained by changing pH and electric conductivity of water to observe the effect of acidity and ionic strength. The effects of fluid temperature was examined by comparing two sets of results obtained at room temperature (26 ± 3 °C) and at high temperature (85 ± 5 °C). In order to investigate the effect of debris concentration, three sets of tests with different debris quantity of 6.6g, 15g, and 40g were conducted. These tests were also analyzed in terms of debris bypass against time. For the sensitivity of fluid velocity on debris bypass, three sets of tests at different approach velocities of 0.31 cm/s, 0.56 cm/s, and 3.11 cm/s were conducted. The quantity of debris bypass were recorded in terms of the weight in grams. Temperature and relative humidity in the laboratory were recorded

during the weight measurements of the filter bags performed before and after each test. The only purpose of such additional measurements was to verify the experimental environment conditions did not significantly change between tests or within the phase of a single test. Except for high temperature tests, all the tests were performed at room temperature.

IV.2.1. Water type sensitivity test results

In order to understand the effect of water type on quantity of debris bypass four different types of water were examined including DI water, 1x (typical concentration) buffered borated water (BA: 16 g/l, TSP: 3 g/l), 2x buffered borated water (BA: 32 g/l, TSP: 6g/l), and Texas A&M University (TAMU) tap water. The source of tap water was indicated since characteristics of tap water changes from place to place. Two different water quality reports are added on Appendix F as examples. All tests were conducted at room temperature (26 ± 3 °C). The tests were repeated at least four times in order to have a representative statistical sample to be used for the comparison of the results. For 3x buffered borated water (BA: 48 g/l, TSP: 9 g/l), simulated TAMU tap water, and simulated Boston tap water, just one additional test for each were conducted for an extended comparison.

IV.2.1.1. Experimental results

Table IV.2.1 summarizes the results of the four tests performed using DI water. The average weight of the debris bypass is 0.32g and the standard deviation is 0.06g.

Table IV.2. 1. DI water test results

Test #	M _{initial} (g)	M _{final} (g)	M _{debris} (g)
DI-1	51.73	52.02	0.29
DI-2	47.98	48.23	0.25
DI-3	51.13	51.47	0.34
DI-4	51.04	51.42	0.38
Average	-	-	0.32
Stdev	-	-	0.06

Table IV.2.2 summarizes the results of the four tests performed with TAMU tap water (TT). The results, in terms of amount of debris bypass collected, showed a satisfactory repeatability. The average weight of the debris bypass is 0.46g and the standard deviation is 0.03g.

Table IV.2. 2. TAMU tap water test results

Test #	M _{initial} (g)	M _{final} (g)	M _{debris} (g)
TT-1	46.35	46.78	0.43
TT-2	47.39	47.88	0.49
TT-3	50.67	51.11	0.44
TT-4	49.78	50.23	0.48
TT-5	43.61	44.07	0.46
TT-6	46.89	47.33	0.44
TT-7	50.59	51.08	0.49
Average	N/A	N/A	0.46
Stdev	N/A	N/A	0.03

Stdev: Standard deviation, N/A: Not available

Table IV.2.3 summarizes the results of the four tests performed 1x BB-DI water at 26 °C. The average weight of the debris bypass is 0.44g and the standard deviation is 0.03g. The results showed a satisfactory repeatability in terms of amount of debris bypass collected.

Table IV.2. 3. 1x buffered borated water test results

Test #	M _{initial} (g)	M _{final} (g)	M _{debris} (g)
1xBB-1	50.44	50.89	0.45
1xBB-2	55.44	55.91	0.47
1xBB-3	45.96	46.37	0.41
1xBB-4	47.78	48.21	0.43
Average	N/A	N/A	0.44
Stdev	N/A	N/A	0.03

Table IV.2.4 summarizes the results of the four tests performed using 2x BB-DI water. The average weight of the debris bypass is 0.45g and the standard deviation is 0.02g.

Table IV.2. 4. 2x buffered borated water test results

Test #	M _{initial} (g)	M _{final} (g)	M _{debris} (g)
2xBB-1	47.66	48.13	0.47
2xBB-2	50.19	50.64	0.45
2xBB-3	50.93	51.39	0.46
2xBB-4	49.13	49.55	0.42
Average	N/A	N/A	0.45
Stdev	N/A	N/A	0.02

Table IV.2.5 summarizes the results of the 3x concentrated buffered borated (3xBB) water test, the simulated TAMU tap (STT) water test, and the simulated Boston tap (SBT) water test.

Table IV.2. 5. Additional water type test results

Test #	M _{initial} (g)	M _{final} (g)	M _{debris} (g)
3xBB-1	47.24	47.65	0.41
STT*-1	48.99	49.46	0.47
SBT**-1	48.76	49.11	0.35

*STT: simulated TAMU tap water, **SBT: simulated Boston tap water

These results showed good agreement with the trend found in previous water type sensitivity tests.

IV.2.1.2. Summary of water type test results

Table IV.2.6 summarizes the average and the variance of the quantity of debris bypass for each type of water in terms of grams and fraction.

Table IV.2. 6. Summary of debris bypass quantity in different water types

Water Type	Number of Tests	Quantity Injected ^a (g)	Average Bypass (g)	Standard Deviation (g)	Average Fraction (%)	Standard Deviation (%)
DI	4	6.60	0.32	0.06 g	4.85	0.86 %
TT	7	6.60	0.46	0.03 g	6.97	0.33 %
1xBB	4	6.60	0.44	0.03 g	6.67	0.45 %
2xBB	4	6.60	0.45	0.02 g	6.82	0.33 %
3xBB	1	6.60	0.41	-	6.21	-
STT*	1	6.60	0.47	-	7.12	-
SBT**	1	6.60	0.35	-	5.30	-

^a accuracy: ± 0.01 g

*STT: simulated TAMU tap water, **SBT: simulated Boston tap water

3x concentration of buffered borated water and two simulated tap water tests were conducted just one time for each. The results of the three different buffered borated water tests and the DI water test are presented in Figure IV.2.1

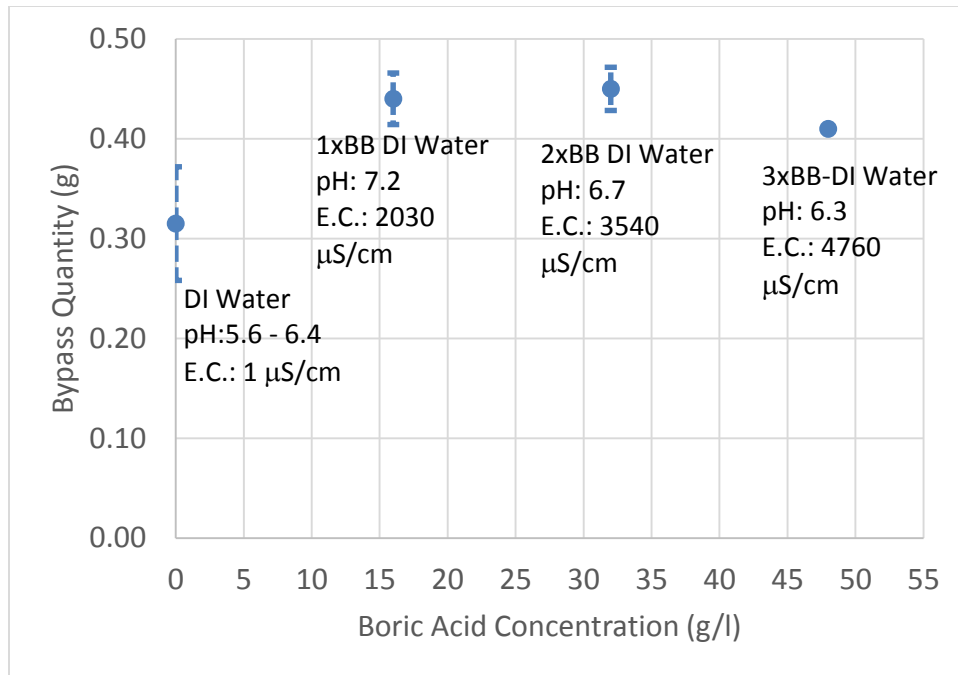


Figure IV.2. 1. Bypass of the buffered borated water tests and the di water test

There exists clear difference between the buffered borated water tests and the DI water tests. However, among the buffered borated water tests, difference was not clear, hence additional tests were required to separate parameters including pH and electrical conductivity which will be discussed in the next section.

IV.2.1.3. Statistical analysis

The tests performed with different types of water were compared statistically. The following analyses were meant to determine whether or not there are statistically significant differences between two different water types in terms of debris bypass quantity, which is known as Welch's t-test [47]. t-test checks if two groups are statistically different from each other as following.

$$t = \frac{\text{variance between groups}}{\text{variance within groups}} \quad (\text{IV.2.1})$$

The variance between groups can be calculated by subtracting the mean value of one group, \bar{W}_{group1} , from the other, \bar{W}_{group2} , defined in Equations (IV.2.2) and (IV.2.3).

$$\bar{W}_{group1} = \frac{1}{N_{group1}} \sum_{i=1}^{N_{group1}} W_{group1,i} \quad (\text{IV.2.2})$$

$$\bar{W}_{group2} = \frac{1}{N_{group2}} \sum_{i=1}^{N_{group2}} W_{group2,i} \quad (\text{IV.2.3})$$

where N_{group1} and N_{group2} are the number of samples of each group, and $W_{group1,i}$ and $W_{group2,i}$ are the values of the i^{th} sample of group1 and group2, respectively.

The variance within groups is calculated by the sum of both variance values which are defined in Equations (IV.2.4) and (IV.2.5).

$$S_{group1}^2 = \frac{1}{(N_{group1} - 1)} \sum_{i=1}^{N_{group1}} \left(W_{group1,i} - \bar{W}_{group1} \right)^2 \quad (IV.2.4)$$

$$S_{group2}^2 = \frac{1}{(N_{group2} - 1)} \sum_{i=1}^{N_{group2}} \left(W_{group2,i} - \bar{W}_{group2} \right)^2 \quad (IV2.5)$$

Finally, t value is calculated as shown in Equation (IV.2.6).

$$t = \frac{\bar{W}_{group1} - \bar{W}_{group2}}{\sqrt{\frac{S_{group1}^2}{N_{group1}} + \frac{S_{gourp2}^2}{N_{group2}}}} \quad (IV.2.6)$$

Equations (IV.2.1) and (IV.2.6) show that t value decreases when the average values of the two groups are similar or the variance of each group is large so that their distributions more overlap each other (an example using two groups with 4 tests for each are provided in Appendix E). A critical t value, t_{crit} , is required to check the calculated t value. The t_{crit} can be found in t-tables [64] using the degree of freedom, ν , calculated by equation (IV.2.7) which is known as the Welch-Satterthwaite equation:

$$v = \frac{\left(\frac{S_{group1}^2}{N_{group1}} + \frac{S_{group2}^2}{N_{group2}} \right)^2}{\frac{S_{group1}^4}{N_{group1}^2(N_{group1}-1)} + \frac{S_{group2}^4}{N_{group2}^2(N_{group2}-1)}} \quad (IV.2.7)$$

The Welch's t-test approach applied to the statistical analysis of the tests results suggest that, if $t > t_{crit}$, a statistical significant difference exists, whilst no statistically significance difference exists if $t < t_{crit}$. Even though one may argue the validity of normality assumption for the population using only 4 samples (i.e. 4 tests), in statistical literature it is common to assume normality even for small sample sizes, generally for the following reasons:

- a. Given that all test parameters remain constant, under the central theorem limit, the volume of screen penetration will naturally have a normal distribution if enough tests are performed.
- b. Even moderate departures from normality will not seriously affect and influence results.
- c. The alternative to t-test, which assumes underlying normal population, would be non-parametric methods, which will generally have significantly low power.

In order to obtain t -values and degree of freedom values the mean values and variances of debris bypass are calculated as shown in Table IV.2.7.

Table IV.2. 7. Summary of debris bypass quantity in different water types

Water Type	Mean Bypass		Variance of Bypass	
	Symbol	Value (g)	Symbol	Value (g ²)
DI	\bar{W}_{DI}	0.32	S_{DI}^2	0.00323
TT	\bar{W}_{TT}	0.46	S_{TT}^2	0.00065
1xBBB	\bar{W}_{1xBBB}	0.44	S_{1xBBB}^2	0.00067
2xBBB	\bar{W}_{2xBBB}	0.45	S_{2xBBB}^2	0.0047

The t-statistic parameter and the degree of freedom to compare two groups of water was calculated. Then, assuming a level of confidence α equal to 0.05, the critical t-value, t_{crit} , can be found from the t-table. Table IV.2.8 summarizes the results of the statistical analyses.

Table IV.2. 8. Summary of statistical analyses

Comparison Pair	t-static		t-critical	Statistical Comparison
DI vs. 1x BB-DI	4.003	>	2.741	Significant Difference
DI vs. 2x BB-DI	4.439	>	2.832	Significant Difference
DI vs. TAMU Tap	4.879	>	2.878	Significant Difference
1x BB-DI vs. 2x BB-DI	0.594	<	2.471	No Significant Difference
1x BB-DI vs. TAMU Tap	1.331	<	2.423	No Significant Difference
2x BB-DI vs. TAMU Tap	0.790	<	2.343	No Significant Difference

Based on the results, it was found that there existed a statistically significant difference between the weights of debris bypass in DI water and BB-DI waters for the selected boundary conditions with an approach velocity of 0.01 ft/s (0.305 cm/s) and debris concentration of 0.09 vol.% (0.0034 wt.%) for one turnover time. However, no statistically significant difference between 1xBB DI water and 2xBB DI water was found for the selected boundary conditions. Also, TAMU tap water showed no statistically significant different trend of debris bypass

IV.2.2 Water chemistry effect analysis

Table IV.2.9 presents the pH and electrical conductivity (EC) for different types of water including DI water, TAMU tap water, and chemical solutions dissolved in DI water.

Table IV.2. 9. Water chemistry conditions

Water Type	pH	EC* [$\mu\text{S}/\text{cm}$]	Bypass (g)
DI	5.6 ~ 6.4	1	0.32
1xBB	7.2	2030	0.45
2xBB	6.7	3540	0.44
3xBB	6.3	4760	0.41
TT	8.6	840	0.46
**CNa ₂ O ₃ 1 g/l	11.2	1703	0.55
**NaCl 1 g/l	6.7	1752	0.37
**NaCl 5 g/l	6.5	7290	0.28
**NaCl 10 g/l	6.6	15500	0.20
**H ₃ BO ₃ 1g/l	4.4	10	0.17

* Electrical Conductivity, $S = \Omega^{-1}$

** Chemicals dissolved in DI water

Figure IV.2.2 shows the weight of the debris bypass in terms of grams at different pH values from Table IV.2.6.

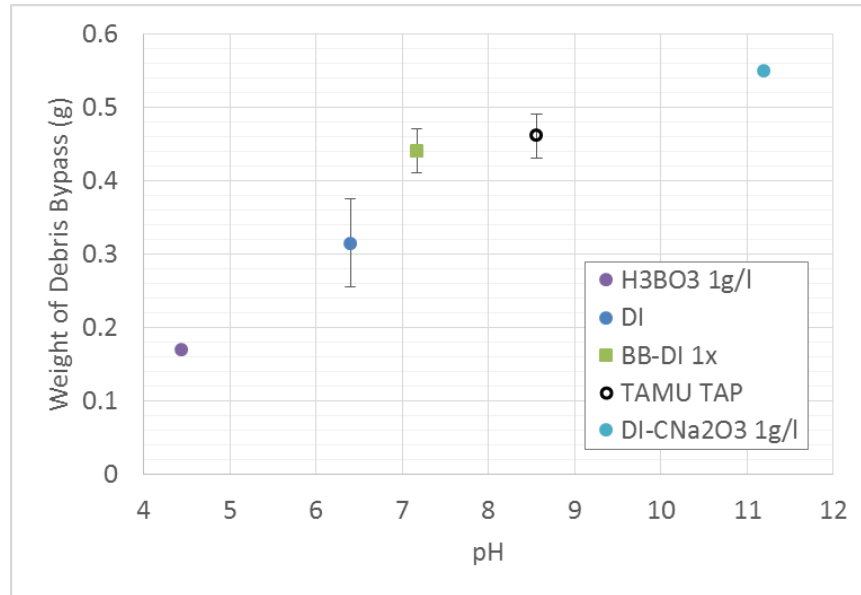


Figure IV.2. 2. pH effect on the weight of debris penetration

Figure IV.2.2 clearly shows that pH affected the quantity of debris bypass in the view of the full range of pH, though two results at pH higher than 7 did not show significant difference. The effect of pH may be explained by the electrical double layer repulsion in the depth filtration with the interaction energy. The electrical double layers on the surface of pores and around the debris overlap, then give rise to repulsive energy of interactions which tend to expel the fine particles from the surfaces. Khilar and Foger [48] summarized equations for double layer repulsion energy, V_{DLR} , of a sphere-plate system for a case of constant potential (Hogg et al. [49]) in Equation (IV.2.8) and for a case of constant charge (Wiese and Healy [50]) in Equation (IV.2.9).

$$V_{DLR} = (\varepsilon a_p / 4) \left[2\psi_{01}\psi_{02} \ln \left(\frac{1 + \exp(-\kappa h)}{1 - \exp(-\kappa h)} \right) + (\psi_{01}^2 + \psi_{02}^2) \ln(1 - \exp(-2\kappa h)) \right] \quad (IV.2.8)$$

$$V_{DLR} = (\varepsilon a_p / 4) \left[2\psi_{01}\psi_{02} \ln \left(\frac{1 + \exp(-\kappa h)}{1 - \exp(-\kappa h)} \right) - (\psi_{01}^2 + \psi_{02}^2) \ln(1 - \exp(-2\kappa h)) \right] \quad (IV.2.9)$$

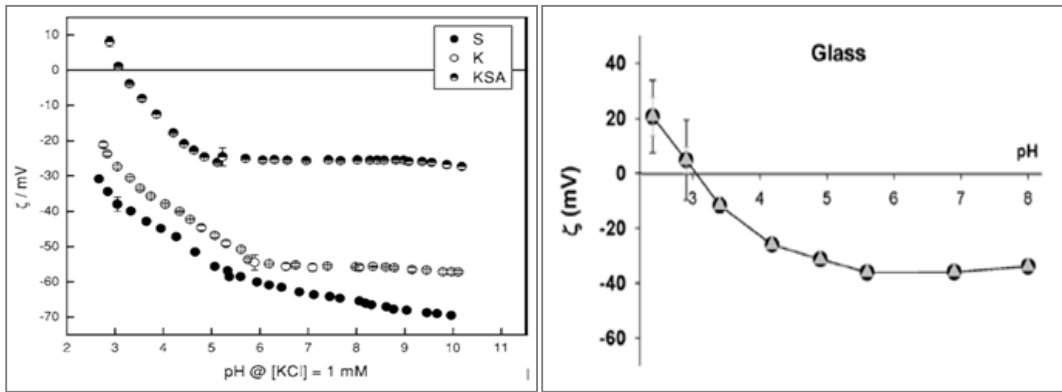
Here, ψ_{01} and ψ_{02} are the electric potentials, a_p is the particle radius, h is the distance of separation, ε is the dielectric constant, and κ is the Deby-Hücke parameter. Since the NUKON fiberglass generated both the fibrous bed and the debris, it can be assumed that ψ_{02} equals ψ_{01} . Then, Equations (IV.2.8) and (IV.2.9) reduce to Equations (IV.2.10) and (IV.2.11), respectively.

$$V_{DLR} = (\varepsilon a_p / 4) \psi_{01}^2 \left[\ln \frac{(1 + \exp(-\kappa h))^3}{1 - \exp(-\kappa h)} \right] \quad (IV.2.10)$$

$$V_{DLR} = (\varepsilon a_p / 4) \psi_{01}^2 \left[\ln \frac{1 + \exp(-\kappa h)}{(1 - \exp(-\kappa h))^3} \right] \quad (IV.2.11)$$

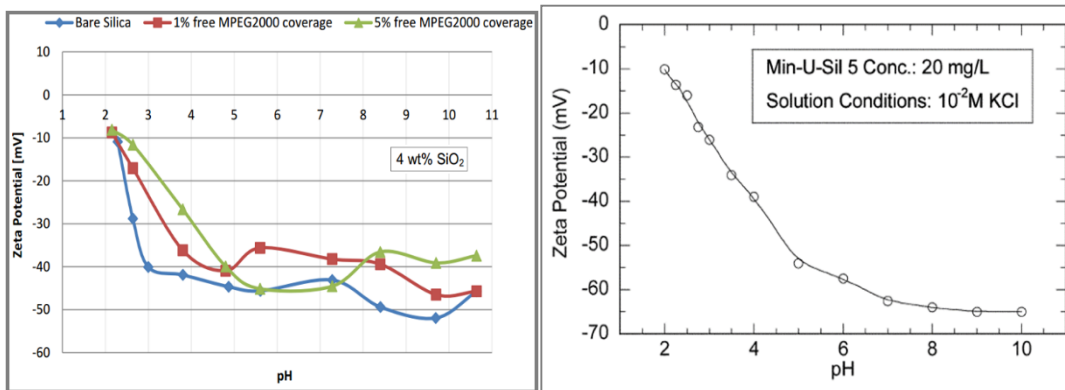
The electric potential ψ_{01} of the double layer can be replaced by the measured zeta potential. Then Equations (IV.2.10) and (IV.2.11) clearly show that the zeta potential increases the repulsion energy which lower the filtering efficiency. Eventually this increased repulsion energy results in greater debris bypass by decreasing probability for

the debris to agglomerate. Several researchers including Kim and Lawler [51], Bismarck et al. [52], Demircioglu [53], and Gallardo-Moreno et al. [54] reported experimental data of the pH effect on the zeta potential of glass materials, in which higher pH increased zeta potential as shown in Figure IV.2.3.



(a) Bismarck et al. [51]

(b) Gallardo-Moreno et al. [54]



(c) Kim and Lawler [52]

(d) Demircioglu [53]

Figure IV.2. 3. pH vs. zeta potential of glass (a, b) and silica (c, d) materials

It showed that some types of glass exhibited a well-established plateau in the range of $6 < \text{pH} < 10$. This plateau is similar to that the bypass quantities at higher than pH 7 are

not significantly different in Figure IV.2.3 as discussed in the previous section in detail with statistical analyses. Figure IV.2.4 is a plot of the quantity of debris bypass against electrical conductivity (EC). Since EC is one of the indicators of ionic strength, I , in a chemical solution, the effect of EC might be considered as the effect of ionic strength. There are several methods available to calculate ionic strength based on EC such as proportional ionic strength linear method by Russell [55], inverse Marion-Babcock nonlinear method [56, 57], and a method based on the diffusion coefficient by Parkhurst and Appelo [58].

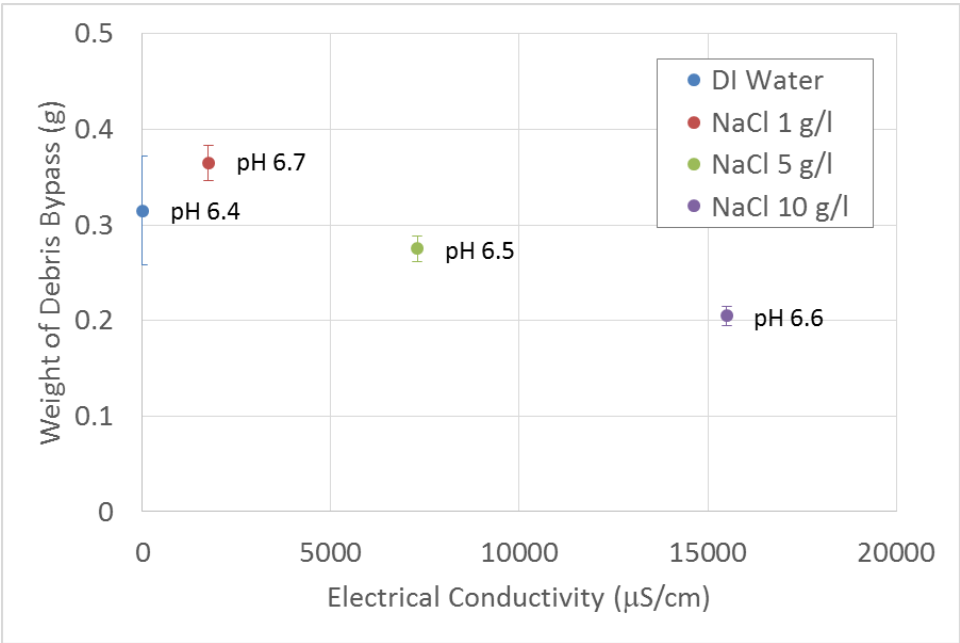


Figure IV.2. 4. EC effect on the weight of debris penetration

The comparison of TAMU tap, 1xBB DI water, and 2xBB DI water showed a decreasing quantity of debris bypass as EC increases. It agrees with the results of Kolakowski and Matijevic [59] and Kia and Fogler [60] that the zeta potential decreased as the electrolyte concentration increased. It is known that higher ionic strength compresses the thickness of the electric double layer, which decreases the double layer potential. Carneiro-da-Cunha et al. [61] reported that the effect of pH is much stronger than that of ionic strength and other factors on an electrostatic self-assembly process. This shows agreement with that the quantity of debris bypass in DI water was significantly smaller than in other types of water, even though DI water has much lower EC. Also, the ionic composition of medium affects the zeta potential as reported by Kolakowski and Matijevic [59] in which a HNO₃ solution at pH 4.0 had the zeta potential of -63mV, whereas a NaOH solution at pH 9.6 had the zeta potential of -18mV. This is not consistent with what observed in a single electrolyte as shown in Fig. 7. Thus, in order to clearly separate the effects of ionic strength and pH, additional studies with different chemical components might be required.

IV.2.3 Temperature effect test results

Before conducting high temperature tests, three tap water tests at 26 ± 3 °C were conducted to prove that the high temperature horizontal facility generates results within the standard deviation of the room temperature test results using the low temperature facility. The results of the high temperature horizontal facility were confirmed to be within the range of the tests performed previously, so, in total, seven room temperature

test results were available to be compared to high temperature tests. Table IV.2.10 summarizes the results of the eight tests performed with tap water approximately within 82.8 ± 8 °C. Since the first four tests showed greater standard deviation than the room temperature tests, additional four tests were conducted to obtain repeatability. The average weight of the debris bypass of the eight tests was 0.45g and the standard deviation was 0.08g.

Table IV.2. 10. High temperature TAMU tap water test results

Test #	Debris Bypass (g)			Temperature (°C)		
	M _{initial}	M _{final}	M _{debris}	Max	Min	Mean
HT-1	55.08	55.44	0.36	88.8	79.4	83.9
HT-2	48.38	48.74	0.36	86.0	78.2	82.3
HT-3	47.64	48.10	0.46	83.5	75.5	79.5
HT-4	48.87	49.43	0.56	86.0	77.4	81.8
HT-5	50.41	50.92	0.51	85.0	76.6	81.0
HT-6	44.23	44.77	0.54	92.5	80.6	85.3
HT-7	50.51	50.97	0.46	89.4	80.1	84.5
HT-8	46.35	46.71	0.36	88.6	79.8	84.3
Average	N/A	N/A	0.45	87.5	78.4	82.8
Stdev	N/A	N/A	0.08	2.9	1.8	2.0

During the high temperature experiments, the temperature history of water was recorded as shown in Figure IV.2.5.

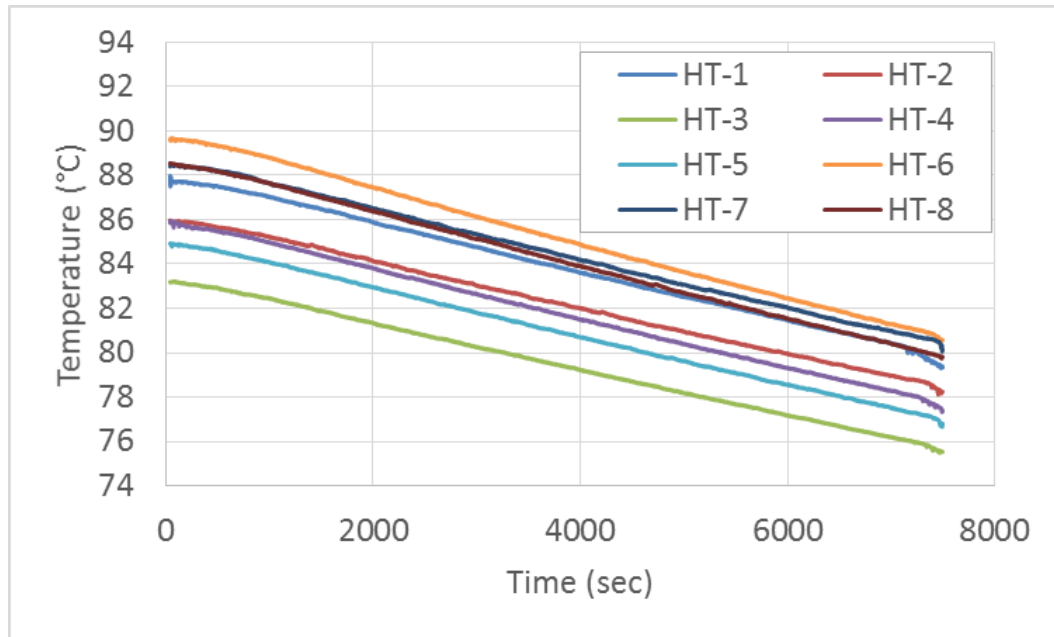


Figure IV.2. 5. Temperature history of high temperature test

The mean temperature of each test ranged between 79.5 °C and 85.3 °C. In order to check if there was any effect of temperature the weight of debris bypass versus the measured average temperature was plotted in Figure IV.2.6. It shows that the average temperature in high temperature range resulted no significant effect on the weight of debris bypass.

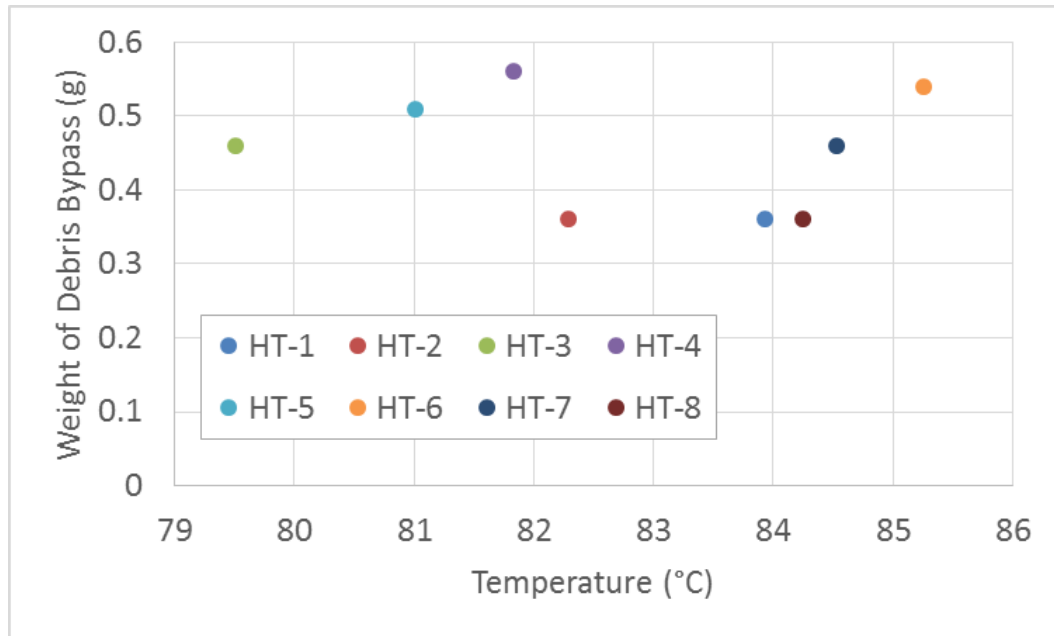


Figure IV.2. 6. Effect of average temperature on weight of debris bypass for high temperature tests

A statistical comparison between the high temperature tests and room temperature tests was performed following the same method of Welch's t-test described previously. The mean, Equation (IV.2.12), and variance, Equation (IV.2.13), of the tap water results at room temperature were recalled:

$$\bar{W}_{HT} = \frac{1}{8} \sum_{i=1}^8 W_{HT,i} = 0.45 \quad (\text{IV.2.12})$$

$$S_{TT}^2 = \frac{1}{7} \sum_{i=1}^7 (W_{TT,i} - \bar{W}_{TT})^2 = 0.00067 \quad (\text{IV.2.13})$$

The mean and the variance of high temperature tests were calculated in Equations (IV.2.14) and (IV.2.15), respectively.

$$\bar{W}_{HT} = \frac{1}{8} \sum_{i=1}^8 W_{HT,i} = 0.45 \quad (\text{IV.2.14})$$

$$S_{HT}^2 = \frac{1}{8} \sum_{i=1}^8 (W_{HT,i} - \bar{W}_{HT})^2 = 0.00711 \quad (\text{IV.2.15})$$

The t-statistic parameter was then calculated in Equation (IV.2.16):

$$t = \frac{\bar{W}_{HT} - \bar{W}_{TT}}{\sqrt{\frac{S_{HT}^2}{8} + \frac{S_{TT}^2}{7}}} = 0.32 \quad (\text{IV.2.16})$$

The degree of freedom was calculated using the Welch-Satterthwaite equation (Equation (IV.2.17) :

$$\nu = \frac{\left(\frac{S_{HT}^2}{8} + \frac{S_{TT}^2}{7} \right)^2}{\frac{S_{HT}^4}{448} + \frac{S_{TT}^4}{294}} = 8.4820 \quad (\text{IV.2.17})$$

Assuming a level of confidence α equal to 0.05 (95%) with the calculated degree of freedom, Equation (IV.2.17), critical t-value was found to be $t_{crit} \approx 2.28$. Based on the calculated t-statistic parameter (IV.2.16) and the value of t_{crit} , for the sets of tests performed, the following condition was found:

$$t = 0.1711 < t_{crit} \approx 2.28 \quad (\text{IV.2.18})$$

Water temperature did not statistically significantly affect the quantity of debris bypass. However, high temperature tests showed greater standard deviation, therefore, it will be more conservative to use this standard deviation, 17%, of the high temperature tests as the uncertainty of the bypass quantity.

IV.2.4 Effect of debris concentration

At the early phase of debris bypass, higher debris concentration resulted in greater amount of debris bypass. However, more transportation of debris results in thicker fibrous beds, which are a filter in another point of view. Also, as time goes, the concentration of debris approaching the strainer decreases. Thus, the debris bypass should be investigated as a function of injected concentration and time. Tables IV.2.11 and IV.2.12 presents the bypass test results with different amount of debris injected and at different termination times in the horizontal facility and the vertical facility, respectively.

Table IV.2. 11. Debris bypass in the horizontal loop* experiments

U (cm/s)	Injection (g)	Bypass (g)				
		$N_T^{**} = 0.25$	$N_T = 0.5$	$N_T = 1$	$N_T = 2$	$N_T = 10$
0.31	6.6	0.23	0.3±0.04	0.46±0.03	0.57±0.01	0.57±0.01
	15	-	-	0.62	-	1.1±0.01
	40	-	-	1.07	-	1.41
3.11	6.6	-	-	0.28	-	0.43
	40	-	-	0.42±0.04	-	0.42 ±0.09

* Strainer surface area of the vertical loop is 81.07 cm²

** N_T is number of turnovers defined in Equation (IV.2.20)

Table IV.2. 12. Debris bypass in the vertical loop* experiments

U (cm/s)	NUKON (g)	Bypass (g)		
		$N_T = 1$	$N_T = 2.25$	$N_T = 10$
0.31	6.6	0.77	1.03 ± 0.05	-
	40	1.65	-	2.69
3.11	6.6	0.46	0.74 ± 0.06	-
	40	1.30	-	-

* Strainer surface area of the vertical loop is 182.41 cm²

Each facility has its own strainer size which changes the flow rate even at the same liquid approach velocity. This is also true for commercial PWRs, and there are several design factors affecting the debris bypass condition such as the total volume of water collected in the sump, the surface area of the strainer, and flow rate. Thus, the quantity of debris bypass should be analyzed using grams per unit surface area to generalize the results of different facilities. Figure IV.2.7 presents the total quantity of bypass per unit surface area with different quantities of injection per unit surface area. The lowest weight of debris injected was selected to cover 99% of the postulated accidents in South Texas Project (STP) nuclear power plant based on the probabilistic risk analysis [37].

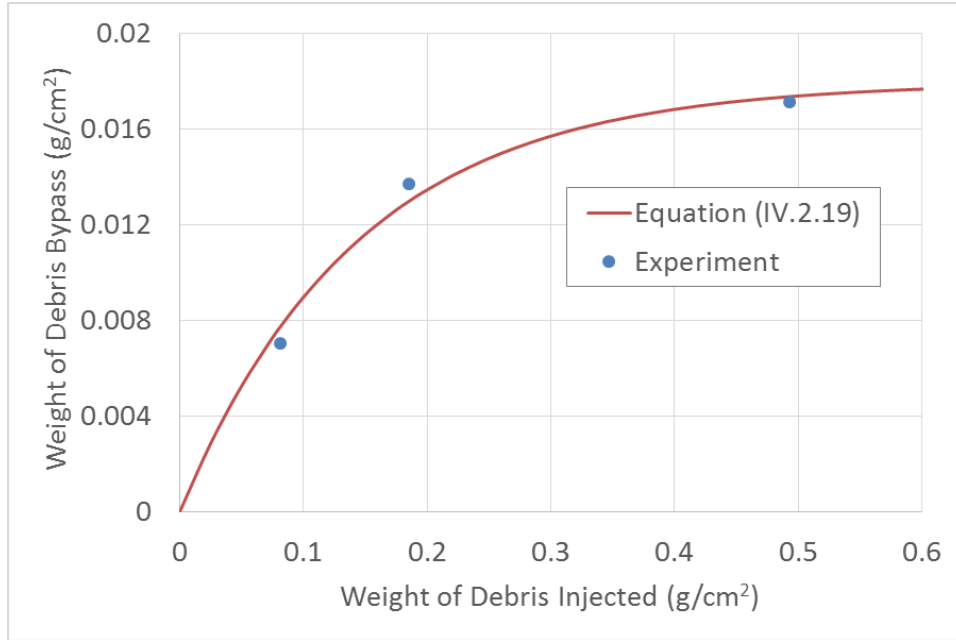


Figure IV.2. 7. Quantity of debris bypass as a function of debris injection concentration in the horizontal test facility

In order to have an acceptable margin additional tests were conducted with double concentration and five times concentration. Equation (IV.2.19) was developed based on the experimental results in Figure IV.2.7.

$$w_{\max} = w_{\infty} \left(1 - e^{-w_{\text{injected}}/\tau_w}\right) = 0.01795 \left(1 - e^{-w_{\text{injected}}/0.1443}\right) \quad (\text{IV.2.19})$$

where w_{\max} is the maximum weight of debris bypass per unit surface area (g/cm²) of the strainer when w_{injected} of debris (g/cm²) is injected. w_{∞} and τ_w were experimentally determined coefficients for the present study. With 95% confidence bounds, w_{∞} and τ_w were calculated to be 0.01795 ± 00407 and 0.1443 ± 0.08542 , respectively. The sum of

squares due to error (SSE) was 1.069×10^{-6} , R-square was 0.9938, and root mean square error (RMSE) was 0.0007311. The concentration of debris approaching the strainer is a function of number of turnovers, N_T , defined in Equation (IV.2.20).

$$N_T = \frac{\text{Flow rate} \times \text{Time}}{\text{Volume of Water in the Tank}} = \frac{UAt}{V} \quad (\text{IV.2.20})$$

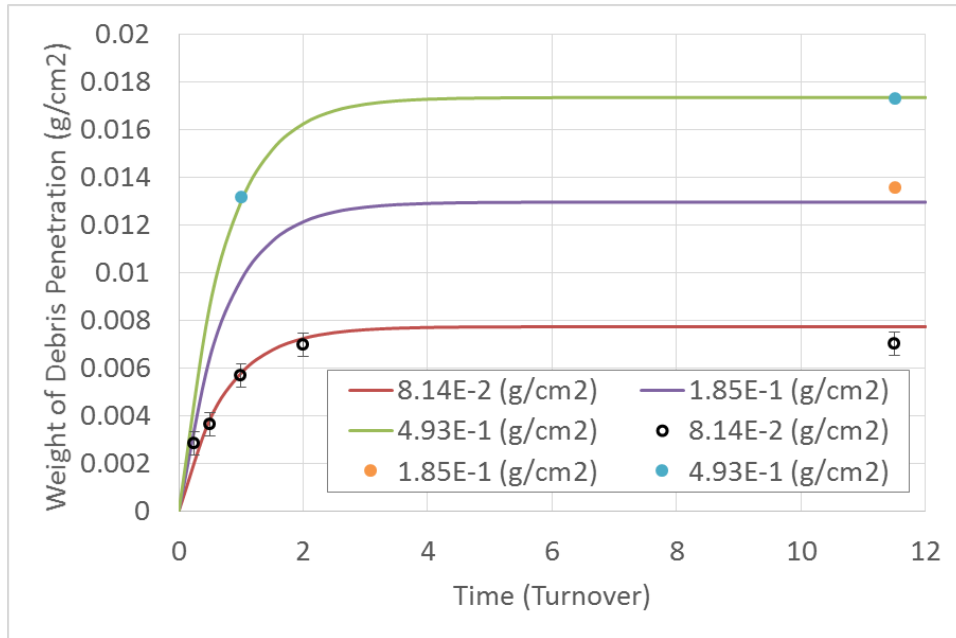


Figure IV.2. 8. Quantity of debris bypass vs. time at different concentrations in the horizontal test facility (lines: Equation (IV.2.21), dots: Experiments)

The quantity of debris bypass per unit surface area of a strainer, w_{bypass} (g/cm^2), was obtained as a function of injected quantity per unit surface area of the strainer, flow rate, volume of water in the sump, and time as shown in Equation (IV.2.21).

$$w_{bypass} = w_{\max} \left(1 - e^{-N_T/\tau}\right) = w_{\infty} \left(1 - e^{-w_{injected}/\tau_w}\right) \left(1 - e^{-N_T/\tau}\right) \quad (\text{IV.2.21})$$

With 95% confidence bounds, τ was experimentally determined to be 0.7263 ± 0.2224 .

The SSE was 1.069×10^{-06} , the R-square was 0.9349, and the RMSE was 0.0004908.

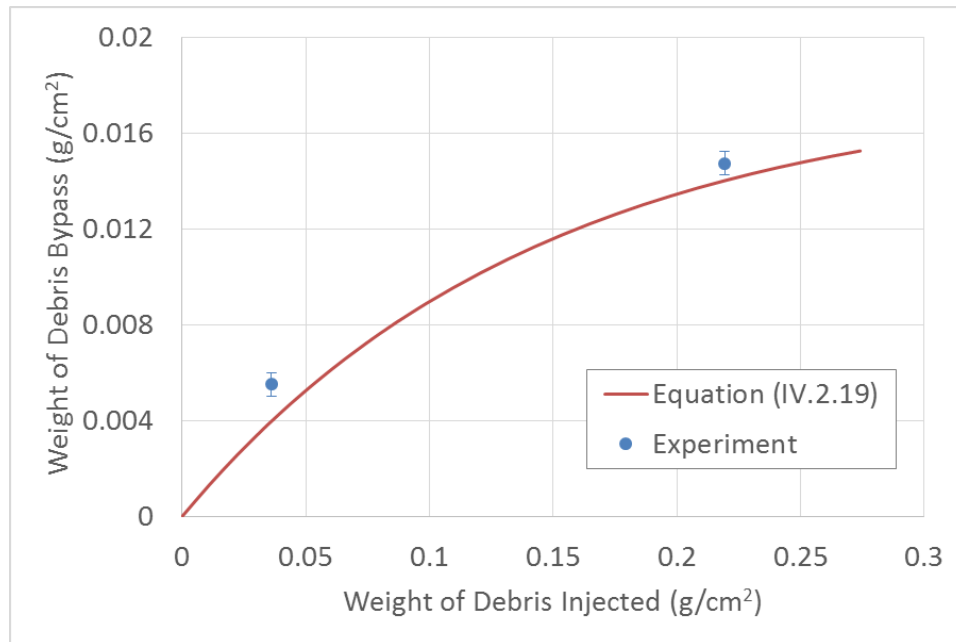


Figure IV.2. 9. Quantity of debris bypass as a function of debris injection concentration in the vertical test facility

As shown in Figure IV.2.9, the model (Equation (IV.2.23)) predicted the quantity of debris bypass in the vertical system with an accuracy of 5% for large amount of debris injection (40g). However, at low concentration (0.036 g/cm²), it under predicted the amount by 28%. This type of under prediction can be also found in the small number of turnovers in Figure IV.2.8. A possible reason is that the debris bed is not built up enough

to form a representative porous medium which functions as a filter with small quantity of debris transported either in low injection concentration or in early phases of the bed generation.

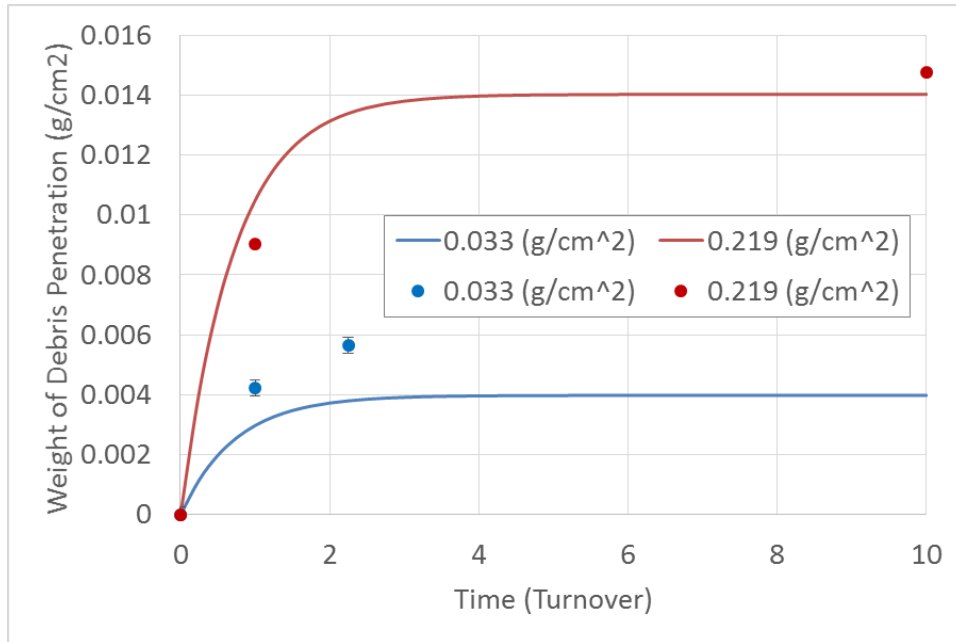


Figure IV.2. 10. Quantity of debris bypass vs. time at different concentrations in the vertical test facility (lines: Equation (IV.2.21), dots: Experiments)

The models, so far, predicted the total quantity of debris bypass in terms of grams per unit surface area. In further works to develop a filtration efficiency model additional investigations focused on instantaneous bypass of debris will be required.

IV.2.5. Effect of fluid approach velocity

The effect of fluid approach velocity on the quantity of debris bypass was experimentally investigated at 0.31 cm/s, 0.65 cm/s, and 3.11 cm/s. Additionally, the approach velocity effect on the debris bypass for the conditions with different debris concentrations at different turnovers was tested. The summary of the tests is presented in Table IV.2.13.

Table IV.2. 13. Summary of fluid approach velocity effect tests

Facility	Approach Velocity (cm/s)	Debris Injected (g)	Turnovers	Debris Bypass (g)
Horizontal	0.31	6.6	1	0.46 ± 0.03
Horizontal	0.31	6.6	2	0.57 ± 0.01
Horizontal	0.31	6.6	10	0.57 ± 0.01
Horizontal	0.31	40	1	1.07
Horizontal	0.31	40	10	1.41 ± 0.02
Horizontal	0.65	6.6	2	0.56 ± 0.01
Horizontal	3.11	6.6	1	0.28
Horizontal	3.11	6.6	10	0.43
Horizontal	3.11	40	1	0.42 ± 0.09
Horizontal	3.11	40	10	0.42 ± 0.04
Vertical	0.31	6.6	1	0.77
Vertical	0.31	6.6	2.25	1.03 ± 0.05
Vertical	0.31	40	1	1.65
Vertical	3.11	6.6	1	0.46
Vertical	3.11	6.6	2.25	0.74 ± 0.06
Vertical	3.11	40	1	1.30

Two low approach velocities of 0.31 cm/s and 0.65 cm/s showed almost the same quantity of debris bypass. Figure IV.2.11 more clearly presents the graphical comparison of the quantities of debris bypass at different approach velocity.

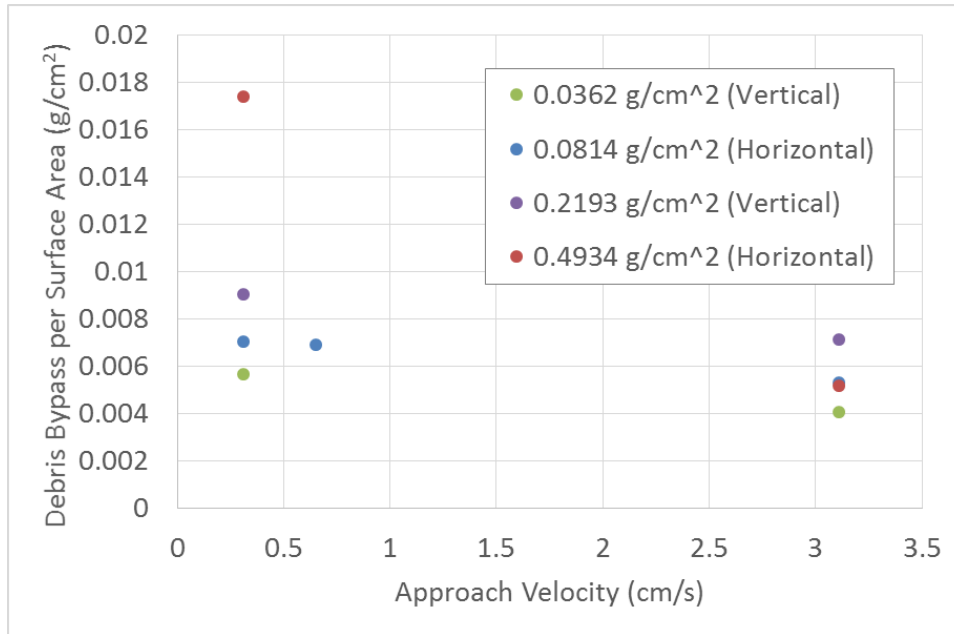


Figure IV.2. 11. Quantity of debris bypass vs. approach velocity for different injection concentrations

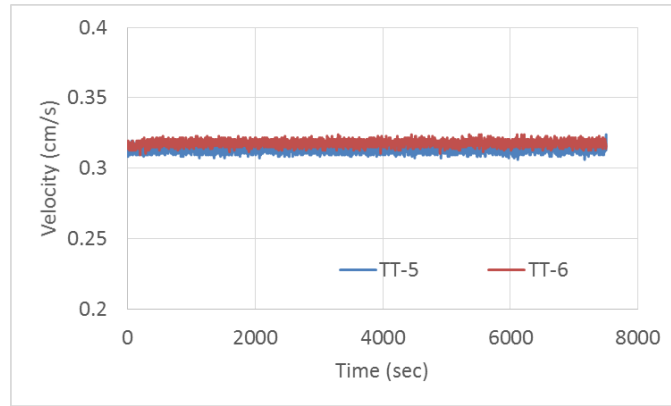
At higher fluid approach velocity, it is known that more penetration by Khilar (1981) [62] and Ryan and Gschward (1994) [63] when the structure of a porous filter is unchanged. However, the fibrous porous media in this study is compressible filter, thus the hydraulic pressure resulted more compression of fibrous bed and, consequently, the porosity of the bed decreased shrinking the pore size.

IV.2.6 Effect of flow fluctuation

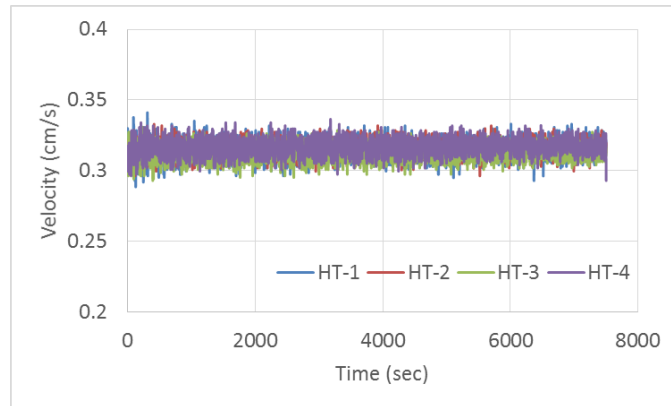
The high temperature system was equipped with external heaters on the returning pipe line downstream of the pump. Those heaters were used to keep the constant temperature of the system. After carrying out several tests with and without the external heaters, it was found that external heaters became a source of flow fluctuation and that more debris bypass was measured when the flow fluctuated. The quantity of debris bypass with and without the external heaters are presented in Table IV.2.14 and the flow fluctuations are plotted in Figure IV.2.12.

Table IV.2. 14. Quantity of debris bypass at different flow fluctuations

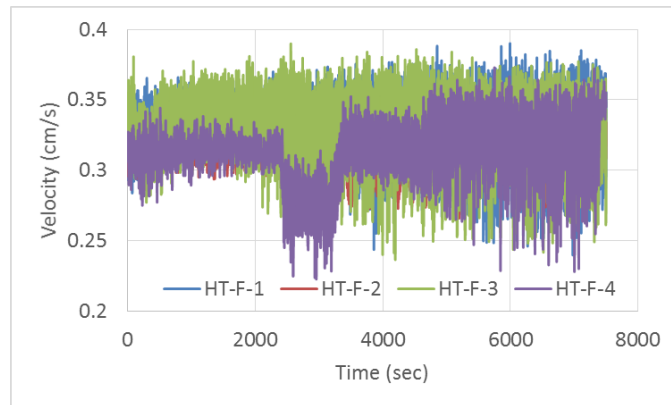
Room Temperature	Test #	TT-5	TT-6	-	-
	Bypass (g)	0.46	0.44	-	-
Weak Fluctuation High Temperature	Test #	HT-1	HT-2	HT-3	HT-4
	Bypass (g)	0.36	0.36	0.46	0.56
Strong Fluctuation High Temperature	Test #	HT-F-1	HT-F-2	HT-F-3	HT-F-4
	Bypass (g)	0.68	0.64	0.71	0.65



(a) Room temperature



(b) Weak fluctuation at high temperature without external heaters



(c) Strong fluctuation at high temperature with external heaters

Figure IV.2. 12. Flow fluctuations at (a) room temperature, (b) high temperature without external heaters, and (c) high temperature with external heaters

Although the tests HT-1 ~ HT-4 showed more fluctuation than the room temperature tests TT-5 and TT-6, the mean values of debris bypass were similar. However, as recalled from Table IV.2.14, the standard deviations showed large difference. It can be interpreted that fluctuation may cause greater uncertainty of debris bypass, even if there is a probability that temperature affected such the larger standard deviation of debris bypass. One possible source of the fluctuation is local boiling caused by the heaters, however, it should be experimentally validated. Local flow fluctuation near the strainer was measured using a Laser Doppler Velocimetry (LDV). It showed huge fluctuation caused by the mixing propeller regardless of the external heaters. Therefore it seemed bypass was more affected by the fluctuation of mean velocity than turbulence upstream of the strainer. It is clear that fluctuation is strongly related to the debris bypass. In the ECCS of a PWR, there might be multiple sources generating vibration of the pipe lines or fluctuation of coolant flow in a LOCA condition. Therefore, additional studies to calculate possible magnitude of mechanical vibration of the pipe lines and coolant fluctuation including flow rate and pressure should be conducted for more accurate and conservative prediction.

IV.3. Debris size characterization

A debris size characterization system was developed using two different magnifications. This system was applied to a NUKON sample prepared using NEI protocol at Texas A&M University and three samples for the Vogtle nuclear power plant operated by the Southern Nuclear Company (SNC) and four sets of samples for STP produced by Alden

Research Laboratory (ARL). The samples for each set were taken at different times during experiments carried out to study the debris bypass behavior by ARL. Figure IV.3.1 shows the containers as received.

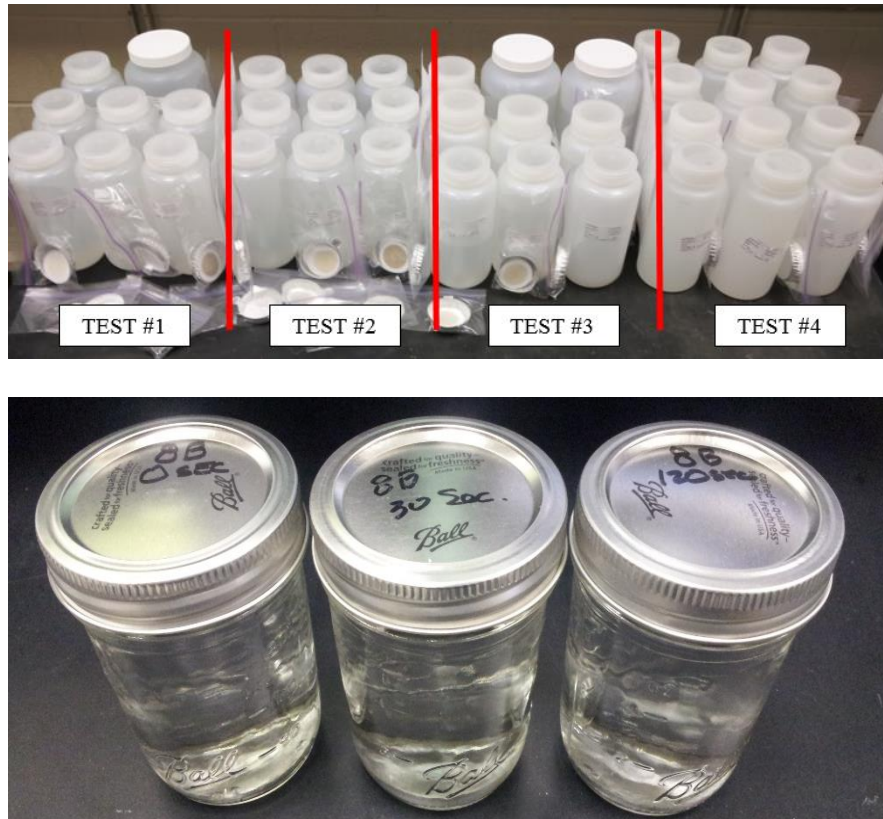


Figure IV.3. 1. Debris samples in containers - four sets of samples for STP (top) and three samples for Vogtle (bottom).

The samples that came from ARL were prepared using NEI protocol as well. Different samples during each test were taken downstream of the strainer at different turnovers using an isokinetic sampling port for STP. The SNC samples were simply taken from the water tank. The samples selected for the debris size characterization are the following:

- NEI Preparation 0.9 Volume% (NEI 0.9 vol.%) - TAMU
- STP Test #4, Sample #2 (T#4-S#2) - Sampled at 5 min since fiber addition
- Vogtle 8B-0SEC - 0 sec from the water tank in the ARL test facility

Figure IV.3.2 presents the samples in glass vials for eye-view observation. Even an eye observation of the samples showed the presence of a limited number of large fibers (approximately 1 cm, see areas inside the circles) which were not found in the STP sample.

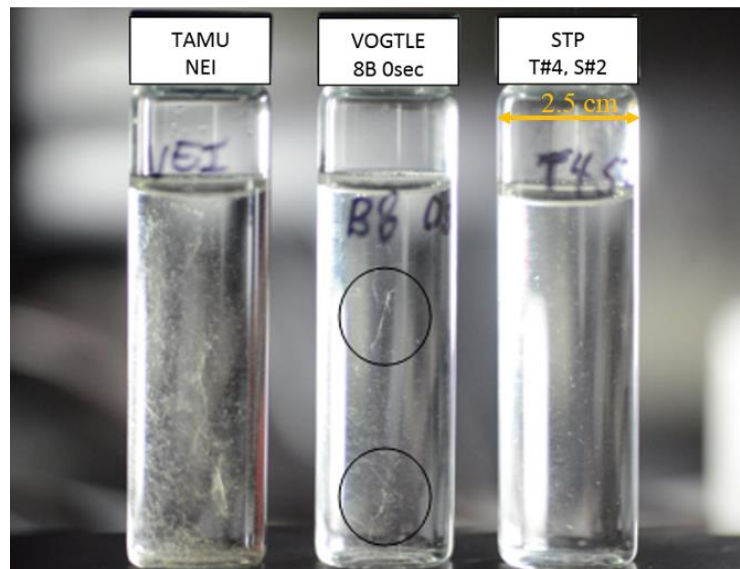


Figure IV.3. 2. Samples in glass vials

For each sample listed above, four independent measurements were performed to achieve statistically reasonable results. Each measurement started from a new sample which was prepared following the procedure described previously. Pictures were also

post-processed to achieve a better illumination and contrast. In this characterization the maximum feret length (or maximum caliper diameter) in Figure IV.3.3 was used as defined on the NIST website. (<http://www.nist.gov/lispix/doc/particle-form/morph-param.htm>)

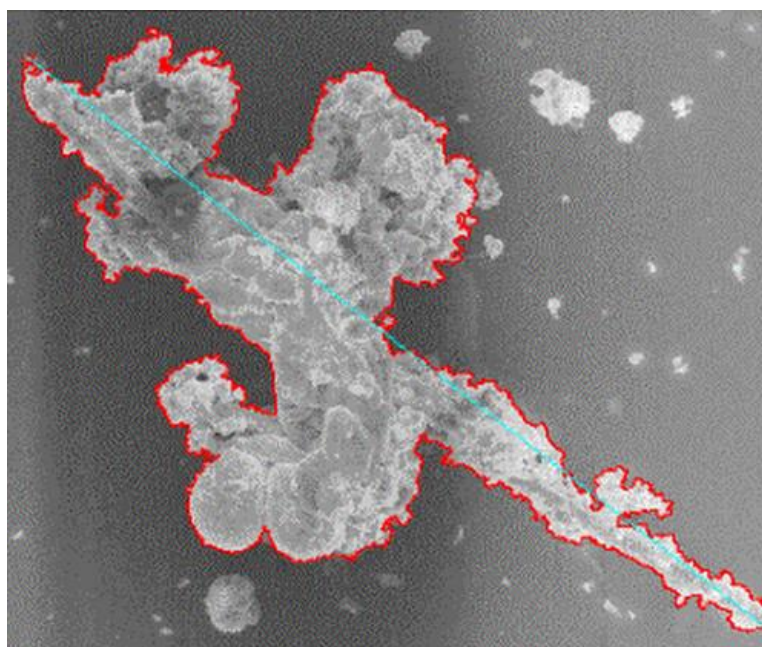


Figure IV.3. 3. Maximum feret length (caliper diameter)

Pictures of the samples (Vogtle top, STP middle, and NEI bottom) were taken with the microscope, as shown in Figures IV.3.4 and IV.3.5 with 2x magnification and 20x magnification, respectively.

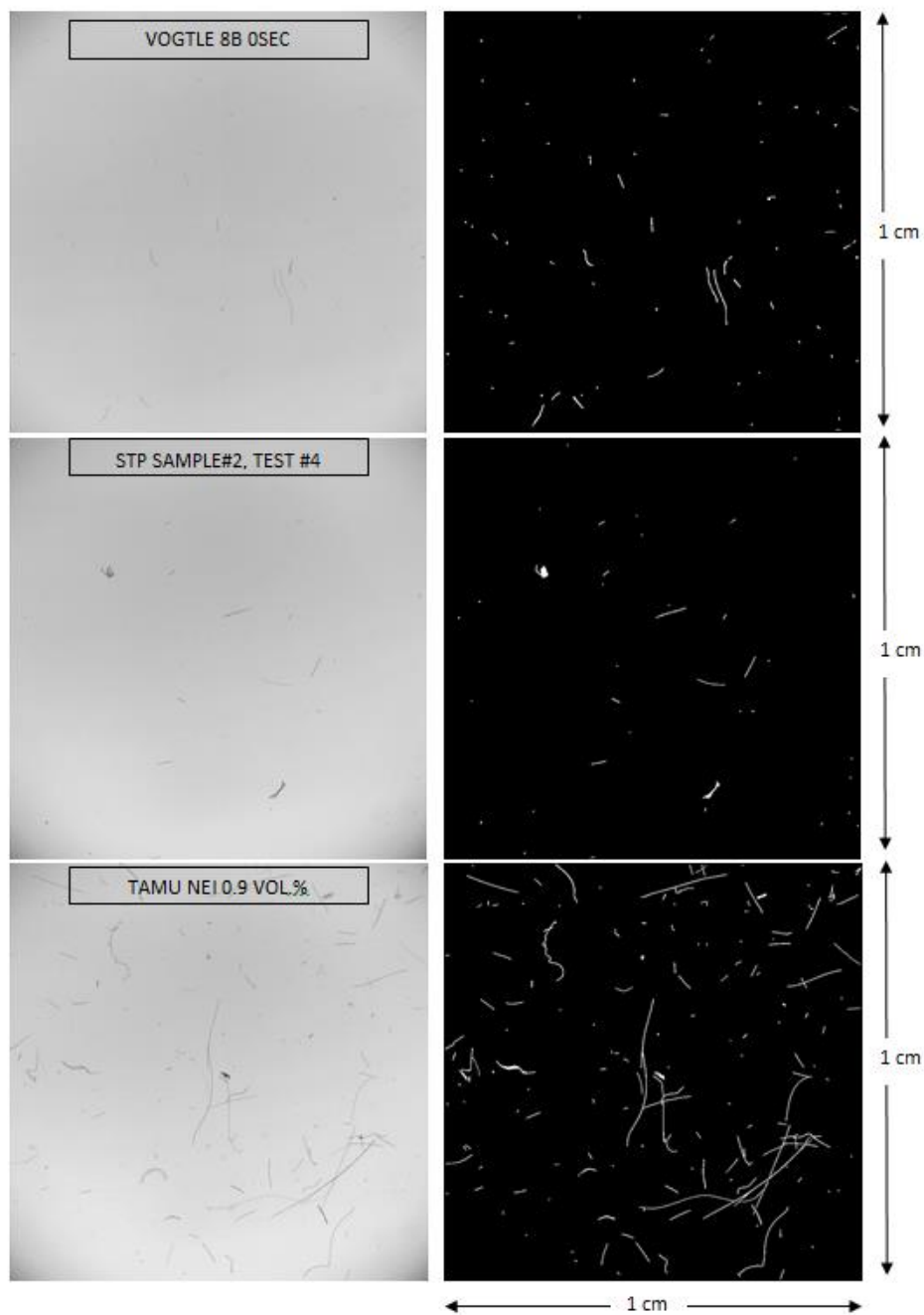


Figure IV.3. 4. Picture of samples with 2x magnification

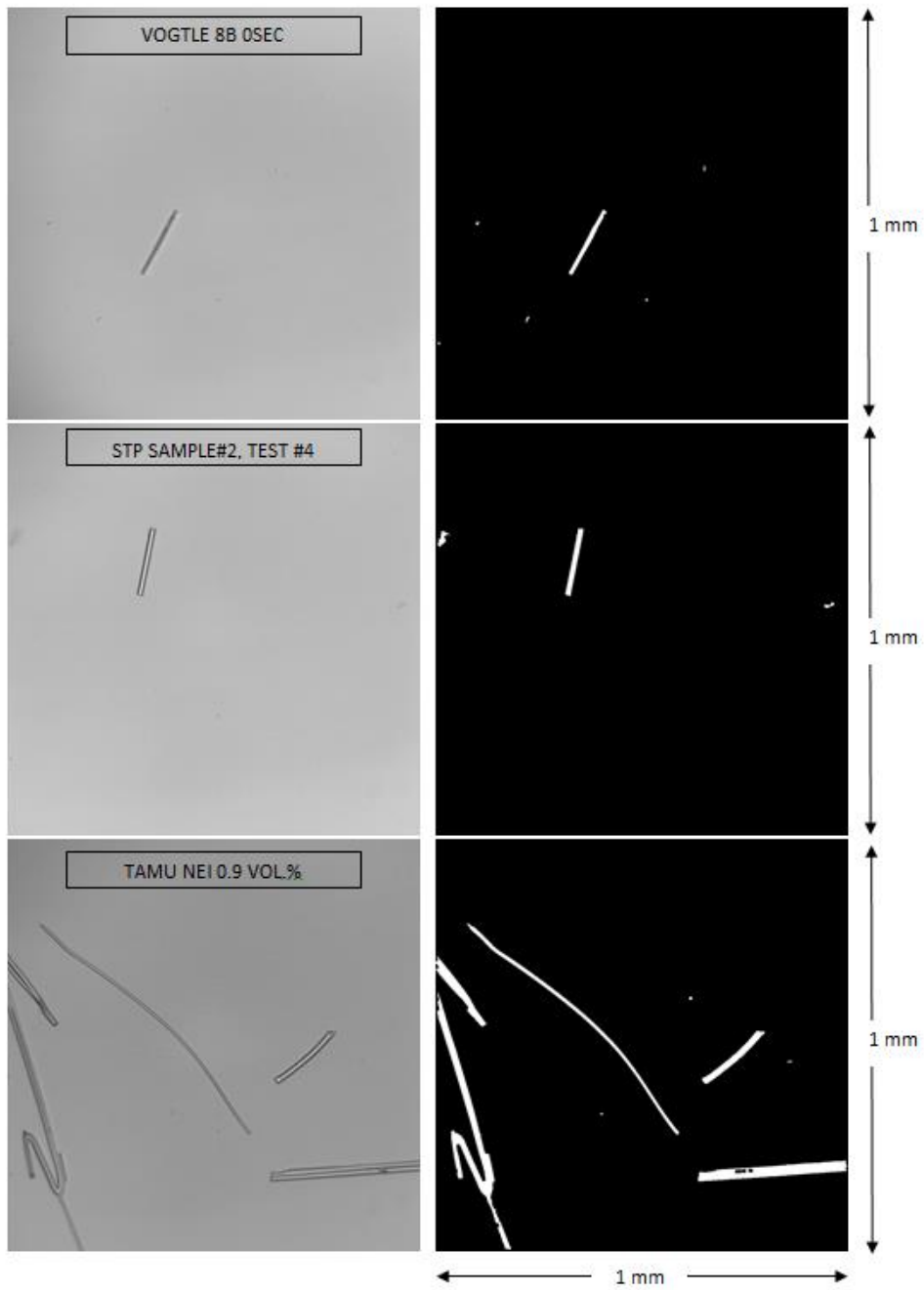


Figure IV.3. 5. Picture of samples with 20x magnification

The characterization results are shown in terms of:

- Volume % Vs Debris Size (Feret Length), X-axis linear scale (Figure IV.3.6)
- Volume % Vs Debris Size (Feret Length), X-axis log scale (Figure IV.3.7)
- Volume % CDF Vs Debris Size (Feret Length), X-axis linear scale (Figure IV.3.8)
- Volume % CDF Vs Debris Size (Feret Length), X-axis log scale (Figure IV.3.9)
- Count Vs Debris Size (Feret Length), X-axis linear scale (Figure IV.3.10)
- Count Vs Debris Size (Feret Length), X-axis log scale (Figure IV.3.11)
- Count CDF Vs Debris Size (Feret Length), X-axis linear scale (Figure IV.3.12)
- Count CDF Vs Debris Size (Feret Length), X-axis log scale (Figure IV.3.13)

The standard deviations of cumulative distribution functions (CDFs) are cumulative as CDFs, thus those increases as integrated.

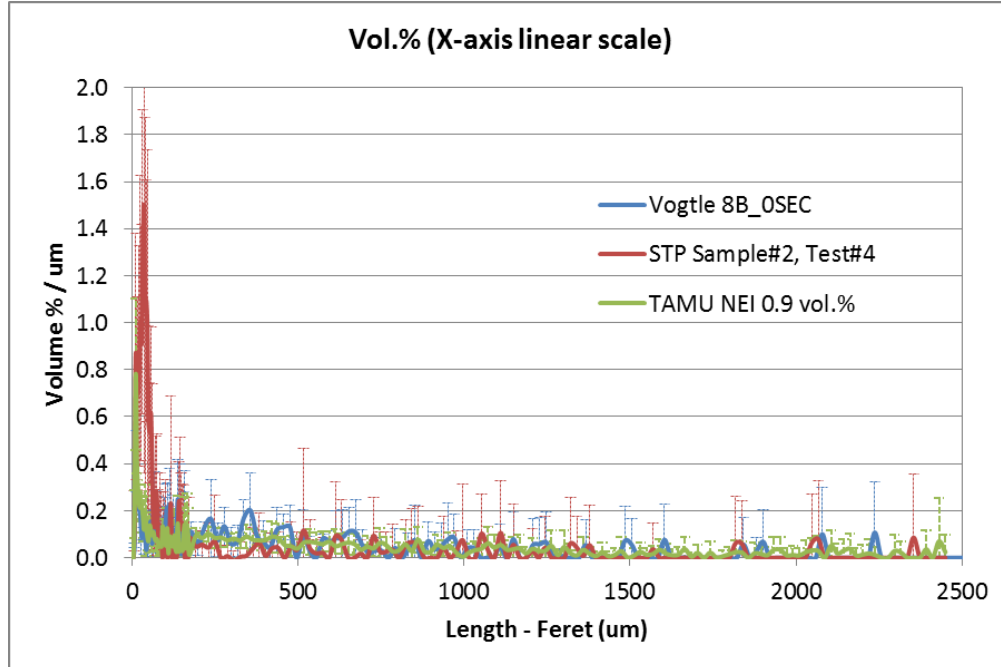


Figure IV.3. 6. Volume % vs. debris size (feret length), x-axis linear scale

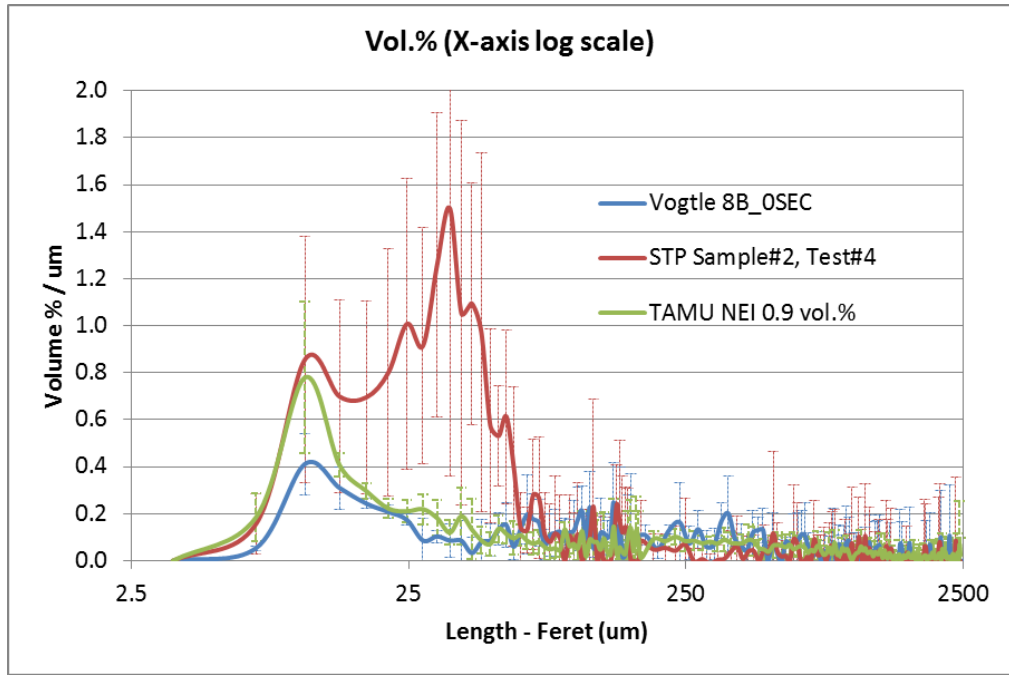


Figure IV.3. 7. Volume % vs. debris size (feret length), x-axis log scale

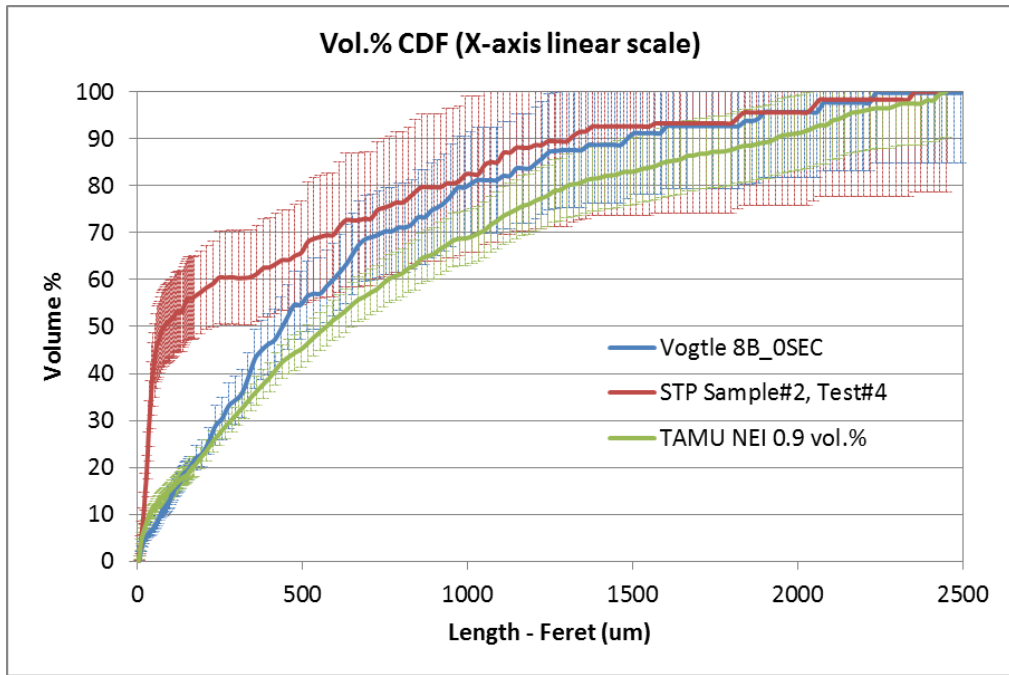


Figure IV.3. 8. Volume % CDF vs. debris size (feret length), x-axis linear scale

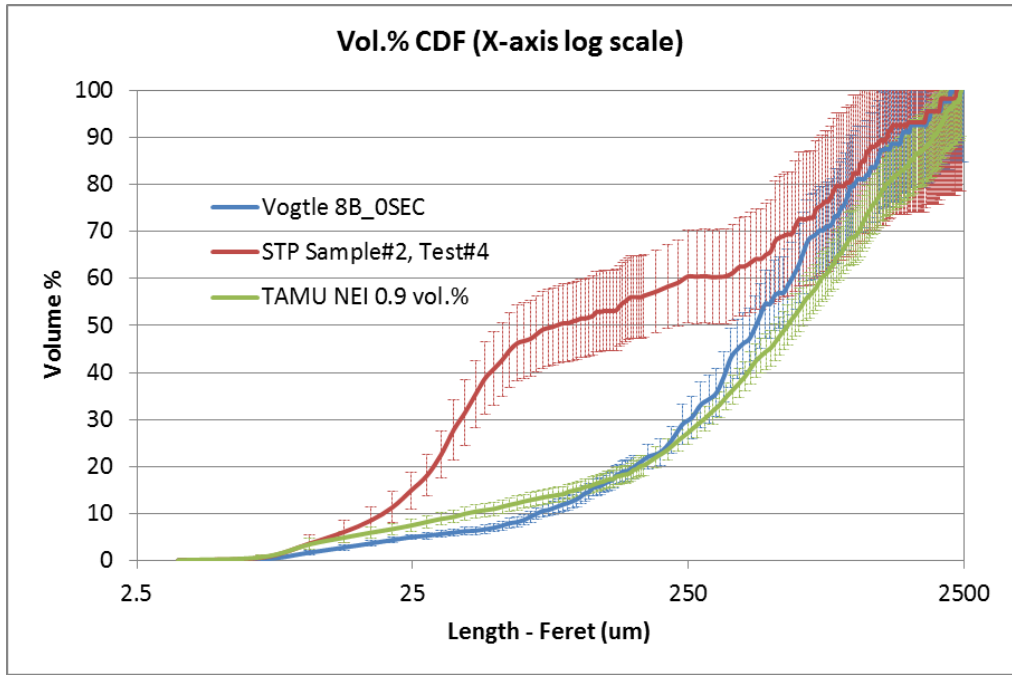


Figure IV.3. 9. Volume % CDF vs. debris size (feret length), x-axis log scale

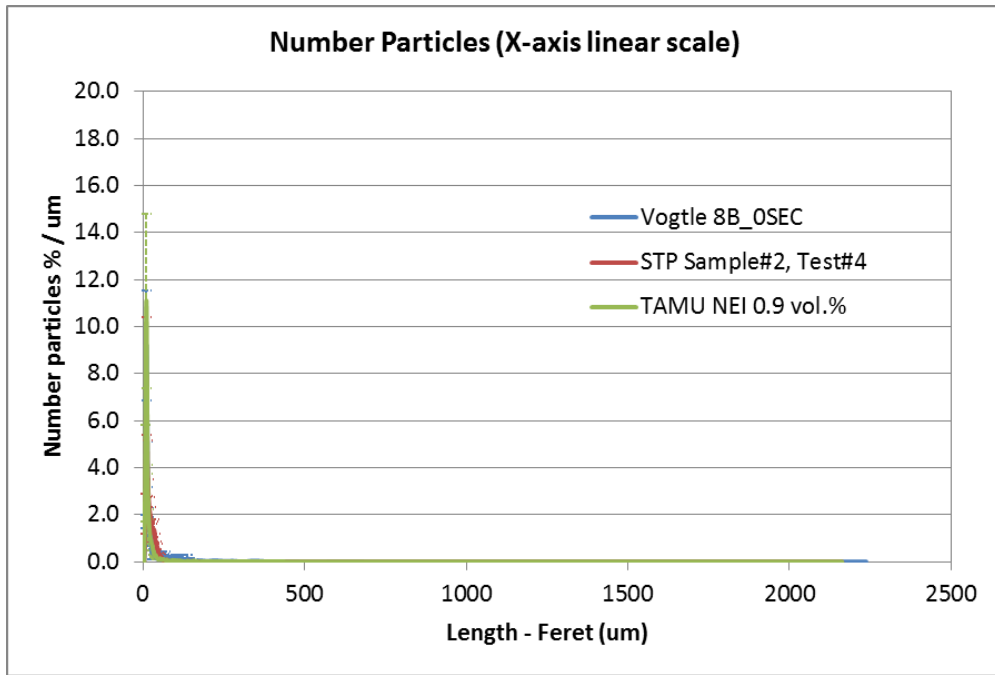


Figure IV.3.10. Count vs. debris size (feret length), x-axis linear scale

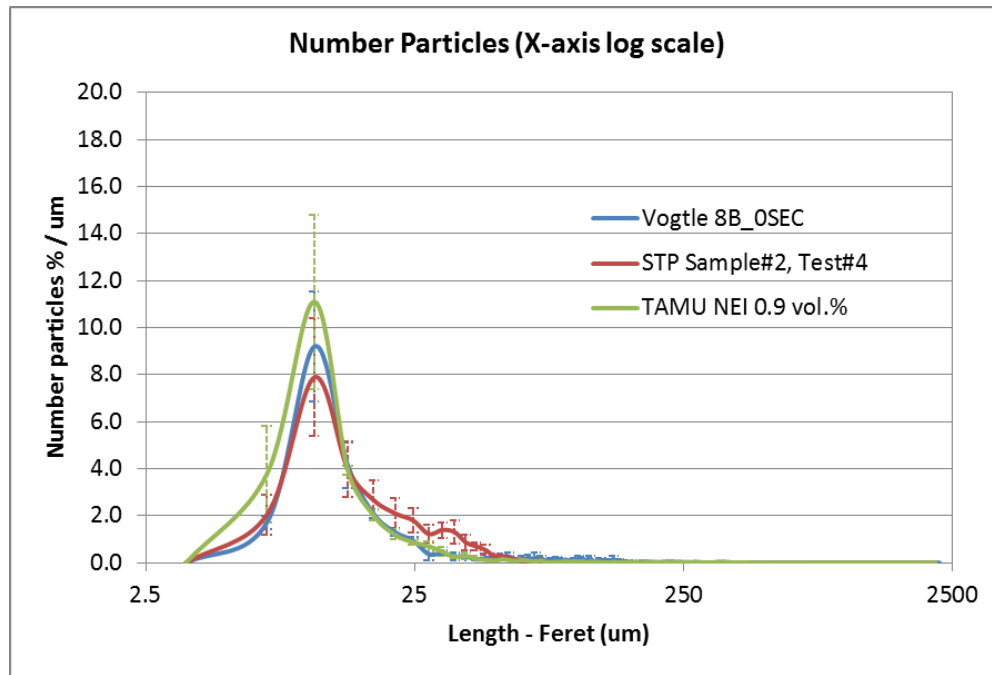


Figure IV.3.11. Count vs. Debris size (feret length), x-axis log scale

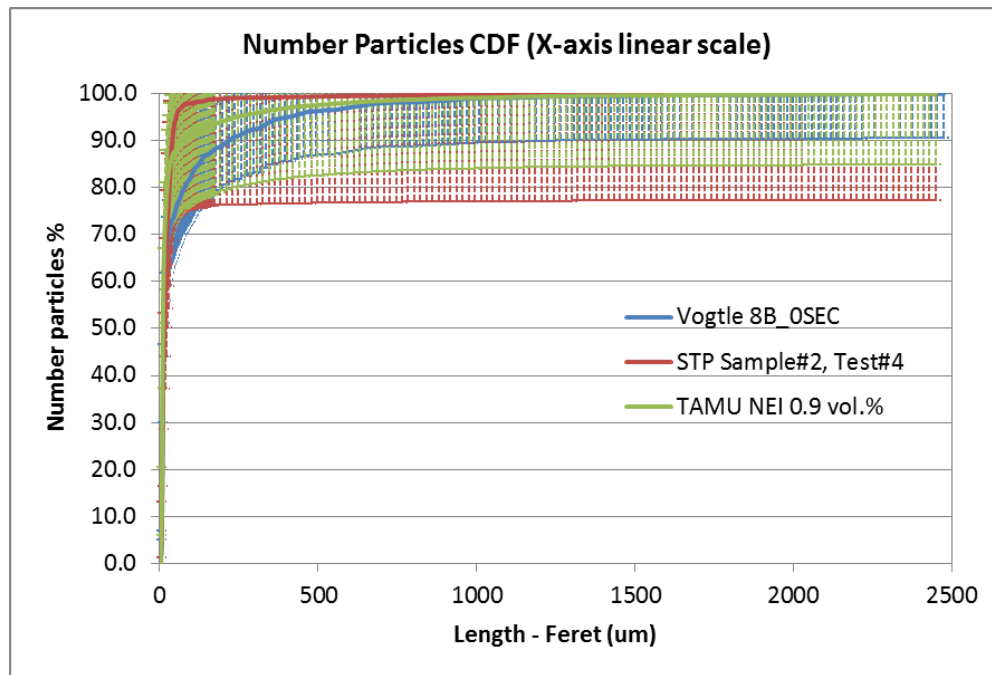


Figure IV.3.12. Count CDF vs. debris size (feret length), x-axis linear scale

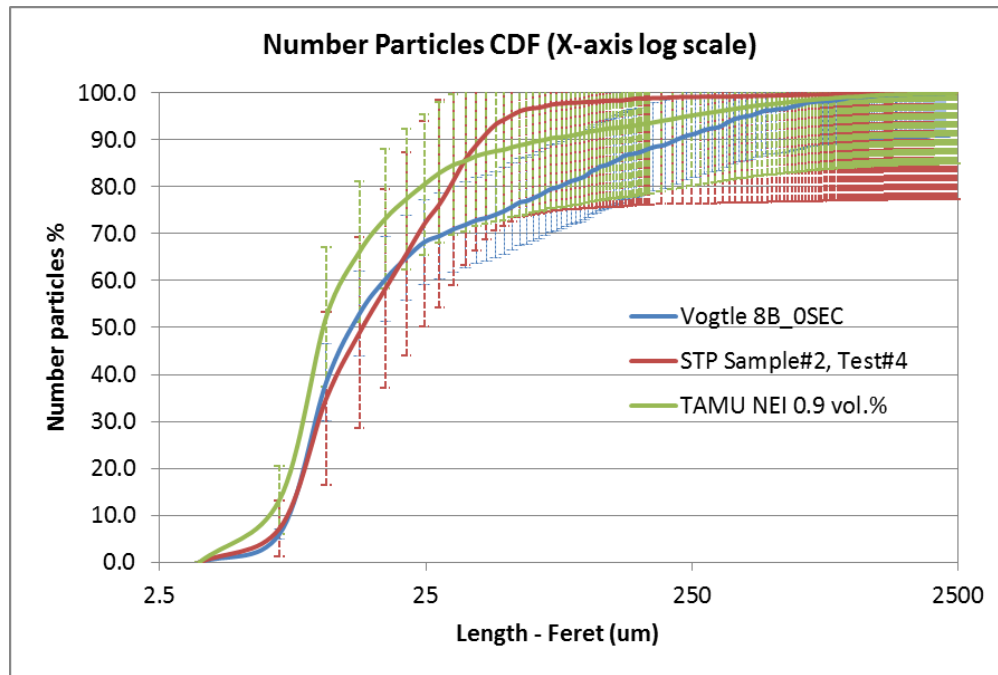


Figure IV.3.13. Count CDF vs. debris size (feret length), x-axis log scale

The comparison of the characterization results showed a difference in the range of the smaller particle sizes. This is easily visible by looking at the vol.% CDFs in Figures IV.3.8, IV.3.9, IV.3.12, and IV.3.13: The curve corresponding to the sample Vogtle 8B-0sec (blue line) lays below the one corresponding to the STP sample (red line). This means that the volume fraction of the particles smaller than $\sim 500 \mu\text{m}$ for the sample 8B-0sec is smaller than that of the STP sample. For larger particles ($500 \mu\text{m}$ up to 2.5 mm) the distributions of the two samples were found to be similar. A small number of large fibers ($>2.5 \text{ mm}$) were found in the Vogtle sample (Figure IV.3.2). The size larger than 2.5 mm was out of this measurement range. In further works, a newer version of the technique will cover the debris larger than 2.5 mm .

CHAPTER V

CONCLUSIONS

The objectives of this research were categorized into three topics: (i) Head loss through Fibrous Beds generated by dilute suspensions of NUKON fiberglass insulation on the sump strainers, (ii) Debris bypass through the sump strainers, and (iii) Development of Debris Size Characterization System.

Head loss through fibrous beds were investigated experimentally, and a head loss model with a compression model in terms of porosity as a function of pressure drop were developed. The head loss model was developed based on Lord's empirical correlation as a function of bed thickness, porosity, approach velocity, and viscosity. Experimental data obtained from the horizontal test facility with samples prepared using shredder method were used to develop the model. Then, the model was applied to the experimental test results using NEI preparation protocol in the horizontal test facility and the vertical test facility. The head loss model predicted pressure drop in an acceptable range for both the horizontal test facility and the vertical test facility. The compression model was developed based on the observation of the debris bed build-up using NEI preparation in the horizontal test facility. For the experimental data obtained using shredder method in the horizontal test facility, the compression model predicted accurately thickness of debris bed for the highest approach velocity where the porosity started being affected by the flow. For the lower approach velocities, porosity of the beds were not correctly predicted since the shredder method generated the debris

maintaining the original porosity of 0.986, thus, the initial porosity using the volume fraction of the fiberglass in the tank was not correctly estimated. For the vertical test results, although there were still some inaccuracy, the models proposed in this study showed better agreement with the head loss and compression for pure fibrous porous media made of NUKON than the models previously proposed in other works. In further works, these models may be applicable to study the effect of additional chemicals and particles on head loss through fibrous beds as bases.

Debris bypass was investigated in terms of total quantity of debris bypass collected downstream of the strainer. The test conditions were selected by changing types of water, concentration of debris, approach velocity, water temperature. Higher pH resulted in greater quantity of debris penetration. This trend was explained with the electrical double layer repulsion with the relation between zeta potential and pH. For the EC higher than 840 $\mu\text{S}/\text{cm}$, the quantity of debris bypass was inversely proportional to EC which can be a measure of ionic strength. The result agrees with the idea that higher ionic strength compresses the electrical double layer which cause repulsive energy among particles and surfaces to decrease. Statistical analyses showed that DI water has a significant difference from the typical chemical solution BB-DI 1x water and TAMU tap water. In the pair of TAMU tap water and BB-DI 1x water tests for the selected condition of approaching velocity (0.305 cm/s) and concentration of debris (0.09 volume%, 0.0034 weight%), no statistically significant difference existed in terms of debris bypass. In a limited condition, a model of debris bypass as a function of injection concentration and time was proposed and showed good agreement with the experimental

data. Approach velocity in the given conditions tended to decrease the quantity of debris bypass; it might be because of compression of porous media reducing pore size.

Fluctuation in the flow resulted in more penetration of debris, therefore, the effect of flow fluctuation or mechanical vibration should be investigated in the future works to confine the phenomena in a more conservative range.

To characterize the shape and size of irregular-shaped debris a microscope system was developed. The system was validated using NIST standard materials and applied to three samples of NEI prepared NUKON at TAMU, a NEI prepared sample taken at time 0 s in the SNC strainer test by ARL, and a NEI prepared sample taken downstream of the strainer from the STP strainer test by ARL. It showed clearly that particles smaller than 250 μm passed through the strainer and occupied most of the fraction of the sample taken downstream of the strainer. Additional tests and analyses are being conducted to understand the filtration of fine debris for different range of sizes at different time periods from the injection of debris into the sump.

Although there were many efforts to resolve the issue of debris accumulation on the sump strainer and bypass through the strainer, it has not been fully understood. This study also did not resolved all the issues, however, it produced reliable experimental data satisfying the conditions accepted for the modified strainer designs and the debris preparation recently within a limited conditions but acceptable range of typical conditions of PWR. Based on the experimental data, this study proposed a head loss model, a compression model, and a debris bypass model, then, it validated by conducting additional tests. In future works, additional studies on the effect of chemicals and

particles on head loss and debris bypass are required. The present models may be able to provide a basis and be modified on demands.

REFERENCES

1. Marmoret, L., Lewandowski, M., & Perwuelz, A. (2012). An air permeability study of anisotropic glass wool fibrous products. *Transport in Porous Media*, 93(1), 79-97.
2. Abe, I., Sato, K., Abe, H., & Naito, M. (2008). Formation of porous fumed silica coating on the surface of glass fibers by a dry mechanical processing technique. *Advanced Powder Technology*, 19(4), 311-320.
3. Davies, C. N. (1983). Filtration of aerosols. *Journal of Aerosol Science*, 14(2), 147-161.
4. Spielman, L., & Goren, S. L. (1968). Model for predicting pressure drop and filtration efficiency in fibrous media. *Environmental Science & Technology*, 2(4), 279-287.
5. Leung, W. W. F., & Hung, C. H. (2008). Investigation on pressure drop evolution of fibrous filter operating in aerodynamic slip regime under continuous loading of sub-micron aerosols. *Separation and Purification Technology*, 63(3), 691-700.
6. Radhakrishnan, T., & Neelakantan, P. (1990). Airflow through fiber plugs part i: review of theory and its limitations. *Textile Research Journal*, 60(5), 293-296.
7. Lord, E. (1955). 10—Air flow through plugs of textile fibres part 1—general flow relations. *Journal of the Textile Institute Transactions*, 46(3), T191-T213.
8. Wang, J., Hrymak, A., & Pelton, R. (2002). Compactable porous and fibrous beds formed from dilute pulp suspensions. *Industrial & Engineering Chemistry Research*, 41(3), 572-578.

9. Singh, R., Lavrykov, S., & Ramarao, B. V. (2009). Permeability of pulp fiber mats with filler particles. *Colloids and Surfaces A: Physicochemical and Engineering Aspects*, 333(1), 96-107.
10. Jackson, G. W., & James, D. F. (1986). The permeability of fibrous porous media. *The Canadian Journal of Chemical Engineering*, 64(3), 364-374.
11. Fard, M. R. (2011). Resolution of generic safety issues. *United States Nuclear Regulatory Commission NUREG-0933*.
12. Zigler, G., Brideau, J., Rao, D. V., Shaffer, C., Souto, F., & Thomas, W. (1995). Parametric study of the potential for BWR ECCS strainer blockage due to LOCA generated debris. *United States Nuclear Regulatory Commission final report NUREG/CR-6224, Science and Engineering Associates, Inc., report SEA-93-554-06-A, 1*, 163.
13. Rao, D. V., Shaffer, C. J., & Leonard, M. T. (2003). Knowledge base for the effect of debris on pressurized water reactor emergency core cooling sump performance. *United States Nuclear Regulatory Commission NUREG/CR-6808, LA-UR-03-0880*.
14. Boger, B. A., Architzel, R., Webb, M., & Cullison, D. (2004). Potential impact of debris blockage on Emergency recirculation during design Basis accidents at pressurized-water Reactors. *United States Nuclear Regulatory Commission Generic Letter 2004-02, ML042360586*.
15. Muskat, M. (1981). *Physical principles of oil production*. Springer.
16. Blake, F. C. (1922). The resistance of packing to fluid flow. *Transactions of the American Institute of Chemical Engineers*, 14, 415-421.

17. Kaviany, M. (1991). *Principles of heat transfer in porous media*. Springer-Verlag.
18. Ergun, S. (1952). Fluid flow through packed columns. *Chemical Engineering Progress*, 48, 89-94.
19. Carman, P. C. (1956). *Flow of gases through porous media*. Academic Press.
20. Davies, C. N. (1950). The separation of airborne dust and particles. *Arhiv za Higijenu Rada*, 1(4), 393-427.
21. Ingmanson, W. L., Andrews, B. D., & Johnson, R. C. (1959). Internal pressure distributions in compressible mats under fluid stress. *Tappi Journal*, 42(10), 840-849.
22. Happel, J. (1959). Viscous flow relative to arrays of cylinders. *AIChE Journal*, 5(2), 174-177.
23. Kuwabara, S. (1959). The forces experienced by randomly distributed parallel circular cylinders or spheres in a viscous flow at small Reynolds numbers. *Journal of the Physical Society of Japan*, 14(4), 527-532.
24. Drummond, J. E., & Tahir, M. I. (1984). Laminar viscous flow through regular arrays of parallel solid cylinders. *International Journal of Multiphase Flow*, 10(5), 515-540.
25. Krotiuk, W.J. (2007). Development of a pressure drop calculation method for debris-covered sump screens in support of generic safety issue 191. *United States Nuclear Regulatory Commission report NUREG-1862*.

26. Wu, W. T., Liu, J. F., Li, W. J., & Hsieh, W. H. (2005). Measurement and correlation of hydraulic resistance of flow through woven metal screens. *International Journal of Heat and Mass Transfer*, 48(14), 3008-3017.
27. Jönsson, K., & Jönsson, B. T. (1992). Fluid flow in compressible porous media: I: Steady-state conditions. *AIChE Journal*, 38(9), 1340-1348.
28. Meyer, H. (1962). A filtration theory for compressible fibrous beds formed from dilute suspensions. *Tappi Journal*, 45(4), 296-310.
29. Grahn, A., Krepper, E., Alt, S., & Kästner, W. (2008). Implementation of a strainer model for calculating the pressure drop across beds of compressible, fibrous materials. *Nuclear Engineering and Design*, 238(10), 2546-2553.
30. Hutten, I. M. (2007). *Handbook of nonwoven filter media*. Elsevier.
31. Purchas, D., & Sutherland, K. (Eds.). (2002). *Handbook of filter media*. Elsevier.
32. Krepper, E., Cartland-Glover, G., Grahn, A., Weiss, F. P., Alt, S., Hampel, R., & Seeliger, A. (2010). CFD-modeling of insulation debris transport phenomena in water flow. *Nuclear Engineering and Design*, 240(9), 2357-2364.
33. Krepper, E., Glover, G. C., Grahn, A., Weiss, F. P., Alt, S., Hampel, R., & Seeliger, A. (2008). Numerical and experimental investigations for insulation particle transport phenomena in water flow. *Annals of Nuclear Energy*, 35(8), 1564-1579.
34. Merkus, H. G. (2008). *Particle size measurements*. Springer.
35. Allen, T. (2003). *Powder sampling and particle size determination*. Elsevier.

36. Butler, J. C. (2012). Fibrous debris preparation procedure for ECCS recirculation sump strainer testing, revision 1. *United States Nuclear Regulatory Commission package ML120481061*.
37. Powell, G. T. (2013). STP pilot submittal and request for exemption for a risk-informed approach to resolve generic safety issue (GSI)-191. *United States Nuclear Regulatory Commission package ML13323A128, NOC-AE-13002954, Docket Nos. STN 50-498 and STN 50-499*.
38. Wiggins, E. J., Campbell, W. B., & Maass, O. (1939). Determination of the specific surface of fibrous materials. *Canadian Journal of Research*, 17(10), 318-324.
39. Brown, J. C. (1950). Determination of the exposed specific surface of pulp fibers from air permeability measurements. *Tappi Journal*, 33(3), 130-137.
40. Nuclear Energy Institute. (2004). Pressurized water reactor sump performance evaluation methodology revision 0. *United States Nuclear Regulatory Commission document ML050550138*.
41. Crawford, R., Jones, G. F., You, L., & Wu, Q. (2011). Compression-dependent permeability measurement for random soft porous media and its implications to lift generation. *Chemical Engineering Science*, 66(3), 294-302.
42. Kyan, C. P., Wasan, D. T., & Kintner, R. C. (1970). Flow of single-phase fluids through fibrous beds. *Industrial & Engineering Chemistry Fundamentals*, 9(4), 596-603.
43. Enderlin, C. W., Wells, B. E., White, M., Nigl, F., Rector, D. R., Peters, T. J., & Guzman, A. D. (2007). Experimental measurements of pressure drop across sump

screen debris beds in support of generic safety issue 191. *Pacific Northwest National Laboratory*.

44. Leonard, M. T., Letellier, B. C., Rao, D. V., Roesch, W. A., Madrid, J. D., Maji, A. K., & Garcia, J. (2005). *GSI-191: Experimental studies of loss-of-coolant-accident-generated debris accumulation and head loss with emphasis on the effects of calcium silicate insulation*. Division of Engineering Technology, Office of Nuclear Regulatory Research, US Nuclear Regulatory Commission.
45. Rao, D. V., & Souto, F. J. (1996). *Experimental study of head loss and filtration for LOCA debris*. Division of Engineering Technology, Office of Nuclear Regulatory Research, US Nuclear Regulatory Commission.
46. Wallis, G. B. (1969). *One-dimensional two-phase flow*. McGraw-Hill.
47. Sawilowsky, S. S. (2002). Fermat, Schubert, Einstein, and Behrens-Fisher: The probable difference between two means when $\sigma_1 \neq \sigma_2$.
48. Khilar, K. C., & Fogler, H. S. (1998). *Migrations of fines in porous media* (Vol. 12). Springer.
49. Hogg, R. T. W. D. W., Healy, T. W., & Fuerstenau, D. W. (1966). Mutual coagulation of colloidal dispersions. *Transactions of the Faraday Society*, 62, 1638-1651.
50. Wiese, G. R., & Healy, T. W. (1970). Effect of particle size on colloid stability. *Transactions of the Faraday Society*, 66, 490-499.

51. Kim, J., & Lawler, D. F. (2005). Characteristics of zeta potential distribution in silica particles. *Bulletin-Korean Chemical Society*, 26(7), 1083.
52. Bismarck, A., Boccaccini, A. R., Egia-Ajuriagojeaskoa, E., Hülsenberg, D., & Leutbecher, T. (2004). Surface characterization of glass fibers made from silicate waste: Zeta-potential and contact angle measurements. *Journal of Materials Science*, 39(2), 401-412.
53. Demircioglu, D. (2011). *Surface Active Silica Sols, Effect of PEG-Silica Interactions* (Masters' thesis, Chalmers University of Technology).
54. Gallardo-Moreno, A. M., Vadillo-Rodríguez, V., Perera-Núñez, J., Bruque, J. M., & González-Martín, M. L. (2012). The zeta potential of extended dielectrics and conductors in terms of streaming potential and streaming current measurements. *Physical Chemistry Chemical Physics*, 14(27), 9758-9767.
55. Russell, L. L. (1976). Chemical aspects of ground water recharge with wastewaters. Available from University Microfilms International, Ann Arbor Michigan 48106.
56. Marion, G. M., & Babcock, K. L. (1976). Predicting specific conductance and salt concentration in dilute aqueous solutions. *Soil Science*, 122(4), 181-187.
57. Sposito, G. (2008). *The chemistry of soils*. Oxford University Press.
58. Parkhurst, D. L., & Appelo, C. A. J. (1995). *User's guide to PHREEQC: a computer program for speciation, batch-reaction, one-dimensional transport, and inverse geochemical calculations*. University of Michigan Library

59. Kolakowski, J. E., & Matijević, E. (1979). Particle adhesion and removal in model systems. Part 1.—Monodispersed chromium hydroxide on glass. *Journal of the Chemical Society, Faraday Transactions 1: Physical Chemistry in Condensed Phases*, 75, 65-78.
60. Kia, S. F., Fogler, H. S., & Reed, M. G. (1987). Effect of pH on colloiddally induced fines migration. *Journal of colloid and interface science*, 118(1), 158-168.
61. Carneiro-da-Cunha, M. G., Cerqueira, M. A., Souza, B. W., Teixeira, J. A., & Vicente, A. A. (2011). Influence of concentration, ionic strength and pH on zeta potential and mean hydrodynamic diameter of edible polysaccharide solutions envisaged for multilayered films production. *Carbohydrate Polymers*, 85(3), 522-528.
62. Khilar, K. C. (1981). *The water sensitivity of Berea sandstone* (Doctoral dissertation, University of Michigan).
63. Ryan, J. N., & Gschwend, P. M. (1994). Effects of ionic strength and flow rate on colloid release: Relating kinetics to intersurface potential energy. *Journal of Colloid and Interface Science*, 164(1), 21-34.
64. Natrella, M. (2010). *NIST/SEMATECH e-handbook of statistical methods*.

APPENDIX A

PRELIMINARY INVESTIGATION ON THE MIXING PROPELLER EFFECTS

Preliminary tests were performed in preparation for another experiment to study the pressure drop through a strainer. To check the effect of the propeller on the pressure drop measurements a dedicated test was performed without debris. The test can be described by the following steps:

STEP1: The horizontal test facility was filled with tap water at room temperature without debris, and the approach velocity of flow was setup to 0.52 cm/s.

STEP2: The pressure drop through the strainer was measured using a Honeywell TJE differential pressure transducer (accuracy = 6.8948 Pa) with the mixing propeller off for 550 seconds.

STEP3: The measurement described in STEP2 was repeated with the mixing propeller turned on for 550 seconds.

STEP4: The two results were compared (see Figure A1)

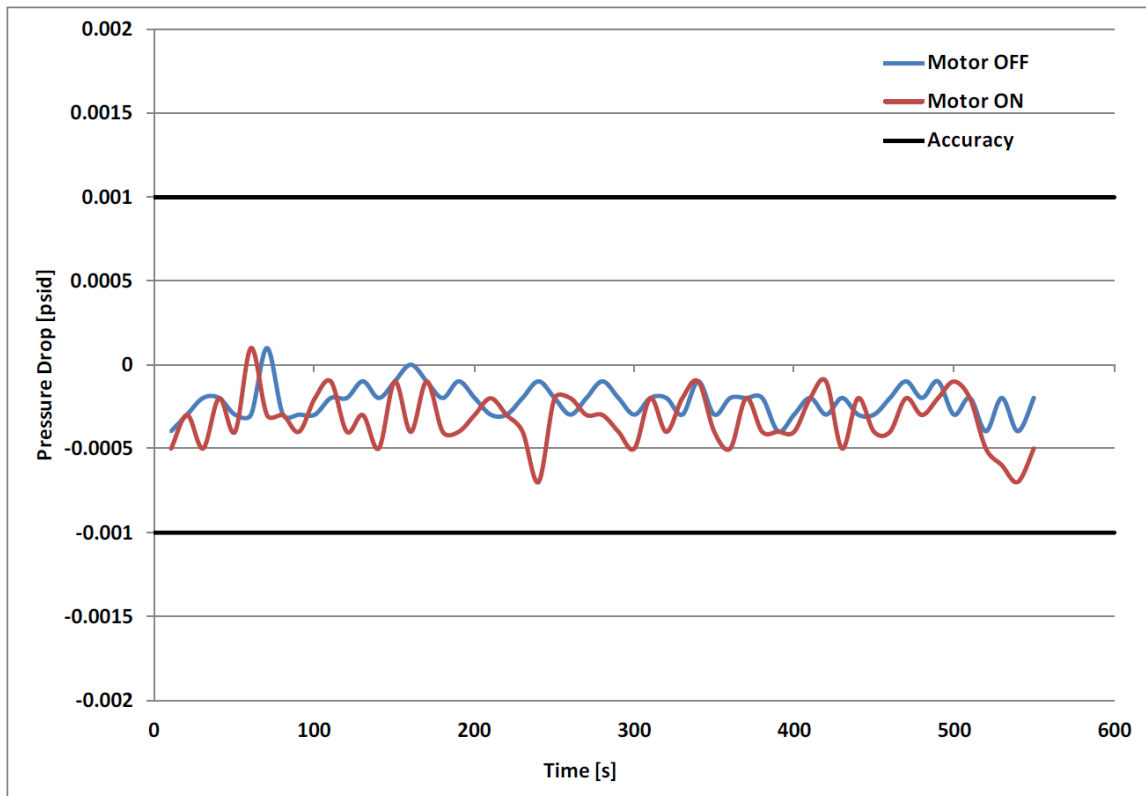


Figure A1. Pressure Drop through the Screen Plate

The results obtained showed no significant effect of the mixing propeller on the pressure drop through the screen plate.

APPENDIX B

DRYING TIME AND EQUILIBRIUM TIME ESTIMATION

A clean filter bag was used to conduct the preliminary experiment to estimate the drying time (time required to fully dry the wet filter bag) and equilibrium time (time required for the weight measurement to become stable after the drying period). The filter bag was weighed at the beginning of the experiment. The selected filter bag weight for this measurement set was 46.90g. The filter was immersed into de-ionized (DI) water for a few minutes and then placed on the heated plate at 50 °C. Continuous measurements of the weight of the filter were taken during the drying period until a stable value was achieved, confirming that all the water was removed (filter bag fully dry). After this period, the filter bag was positioned on the scale and the weight was observed to increase until a new steady-state (equilibrium) was achieved. The final weight measured at the end of the equilibrium time was found to be the same (46.90g) of the initial weight of the filter. Figure C1 shows the measurements taken during the entire procedure. Figure B2 shows a zoom of the curve during the equilibrium phase.

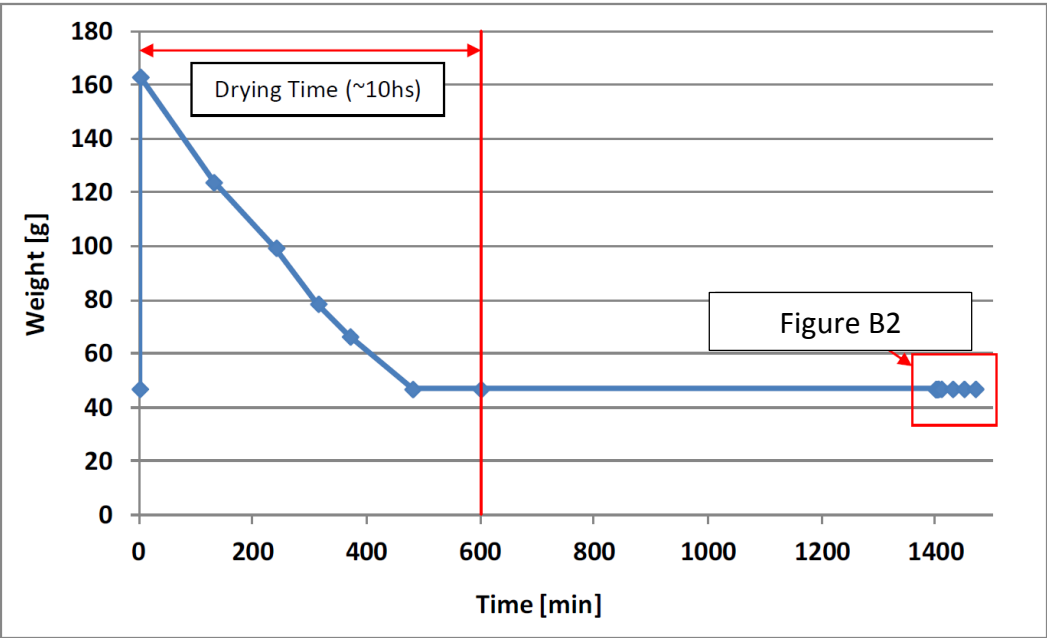


Figure B1. Filter Bag Weight Measurements – Overview

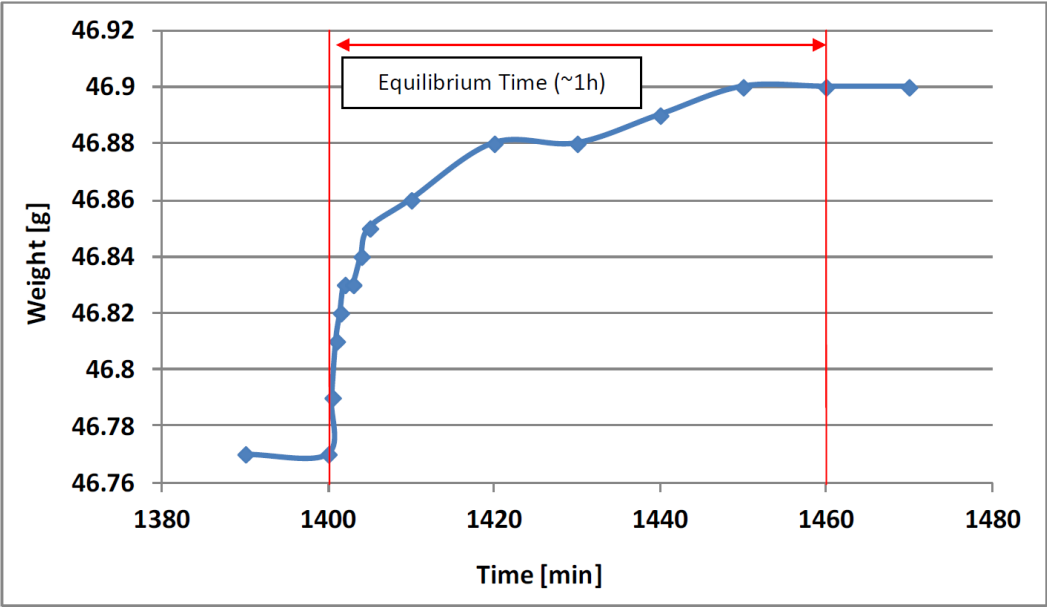


Figure B2. Filter Bag Weight Measurements – Zoom at the Equilibrium Phase

APPENDIX C

PRELIMINARY MEASUREMENTS FOR THE FILTER WASHOUT PROCEDURE

Estimation of the Weight of Water Retained in the Filter Bag

Filter Bag Dry Weight (before immersing into buffered/borated water): 46.44g

Filter Bag Wet Weight (after immersing into buffered/borated water): 161.20g

Weight of water retained in the filter bag: $161.20 - 46.44 = 114.76$ g

Verification of the Complete Boric Acid/TSP Removal without Debris

Filter Bag Dry Weight (before immersing into buffered/borated water): 47.12g

Filter Bag Dry Weight (after immersing into buffered/borated water and washing):

47.12g

Verification of the Complete Boric Acid/TSP Removal with Debris

Filter Bag Dry Weight (before immersing into buffered/borated water): 48.59g

Debris added: 0.28 g

Total Filter Bag Weight (before immersing into buffered/borated water): 48.87g

Filter Bag Dry Weight (after immersing into buffered/borated water and washing):

48.87g

APPENDIX D

HEAD LOSS AND COMPRESSION - MATLAB CODE

```
function varargout =
DEBRIS_HEAD_LOSS_POROUS_MEDIA_MODELING_GUI(varargin)
% DEBRIS_HEAD_LOSS_POROUS_MEDIA_MODELING_GUI MATLAB code for
DEBRIS_HEAD_LOSS_POROUS_MEDIA_MODELING_GUI.fig
%     DEBRIS_HEAD_LOSS_POROUS_MEDIA_MODELING_GUI, by itself, creates a
new DEBRIS_HEAD_LOSS_POROUS_MEDIA_MODELING_GUI or raises the existing
%     singleton*.
%
%     H = DEBRIS_HEAD_LOSS_POROUS_MEDIA_MODELING_GUI returns the
handle to a new DEBRIS_HEAD_LOSS_POROUS_MEDIA_MODELING_GUI or the
handle to
%     the existing singleton*.
%
%
DEBRIS_HEAD_LOSS_POROUS_MEDIA_MODELING_GUI('CALLBACK',hObject,eventData
,handles,...) calls the local
%     function named CALLBACK in
DEBRIS_HEAD_LOSS_POROUS_MEDIA_MODELING_GUI.M with the given input
arguments.
%
%
DEBRIS_HEAD_LOSS_POROUS_MEDIA_MODELING_GUI('Property','Value',...)
creates a new DEBRIS_HEAD_LOSS_POROUS_MEDIA_MODELING_GUI or raises the
%     existing singleton*. Starting from the left, property value
pairs are
%     applied to the GUI before
DEBRIS_HEAD_LOSS_POROUS_MEDIA_MODELING_GUI_OpeningFcn gets called. An
%     unrecognized property name or invalid value makes property
application
%     stop. All inputs are passed to
DEBRIS_HEAD_LOSS_POROUS_MEDIA_MODELING_GUI_OpeningFcn via varargin.
%
%     *See GUI Options on GUIDE's Tools menu. Choose "GUI allows only
one
%     instance to run (singleton)".
%
% See also: GUIDE, GUIDATA, GUIHANDLES

% Edit the above text to modify the response to help
DEBRIS_HEAD_LOSS_POROUS_MEDIA_MODELING_GUI

% Last Modified by GUIDE v2.5 26-Feb-2014 22:16:01

% Begin initialization code - DO NOT EDIT
```

```

gui_Singleton = 1;
gui_State = struct('gui_Name',       mfilename, ...
                  'gui_Singleton',  gui_Singleton, ...
                  'gui_OpeningFcn', @DEBRIS_HEAD_LOSS_POROUS_MEDIA_MODELING_GUI_OpeningFcn, ...
                  'gui_OutputFcn',  @DEBRIS_HEAD_LOSS_POROUS_MEDIA_MODELING_GUI_OutputFcn, ...
                  'gui_LayoutFcn',  [], ...
                  'gui_Callback',   []);
if nargin && ischar(varargin{1})
    gui_State.gui_Callback = str2func(varargin{1});
end

if nargout
    [varargout{1:nargout}] = gui_mainfcn(gui_State, varargin{:});
else
    gui_mainfcn(gui_State, varargin{:});
end
% End initialization code - DO NOT EDIT

% --- Executes just before DEBRIS_HEAD_LOSS_POROUS_MEDIA_MODELING_GUI
% is made visible.
function DEBRIS_HEAD_LOSS_POROUS_MEDIA_MODELING_GUI_OpeningFcn(hObject,
~, handles, varargin)
% This function has no output args, see OutputFcn.
% hObject    handle to figure
% eventdata  reserved - to be defined in a future version of MATLAB
% handles    structure with handles and user data (see GUIDATA)
% varargin   command line arguments to
DEBRIS_HEAD_LOSS_POROUS_MEDIA_MODELING_GUI (see VARARGIN)

% Choose default command line output for
DEBRIS_HEAD_LOSS_POROUS_MEDIA_MODELING_GUI
handles.output = hObject;

% Update handles structure
guidata(hObject, handles);

% UIWAIT makes DEBRIS_HEAD_LOSS_POROUS_MEDIA_MODELING_GUI wait for user
% response (see UIRESUME)
% uiwait(handles.figure1);

% --- Outputs from this function are returned to the command line.
function varargout =
DEBRIS_HEAD_LOSS_POROUS_MEDIA_MODELING_GUI_OutputFcn(~, ~, handles)
% varargout  cell array for returning output args (see VARARGOUT);
% hObject    handle to figure
% eventdata  reserved - to be defined in a future version of MATLAB
% handles    structure with handles and user data (see GUIDATA)

```

```

% Get default command line output from handles structure
varargout{1} = handles.output;

%%%%%%%%%%%%%%%%%%%%%%%%%%%%%%%%%%%%%%%%%%%%%%%%%%%%%%%%%%%%%%%%%%%%%%%%
%%%%%%%%%%%%%%%%%%%%%%%%%%%%%%%%%%%%%%%%%%%%%%%%%%%%%%%%%%%%%%%%%%%%%%%%
%%%%%%%%%%%%%%%%%%%%%%%%%%%%%%%%%%%%%%%%%%%%%%%%%%%%%%%%%%%%%%%%%%%%%%%%
%%%%%%%%%%%%%%%%%%%%%%%%%%%%%%%%%%%%%%%%%%%%%%%%%%%%%%%%%%%%%%%%%%%%%%%%
%%%%%%%%%%%%%%%%%%%%%%%%%%%%%%%%%%%%%%%%%%%%%%%%%%%%%%%%%%%%%%%%%%%%%%%% Flow Setup %%%%%%%%%%%%%%%%%%%%%%%%%%%%%%%%%%%%%%%%%%%%%%%%%%%%%%%%%%%%%%%%%%%%%%%%%

function flow_rate_Callback(hObject, eventdata, handles)
% hObject      handle to flow_rate (see GCBO)
% eventdata    reserved - to be defined in a future version of MATLAB
% handles      structure with handles and user data (see GUIDATA)

% Hints: get(hObject,'String') returns contents of flow_rate as text
%         str2double(get(hObject,'String')) returns contents of
flow_rate as a double
flow_rate = str2double(get(hObject, 'String'));
if isnan(flow_rate)
    set(hObject, 'String', 0);
    errordlg('Input must be a number','Error');
end
% Save the new density value
handles.flow_setup.flow_rate = flow_rate;
guidata(hObject,handles)

% --- Executes during object creation, after setting all properties.
function flow_rate_CreateFcn(hObject, eventdata, handles)
% hObject      handle to flow_rate (see GCBO)
% eventdata    reserved - to be defined in a future version of MATLAB
% handles      empty - handles not created until after all CreateFcns
called

% Hint: edit controls usually have a white background on Windows.
%         See ISPC and COMPUTER.
if ispc && isequal(get(hObject,'BackgroundColor'),
get(0,'defaultUicontrolBackgroundColor'))
    set(hObject,'BackgroundColor','white');
end

function velo_Callback(hObject, eventdata, handles)
% hObject      handle to velo (see GCBO)
% eventdata    reserved - to be defined in a future version of MATLAB
% handles      structure with handles and user data (see GUIDATA)

% Hints: get(hObject,'String') returns contents of velo as text
%         str2double(get(hObject,'String')) returns contents of velo as
a double
velo = str2double(get(hObject, 'String'));
if isnan(velo)
    set(hObject, 'String', 0);
    errordlg('Input must be a number','Error');
end

```

```

% Save the new density value
handles.flow_setup.velo = velo;
guidata(hObject,handles)

% --- Executes during object creation, after setting all properties.
function velo_CreateFcn(hObject, eventdata, handles)
% hObject    handle to velo (see GCBO)
% eventdata  reserved - to be defined in a future version of MATLAB
% handles    empty - handles not created until after all CreateFcns
called

% Hint: edit controls usually have a white background on Windows.
%         See ISPC and COMPUTER.
if ispc && isequal(get(hObject,'BackgroundColor'),
get(0,'defaultUicontrolBackgroundColor'))
    set(hObject,'BackgroundColor','white');
end

function temp_water_Callback(hObject, eventdata, handles)
% hObject    handle to temp_water (see GCBO)
% eventdata  reserved - to be defined in a future version of MATLAB
% handles    structure with handles and user data (see GUIDATA)

% Hints: get(hObject,'String') returns contents of temp_water as text
%         str2double(get(hObject,'String')) returns contents of
temp_water as a double
temp = str2double(get(hObject, 'String'));
if isnan(temp)
    set(hObject, 'String', 0);
    errordlg('Input must be a number','Error');
end
% Save the new density value
handles.flow_setup.temp = temp;
guidata(hObject,handles)

% --- Executes during object creation, after setting all properties.
function temp_water_CreateFcn(hObject, eventdata, handles)
% hObject    handle to temp_water (see GCBO)
% eventdata  reserved - to be defined in a future version of MATLAB
% handles    empty - handles not created until after all CreateFcns
called

% Hint: edit controls usually have a white background on Windows.
%         See ISPC and COMPUTER.
if ispc && isequal(get(hObject,'BackgroundColor'),
get(0,'defaultUicontrolBackgroundColor'))
    set(hObject,'BackgroundColor','white');
end

function viscosity_Callback(hObject, eventdata, handles)
% hObject    handle to viscosity (see GCBO)
% eventdata  reserved - to be defined in a future version of MATLAB

```



```

% handles      structure with handles and user data (see GUIDATA)

% Hints: get(hObject,'String') returns contents of viscosity as text
%         str2double(get(hObject,'String')) returns contents of
viscosity as a double
viscosity = str2double(get(hObject, 'String'));
if isnan(viscosity)
    viscosity = 1.002*10^-3;

end
% Save the new density value
handles.flow_setup.viscosity = viscosity;
guidata(hObject,handles)

% --- Executes during object creation, after setting all properties.
function viscosity_CreateFcn(hObject, eventdata, handles)
% hObject      handle to viscosity (see GCBO)
% eventdata    reserved - to be defined in a future version of MATLAB
% handles      empty - handles not created until after all CreateFcns
called

% Hint: edit controls usually have a white background on Windows.
%           See ISPC and COMPUTER.
if ispc && isequal(get(hObject,'BackgroundColor'),
get(0,'defaultUicontrolBackgroundColor'))
    set(hObject,'BackgroundColor','white');
end

%%%%%%%%%%%%%%%%%%%%%%%%%%%%%%%%%%%%%%%%%%%%%%%%%%%%%%%%%%%%%%%%%%%%%%%%
%%%%%%%%%%%%%%%%%%%%%%%%%%%%%%%%%%%%%%%%%%%%%%%%%%%%%%%%%%%%%%%%%%%%%%%%
%%%%%%%%%%%%%%%%%%%%%%%%%%%%%%%%%%%%%%%%%%%%%%%%%%%%%%%%%%%%%%%%%%%%%%%%
%%%%%%%%%%%%%%%%%%%%%%%%%%%%%%%%%%%%%%%%%%%%%%%%%%%%%%%%%%%%%%%%%%%%%%%% Debris Property %%%%%%%%%%%%%%%%%%%%%%%%%%%%%%%%%%%%%%%%%%%%%%%%%%%%%%%%%%%%%%%%%%%%%%%%%

function w_deb_Callback(hObject, eventdata, handles)
% hObject      handle to w_deb (see GCBO)
% eventdata    reserved - to be defined in a future version of MATLAB
% handles      structure with handles and user data (see GUIDATA)

% Hints: get(hObject,'String') returns contents of w_deb as text
%         str2double(get(hObject,'String')) returns contents of w_deb as
a double
w_deb = str2double(get(hObject, 'String'));
if isnan(w_deb)
    set(hObject, 'String', 0);
    errorldg('Input must be a number','Error');
end
% Save the new density value
handles.debris_setup.w_deb = w_deb;
guidata(hObject,handles)

```

```

% --- Executes during object creation, after setting all properties.
function w_deb_CreateFcn(hObject, eventdata, handles)
% hObject    handle to w_deb (see GCBO)
% eventdata  reserved - to be defined in a future version of MATLAB
% handles    empty - handles not created until after all CreateFcns
called

% Hint: edit controls usually have a white background on Windows.
%         See ISPC and COMPUTER.
if ispc && isequal(get(hObject,'BackgroundColor'),
get(0,'defaultUicontrolBackgroundColor'))
    set(hObject,'BackgroundColor','white');
end

function den_deb_Callback(hObject, eventdata, handles)
% hObject    handle to den_deb (see GCBO)
% eventdata  reserved - to be defined in a future version of MATLAB
% handles    structure with handles and user data (see GUIDATA)

% Hints: get(hObject,'String') returns contents of den_deb as text
%         str2double(get(hObject,'String')) returns contents of den_deb
as a double
den_deb = str2double(get(hObject, 'String'));
if isnan(den_deb)
    set(hObject, 'String', 0);
    errordlg('Input must be a number','Error');
end
% Save the new density value
handles.debris_setup.den_deb = den_deb;
guidata(hObject,handles)

% --- Executes during object creation, after setting all properties.
function den_deb_CreateFcn(hObject, eventdata, handles)
% hObject    handle to den_deb (see GCBO)
% eventdata  reserved - to be defined in a future version of MATLAB
% handles    empty - handles not created until after all CreateFcns
called

% Hint: edit controls usually have a white background on Windows.
%         See ISPC and COMPUTER.
if ispc && isequal(get(hObject,'BackgroundColor'),
get(0,'defaultUicontrolBackgroundColor'))
    set(hObject,'BackgroundColor','white');
end

function conc_deb_Callback(hObject, eventdata, handles)

```

```

% hObject    handle to conc_deb (see GCBO)
% eventdata  reserved - to be defined in a future version of MATLAB
% handles     structure with handles and user data (see GUIDATA)

% Hints: get(hObject,'String') returns contents of conc_deb as text
%         str2double(get(hObject,'String')) returns contents of conc_deb
as a double
conc_deb = str2double(get(hObject, 'String'));
if isnan(conc_deb)
    set(hObject, 'String', 0);
    errordlg('Input must be a number','Error');
end
handles.debris_setup.conc_deb = conc_deb;
guidata(hObject,handles)

% --- Executes during object creation, after setting all properties.
function conc_deb_CreateFcn(hObject, eventdata, handles)
% hObject    handle to conc_deb (see GCBO)
% eventdata  reserved - to be defined in a future version of MATLAB
% handles     empty - handles not created until after all CreateFcns
called

% Hint: edit controls usually have a white background on Windows.
%         See ISPC and COMPUTER.
if ispc && isequal(get(hObject,'BackgroundColor'),
get(0,'defaultUicontrolBackgroundColor'))
    set(hObject,'BackgroundColor','white');
end

function dia_deb_Callback(hObject, eventdata, handles)
% hObject    handle to dia_deb (see GCBO)
% eventdata  reserved - to be defined in a future version of MATLAB
% handles     structure with handles and user data (see GUIDATA)

% Hints: get(hObject,'String') returns contents of dia_deb as text
%         str2double(get(hObject,'String')) returns contents of dia_deb
as a double
dia_deb = str2double(get(hObject, 'String'));
if isnan(dia_deb)
    set(hObject, 'String', 0);
    errordlg('Input must be a number','Error');
end
handles.debris_setup.dia_deb = dia_deb;
guidata(hObject,handles)

% --- Executes during object creation, after setting all properties.
function dia_deb_CreateFcn(hObject, eventdata, handles)
% hObject    handle to dia_deb (see GCBO)
% eventdata  reserved - to be defined in a future version of MATLAB

```

```

% handles      empty - handles not created until after all CreateFcns
called

% Hint: edit controls usually have a white background on Windows.
%       See ISPC and COMPUTER.
if ispc && isequal(get(hObject,'BackgroundColor'),
get(0,'defaultUicontrolBackgroundColor'))
    set(hObject,'BackgroundColor','white');
end

%%%%%%%%%%%%%%%%%%%%%%%%%%%%%%%%%%%%%%%%%%%%%%%%%%%%%%%%%%%%%%%%%%%%%%%%
%%%%%%%%%%%%%%%%%%%%%%%%%%%%%%%%%%%%%%%%%%%%%%%%%%%%%%%%%%%%%%%%%%%%%%%% Debris Property %%%%%%%%%
%%%%%%%%%%%%%%%%%%%%%%%%%%%%%%%%%%%%%%%%%%%%%%%%%%%%%%%%%%%%%%%%%%%%%%%%
%%%%%%%%%%%%%%%%%%%%%%%%%%%%%%%%%%%%%%%%%%%%%%%%%%%%%%%%%%%%%%%%%%%%%%%%

% --- Executes on button press in poro_cal.
function poro_cal_Callback(hObject, eventdata, handles)
% hObject      handle to poro_cal (see GCBO)
% eventdata    reserved - to be defined in a future version of MATLAB
% handles      structure with handles and user data (see GUIDATA)
velo_cal =
handles.flow_setup.flow_rate/handles.system_setup.size_strainer;
flow_rate = handles.flow_setup.velo*handles.system_setup.size_strainer;
conc_deb = handles.debris_setup.w_deb / handles.debris_setup.den_deb /
handles.system_setup.vol_water;
set(handles.velo_cal, 'String', velo_cal);
set(handles.flow_rate_cal, 'String', flow_rate);
set(handles.conc_cal, 'String', conc_deb);
%%%%%%%%%%%%%%%%%%%%%%%%%%%%%%%%%%%%%%%%%%%%%%%%%%%%%%%%%%%%%%%%%%%%%%%%
%%%%%%%%%%%%%%%%%%%%%%%%%%%%%%%%%%%%%%%%%%%%%%%%%%%%%%%%%%%%%%%%%%%%%%%%
% Fluid conditions
U = handles.flow_setup.velo * 0.01; % Approach Velocity (m/s)
u = handles.flow_setup.viscosity; % Viscosity (Pa.s)
rw = 998;
% Strainer
A = handles.system_setup.size_strainer; % Strainer surface area (cm^2)

% Material porperties
r = handles.debris_setup.den_deb; % Density (g/cm^3)
D = handles.debris_setup.dia_deb*10^-6; % Fiber diameter (m)
Sv = (4/D);
Sv2 = (4/D)^2; % Specific surface area

S2uU = Sv2*u*U; %Specific surface^2 * Viscosity * Velocity

% Kozeny constant model coefficient
% Davies %%%%%%%%%
% a = 4.0;
% b = 56;

```

```

%%%%%%%%%%%%%%%%%%%%%%%%%%%%%%%%%%%%%%%%%%%%%%%%%%%%%%%%%%%%%%%%%%%%%%%%
% Ingmanson et al. %%%%%%%%%
a = 3.5;
b = 57;
%%%%%%%%%%%%%%%%%%%%%%%%%%%%%%%%%%%%%%%%%%%%%%%%%%%%%%%%%%%%%%%%%%%%%%%%
% Lee et al. %%%%%%%%%
% a = 2.1;
% b = 146;
%%%%%%%%%%%%%%%%%%%%%%%%%%%%%%%%%%%%%%%%%%%%%%%%%%%%%%%%%%%%%%%%%%%%%%%%
% Lee et al. (Lord) %%%%%%%%%
% a = 1.41 - 2;
% b = 0.903;

% NUREG-1862

% Compression model coefficient
e0 = 0.9998;
N = 0.0022;
% N = 0.002;
M = 0.288;
% M = 0.255;
% Bed thickness

dL = 0.001;

i = 0;
w_tot = 0;
w_inj = handles.debris_setup.w_deb;
while w_tot < w_inj

    i = i + 1;
    L = i*0.001;
    n = L/dL;
    x = L/n : L/n : L;

    e(1) = e0; % Porosity
    p(1) = 0; % Pressure

%     if dL <= 0.001
%         n = n + 1;
%     end

    for j = 2 : n
        jj = j-1;

%Davies - Lee
%         p(j) = p(jj) + (1-e(jj))^1.5*(a*(1+b*(1-e(jj))^3))*S2u*dL +
0.66*Sv*(1-e(jj))/e(jj)^3*rw*U^2*dL;
%Lord - Lee

```

```

%           p(j) = p(jj) + 1/b*(1-e(jj))^a/e(jj)^2*(1-
e(jj))^2/e(jj)^3*S2uU*dL + 0.66*Sv*(1-e(jj))/e(jj)^3*rw*U^2*dL;

%NUREG-1862

        X(jj) = e(jj)/(1-e(jj));
        K(jj) = -0.5+0.5*log(1+X(jj))+1/(2+2*X(jj)+X(jj)^2);

        p(j) = p(jj) + S2uU*X(jj)^3/(K(jj)*(1+X(jj))^2)*(1-
e(jj))^2/e(jj)^3*dL + 1.95*((1-e(jj))/(rw*U*D/u))^0.071*rw*U^2*Sv*(1-
e(jj))/e(jj)^3*dL;

        e(j) = e0 - N*p(j)^M;

end

w_tot = sum((1-e)*r*A*dL*100);

Bed(i).porosity = e;
Bed(i).pressure = p;
Bed(i).thickenss = L*100;
Bed(i).weight = w_tot;
Bed(i).x = 100*(max(x) - x);

i_final = i
j
n

end

% for i = 1 : i_final
%     dP(i) = max(Bed(i).pressure);
%     dx(i) = max(Bed(i).x);
% end

% popup_sel_index = get(handles.popupmenu1, 'Value');
% switch popup_sel_index
%     case 1
%         plot(rand(5));
%     case 2
%         plot(sin(1:0.01:25.99));
%     case 3
%         bar(1:.5:10);
%     case 4
%         plot(membrane);
%     case 5
%         surf(peaks);
% end

L = L*100;
P = max(Bed(i_final).pressure);

```

```

axes(handles.porosity_ax);
cla;
plot(Bed(i_final).x,Bed(i_final).porosity);

axes(handles.pressure_ax);
cla;
plot(Bed(i_final).x,Bed(i_final).pressure);
%%%%%%%%%%%%%%%%%%%%%%%%%%%%%%%%%%%%%%%%%%%%%%%%%%%%%%%%%%%%%%%%%%%%%%%%
%%%%%%%%%%%%%%%%%%%%%%%%%%%%%%%%%%%%%%%%%%%%%%%%%%%%%%%%%%%%%%%%%%%%%%%%
set(handles.bed_thickness, 'String', L);
set(handles.head_loss, 'String', P);
set(handles.deb_trans, 'String', w_tot);

% --- Executes on button press in pre_cal.
function pre_cal_Callback(hObject, eventdata, handles)
% hObject      handle to pre_cal (see GCBO)
% eventdata    reserved - to be defined in a future version of MATLAB
% handles      structure with handles and user data (see GUIDATA)

% --- Executes on button press in tick_cal.
function tick_cal_Callback(hObject, eventdata, handles)
% hObject      handle to tick_cal (see GCBO)
% eventdata    reserved - to be defined in a future version of MATLAB
% handles      structure with handles and user data (see GUIDATA)

%%%%%%%%%%%%%%%%%%%%%%%%%%%%%%%%%%%%%%%%%%%%%%%%%%%%%%%%%%%%%%%%%%%%%%%%
%%%%%%%%%%%%%%%%%%%%%%%%%%%%%%%%%%%%%%%%%%%%%%%%%%%%%%%%%%%%%%%%%%%%%%%%
%%%%%%%%%%%%%%%%%%%%%%%%%%%%%%%%%%%%%%%%%%%%%%%%%%%%%%%%%%%%%%%%%%%%%%%%
%%%%%%%%%%%%%%%%%%%%%%%%%%%%%%%%%%%%%%%%%%%%%%%%%%%%%%%%%%%%%%%%%%%%%%%%
%%%%%%%%%%%%%%%%%%%%%%%%%%%%%%%%%%%%%%%%%%%%%%%%%%%%%%%%%%%%%%%%%%%%%%%% System Setup %%%%%%%%%%%%%%%%%%%%%%%%%%%%%%%%%%%%%%%%%%%%%%%%%%%%%%%%%%%%%%%%%%%%%%%%%
%%%%%%%%%%%%%%%%%%%%%%%%%%%%%%%%%%%%%%%%%%%%%%%%%%%%%%%%%%%%%%%%%%%%%%%%
%%%%%%%%%%%%%%%%%%%%%%%%%%%%%%%%%%%%%%%%%%%%%%%%%%%%%%%%%%%%%%%%%%%%%%%%

function num_to_Callback(hObject, eventdata, handles)
% hObject      handle to num_to (see GCBO)
% eventdata    reserved - to be defined in a future version of MATLAB
% handles      structure with handles and user data (see GUIDATA)

% Hints: get(hObject,'String') returns contents of num_to as text
%        str2double(get(hObject,'String')) returns contents of num_to
as a double

% --- Executes during object creation, after setting all properties.
function num_to_CreateFcn(hObject, eventdata, handles)
% hObject      handle to num_to (see GCBO)
% eventdata    reserved - to be defined in a future version of MATLAB
% handles      empty - handles not created until after all CreateFcns
called
% Hint: edit controls usually have a white background on Windows.
%         See ISPC and COMPUTER.

```

```

if ispc && isequal(get(hObject,'BackgroundColor'),
get(0,'defaultUicontrolBackgroundColor'))
    set(hObject,'BackgroundColor','white');
end

function vol_water_Callback(hObject, eventdata, handles)
% hObject    handle to vol_water (see GCBO)
% eventdata  reserved - to be defined in a future version of MATLAB
% handles    structure with handles and user data (see GUIDATA)

% Hints: get(hObject,'String') returns contents of vol_water as text
%         str2double(get(hObject,'String')) returns contents of
vol_water as a double
vol_water = str2double(get(hObject, 'String'));
if isnan(vol_water)
    set(hObject, 'String', 0);
    errordlg('Input must be a number','Error');
end
handles.system_setup.vol_water = vol_water;
guidata(hObject,handles)

% --- Executes during object creation, after setting all properties.
function vol_water_CreateFcn(hObject, eventdata, handles)
% hObject    handle to vol_water (see GCBO)
% eventdata  reserved - to be defined in a future version of MATLAB
% handles    empty - handles not created until after all CreateFcns
called

% Hint: edit controls usually have a white background on Windows.
%         See ISPC and COMPUTER.
if ispc && isequal(get(hObject,'BackgroundColor'),
get(0,'defaultUicontrolBackgroundColor'))
    set(hObject,'BackgroundColor','white');
end

function size_strainer_Callback(hObject, eventdata, handles)
% hObject    handle to size_strainer (see GCBO)
% eventdata  reserved - to be defined in a future version of MATLAB
% handles    structure with handles and user data (see GUIDATA)

% Hints: get(hObject,'String') returns contents of size_strainer as
text
%         str2double(get(hObject,'String')) returns contents of
size_strainer as a double
size_strainer = str2double(get(hObject, 'String'));
if isnan(size_strainer)
    set(hObject, 'String', 0);
    errordlg('Input must be a number','Error');
end
% Save the new density value

```



```

handles.system_setup.size_strainer = size_strainer;
guidata(hObject,handles)

% --- Executes during object creation, after setting all properties.
function size_strainer_CreateFcn(hObject, eventdata, handles)
% hObject    handle to size_strainer (see GCBO)
% eventdata  reserved - to be defined in a future version of MATLAB
% handles    empty - handles not created until after all CreateFcns
called

% Hint: edit controls usually have a white background on Windows.
%         See ISPC and COMPUTER.
if ispc && isequal(get(hObject,'BackgroundColor'),
get(0,'defaultUicontrolBackgroundColor'))
    set(hObject,'BackgroundColor','white');
end

% --- Executes during object creation, after setting all properties.
function flow_rate_cal_CreateFcn(hObject, eventdata, handles)
% hObject    handle to velo_cal (see GCBO)
% eventdata  reserved - to be defined in a future version of MATLAB
% handles    empty - handles not created until after all CreateFcns
called

% --- Executes during object creation, after setting all properties.
function velo_cal_CreateFcn(hObject, eventdata, handles)
% hObject    handle to velo_cal (see GCBO)
% eventdata  reserved - to be defined in a future version of MATLAB
% handles    empty - handles not created until after all CreateFcns
called

% --- Executes during object creation, after setting all properties.
function porosity_ax_CreateFcn(hObject, eventdata, handles)
% hObject    handle to porosity_ax (see GCBO)
% eventdata  reserved - to be defined in a future version of MATLAB
% handles    empty - handles not created until after all CreateFcns
called

% Hint: place code in OpeningFcn to populate porosity_ax

% --- Executes during object creation, after setting all properties.
function pressure_ax_CreateFcn(hObject, eventdata, handles)
% hObject    handle to pressure_ax (see GCBO)
% eventdata  reserved - to be defined in a future version of MATLAB
% handles    empty - handles not created until after all CreateFcns
called

% Hint: place code in OpeningFcn to populate pressure_ax

```

```
% --- Executes during object creation, after setting all properties.  
function bed_thickness_CreateFcn(hObject, eventdata, handles)  
% hObject    handle to bed_thickness (see GCBO)  
% eventdata  reserved - to be defined in a future version of MATLAB  
% handles    empty - handles not created until after all CreateFcns  
called
```

```
% --- Executes during object creation, after setting all properties.  
function head_loss_CreateFcn(hObject, eventdata, handles)  
% hObject    handle to head_loss (see GCBO)  
% eventdata  reserved - to be defined in a future version of MATLAB  
% handles    empty - handles not created until after all CreateFcns  
called
```

```
% --- Executes during object creation, after setting all properties.  
function deb_trans_CreateFcn(hObject, eventdata, handles)  
% hObject    handle to deb_trans (see GCBO)  
% eventdata  reserved - to be defined in a future version of MATLAB  
% handles    empty - handles not created until after all CreateFcns  
called
```

```
% --- Executes during object creation, after setting all properties.  
function uipanel16_CreateFcn(hObject, eventdata, handles)  
% hObject    handle to uipanel16 (see GCBO)  
% eventdata  reserved - to be defined in a future version of MATLAB  
% handles    empty - handles not created until after all CreateFcns  
called
```

APPENDIX E

TEXAS A&M TAP WATER VS. BORATED WATER STATISTICAL ANALYSIS

PROCEDURE BY JEREMY TEJADA

Texas A&M will conduct 4 tests with boronated water and 4 tests with tap water, using the responses from those tests we seek to determine whether or not there is a statistically significant difference between these two types of water as it pertains to screen penetration.

Upon completion, 8 data points will exist and they could be organized as in the table below:

Test #	Tap Water	Boronated Water
1	X_1	Y_1
2	X_2	Y_2
3	X_3	Y_3
4	X_4	Y_4

The following procedure (also known as Welch's *t*-test) can be used to determine whether or not a statistically significant difference exists.

Note: $n_x = 4$ and $n_y = 4$ for this experiment.

1. Compute the response means for each water type:

$$\bar{X} = \frac{1}{n_x} \sum_{i=1}^{n_x} X_i = \frac{1}{4} \sum_{i=1}^4 X_i \quad \text{and} \quad \bar{Y} = \frac{1}{n_y} \sum_{i=1}^{n_y} Y_i = \frac{1}{4} \sum_{i=1}^4 Y_i$$

2. Compute the response variances for each water type:

$$s_x^2 = \left(\frac{1}{n_x - 1} \right) \sum_{i=1}^{n_x} (X_i - \bar{X})^2 = \frac{1}{3} \sum_{i=1}^4 (X_i - \bar{X})^2 \quad \text{and} \quad s_y^2 = \left(\frac{1}{n_y - 1} \right) \sum_{i=1}^{n_y} (Y_i - \bar{Y})^2 = \frac{1}{3} \sum_{i=1}^4 (Y_i - \bar{Y})^2$$

3. Compute the *t*-statistic:

$$t = \frac{\bar{X} - \bar{Y}}{\sqrt{\frac{s_x^2}{n_x} + \frac{s_y^2}{n_y}}} = \frac{\bar{X} - \bar{Y}}{\sqrt{\frac{s_x^2}{4} + \frac{s_y^2}{4}}}$$

4. Compute degrees of freedom (using the Welch-Satterthwaite equation):

$$v = \frac{\left(\frac{s_X^2}{n_X} + \frac{s_Y^2}{n_Y}\right)^2}{\frac{s_X^4}{n_X^2(n_X-1)} + \frac{s_Y^4}{n_Y^2(n_Y-1)}} = \frac{\left(\frac{s_X^2}{4} + \frac{s_Y^2}{4}\right)^2}{\frac{s_X^4}{16(3)} + \frac{s_Y^4}{16(3)}}$$

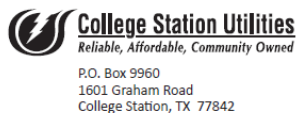
5. Select a value for α (the confidence level). Usually $\alpha = 0.05$ is chosen.
6. Use t -tables to look up the critical t -value (t -crit). You should use the computed degrees of freedom v and $\alpha/2$ (for a two-tailed test). Thus, if $\alpha = 0.05$ is selected, when finding the critical t -value one would look in the 0.025 column in the table below.

<http://itl.nist.gov/div898/handbook/eda/section3/eda3672.htm>

v	0.100	0.050	0.025	0.010	0.005	0.001
1	3.08	6.31	12.71	31.82	63.66	318.31
2	1.89	2.92	4.30	6.97	9.93	22.33
3	1.64	2.35	3.18	4.54	5.84	10.22
4	1.53	2.13	2.78	3.75	4.60	7.17
5	1.48	2.02	2.57	3.37	4.03	5.89
6	1.44	1.94	2.45	3.14	3.71	5.21
7	1.42	1.90	2.37	3.00	3.50	4.78
8	1.40	1.86	2.31	2.90	3.36	4.50
9	1.38	1.83	2.26	2.82	3.25	4.30
10	1.37	1.81	2.23	2.76	3.17	4.14
11	1.36	1.80	2.20	2.72	3.11	4.02
12	1.36	1.78	2.18	2.68	3.06	3.93
13	1.35	1.77	2.16	2.65	3.01	3.85
14	1.35	1.76	2.15	2.62	2.98	3.79
15	1.34	1.75	2.13	2.60	2.95	3.73
16	1.34	1.75	2.12	2.58	2.92	3.69
17	1.33	1.74	2.11	2.57	2.90	3.65
18	1.33	1.73	2.10	2.55	2.88	3.61
19	1.33	1.73	2.09	2.54	2.86	3.58

7. IF $t > t$ -crit, a statistically significant difference exists
 IF $t < t$ -crit, no statistically significant difference exists

APPENDIX F
WATER QUALITY REPORTS



PRSRT STD
U.S. POSTAGE
PAID
PERMIT NO. 77
BRYAN, TX

2012 Drinking Water Quality Report

This report provides a summary of the important information about your drinking water and the efforts made by City of College Station Water Services to provide safe drinking water. Water quality test results shown are required by the Texas Commission on Environmental Quality (TCEQ). Annual drinking water quality reports such as this one are required of every public water system by the 1996 Safe Drinking Water Act to provide information to water customers. Your College Station drinking water system is rated "Superior" by the TCEQ and meets all state and federal government standards.

Special Notice for the *ELDERLY, INFANTS and IMMUNO-COMPROMISED PERSONS*:

You may be more vulnerable to certain microbial contaminants, such as Cryptosporidium, in drinking water. Infants, some elderly, or immuno-compromised persons such as those undergoing chemotherapy for cancer; those who have undergone organ transplants; those who are undergoing treatment with steroids; and people with HIV/AIDS or other immune system disorders can be particularly at risk from infections. You should seek advice about drinking water from your physician or health care provider. Additional guidelines on appropriate means to lessen the risk of infection by Cryptosporidium are available from the **Safe Drinking Water Hotline (1-800-426-4791)**.

Bottled water vs. tap water

In order to ensure that tap water is safe to drink, the Environmental Protection Agency (EPA) prescribes regulations which limit the amount of certain contaminants in water provided by public health systems. FDA regulations establish limits for contaminants in bottled water which must provide the same protection for public health. When drinking water meets federal standards, as College Station's water does, there may not be any health based benefits to purchasing bottled water or point-of-use devices.

But what about contaminants?

Drinking water, including bottled water, may reasonably be expected to contain at least small amounts of some contaminants. The presence of contaminants does not necessarily indicate that water poses a health risk. Contaminants may be found in drinking water that may cause taste, color, or odor problems. These types of problems are not necessarily causes for health concerns. For more information on taste, odor, or color of drinking water, please contact City of College Station Water Services at 979-764-3660. More information about contaminants and potential health effects can be obtained by calling the EPA's Safe Drinking Water Hotline (1-800-426-4791).

Where do we get our drinking water?

Sources of drinking water include rivers, lakes, streams, ponds, reservoirs, springs and wells. As water travels over land or through the ground, it dissolves naturally-occurring minerals (and radioactive materials, in some cases) and can pick up substances resulting from the presence of animal or human activity. Contaminants that may be present in source water before treatment include microbes, inorganic contaminants, pesticides, herbicides, radioactive contaminants, and organic chemical contaminants. College Station relies entirely on groundwater for its drinking water supply, pumping water from eight wells in the Carrizo-Wilcox Aquifer and one well in the Sparta Aquifer. The TCEQ has completed an assessment of your source water and results indicate that some of your sources are susceptible to certain contaminants. The sampling requirements for your water system are based on this susceptibility and previous sample data. Any detection of these contaminants may be found in this Drinking Water Quality (Consumer Confidence) Report. For more information on source water assessments and protection efforts at our system, contact Jennifer Nations at 979-764-6223.

ADDITIONAL PURCHASED WATER SOURCES: The City of College Station maintains water system interconnects with the City of Bryan and Texas A&M University (TAMU) to provide or obtain water on an emergency basis. On March 19, 2012, TAMU supplied 2.07 million gallons of water and the City of Bryan supplied 0.972 million gallons of water. On April 24-25, 2012, the City of Bryan supplied a total of 5.887 million gallons of water. On both occasions, the water was provided to supplement College Station's water system while the Dowling Road Pump Station was out of service during the installation of new high-service pumps. To learn more about TAMU drinking water, please call 979-845-4541. To learn more about Bryan drinking water, please call 979-209-5900.

For more information regarding this report, contact Jennifer Douglass Nations at jnations@cstx.gov or call 979-764-6223.

EN ESPAÑOL: Este reporte incluye información importante sobre el agua para tomar. Para asistencia en español, favor de llamar al teléfono 979-764-3433.

To learn more about your water, visit cstx.gov/water.

2012 WATER QUALITY TEST RESULTS

Inorganic Contaminants

YEAR SAMPLED	SUBSTANCE	HIGHEST AVG. DETECTED	RANGE DETECTED	MCL	MCLG	VIOLATION? Y/N	POSSIBLE SOURCE(S) OF CONTAMINANT
2011	Fluoride	0.44 ppm	0.44 - 0.44 ppm	4 ppm	2 ppm	N	Water additive to promote strong teeth; erosion of natural deposits
2011	Barium	0.0807 ppm	0.0807 - 0.0807 ppm	2 ppm	2 ppm	N	Discharge of drilling wastes or metal refineries; erosion of natural deposits
2012	Nitrate	0.05 ppm	0.05 - 0.05 ppm	10 ppm	10 ppm	N	Runoff from fertilizer; leaching from septic tanks; erosion of natural deposits

Microbiological Contaminants ¹

Year Sampled	Total Coliform MCL	Total Coliform MCLG	Highest Monthly % of Positive Samples	Fecal Coliform or E. Coli MCL	Total No. of Positive E. Coli or Fecal Coliform Samples	Violation? Y/N	Possible Source(s) of Contaminant
2012	5% of monthly samples are (+)	0	2.73 %	1 positive sample	0	N	Naturally present in the environment

¹ Total coliform bacteria are not disease-causing organisms themselves, but they are often found in association with other microbes that are capable of causing disease. They are used as indicators of microbial contamination of drinking water because their absence from water is a good indication that the water is microbiologically safe for human consumption. In 2012, a total of 1,233 samples, at least 101 per month, were collected by Environmental Services personnel and analyzed by the Brazos County Health Department. Out of these 1,233 samples, a total of five tested positive for Total Coliform Bacteria. Following each positive Total Coliform sample, the sample site as well as one sample site upstream and downstream was re-sampled according to established sampling procedures. In addition, Fecal Coliform Bacteria was not detected in any of these monthly tests. There were no violations of the Total Coliform Rule.

Disinfectant Residual, Disinfection By-Products

YEAR SAMPLED	SUBSTANCE	HIGHEST AVERAGE DETECTED	RANGE DETECTED	MIRDL	MIDRLG	VIOLATION? Y/N	POSSIBLE SOURCE(S) OF CONTAMINANT
2012	Chlorine	1.55 ppm	1.01 - 1.94 ppm	4 ppm	2 ppm	N	Disinfectant used to control microbes
2012	Total Trihalomethanes (TTHM)	13.53 ppb	12 - 30.1 ppb	80 ppb	N/A	N	Byproduct of drinking water disinfection
2012	Halooacetic Acids (HAA5)	1.49 ppb	1.7 - 2.4 ppb	60 ppb	N/A	N	Byproduct of drinking water disinfection

² If present, elevated levels of lead can cause serious health problems, especially for pregnant women and young children. Lead in drinking water is primarily from materials and components associated with service lines and home plumbing. This water supply is responsible for providing high quality drinking water, but cannot control the variety of materials used in plumbing components. When your water has been sitting for several hours, you can minimize the potential for lead exposure by flushing your tap for 30 seconds to 2 minutes before using water for drinking or cooking. If you are concerned about lead in your water, you may wish to have your water tested. Information on lead in drinking water, testing methods, and steps you can take to minimize exposure is available from the Safe Drinking Water Hotline or at <http://www.epa.gov/safewater/lead>.

Lead and Copper ²

YEAR SAMPLED	SUBSTANCE	90th PERCENTILE ³	ACTION LEVEL (AL)	ALG	VIOLATION Y/N	# SITES OVER AL	POSSIBLE SOURCE(S) OF CONTAMINANT
2012	Lead	2.16 ppb	15 ppb	0 ppb	N	1	Corrosion of household plumbing systems; erosion of natural deposits
2012	Copper	0.121 ppm	1.3 ppm	1.3 ppm	N	0	Corrosion of household plumbing systems; erosion of natural deposits

³ College Station's water system does not exceed the Action Level for Lead or Copper. 90% of College Station tap water samples measured at or below 2.16 parts per billion (ppb) for lead and 0.121 parts per million (ppm) for copper. The Environmental Protection Agency considers the 90th percentile the same as an "average" value for other contaminants. College Station did not violate the MCL for Lead or Copper in drinking water.

Secondary and Other Non-Regulated Contaminants⁴

YEAR SAMPLED	SUBSTANCE	DETECTED LEVELS	UNITS	LIMIT
2011	Alkalinity (Bicarbonate)	432	mg/L	No recommendation
2011	Alkalinity (Total)	369	mg/L	No recommendation
2011	Carbonate	9	mg/L	No recommendation
2011	Phenolphthalein Alkalinity (as CaCO ₃)	8	mg/L	No recommendation
2011	Calcium	2.82	mg/L	No recommendation
2011	Chloride	52	mg/L	300
2011	Copper	0.0063	N/A	1
2011	Fluoride	0.44	mg/L	2
2011	Manganese	0.0066	mg/L	0.05
2011	pH	8.5	mg/L	> 7.0
2011	Sodium	193	mg/L	No recommendation
2011	Diluted Conductance	897	µmhos/cm	No recommendation
2011	Sulfate	9	mg/L	300
2011	Total Hardness (as CaCO ₃)	7.04	mg/L	No recommendation
2011	Total Dissolved Solids	513	mg/L	1,000

⁴ Many constituents which are often found in drinking water can cause taste, color, and odor problems. The taste and odor constituents are called secondary constituents and are regulated by the State of Texas, not the EPA. These constituents are not causes for health concern but they may greatly affect the appearance and taste of your water.

Public Participation Opportunities

City Council Meetings | College Station City Hall
2nd & 4th Thursday, 7 p.m. | call 979-764-3510

To learn about future public meetings concerning your drinking water, or to request to schedule one, please call the City Secretary's Office at the number above or College Station Water Services at 979-764-3660.

Definitions

The above tables contain scientific terms and measures, some of which may require explanation.

Action Level Goals (ALG): The level of a contaminant in drinking water below which there is no known or expected risk to health. ALGs allow for a margin of safety.

Action Level: The concentration of a contaminant which, if exceeded, triggers treatment or other requirements which a water system must follow.

Average or Avg: Regulatory compliance with some MCLs is based on running annual average of monthly samples.

Maximum Contaminant Level (MCL): The

highest permissible level of a contaminant in drinking water. MCLs are set as close to the MCLGs as feasible using the best available treatment technology.

Maximum Contaminant Level Goal (MCLG): The level of a contaminant in drinking water below which there is no known or expected health risk. MCLGs allow for a margin of safety.

Maximum Residual Disinfectant Level (MRDL): The highest level of a disinfectant allowed in drinking water. There is convincing evidence that addition of a disinfectant is necessary for control of microbial contaminants.

Maximum Residual Disinfectant Level Goal (MRDLG): The level of a drinking water disinfectant

below which there is no known or expected risk to health. MRDLGs do not reflect the benefits of the use of disinfectants to control microbial contaminants.

ABBREVIATIONS

N/A = not applicable
ppm = Parts per million, or milligrams per liter (mg/L). Equivalent to one ounce in 7,500 gallons of water.
ppb = Parts per billion, or micrograms per liter (µg/L). Equivalent to one ounce in 7,500,000 gallons of water.

UTILITY CUSTOMER SERVICE

Bill pay, connect/disconnect utilities
979-764-3535 or epay.cstx.gov

UTILITY HOTLINE

Line breaks, sewer backups, power outages
855-528-4278 [24 hours]



2012 Water Quality Report

Town of Holden, Massachusetts 01520
Holden Department of Public Works
Water & Sewer Division
Public Water Supply Identification No. 2134000
www.Holdenma.gov

We are pleased to present you with this year's Annual Water Quality Report for the calendar year 2012. The intent of this report is to inform you about your drinking water and to provide you with information on where your water comes from, what is found in the water, and how it compares to state and federal standards. The United States Environmental Protection Agency (EPA) and the Massachusetts Department of Environmental Protection (DEP) require the Town to provide this information on an annual basis.

The accompanying tables and descriptions show that our system met all water quality standards. The Department takes pride in ensuring that your drinking water complies with all federal and state requirements.

I. PUBLIC WATER SYSTEM INFORMATION

Address: Town Hall, 1196 Main Street, Holden, Massachusetts 01520
Contact Person: Mark A. Elbag, Jr., P.E., Water and Sewer Superintendent
Telephone No. (508) 210-5550 Fax No. (508) 829-0252
Internet Address: http://www.Holdenma.gov/Pages/HoldenMA_DPW/waterqualityreports

Opportunities for Public Participation

If you would like to participate in discussions regarding your water quality, you may attend a Water & Sewer Advisory Board meeting. If you wish to attend a meeting, please check the Town bulletin board or local access television channel for specific times and dates, or you may call the Holden Department of Public Works Office at (508) 210-5550.

II. YOUR DRINKING WATER SOURCE

Where Does My Drinking Water Come From?

The Town's water supply comes from five (5) wells and two (2) municipal interconnections with the City of Worcester. Each source is listed below:

Source Name	DEP Source ID #	Source Type	Location of Source
Quinapoxet Wells	2134000-02G 2134000-06G	Two (2) Gravel Packed Wells	Adjacent to Wachusett Street
Mill Street Well Field	2134000-03G	Tubular Well Field	Adjacent to Mill Street
Mason Road Well Field	2134000-04G	Tubular Well Field	Adjacent to Mason Road
Spring Street Well	2134000-05G	Gravel Packed Well	Adjacent to Spring Street
Brattle Street Interconnection	2134000-01P	Interconnection with Worcester	Brattle Street
Salisbury Street Interconnection	2134000-02P	Interconnection with Worcester	Salisbury Street

Is My Water Treated?

Water from our Town wells is treated with Potassium Hydroxide for pH adjustment and Sodium Fluoride for Fluoridation. The groundwater in Holden has a naturally low pH, which means it is somewhat acidic and therefore corrosive. The Potassium Hydroxide raises the pH to just above neutral (7.0) so that it is not acidic and corrosive. The Sodium Fluoride is added to provide cavity protection for infants and children. The water that we buy from Worcester is treated at Worcester's Water Filtration Plant. If you would like to learn more about Worcester's water sources and treatment processes, we invite you to visit the Holden Department of Public Works Office located at the Town Hall where we maintain copies of Worcester's Water Quality Report. The one notable difference with Worcester's water is that Worcester chlorinates their water. Therefore, if you reside within the southerly portion of Holden you may occasionally receive chlorinated water. Worcester does not fluoridate their water, and therefore, we add Sodium Fluoride at each of our two (2) municipal interconnections. The water quality of our system is constantly monitored by the Holden Water & Sewer Division and the DEP to determine the effectiveness of existing water treatment and to determine if additional treatment is required.

How Are These Sources Protected?

The Department of Environmental Protection has prepared a Source Water Assessment Program (SWAP) Report for the Town's water supply sources. The SWAP Report assesses the susceptibility of the supplies to contamination. The complete SWAP report is available at Town Hall or online at <http://www.mass.gov/dep/water/drinking/2134000.pdf>

III. SUBSTANCES FOUND IN DRINKING WATER

Sources of drinking water (for both tap water and bottled water) include rivers, lakes, streams, ponds, reservoirs, springs, and wells. As water travels over the surface of the land or through the ground, it dissolves naturally occurring minerals, and in some cases, radioactive material, and can pick up substances resulting from the presence of animals or from human activity.

Contaminants that may be present in source water include:

Microbial contaminants – such as viruses and bacteria, which may come from sewage treatment plants, septic systems, agricultural livestock operations, and wildlife.

Inorganic contaminants – such as salts and metals, which can be naturally-occurring or result from urban stormwater runoff, industrial or domestic wastewater discharges, oil and gas production, mining, and farming.

Pesticides and herbicides – which may come from a variety of sources such as agriculture, urban storm water runoff, and residential uses.

Organic chemical contaminants – these include synthetic and volatile organic chemicals that are by-products of industrial processes and petroleum production. These contaminants can also come from gas stations, urban stormwater runoff, and septic systems.

Radioactive contaminants – which can be naturally occurring or be the result of oil and gas production and mining activities.

In order to ensure that tap water is safe to drink, DEP and EPA prescribe regulations that limit the amount of certain contaminants in water provided by public water systems. The Food and Drug Administration (FDA) and Massachusetts Department of Public Health (DPH) regulations also establish limits for contaminants in bottled water that must provide the same protection for public health. All drinking water, including bottled water, may reasonably be expected to contain at least small amounts of some contaminants. The presence of contaminants does not necessarily indicate

that water poses a health risk. More information about contaminants and potential health effects can be obtained by calling the EPA's Safe Drinking Water Hotline at (800) 426-4791.

Some people may be more vulnerable to contaminants in drinking water than the general population. Immuno-compromised persons such as persons with cancer undergoing chemotherapy, persons who have undergone organ transplants, people with HIV/AIDS or other immune system disorders, some elderly, and some infants can be particularly at risk from infections. These people should seek advice about drinking water from their health care providers. EPA/Centers for Disease Control and Prevention (CDC) guidelines on lowering the risk of infection by *Cryptosporidium* and other microbial contaminants are available from the Safe Drinking Water Hotline at (800) 426-4791.

IV. IMPORTANT DEFINITIONS

Maximum Contaminant Level (MCL) – The highest level of a contaminant that is allowed in drinking water. MCLs are set as close to the MCLGs as feasible using the best available treatment technology.

Maximum Contaminant Level Goal (MCLG) – The level of a contaminant in drinking water below which there is no known or expected risk to health. MCLGs allow for a margin of safety.

Maximum Residual Disinfectant Level (MRDL) – The highest level of a disinfectant (chlorine, chloramines, chlorine dioxide) allowed in drinking water. There is convincing evidence that addition of a disinfectant is necessary for control of microbial contaminants.

Maximum Residual Disinfectant Level Goal (MRDLG) – The level of a drinking water disinfectant (chlorine, chloramines, chlorine dioxide) below which there is no known or expected risk to health. MRDLG's do not reflect the benefits of the use of disinfectants to control microbial contaminants.

Action Level (AL) – The concentration of a contaminant, which, if exceeded, triggers treatment or other requirements that a water system must follow.

90th Percentile – Out of every 10 homes sampled, 9 were at or below this level.

ppm	= parts per million, or milligrams per liter (mg/l)	ND	= Not Detected
ppb	= parts per billion, or micrograms per liter (ug/l)	N/A	= Not Applicable
pCi/l	= picocuries per liter (a measure of radioactivity)		

Secondary Maximum Contaminant Level (SMCL) – These standards are developed to protect the aesthetic qualities of drinking water and are not health based.

Massachusetts Office of Research and Standards Guideline (ORSG) – This is the concentration of a chemical in drinking water, at or below which, adverse health effects are unlikely to occur after chronic (lifetime) exposure. If exceeded, it serves as an indicator of the potential need for further action.

V. WATER QUALITY TESTING RESULTS

What Does This Data Represent?

There are over 100 regulated and unregulated contaminants that we test for. The water quality information presented in the tables below are from the most recent round of testing performed in accordance with the regulations. The tables list anything that was detected during testing. It is important to note that no contaminants were detected above the maximum allowable level.

The Massachusetts Department of Environmental Protection has reduced the monitoring requirements for Nitrate, Gross Alpha, Radon, and Chloromethane because our sources are not at risk of contamination. The last sample collected for these contaminants were taken in 2006, 2009, and 2010 and were found to meet all applicable EPA and DEP standards.

Fluoride is a naturally occurring element in many water supplies in trace amounts. In our system the fluoride level is adjusted to an optimal level averaging one part per million (ppm or mg/l) to improve oral health in children. At this level, it is safe, odorless, colorless, and tasteless. Our water system has been providing this treatment since 1995. There are over 3.9 million people in 140 Massachusetts water systems and 184 million people in the United States who receive the health and economic benefits of fluoridation.

Regulated Contaminant	Date(s) Collected	Max Detect	Range Detected	High Ave.	MCL or MRDL	MCLG or MRDLG	Violation (Y/N)	Possible Source(s) of Contamination
Inorganic Contaminants								
Fluoride (ppm)	Monthly 2012	1.10	0.8-1.10	0.92	4	4	N	Water additive that promotes strong teeth.
Arsenic (ppm)	4/20/11 6/20/11	0.00190	ND-0.00190	NA	0.010	0.010	N	Arsenic can enter the water supply from natural deposits in the earth or from industrial and agricultural pollution.
Nitrate (ppm)	05/08/12	1.55	0.14-1.55	0.58	10	10	N	Runoff from fertilizer use; leaching from septic tanks; sewage; erosion of natural deposits
Nitrite (ppm)	05/08/12	ND	ND	ND	1	1	N	Runoff from fertilizer use; leaching from septic tanks; sewage; erosion of natural
Selenium (ppb)	4/20/11 6/20/11	ND	ND	NA	50	50	N	Discharge from metal refineries; erosion of natural deposits; discharge from mines
Barium (ppm)	4/20/11 6/20/11	0.0380	ND-0.0380	NA	2	2	N	Discharge of drilling wastes; discharge from metal refineries; erosion of natural deposits
Organic Contaminants								
Trichloroethylene (ppb)	Qrtly 2012	1.83	ND-1.83	0.59	5	0	N	Discharge from metal degreasing sites and other factories
1,1,1-Trichloroethane (ppb)	Qrtly 2012	1.80	ND-1.80	0.43	200	200	N	Discharge from use in septic system cleaners
CIS-1,2-Dichloroethylene (ppb)	Qrtly 2012	1.41	ND-1.41	0.42	70	70	N	Breakdown product of trichloroethylene and tetrachloroethylene

Regulated Contaminant	Date(s) Collected	Max Detect	Range Detected	High Ave.	MCL or MRDL	MCLG or MRDLG	Violation (Y/N)	Possible Source(s) of Contamination
Perchlorate (ppb)	3 rd Qtr 2012	ND	ND	NA	2.0	NA	N	Naturally occurring and manmade contaminant increasingly found in groundwater, surface water and soil.
Radioactive Contaminants								
Gross Alpha (pCi/l) (minus uranium)	Qrtly 2006	1.7	ND-1.7	NA	15	0	N	Erosion of natural deposits
Radon (pCi/l)	06/02/06	820	820	NA	10,000	NA	N	Erosion of natural deposits
Radium 226	6/11/12	0.64	0.64	0.64	5 pCi/L	0 pCi/L	N	Erosion of natural deposits
Radium 228	6/11/12	1.30	1.30	1.30	5 pCi/L	0 pCi/L	N	Erosion of natural deposits
Disinfection By-Products								
Total Trihalomethanes (THMs) (ppb)	Qrtly 2012	63.5	23.4-63.5	38.53	80	----	N	Byproduct of drinking water chlorination
Haloacetic Acids (HAA5) (ppb)	Qrtly 2012	27.3	10.0-27.3	15.25	60	----	N	Byproduct of drinking water disinfection
Chlorine (ppm)	Monthly 2012	0.37	0.08-0.37	0.25	4.0	4.0	N	Water additive used to control microbes

(1) **Haloacetic Acids and Trihalomethanes:** The highest-level detected represents the highest running annual average for these contaminants. The range of levels found may have results in excess of the MCL but the running average of all sample locations is used to determine compliance.

Unregulated Contaminant	Date(s) Collected	Range Detected	Average Detected	SMCL	ORSG	Possible Source
Inorganic Contaminants						
Sodium (ppm)	2nd Qtr 2011	11-26	19	----	20	Natural sources; runoff from use as salt on roadways; by-product of treatment process
Sulfate (ppm)	2nd Qtr 2012	7.39-14.3	10.39	250	----	Natural sources
Organic Contaminants						
Chloromethane (ppb)	Qrtly 2012	ND	ND	----	----	Occurs naturally and is also produced in industry
Tetrachloroethylene (ppb)	Qrtly 2012	ND	ND	0.5	----	Often used for dry cleaning clothes

- (2) **Unregulated contaminants** are those for which there are no established drinking water standards. The purpose of unregulated contaminant monitoring is to assist regulatory agencies in determining their occurrence in drinking water and whether future regulation is warranted.

Secondary Contaminant	Date(s) Collected	Range Detected	Average Detected	SMCL	Possible Source
Iron (ppm)	2nd Qtr 2012	0.72	0.14	0.3	Naturally occurring, corrosion of cast iron pipes
Manganese (ppm)	2nd Qtr 2012	0.15	0.04	0.05 (3)	Erosion of natural deposits
Alkalinity (ppm)	2nd Qtr 2012	10.0-68.0	24.0	None	Buffering capacity of water
Aluminum (ppm)	2nd Qtr 2012	ND	0.00	0.2	Byproduct of treatment process, naturally occurring
Chloride (ppm)	2nd Qtr 2012	16.7-36.9	25.38	250	Runoff from road de-icing, use of inorganic fertilizers, landfill leachates, septic tank effluents, animal feeds, industrial effluents, irrigation drainage
Magnesium (ppm)	2nd Qtr 2012	0.97-1.48	1.18	None	Naturally occurring mineral
Hardness (ppm)	2nd Qtr 2012	18-28.2	22.2	None	Naturally occurring mineral
Potassium (ppm)	2nd Qtr 2012	1.1-45	10.12	None	Naturally occurring mineral
Calcium (ppm)	2nd Qtr 2012	5.59-8.86	6.94	None	Naturally occurring mineral
Total Dissolved Solids (TDS) (ppm)	2nd Qtr 2012	63-172	113.6	500	Erosion of natural deposits.

- (3) The EPA has established a lifetime health advisory (HA) value of 0.3 mg/L for manganese to protect against concerns of potential neurological effects, and a One-day and 10-day HA of 1 mg/L for acute exposure.

Lead and Copper

Lead and copper are contaminants that have a very specific and unique set of rules for sampling and testing. Unlike other inorganics, which tend to contaminate a water supply at the source, lead and copper generally enter the water after it has flowed to the consumer's home. These metals typically dissolve from the water pipes within your house if the water is corrosive. Lead usually comes from the lead solder used prior to 1986 to connect the copper tubing in a house's water supply lines. The copper comes from the tubing itself. Ingesting large amounts of copper from drinking water can upset your stomach but there are no long-term health effects unless you suffer from Wilson's Disease. Lead, on the other hand, is known to cause learning impairments in young children and may cause delays in mental and physical development. Elevated lead ingestion may also cause kidney problems or high blood pressure in adults. Lead is therefore, strictly regulated in drinking water. In past years, gasoline and paint were major sources of lead in the environment.

Since both lead and copper enter the water at the point of use (near the tap), sampling and testing for these metals must be performed at homes in the Town rather than at the entry point to the distribution system. Samples had to be collected after the water went unused in the home for at least six (6) hours. This permitted the maximum contact between water and the lead and copper. If the 90th percentile results exceed the action level, further sampling and possible treatment changes might be necessary.

If present, elevated levels of lead can cause serious health problems, especially for pregnant women and young children. Lead in drinking water is primarily from materials and components associated with service lines and home plumbing. The Holden Water & Sewer Division is responsible for providing high quality drinking water, but cannot control the variety of materials used in plumbing components. When your water has been sitting for several hours you can minimize the potential for lead exposure by flushing your tap for 3 seconds to 2 minutes before using water for drinking or cooking. If you are concerned about lead in your water, you may wish to have your water tested. Information on lead in drinking water, testing methods, and steps you can take to minimize exposure is available from the Safe Drinking Water Hotline or at <http://water.epa.gov/drink/info/lead/index.cfm>.

Contaminant	Date(s) Collected	90 th percentile	Action Level	MCLG	No. of sites sampled	No. of sites above Action Level	Possible Source of Contamination
Lead (ppb)	08/11-09/11	0.0018	0.015	0	30	0	Corrosion of household plumbing systems; Erosion of natural deposits
Copper (ppm)	08/11-09/11	0.9200	1.3	1.3	30	0	Corrosion of household plumbing systems; Erosion of natural deposits; Leaching from wood preservatives

VI. COMPLIANCE WITH DRINKING WATER REGULATIONS

Does My Drinking Water Meet Current Health Standards?

We are committed to providing you with the best water quality available. We are proud to report that last year all test results met all applicable health standards regulated by the state and federal government.

VII. CROSS-CONNECTION CONTROL AND BACKFLOW PREVENTION

What is a cross-connection?

A cross-connection occurs whenever the drinking water supply is or could be in contact with potential sources of pollution or contamination. Cross-connections exist in piping arrangements or equipments that allowed the drinking water to come in contact with non-potable liquids, solids or gases (hazardous to humans) in event of a backflow.

What is a backflow?

Backflow is the undesired reverse of the water flow in the drinking water distribution lines. This backward flow of water can occur when the pressure created by an equipment or system such as a boiler or air-conditioning is higher than the water pressure inside the water distribution line (backpressure), or when the pressure in the distribution line drops due to routine occurrences such as water main breaks or heavy water demand causing the water to flow backward inside the water distribution system (backsiphonage). Backflow is a problem that many water consumers are unaware of, a problem that each and every water customer has a responsibility to help prevent.

What can I do to help prevent a cross-connection?

Without the proper protection, something as simple as a garden hose has the potential to contaminate or pollute the drinking water lines in your house. In fact over half of the country's cross-connection incidents involve unprotected garden hoses. There are very simple steps that you as a drinking water user can take to prevent such hazards, they are:

- NEVER submerge a hose in soapy water buckets, pet watering containers, pool, tubs, sinks, drains or chemicals.
- NEVER attach a hose to a garden sprayer without the proper backflow preventer.
- Buy and install a hose bib vacuum breaker in any threaded water fixture. The installation can be as easy as attaching a garden hose to a spigot. This inexpensive device is available at most hardware stores and home-improvement centers.
- Identify and be aware of potential cross-connections to your water line.
- Buy appliances and equipment with a backflow preventer
- Buy and install backflow prevention devices or assemblies for all high and moderate hazard connections.

The Massachusetts Drinking Water Regulations, 310 CMR 22.00, requires all public water systems to have an approved and fully implemented Cross-Connection Control Program (CCCP). The Holden Water Division is working diligently to protect the public health of its drinking water customers from the hazards caused by unprotected cross-connections through the implementation of its cross-connection survey program, elimination or properly protection of all identified cross-connections, the registration of all cross-connections protected by a reduced pressure backflow preventers (RPBPs) or a double check valve assemblies (DCVAs), and the implementation of a testing program for all RPBPs and DCVAs.

For more information on this program please call DPW Water Division at (508)210-5550.

VIII. WATER CONSERVATION

We ask that all customers cooperate to conserve water for the purpose of saving money, and importantly, to save our limited and valued natural resources. If you have an irrigation system and it operates on rainy days you might want to consider using a rain sensor, which when connected to your irrigation system, will not allow your irrigation system to operate if there has been recent precipitation. These devices are inexpensive and relatively easy to install.

In accordance with the requirements of the Water Management Act Final Permit issued to the Town of Holden by DEP, the Town is required to enact a Water Use Restriction from May 1st until September 30th 2012, between the hours of 9AM to 5PM. This ban restricts daily "nonessential" outdoor water use from public water sources, and more information can be found on the Town's website at www.holdenma.gov.

APPENDIX G

VISCOSITY MEASUREMENT

Preparation of the Chemical Solutions

The chemicals used to prepare the solutions were listed in Table G.1. The typical concentration buffered borated (1xBB) solutions were prepared by mixing BA and pH agent (TSP) in deionized (DI) water at room temperature with a magnetic stirrer for around 1 hr. In order to remove dissolved air from inside the samples, DI water and solutions were boiled and degassed under vacuum before any measurement.

Table G.1. Summary of materials used in solutions.

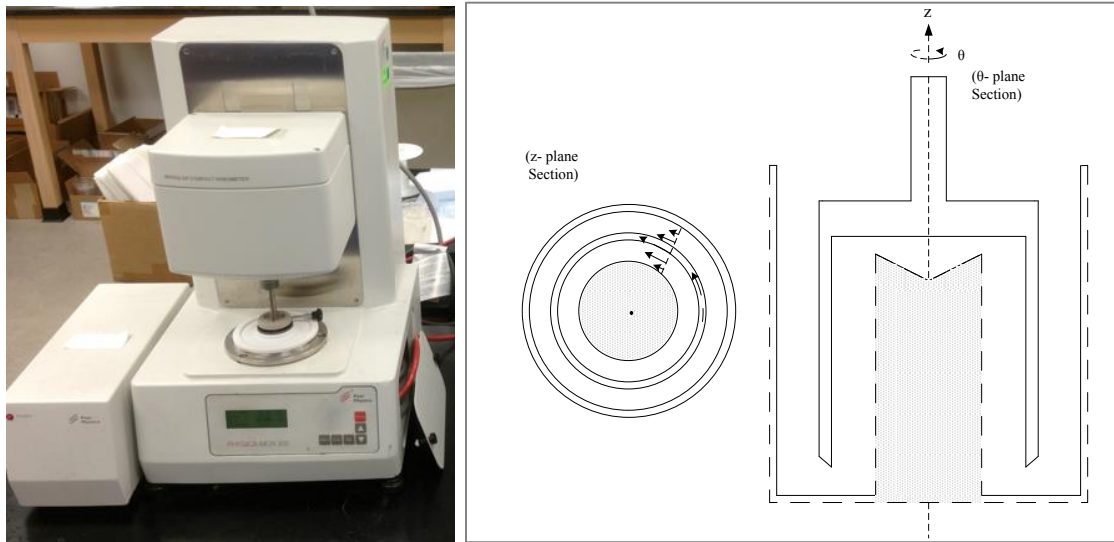
Material	Vendor and Specifications	Water Solubility (g/100 ml)
Boric Acid (BA)	Optibor® Orthoboric Acid	5.04 @ 20°C ⁴
	U.S. Borax Inc.	8.72 @ 40°C ⁴
	(99.9-100.9% H ₃ BO ₃)	14.81 @ 60°C ⁴
	Cat. No. 10043-35-3	
Trisodium Phosphate (TSP)	Technical Grade (Certified to NSF/ANSI 60)	10.64 @ 25°C ⁵
	ICL Performance Products LP Cat. No. 10101-89-0	39.01 @ 60°C ⁵

Viscosity Measurements

Steady shear viscosity measurements were taken using an MCR 300 Modular Compact Rheometer (Anton Paar, Ashland, VA) in Figure G.1.a. We used an embedded double couette cylindrical system (DG 26.7) for the measurements (Figure G.1.b) in order to

increase the surface area and thereby yield a higher force signal and enhanced accuracy.

The specifications of these systems are listed in Table G.2.



(a) (b)
Figure G.1. Viscosity measurement system – (a) MCR 300 Modular Compact Rheometer (Anton Paar, Ashland, VA) and (b) DG 26.7 (double-walled couette).

Table G.2. Specifications of the viscosity measuring system

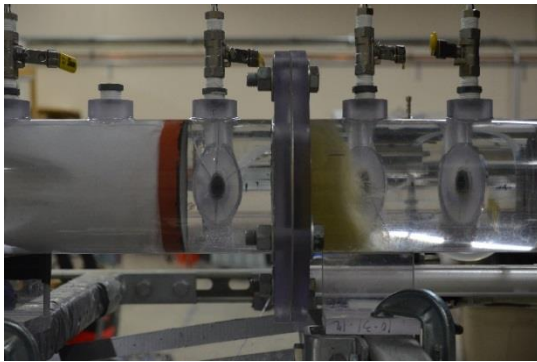
Geometry	Sample volume (ml)	Radius 1 (mm)	Radius 2 (mm)	Gap 1 (mm)	Gap 2 (mm)	Temperature control unit
						<u>TEZ 150 P</u>
DG 26.7	4	13.796 (outer)	12.33 (outer)	0.47	0.42	Temperature range: 20 - 150°C Heating rate: 5 °C /min Cooling rate: 1.6 °C /min Water circulation

The instrument was programmed for constant temperature and equilibration followed by a two-step shear ramp in which the shear rate was increased from 100 to 250 s⁻¹ and immediately decreased from 250 to 100 s⁻¹. We focused on the shear rate values less than 250 s⁻¹ to avoid the inaccuracy due to the secondary flow. The measuring duration was kept at 60 s for each of the five points to lessen the impact of noise in the torque signal and to produce cleaner data. All measurements were repeated at least three times at the temperatures. The temperature was controlled using a circulating water bath (Lauda Model RE106). The measuring cup and cylinder (DG 26.7) were also ultrasonicated around 30 minutes at high temperature (>50°C) before any measurements, in order to prevent the viscosity measurements from being affected by chemical deposition on the surfaces of inner and outer cylinders. The accuracy for viscosity and temperature of an MCR 300 rheometer are ± 0.5% and ± 0.1 °C, respectively. Samples were weighed using a Mettler Toledo AB analytical balance (Model. AB204-S) with ± 0.0001 g accuracy. The viscosity measurement using the MCR 300 rheometer and the present protocol were validated by comparing the measured viscosity of DI water to the viscosity provided by NIST.

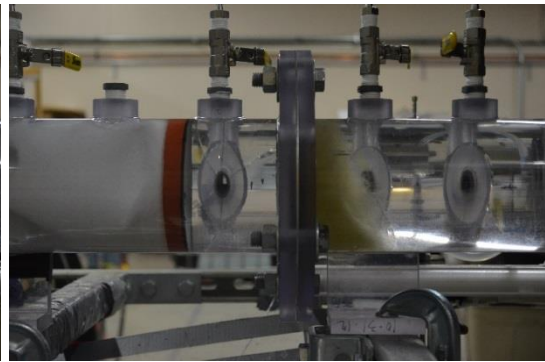
APPENDIX H

DEBRIS BED SNAPSHOTS – END OF TEST

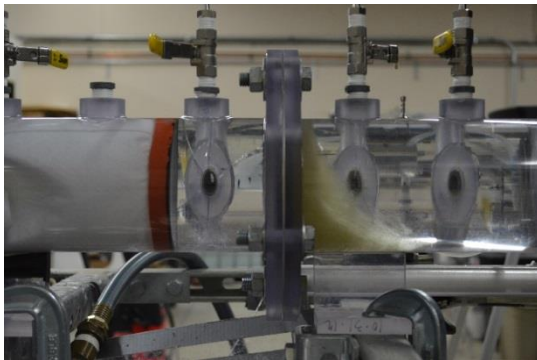
The following pictures are snapshots extracted from the movies recorded during each of the tests performed. The time at which these snapshots were taken is the termination time of the experiment.



(a) DI-1



(b) DI-2

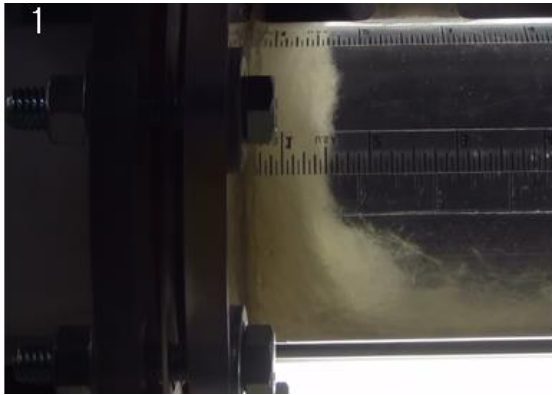


(c) DI-3

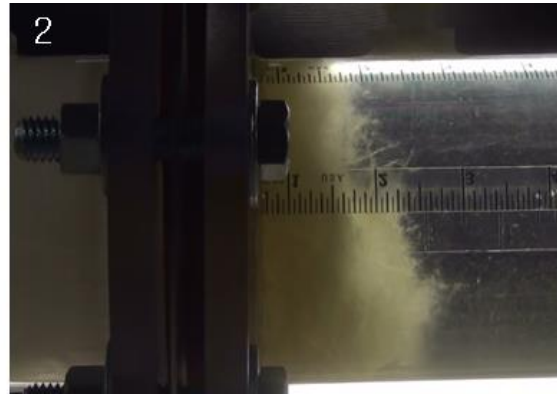


(d) DI-4

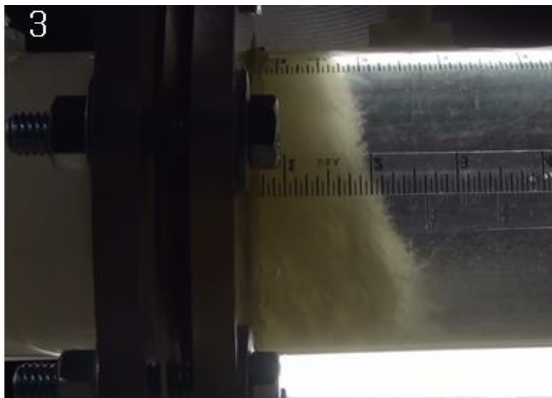
Figure H.1. Debris bed snapshots of DI water experiments – (a) DI-1, (b) DI-2, (c) DI-3, and (d) DI-4



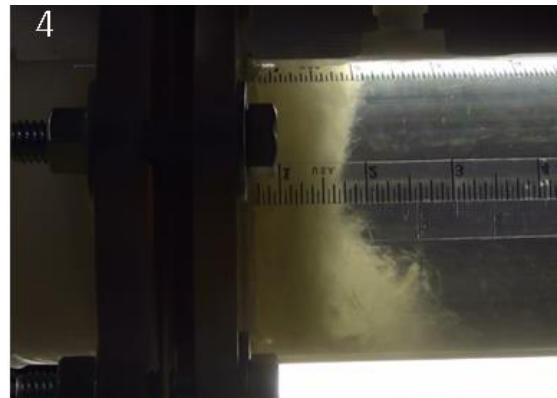
(a) TT-1



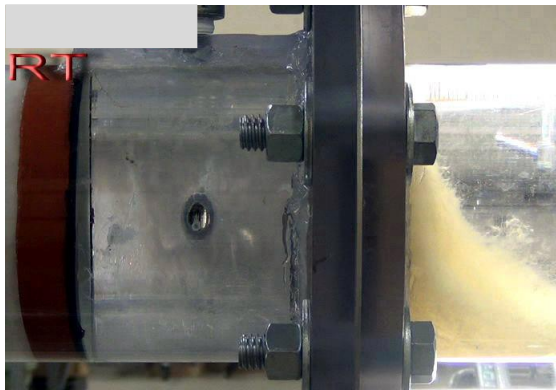
(b) TT-2



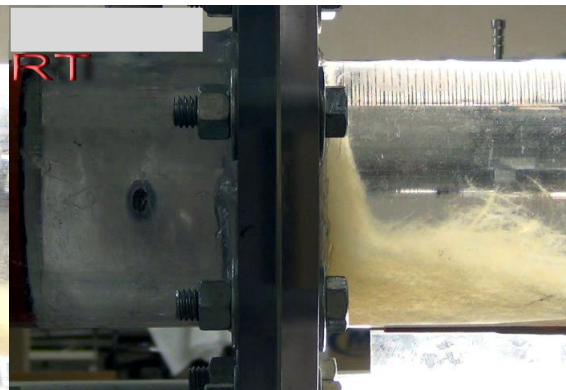
(c) TT-3



(d) TT-4



(e) TT-5

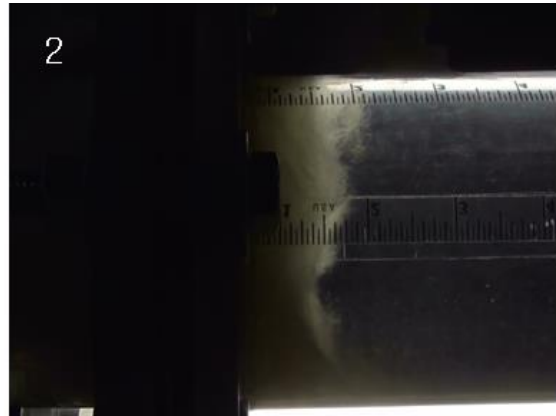


(f) TT-6

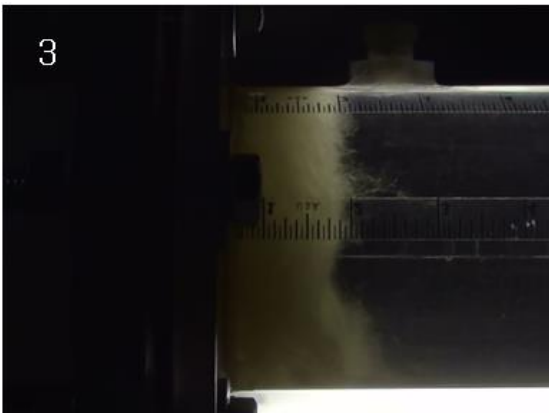
Figure H.2. Debris bed snapshots of TAMU tap water experiments – (a) TT-1, (b) TT-2, (c) TT-3, (d) TT-4, (e) TT-5, and (f) TT-6



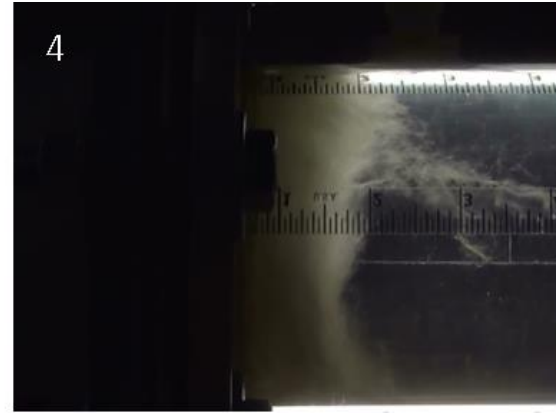
(a) 1xBB-1



(b) 1xBB -2

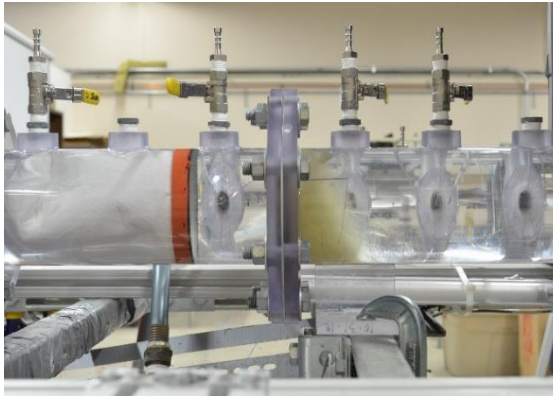


(c) 1xBB -1



(d) 1xBB -2

Figure H.3. Debris bed snapshots of 1x buffered-borate DI water experiments – (a) 1xBB-1, (b) 1xBB-2, (c) 1xBB -3, and (d) 1xBB -4



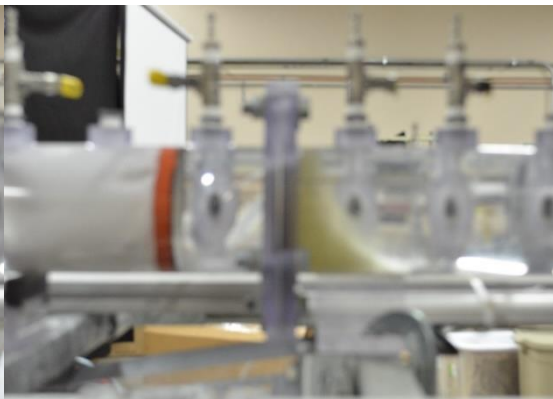
(a) 2xBB-1



(b) 2xBB-2

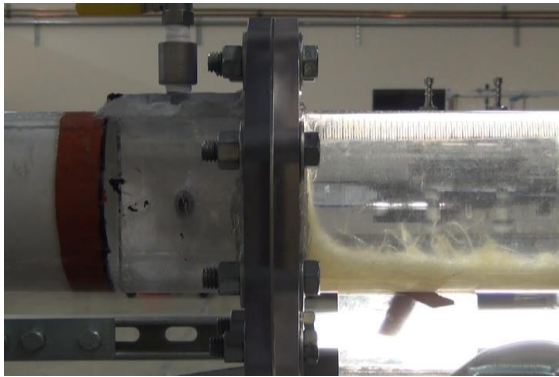


(c) 2xBB-4

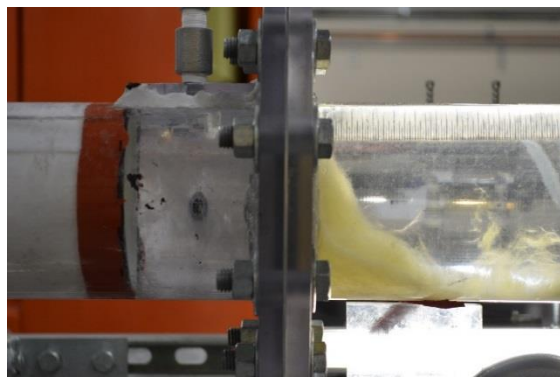


(d) 2xBB-4

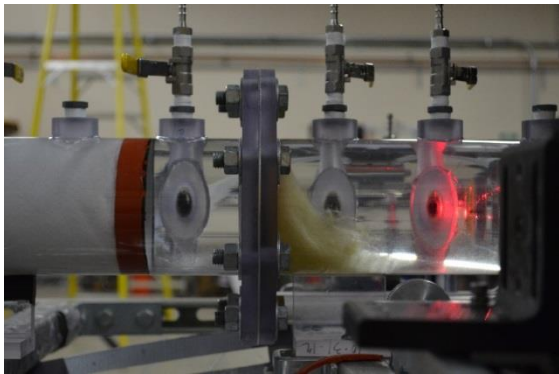
Figure H.4. Debris bed snapshots of 2x buffered-borate DI water experiments – (a) 2xBB-1, (b) 2xBB-2, (c) 2xBB -3, and (d) 2xBB -4



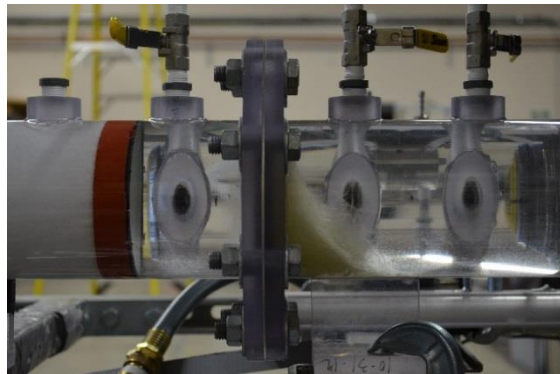
(a)



(b)



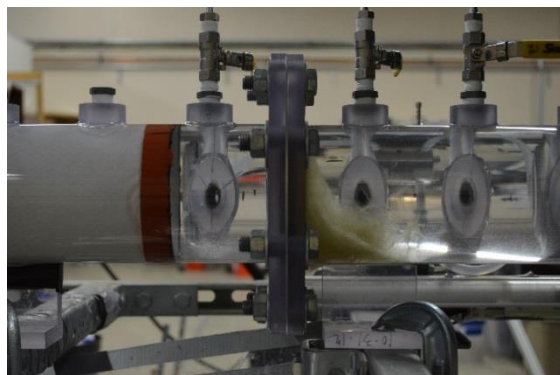
(c)



(d)

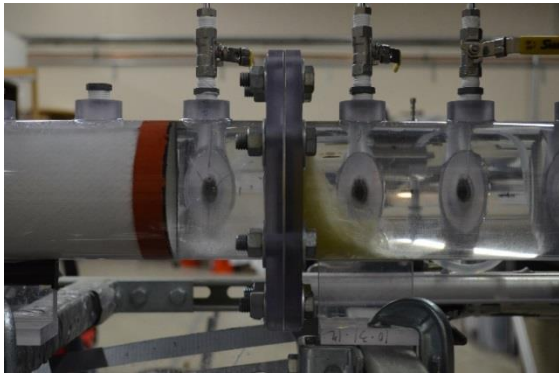


(e)

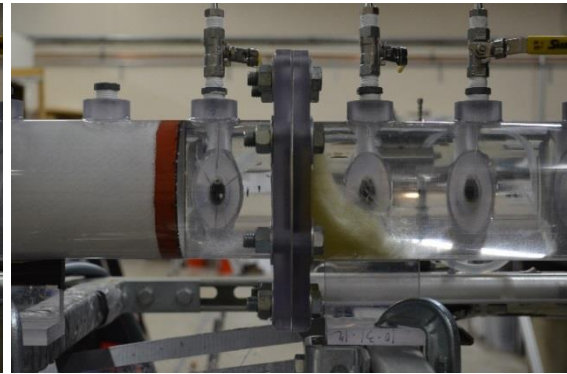


(f)

Figure H.5. Debris bed snapshots of high temperature tests – (a) HT-1, (b) HT-2, (c) HT-3, (d) HT-4, (e) HT-5, (f) HT-6, (g) HT-7, and (h) HT-8



(g)



(h)

Figure H.5. Continued

APPENDIX I

DEBRIS SIZE CHARACTERIZATION MATLAB CODE

```
%% Close, delete and clear all figures, variables and command window
clear all;
close all;
clc;
%%%%%%%%%%%%%%%%%%%%%%%%%%%%%%%%%%%%%%%%%%%%%%%%%%%%%%%%%%%%%%%%%%%%%%%%
%%%%%%%%%%%%%%%%%%%%%%%%%%%%%%%%%%%%%%%%%%%%%%%%%%%%%%%%%%%%%%%%%%%%%%%% Initial Conditions, Image Address
folder_name = 'F:\SAYA\STP\T3S2\20x_T3S2_01072013';
file_name = '20x_T3S2_01_01072013';
file_pre_name = [folder_name, '\', file_name, '\', file_name '_000'];
img_save_name = [folder_name, '_3\', file_name, '_Result\IMG\'
file_name, '_Result_000'];
img_save_name_ind = [folder_name, '_3\', file_name, '_Result\IMG_IND\'
file_name, '_Result_000'];
data_save_name = [folder_name, '_3\', file_name, '_Result\DAT\'
file_name, '_Result_000'];

file_ext = '.tif';
data_ext = '.dat';

start_image_number = 0;
image_interval = 1;
finish_image_number = 440;

im_size = 1024;

ip_op = 1; %image processing option: 1:internal function 0: processed
image
f_op = 0; %filtering options: 1:filter 0:threshold
th_level = 140;
th_level = th_level / 255;

f_r_low = 0.135;
f_r_high = 0.99;

p_th = 25;

i_1 = im_size/4 + 1;
i_2 = im_size/4*3;
j_1 = im_size/4 + 1;
j_2 = im_size/4*3;

%%%%%%%%%%%%%%%%%%%%%%%%%%%%%%%%%%%%%%%%%%%%%%%%%%%%%%%%%%%%%%%%%%%%%%%%
% Test Image
```

```

%%%%%%%%%%%%%%%%%%%%%%%%%%%%%%%%%%%%%%%%%%%%%%%%%%%%%%%%%%%%%%%%%%%%%%%%
count_1 = 0;
for image_number = start_image_number : image_interval :
finish_image_number
    count_1 = count_1 + 1;

    num_str = num2str(image_number);

% get image addresses
    f_num_str_buff = num_str;

    if image_number < 10000
        num_str = ['0' , f_num_str_buff];
    end
    if image_number < 1000
        num_str = ['00' , f_num_str_buff];
    end
    if image_number < 100
        num_str = ['000' , f_num_str_buff];
    end
    if image_number < 10
        num_str = ['0000' , f_num_str_buff];
    end

    image_address = [file_pre_name , num_str, file_ext];

    img_test_rgb = (imread(image_address));
    [i_s_t, j_s_t, k_s_t] = size(img_test_rgb);

    if k_s_t > 1
        img_test = rgb2gray(img_test_rgb);
    else
        img_test = img_test_rgb;
    end
    I = img_test;
%     figure, imshow(I);
% Parameter Initialization
        Particle_Img(1,1) = 0;
        Particle_Img(1,1) = 0;
        Particle_Loc(1,1) = 0;
        Particle_Q(1,1) = 0;
        Particle_Perimeter_0(1,1) = 0;
        Particle_Perimeter_1(1,1) = 0;
        Particle_Length_0(1,1) = 0;
        Particle_Length_1(1,1) = 0;
        Particle_Area(1,1) = 0;
        Particle_Feret_Max(1,1) = 0;
        Particle_Feret_min(1,1) = 0;

    if ip_op == 1
        if f_op == 1

```

```

        f_size = 21;
        [f1,f2] = freqspace(f_size,'meshgrid');
        Hd = ones(f_size);
        r = sqrt(f1.^2 + f2.^2);
        Hd((r<f_r_low)|(r>f_r_high)) = 0;

        h = fwind1(Hd,hamming(f_size));
        freqz2(h);
        Y = filter2(h,I);
        figure, imshow(I);

        BW = im2bw(Y, 0.5);

    else
        BW = im2bw(I, th_level);
    end
else
    BW = I;
end

BW = 1 - BW;
CC = bwconncomp(BW);

for i = 1 : CC.NumObjects

    if size(CC.PixelIdxList{i}) < p_th
        BW(CC.PixelIdxList{i}) = 0;
    end
end

se = strel('disk',4);
BW = imclose(BW,se);
CC = bwconncomp(BW);
L = labelmatrix(CC);
BWL = bwlabel(BW,4);
BWP = bwperim(BW,4);

for i = 1 : CC.NumObjects
    I3 = uint8(zeros(i_s_t,j_s_t));
    I3(CC.PixelIdxList{i}) = 255;

    [i_buff_1 i_buff_2] = size(CC.PixelIdxList{i});
    i_buff = rem(CC.PixelIdxList{i},1024);
    for i_buff_3 = 1 : i_buff_1

        if i_buff(i_buff_3) == 0;
            i_buff(i_buff_3) = 1024;
        end
    end
    i_min = min(i_buff);
    i_max = max(i_buff);

```

```

[j_buff_1 j_buff_2] = size(CC.PixelIdxList{i});
j_buff = CC.PixelIdxList{i};
for j_buff_3 = 1 : j_buff_1
    j_buff_4 = floor(CC.PixelIdxList{i}/1024) + 1;
    if rem(j_buff(j_buff_3),1024) == 0
        j_buff_4(j_buff_3) = j_buff_4(j_buff_3) - 1;
    end
end
j_min = min(j_buff_4);
j_max = max(j_buff_4);

if i_min > i_1 && i_max < i_2 && j_min > j_1 && j_max < j_2
    I4 = im2bw(I3(i_min:i_max,j_min:j_max),0.5);
    I4_BW4 = bwperim(I4,4);
    I4_BW8 = bwperim(I4,8);
    I4_BWA = bwarea(I4);
    I4_BWF = imFeretDiameter(I4);

    I4_P0 = (sum(sum(I4_BW8))+sum(sum(I4_BW4)))/2;
    I4_P = regionprops(I4,'perimeter');
    I4_P1 = I4_P.Perimeter;

%
    I4_CC = bwconncomp(I4_BW);
    Particle_Img(i,1) = image_number;
    Particle_Loc(i,1) = 1;
    Particle_Q(i,1) = 1;
    Particle_Perimeter_0(i,1) = I4_P0;
    Particle_Perimeter_1(i,1) = I4_P1;
    Particle_Length_0(i,1) = Particle_Perimeter_0(i,1) / 2;
    Particle_Length_1(i,1) = Particle_Perimeter_1(i,1) / 2;
    Particle_Area(i,1) = I4_BWA;
    Particle_Feret_Max(i,1) = max(max(I4_BWF));
    Particle_Feret_min(i,1) = min(min(I4_BWF));

elseif i_min < i_2 && i_max > i_1 && j_min < j_2 && j_max >
j_1

    i_min_2 = max(i_min,i_1);
    i_max_2 = min(i_max,i_2);
    j_min_2 = max(j_min,j_1);
    j_max_2 = min(j_max,j_2);

    I4 = im2bw(I3(i_min:i_max,j_min:j_max),0.5);
    I4_BW4 = bwperim(I4,4);
    I4_BW8 = bwperim(I4,8);
    I4_BWA = bwarea(I4);
    I4_BWF = imFeretDiameter(I4);

    I4_P0 = (sum(sum(I4_BW8))+sum(sum(I4_BW4)))/2;
    I4_P = regionprops(I4,'Perimeter');
    I4_P1 = I4_P.Perimeter;

```

```

I5 = im2bw(I3(i_min_2:i_max_2,j_min_2:j_max_2),0.5);
I5_BWA = bwarea(I5);

if max(max(I5)) > 0
    I4I5 = I5_BWA / I4_BWA;
else
    I4I5 = 0;
end

%
    I4_CC = bwconncomp(I4_BW);
Particle_Img(i,1) = image_number;
Particle_Loc(i,1) = 2;
Particle_Q(i,1) = I4I5;
Particle_Perimeter_0(i,1) = I4_P0;
Particle_Perimeter_1(i,1) = I4_P1;
Particle_Length_0(i,1) = Particle_Perimeter_0(i,1) / 2;
Particle_Length_1(i,1) = Particle_Perimeter_1(i,1) / 2;
Particle_Area(i,1) = I4_BWA;
Particle_Feret_Max(i,1) = max(max(I4_BWF));
Particle_Feret_min(i,1) = min(min(I4_BWF));

else

I4 = im2bw(I3(i_min:i_max,j_min:j_max),0.5);
I4_BW4 = bwperim(I4,4);
I4_BW8 = bwperim(I4,8);
I4_BWA = bwarea(I4);
I4_BWF = imFeretDiameter(I4);

I4_P0 = (sum(sum(I4_BW8))+sum(sum(I4_BW4)))/2;
I4_P = regionprops(I4,'Perimeter');
I4_P1 = I4_P.Perimeter;

%
    I4_CC = bwconncomp(I4_BW);
Particle_Img(i,1) = image_number;
Particle_Loc(i,1) = 0;
Particle_Q(i,1) = 0;
Particle_Perimeter_0(i,1) = I4_P0;
Particle_Perimeter_1(i,1) = I4_P1;
Particle_Length_0(i,1) = Particle_Perimeter_0(i,1) / 2;
Particle_Length_1(i,1) = Particle_Perimeter_1(i,1) / 2;
Particle_Area(i,1) = I4_BWA;
Particle_Feret_Max(i,1) = max(max(I4_BWF));
Particle_Feret_min(i,1) = min(min(I4_BWF));
end

%
if Particle_Length_1(i,1) > 256
%
    Particle_Perimeter_0(i,1) = 0;
%
    Particle_Perimeter_1(i,1) = 0;
%
    Particle_Length_0(i,1) = 0;
%
    Particle_Length_1(i,1) = 0;

```

```

%         Particle_Area(i,1) = 0;
%         Particle_Feret_Max(i,1) = 0;
%         Particle_Feret_min(i,1) = 0;
%     end
%     figure, imshow(I4_BW4);
%     Save all the particles
%         num_str2 = num2str(i);
%         img_save_name_2 = [img_save_name_ind , num_str, '_shape',
num_str2, file_ext];
%         imwrite(I4, img_save_name_2, 'tif');
%     clear I4;
end
    Particle_Info = [Particle_Img, Particle_Loc, Particle_Q,
Particle_Perimeter_0, Particle_Length_0, Particle_Perimeter_1,
Particle_Length_1, Particle_Area, Particle_Feret_Max,
Particle_Feret_min];
    data_save_name_1 = [data_save_name , num_str, '_shape',
data_ext];
    save(data_save_name_1, 'Particle_Info', '-ascii');
    data_save_name_1 = [data_save_name , '00000_shape_total',
data_ext];
    save(data_save_name_1, 'Particle_Info', '-ascii', '-append');

    clear Particle_Img;
    clear Particle_Loc;
    clear Particle_Q;
    clear Particle_Perimeter_0;
    clear Particle_Perimeter_1;
    clear Particle_Length_0;
    clear Particle_Length_1;
    clear Particle_Area;
    clear Particle_Feret_Max;
    clear Particle_Feret_min;

%     figure, imshow(BW);
    img_save_name_1 = [img_save_name , num_str, '_shape_info',
file_ext];
    imwrite(BW, img_save_name_1, 'tif');

end

figure();

```

APPENDIX J

FIBROUS DEBRIS SEM IMAGES

JEOL JSM-7500F Images

The JEOL JSM-7500F is an ultra-high resolution field emission scanning electron microscope (FE-SEM) equipped with a high brightness conical FE gun and a low aberration conical objective lens).



Figure J.1. JEOL JSM-7500F SEM Overview (Texas A&M University)

The improved overall stability of the JSM-7500F enables to readily observe specimens at magnifications up to 1,000,000x with the guaranteed resolution of 1 nm.

Resolution: 1.0 nm guaranteed at 15kV / 2.2 nm guaranteed at 1.0kV

Mag. range: 25x to 19,000x in LM mode / 100x to 650,000x in SEM mode

Accessories associated with the JSM-7500 include: conventional in-chamber Everhart-Thornley and through-the-lens secondary detectors, low angle back-scattered electron detector (LBE), IR-CCD chamber camera, Oxford EDS system equipped with X-ray mapping and digital imaging.

JEOL JSM-6400 Images

This software-oriented, analytical-grade SEM, is capable of acquiring and digitizing images. Acceleration voltages from 0.2 to 40kV, a magnification range of 10 to 300,000x, and a guaranteed resolution of 3.5nm allow an operator to achieve excellent results on a wide variety of samples.



Figure J.2. JEOL JSM-6400 SEM Overview (Texas A&M University)

SEM Images of STP samples of test #3 are presented in Figures J.3 ~ J.11. Four images with 10x, 25x, 100x, and 400x were taken for each sample.

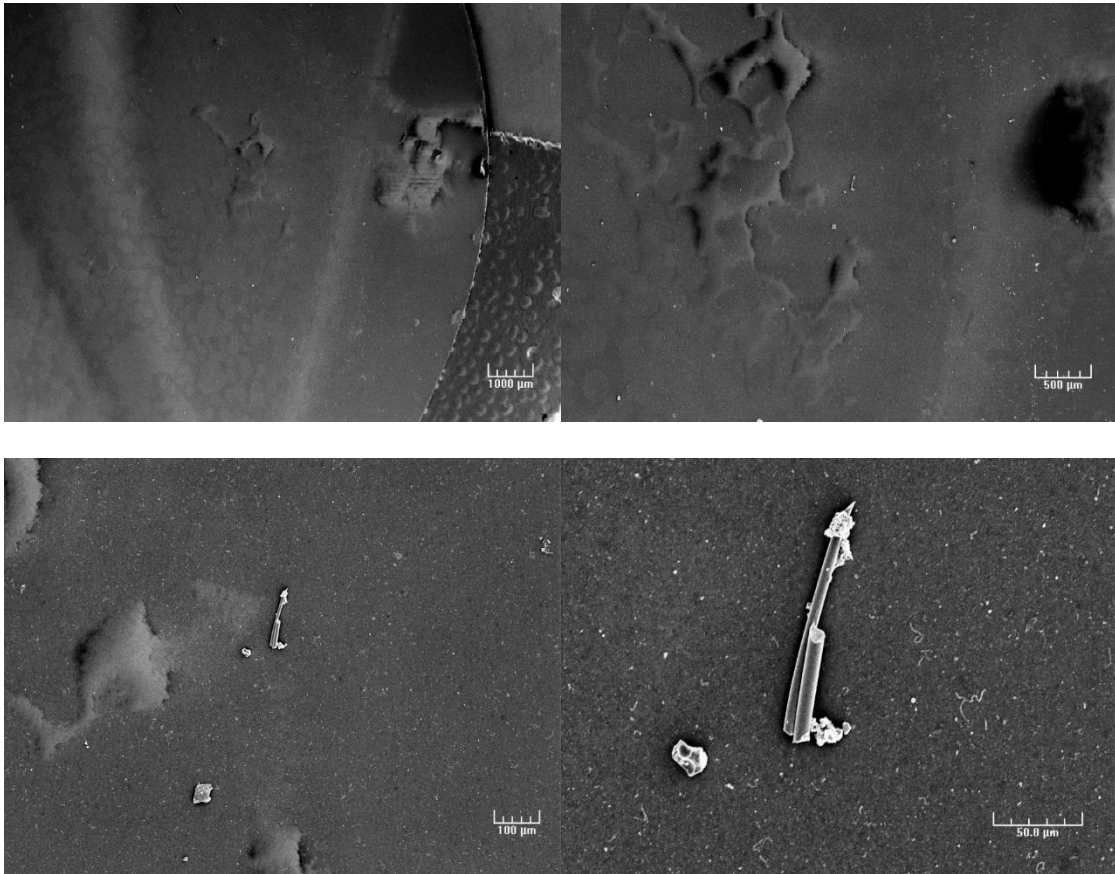


Figure J.3. STP debris sample Test#3-Sample#0 – (left-top) 10x, (right-top) 25x, (left-bottom) 100x, and (right-bottom) 400x

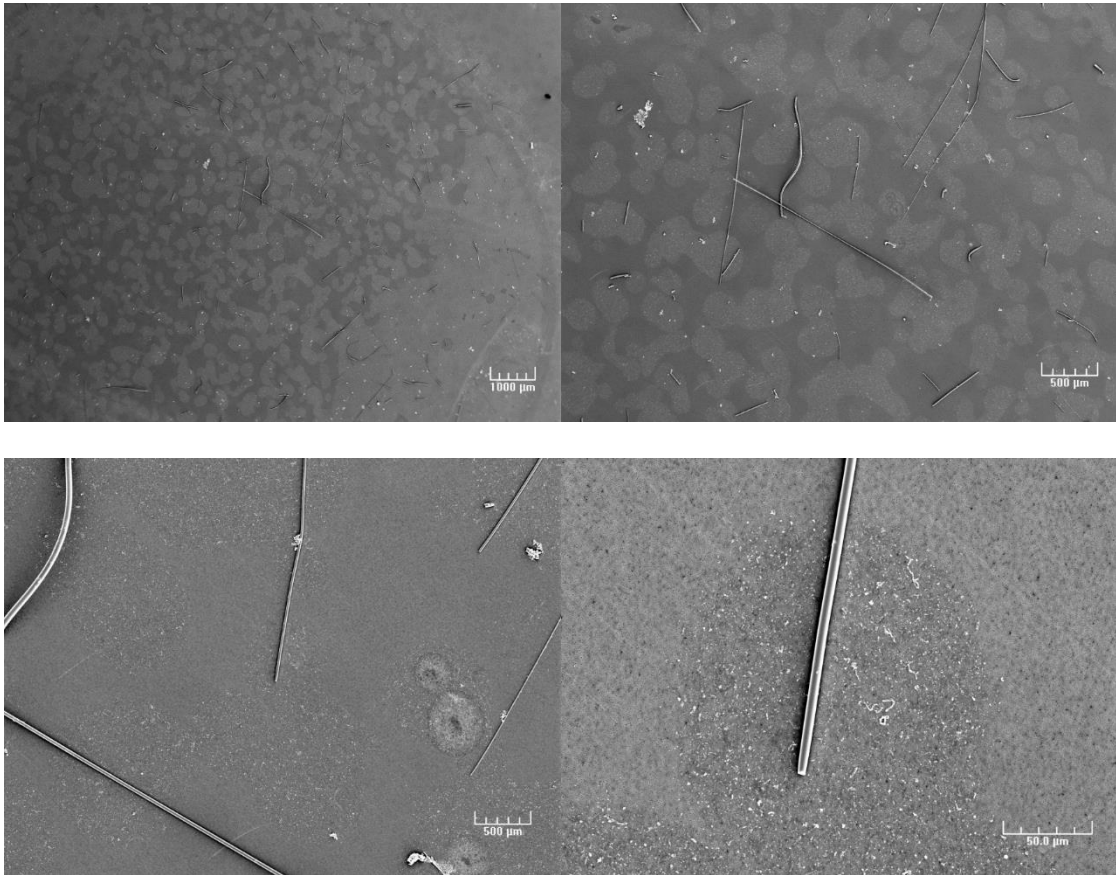


Figure J.4. STP debris sample Test#3-Sample#1 – (left-top) 10x, (right-top) 25x, (left-bottom) 100x, and (right-bottom) 400x

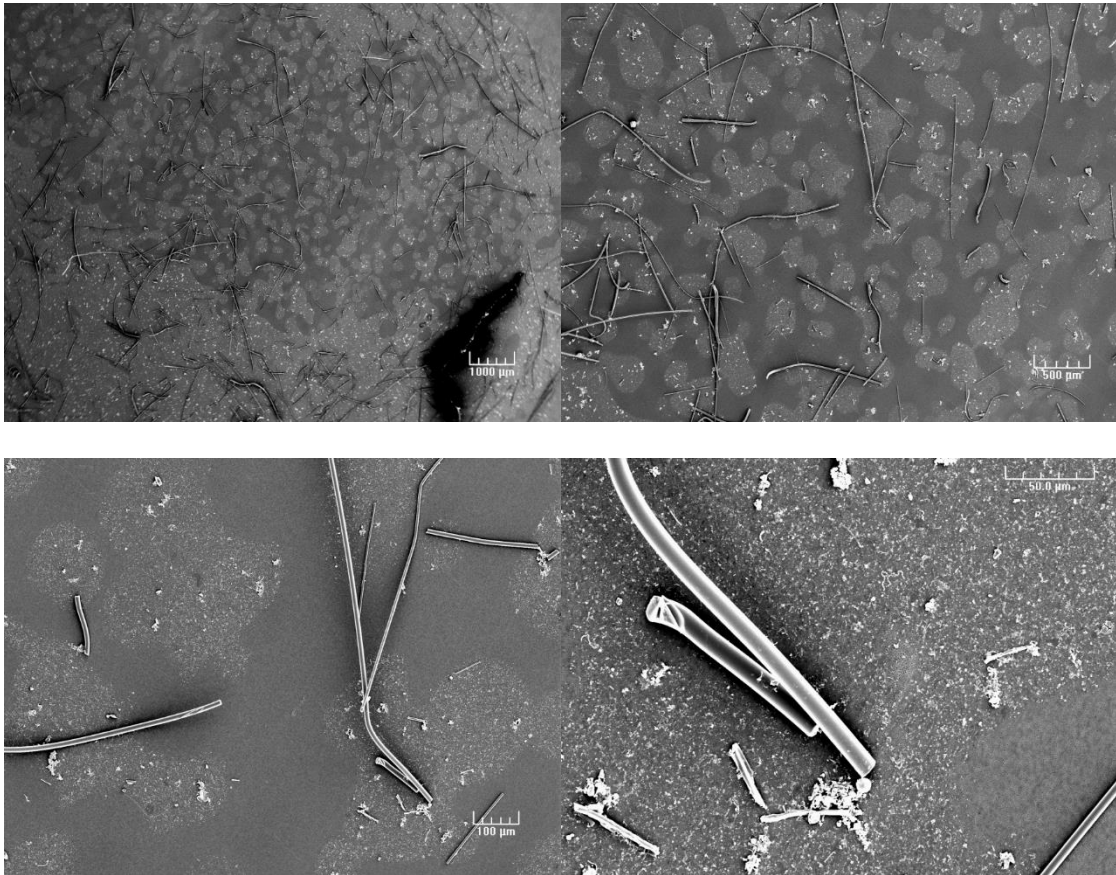


Figure J.5. STP debris sample Test#3-Sample#2 – (left-top) 10x, (right-top) 25x, (left-bottom) 100x, and (right-bottom) 400x

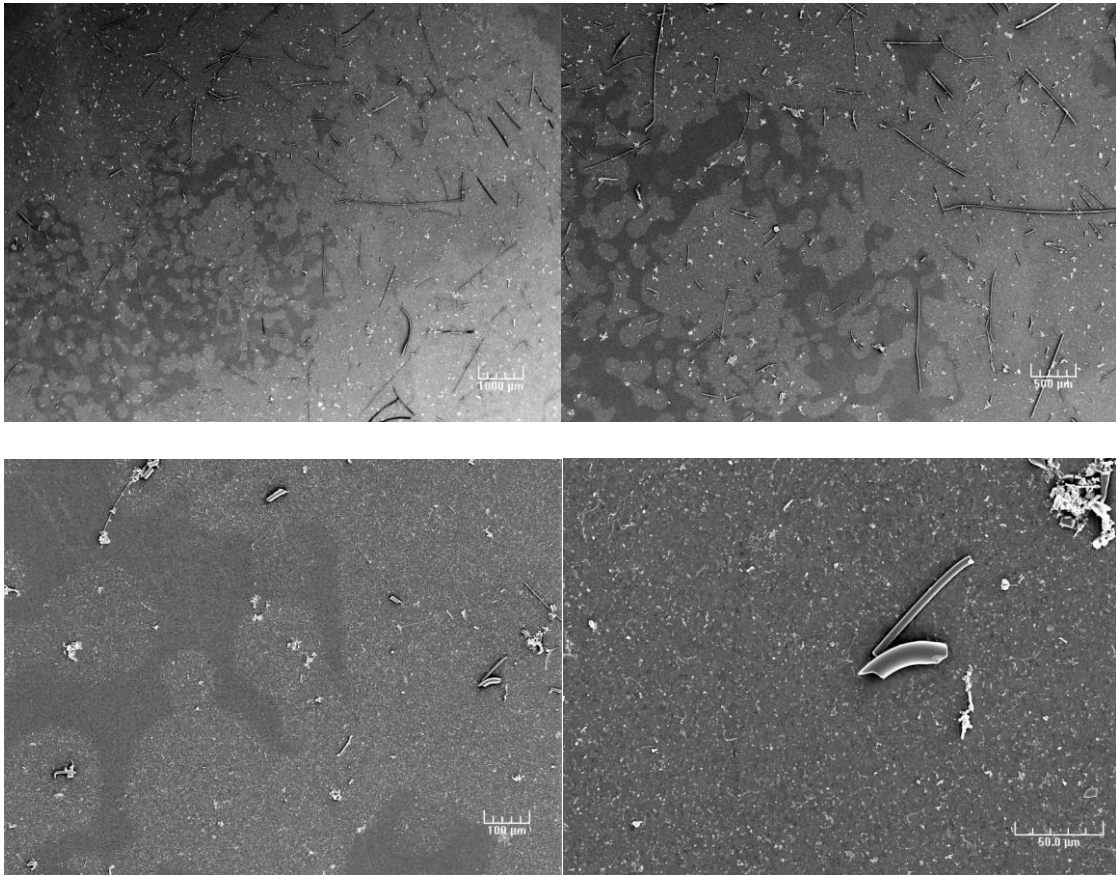


Figure J.6. STP debris sample Test#3-Sample#3 – (left-top) 10x, (right-top) 25x, (left-bottom) 100x, and (right-bottom) 400x

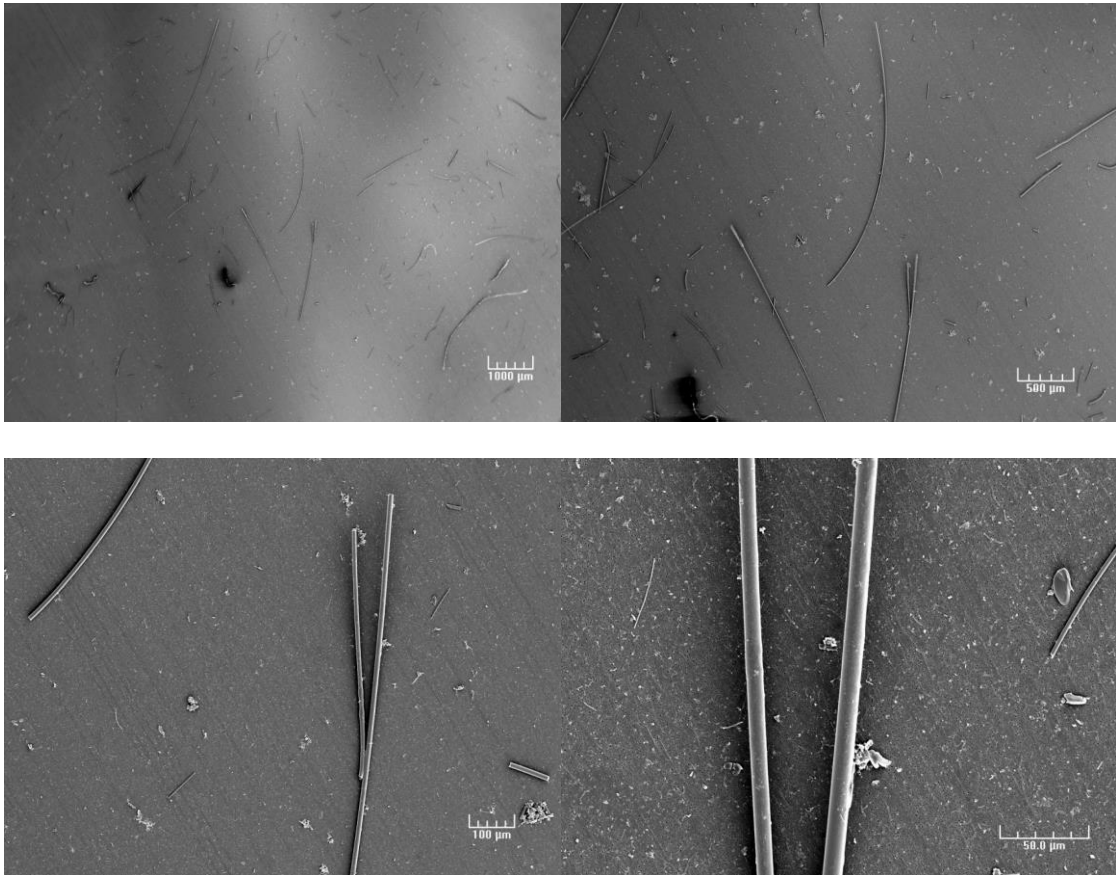


Figure J.7. STP debris sample Test#3-Sample#4 – (left-top) 10x, (right-top) 25x, (left-bottom) 100x, and (right-bottom) 400x

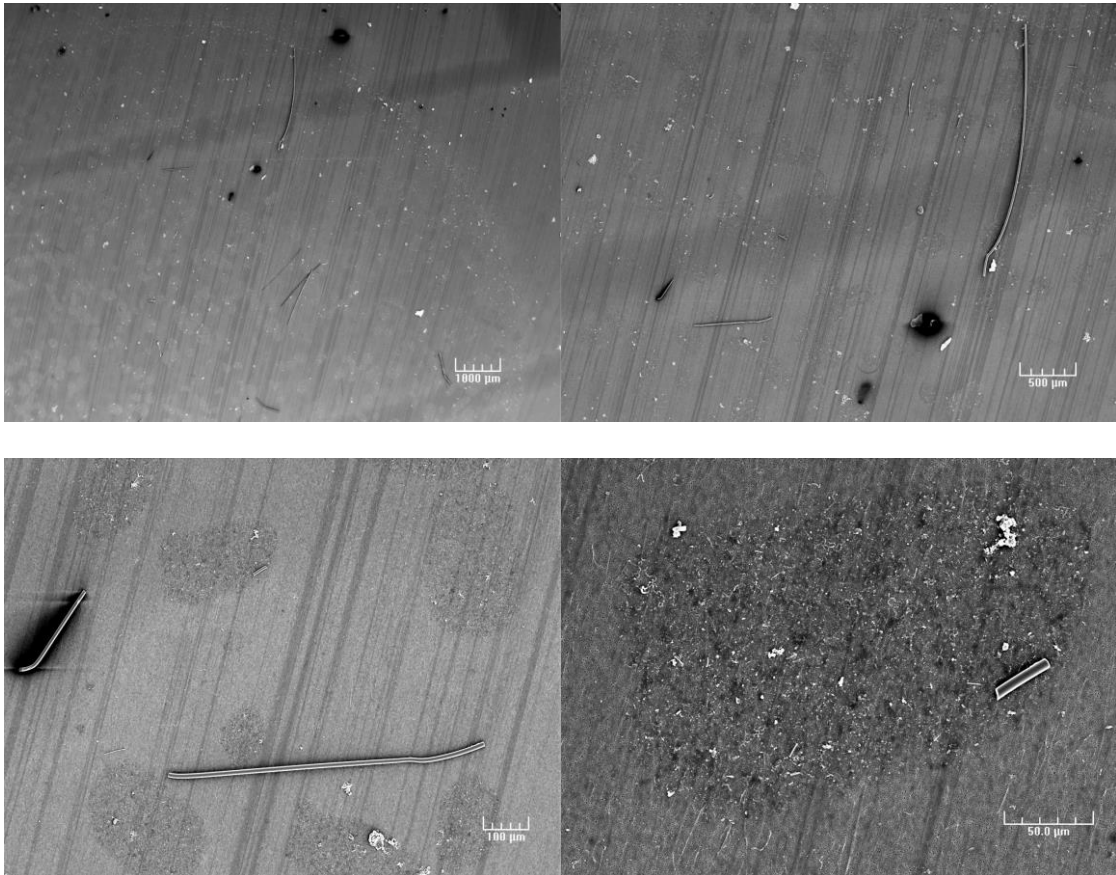


Figure J.8. STP debris sample Test#3-Sample#5 – (left-top) 10x, (right-top) 25x, (left-bottom) 100x, and (right-bottom) 400x

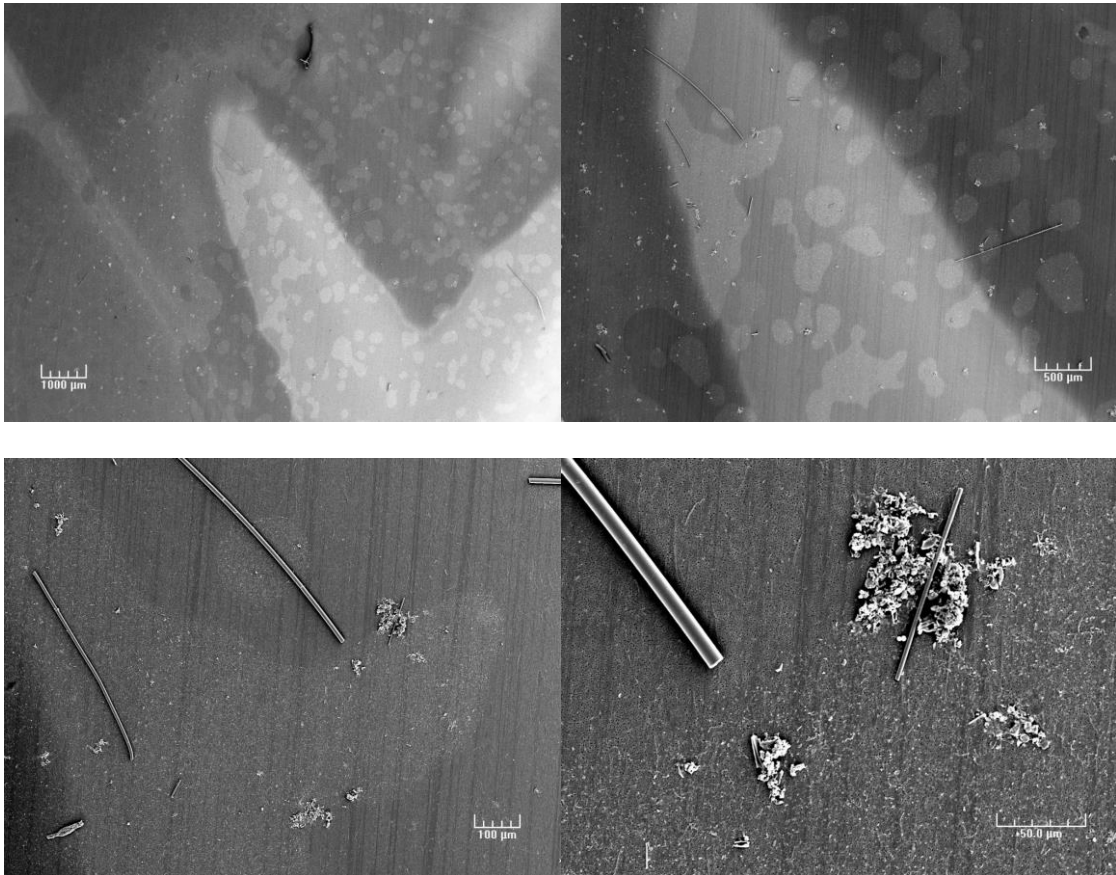


Figure J.9. STP debris sample Test#3-Sample#6 – (left-top) 10x, (right-top) 25x, (left-bottom) 100x, and (right-bottom) 400x

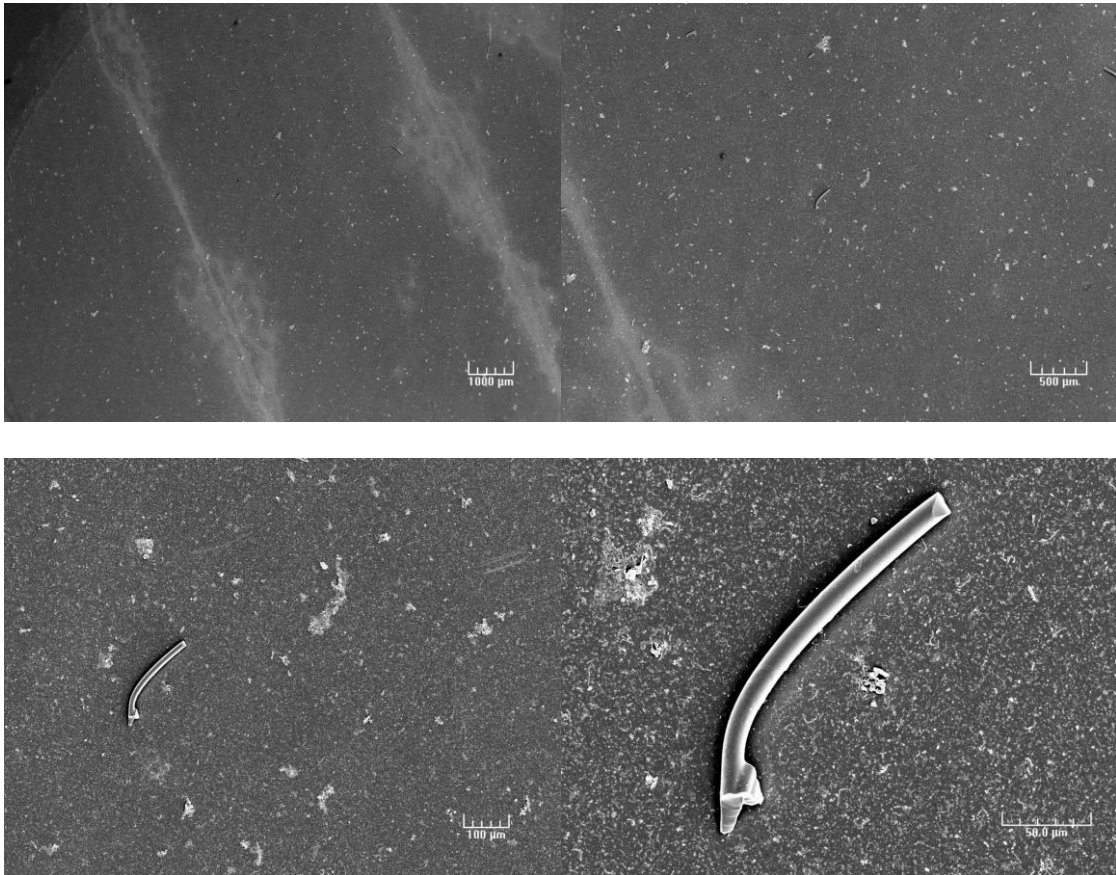


Figure J.10. STP debris sample Test#3-Sample#7 – (left-top) 10x, (right-top) 25x, (left-bottom) 100x, and (right-bottom) 400x

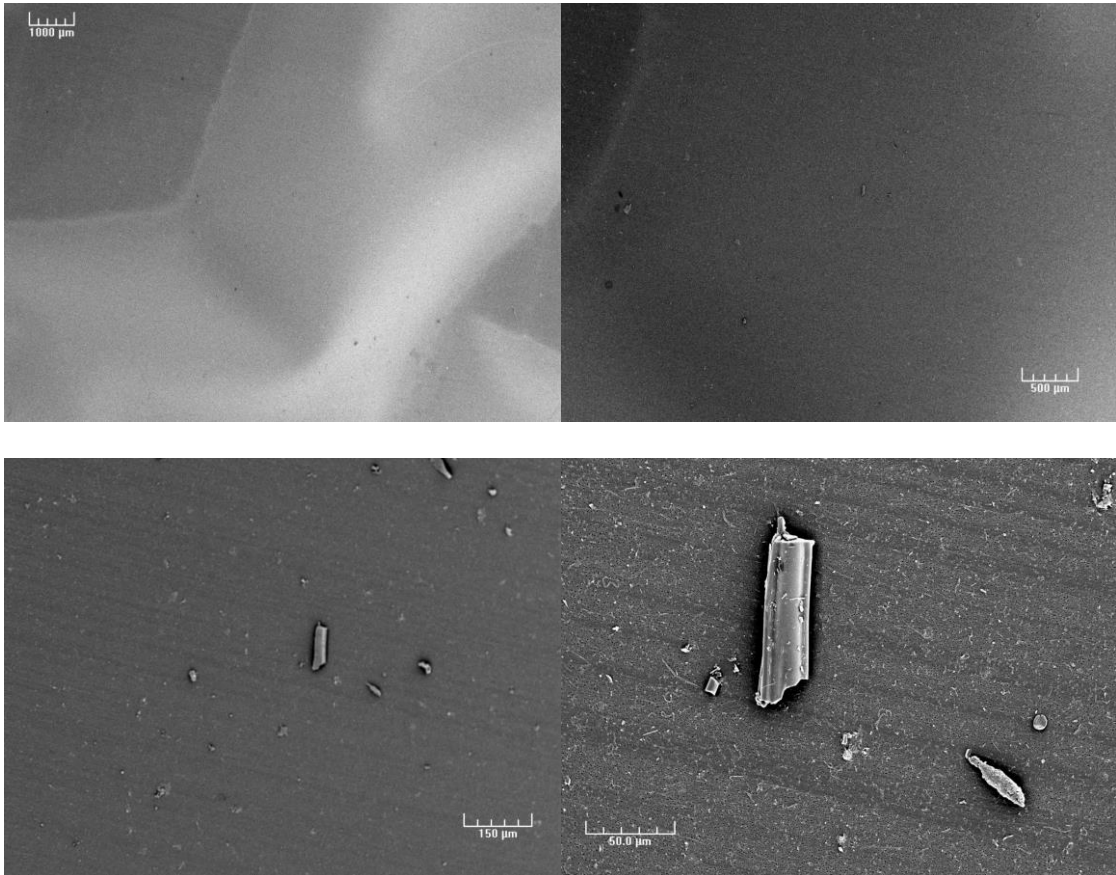


Figure J.11. STP debris sample Test#3-Sample#8 – (left-top) 10x, (right-top) 25x, (left-bottom) 100x, and (right-bottom) 400x